Geneeskundige **S**tichting **K**oningin **E**lisabeth
Fondation **M**édicale **R**eine **E**lisabeth
Königin-**E**lisabeth-**S**tiftung für **M**edizin
Queen **E**lisabeth **M**edical **F**oundation

Verslag – Rapport – Bericht – Report

_____

2022

G.S.K.E. – F.M.R.E. – K.E.S.M. – Q.E.M.F.

www.fmre-gske.be
www.fmre-gske.eu
www.fmre-gske.com

Final reports of the research projects of young researchers, supported by the Queen Elisabeth Medical Fondation in collaboration with the following professors and doctors (2022)

Interuniversitaire onderzoeksprojecten 2020-2022 gefinancierd door de G.S.K.E.

Projets de recherche interuniversitaire 2020-2022 subventionnés par la F.M.R.E.

Interuniversity research projects 2020-2022 funded by the Q.E.M.F.

Universiteiten met onderzoeksprogramma's die gesteund worden door de G.S.K.E.

Universités ayant des programmes de recherche subventionnés par la F.M.R.E.

Universities having research programs supported by the Q.E.M.F.

→ Universiteit Antwerpen (UAntwerpen)
→ Universiteit Gent (UGent)

→ Vrije Universiteit Brussel (VUB)
→ Katholieke Universiteit Leuven (KU Leuven)

Brussel/Bruxelles/Brussels

België
Belgique
Belgium

Europa
Europe

→ Univeristé de Mons (UMONS)

→ Université de Liège (ULg)
→ Université Catholique de Louvain (UCLouvain)

Interuniversitaire onderzoeksprojecten 2020-2022 gefinancierd door de G.S.K.E.
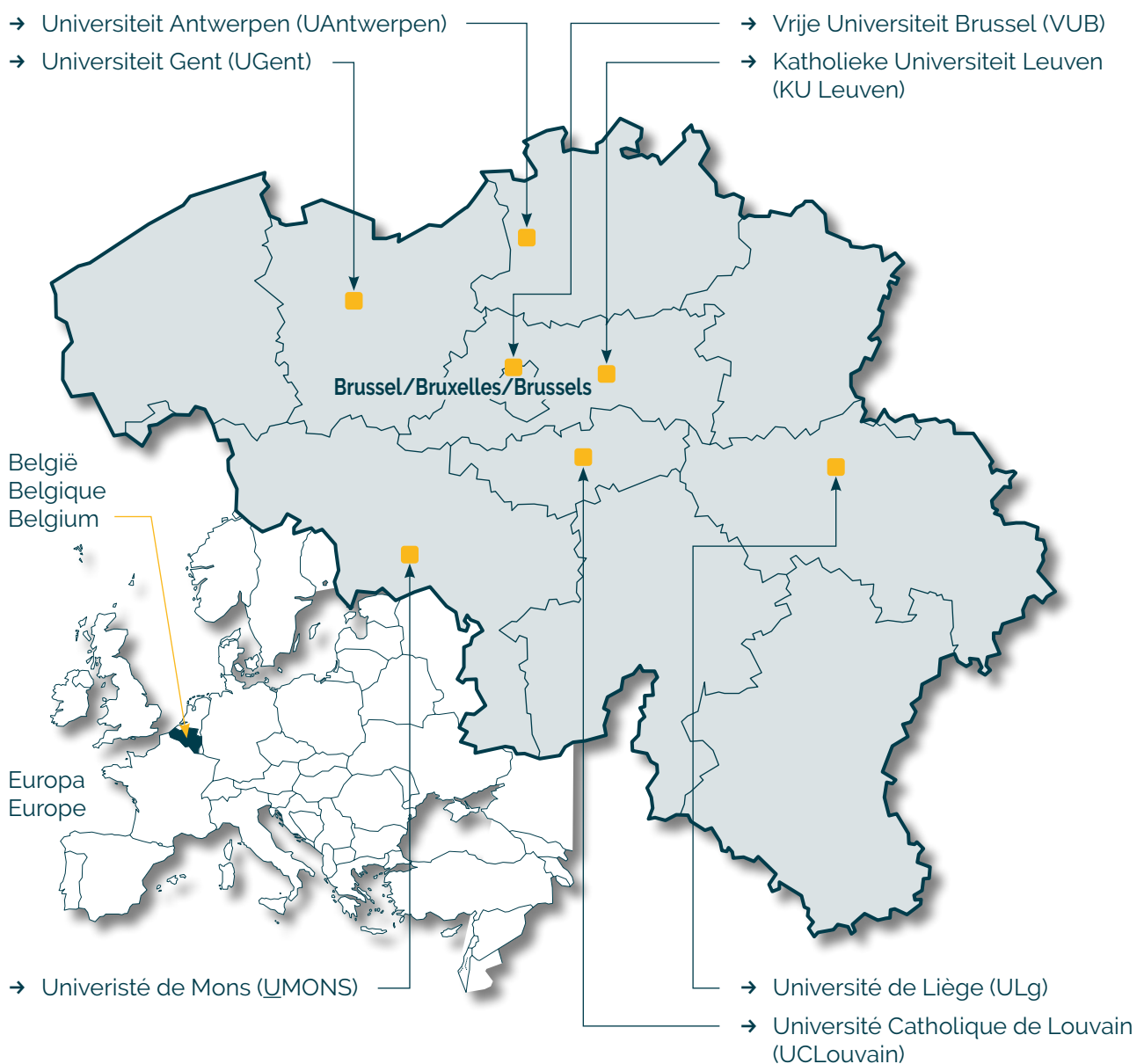
Projets de recherche interuniversitaire 2020-2022 subventionnés par la F.M.R.E.

Interuniversity research projects 2020-2022 funded by the Q.E.M.F.

Prof. dr. Jean-Noël Octave (UCLouvain)
Prof. dr. Philippe Gailly (UCLouvain)
Prof. dr. Nathalie Pierrot (UCLouvain)
Prof. dr. Laurence Ris (UMONS)
Prof. dr. Paul Boon (UGent)
Involvement of PPARα activation in the control of synaptic function by APP

Prof. dr. Sebastiaan Engelborghs (VUB)
Prof. dr. Chris Baeken (UGent)
Unraveling the link between depression and dementia to improve diagnostic and treatment options

Prof. dr. Vincent Van Rompaey (UAntwerpen)
Prof. dr. Peter Ponsaerts (UAntwerpen)
Prof. dr. Guy Van Camp (UAntwerpen)
Prof. Rik Gijsbers (KU Leuven)
Development of allele-specific CRISPR-nuclease gene therapy for late-onset sensorineural hearing impairment in a new humanized DFNA9 mouse model

Prof. dr. An Goris (KU Leuven)
Prof. Nathalie Cools (UAntwerpen)
Deep sequencing of myelin-reactive T-cells to elucidate new disease mechanisms and identify correlates for treatment responsiveness

Prof. dr. Pascal Kienlen-Campard (UCLouvain)
Prof. dr. Loïc Quinton (ULg)
Prof. dr. Jan Gettemans (UGent)
New analytical tools to identify and target pathogenic hexameric Aβ assemblies in Alzheimer's disease

Final report of the interuniversity research project of

Prof. dr. Jean-Noël Octave (UCLouvain)
Prof. dr. Philippe Gailly (UCLouvain)
Prof. dr. Nathalie Pierrot (UCLouvain)
Prof. dr. Laurence Ris (UMONS)
Prof. dr. Paul Boon (UGent)
Robrecht Raedt (UGent)

Prof. dr. Jean-Noël Octave (UCLouvain)
Faculty of Pharmacy and Biomedical Sciences
Institute of neuroscience (IONS)
CEMO
Avenue Hippocrate 54/B1.54.10
1200 Woluwe-Saint-Lambert
jean-noel.octave@uclouvain.be

Prof. dr. Philippe Gailly (UCLouvain)
Institute of Neuroscience (IoNS)
Laboratory of Cell Physiology (FYCL)
Avenue Mounier, 53 - B1.53.17
1200 Brussels
philippe.gailly@uclouvain.be
Tel. + 32 (0)2 764 55 42

Prof. dr. Nathalie Pierrot (UCLouvain)
Institute of Neuroscience (IONS)
CEMO
Avenue Mounier 53/B1.53.03
1200 Woluwe-Saint-Lambert
nathalie.pierrot@uclouvain.be

Prof dr. Laurence Ris (UMONS)
Lecturer, head of the department of Neuroscience
Faculty of Medicine and Pharmacy
6A, avenue du Champ de Mars 7000 Mons
laurence.ris@umons.ac.be

Prof. dr. Paul Boon (UGent)
Professor and chairman Department of Neurology
Chairman Division of Head, Movement and Senses
Ghent University Hospital - Ghent University
10 Corneel Heymanslaan
9000 Gent
Paul.boon@ugent.be

Robrecht Raedt (UGent)

Involvement of PPARa activation in the control of synaptic function by APP.

1.   The context

With a prevalence doubling every 5 years beyond 65, Alzheimer's disease (AD) is a devastating neurodegenerative disorder, which is the most common cause of dementia in the elderly. Together with a progressive loss of cognitive functions, AD is characterized by the existence of extracellular senile plaques containing the amyloid-β (Aβ) peptide generated from the sequential proteolytic processing of its precursor, the amyloid precursor protein (APP).

Although amyloid deposition occurring in the hippocampus and the cerebral cortex of AD patients potentially explains deficits in memory and cognitive function observed [1], it remains difficult to influence the course of AD by removing amyloid deposits. Indeed, even if immunotherapy efficiently removes senile plaques from AD brains, clinical trials indicate that cognition is not improved in AD patients. Therefore, a better knowledge of the underlying physiopathological mechanisms involved early in the neurodegenerative process is required. In particular, a considerable bulk of evidence supports that synaptic function is affected at the earliest stages of AD. Indeed, synaptic dysfunction leading to atypical neural synchrony and oscillations observed in AD brain might play an early role in the establishment of pathogenic cascades leading to AD and could contribute to cognitive deficits [2,3].

Synaptic deficits occur very early in AD patients [4]. Moreover, it was reported that people at risk for AD (*e.g.* ApoE4 carriers, see below) display increased neuronal excitability without dementia [5] and that cognitive and synaptic dysfunctions arise before the formation of plaques in transgenic mouse models of AD [6]. Using different methodological approaches, including electroencephalography (EEG) [7,8], a lack of functional connectivity between brain areas has been highlighted in AD [9,10].

We previously reported that increase or decrease in APP expression modulates both excitatory and inhibitory neuronal activity in primary rat cortical networks [11-13]. These data suggest an **essential role of APP in the control of both excitatory and inhibitory neurotransmissions, which have to be perfectly balanced to regulate cognitive function.**

In the vast majority of late-onset sporadic AD cases (+/- 99 %), the source of Aβ accumulation in the brain is still unknown. Nevertheless, it is well established that the epsilon 4 allele of the *apolipoprotein E* (*ApoE*) gene, encoding the main transporter of cholesterol in the brain, is a genetic risk factor for AD[14]. Therefore, a **relationship between AD and lipid metabolism has been established.** We have previously demonstrated that the expression of the neuronal human APP

(hAPP) isoform in cortical networks controls cholesterol turnover, needed for neuronal activity [15], by interacting with the sterol regulatory element binding protein 1 (SREBP1), a transcription factor that regulates expression of sterol- and lipogenic genes [16,17]. We reported that **hAPP expression inhibits biosynthesis of both cholesterol and fatty acids (FAs) in cortical cells in culture** [15].

FAs are the major constituents of brain lipids [18] and play a critical role in brain development and functioning [19]. Among them, essential brain polyunsaturated FAs (PUFAs) play a critical role in neurogenesis, synaptic function, inflammation, glucose homeostasis, mood and cognition [20].

PUFAs are ligands for retinoid X and peroxisome proliferator-activated receptors (RXRs and PPARs, respectively) [21], two nuclear receptors forming permissive heterodimers that belong to the superfamily of ligand-dependent transcription factors [22]. PPARs act principally as lipid sensors [23] and due to their anti-inflammatory effects, PPARs activation with specific agonists emerged as promising approaches for treating brain pathologies in several mouse models of Parkinson, Huntington and Alzheimer diseases [24,25]. Recent *in vitro* and *in vivo* evidence point to PPARα as a promising therapeutic target in AD that we have recently reviewed[26]. Indeed, it was shown that PPARα agonists improved amyloid and tau pathologies, decreased neuroinflammation, ameliorated glucose and lipid dyshomeostasis and improved behavior in mouse models of AD [27].

We recently reported that **PPARa expression also plays a crucial role in synaptic function. Activation of PPARα with a specific agonist improves synaptic plasticity in a transgenic mouse model of AD** [28]. However, the cellular and molecular mechanisms underlying such effects are poorly understood.

2.   Results.

2.1.   How does APP modulate excitatory / inhibitory neurotransmission ?
The function of the APP is not fully understood, but its cleavage product Aβ together with neurofibrillary tangles constitute the hallmarks of AD. Yet, imbalance of excitatory and inhibitory neurotransmission accompanied by loss of synaptic functions, has been reported much earlier and independent of any detectable pathological markers. Recently, soluble APP fragments have been shown to bind to presynaptic GABA$_B$ receptors (GABA$_B$Rs), subsequently decreasing the probability of neurotransmitter release [29]. We recently showed that overexpression of wild-type human APP in mice (hAPPwt [30]) causes early cognitive impairment, neuronal loss, and electrophysiological abnormalities in the absence of amyloid plaques and at very low levels of Aβ. hAPPwt mice exhibited neuronal overexcitation that was evident in EEG and increased long-term potentiation (LTP). Overexpression of hAPPwt did not alter GABAergic/glutamatergic receptor components or GABA production ability. Nonetheless, we detected a decrease of GABA but not glutamate that could be linked to soluble APP fragments, acting on presynaptic GABA$_B$Rs and subsequently reducing GABA release. By using CGP36216, a specific presynaptic GABA$_B$R antagonist, we were able to rescue hyperexcitation in hAPPwt animals. Our results provide evidence that APP plays a crucial role in regulating inhibitory neurotransmission (Fig. 1). Interestingly, in the opposite situation, i.e. in APP knockout mice, we observed an increase of GABA production that was caused by a down-regulation of NPAS4, a inducible transcription factor induced by neuronal depolarisation (Fig. 2). These results have been published in 2020 and 2021 (Kreis et al., 2021 and Opsomer et al., 2020; see references below and pdf papers attached)

2.2.   Role of KCC2 in neuronal hyperexcitability and in memory formation.
The postsynaptic inhibition through GABA$_A$ receptors (GABA$_A$R) relies on two mechanisms, a shunting effect due to an increase of the postsynaptic membrane conductance and, in mature neurons, a hyperpolarization effect due to an entry of chloride into postsynaptic neurons. The second effect requires the action of the K$^+$-Cl$^-$ cotransporter KCC2 which extrudes Cl$^-$ from the cell and maintains its cytosolic concentration very low. Neuronal chloride equilibrium seems to be dysregulated in several neurological and psychiatric conditions such as epilepsy, anxiety, schizophrenia, Down syndrome or Alzheimer's disease.

Based on *in vitro* results (cells in culture), we hypothesized that hyperexcitability observed in APP-overexpressing neurons could be related to an APP-induced reduction of the expression

of KCC2, a K^+-Cl^- transporter responsible for the extrusion of Cl^- in mature neurons [13]. However, we did not observe any change in the expression of KCC2 and NKCC1 (the Na^+, K^+, Cl^- transporter responsible for the influx of Cl- in neurons) *in vivo*, in mice overexpressing hAPPwt, suggesting that the excitatory / inhibitory imbalance was not due to the accumulation of chloride in neurons (Kreis et al, 2021). It is however important to note that APP is not systematically overexpressed in sporadic AD, but that its metabolism and/or function are highly impaired. We previously extended our analysis by examining KCC2 and NKCC1 expression in frontal cortex brain tissues from human control subjects and patients suffering from dementia clinically diagnosed with late onset AD [13]. Interestingly, while NKCC1 expression remained unchanged, we detected a significant decrease in KCC2 expression in the brains of these patients (Fig. 3). A potential involvement of Aβ in APP dependent KCC2 regulation cannot be excluded and one could speculate that increased levels of Aβ combined to an alteration in the physiological function of APP could influence KCC2 expression in AD.

We therefore investigated the consequences of a reduction of expression of KCC2 on spatial reference memory and working memory in vivo as well as LTP on brain slices, in a murine model where KCC2 can be specifically reduced in glutamatergic neurons at a specific time point (KCC2$^{lox/lox}$ – CamKII CreERT2 mice) (Collaboration with Thomas Jentsch, Germany).
Tamoxifen-induced conditional deletion of KCC2 in glutamatergic neurons of the forebrain was performed at 3 months of age and resulted in spatial and nonspatial learning impairment. On brain slices, stimulation of Schaffer collaterals by a theta burst induced a long-term potentiation (LTP). The lack of KCC2 did not affect potentiation of field excitatory postsynaptic potentials (fEPSP) measured in the stratum radiatum (dendrites) but increased population spike (PS) amplitudes measured in the CA1 somatic layer, suggesting a reinforcement of the EPSP-PS potentiation, i.e., an increased ability of EPSPs to generate action potentials. At the cellular level, KCC2 deletion induced a positive shift in the reversal potential of GABA$_A$R-driven Cl^- currents (E_{GABA}) suggesting an intracellular accumulation of chloride subsequent to the downregulation of KCC2. After treatment with bumetanide, an antagonist of the Na^+-K^+-Cl^- cotransporter NKCC1, memory impairment, chloride accumulation and EPSP-PS potentiation were rescued in mice lacking KCC2. These results emphasizing the importance of chloride equilibrium and GABA inhibiting ability in synaptic plasticity and memory formation, will be published in 2023 (Kreis et al., see reference below)

2.3. Regulation of PPARα by APP affects the pharmacological modulation of synaptic activity.

Among genetic susceptibility loci associated with late-onset Alzheimer disease (LOAD), genetic polymorphisms identified in genes encoding lipid carriers led to the hypothesis that a disruption of lipid metabolism could promote disease progression. We previously reported that APP involved in AD physiopathology impairs lipid synthesis needed for cortical networks' activity and that activation of peroxisome proliferator–activated receptor α (PPARα), a metabolic regulator involved in lipid metabolism, improves synaptic plasticity in an AD mouse model. These observations led us to investigate a possible correlation between PPARα function and full-length APP expression. Here, we report that PPARα expression and activation were inversely related to APP expression both in LOAD brains and in early-onset AD (EOAD) cases with a duplication of the APP gene, but not in control human brains. Moreover, human APP expression decreased PPARα expression and its related target genes in transgenic mice and in cultured cortical cells, while opposite results were observed in APP-silenced cortical networks (Fig. 4).
In cultured neurons, APP-mediated decrease or increase in synaptic activity was corrected by a PPARα-specific agonist and antagonist, respectively. APP-mediated control of synaptic activity was abolished following PPARα deficiency, indicating a key function of PPARα in this process.

These results have been published in 2021 (Sáez-Orellana et al., 2020 and 2021 see references below and pdf papers attached)

2.4. PPARa activation in hAPPwt animals

In order to confirm the involvement of PPARα activation in the control of synaptic function by APP we further investigated the effect of a PPARα agonist in hAPP mice in vivo. Therefore, hAPP mice (n=5) and wildtype (WT) littermates (n=5) were stereotactically implanted with a tripolar recording electrode with electrode tips located in parietal cortex, hippocampal CA1 and dentate gyrus. Spontaneous EEG was recorded and compared upon PPARα activation with the WY14643 agonist (40 dissolved in saline with 10% Tween-80 and 20% DMSO). Epileptic spikes were observed on the EEG in hAPPwt animals only as described previously (in our paper published in 2021 by Kreis et al.) and were quantified during an 8 hour period immediately before and after treatment with WY14643. Unexpectedly we found an increase rather than a decrease in epileptic spikes upon PPARα activation (Figure 5). Although these results were unexpected, it does suggest an involvement of PPARα in the generation of epileptic spikes in hAPP overexpressing mice.

Furthermore, ex vivo basal synaptic transmission has been investigated by extracellular recordings on acute hippocampal slices of hAPP and WT mice. The causal effect of PPARα activity on the observed deficits has been evaluated by treating slices with the WY14643 PPARα agonist (10 µM) for 2 h. Basal synaptic transmission has been recorded before and after kainate (2 µM) application in the presence or absence of PPARα agonist.
Our results showed a significant reduction of maximal EPSP amplitude in hAPP mice compared to WT ($p < 0.016$). This difference was increased in the presence of PPARα agonist mainly due to a positive effect of the agonist on WT slices.
Kainate application reduced the fEPSP amplitude and slope both in WT and in hAPP mice but the effect was more severe and significant (paired t-test, $p < 0.001$) in hAPP mice where epilepsy was observed. The application of PPARα agonist reduced this effect in hAPP mice

These results showed that PPARα might play a role in the effect of hAPP on the generation of epileptic spikes in the hippocampus and kainite effects. Moreover, they showed that hAPP mice are more sensitive to kainate and more susceptible to develop epilepsy (Figure 6).

Furthermore, results obtained from WT and hAPP mice have been compared to $App^{-/-}$ mice with and without GW6471 PPARα antagonist (5 µM, dose used in organotypic slices [31]). However, we observed no difference between KO and WT mice and no effect of the perfusion of PPARα antagonist on input/output curves.

3.   Papers published in 2020-2022 (research supported by FMRS-GSKE).

– Kreis A, Desloovere J, Suelves N, Pierrot N, Yerna X, Issa F, Schakman O, Gualdani R, De Clippele M, Tajeddine N, Kienlen-Campard P, Raedt R, Octave JN, Gailly P (2021)
Overexpression of wild-type human amyloid precursor protein alters GABAergic transmission
Scientific reports 11 (1), 1-18
IF : 6.5
Q1

– Kreis A, Yerna X, Schakman O, Issa F, de Clippele M, Tajeddine N, Pierrot N, Octave JN, Gualdani R, Gailly P. (2023)
Conditional deletion of KCC2 impairs synaptic plasticity and both spatial and nonspatial memory.
Frontiers in Molecular Neuroscience (paper in revision)
Opsomer R, Contino S, Perrin F, Gualdani R, Tasiaux B, Doyen P, Vergouts M, Vrancx C, Doshina A, Pierrot N, Octave JN, Gailly P, Stanga S, Kienlen-Campard P. (2020)
Amyloid Precursor Protein (APP) Controls the Expression of the Transcriptional Activator Neuronal PAS Domain Protein 4 (NPAS4) and Synaptic GABA Release.
eNeuro. 2020 May 28;7(3):ENEURO.0322-19.2020. doi: 10.1523/ENEURO.0322-19.2020.

– Sáez-Orellana F, Octave JN, Pierrot N. (2020)
Alzheimer's Disease, a Lipid Story: Involvement of Peroxisome Proliferator-Activated Receptor α.
Cells 9(5):1215. doi: 10.3390/cells9051215.
IF: 7.6
Q1 (General Biochemistry, Genetics and Molecular Biology)
Q2 (Cell Biology)

– Sáez-Orellana F, Leroy T, Ribeiro F, Kreis A, Leroy K, Lalloyer F, Baugé E, Staels B, Duyckaerts C, Brion JP, Gailly P, Octave JN, Pierrot N (2021)
Regulation of PPARα by APP in Alzheimer disease affects the pharmacological modulation of synaptic activity.
Journal of Clinical Investigation Insight 6 (16) JCI : e150099
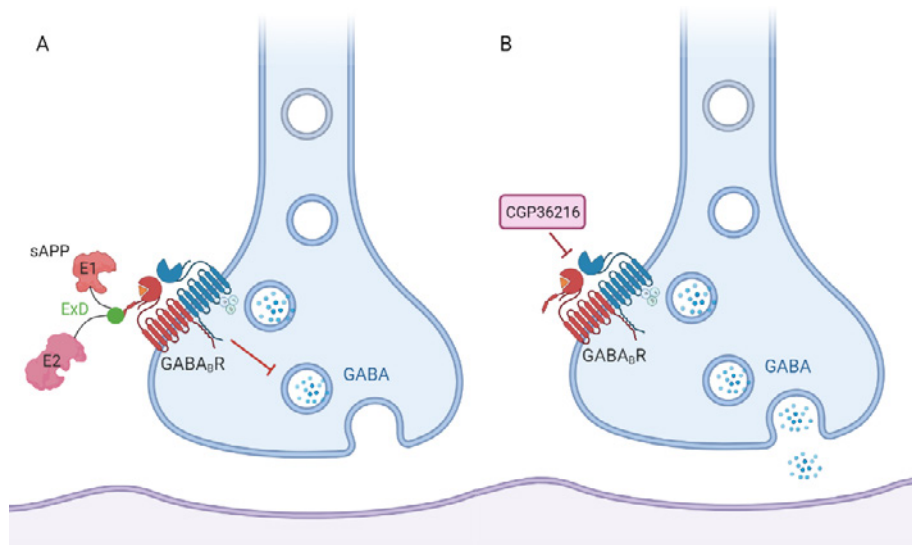IF : 8.35
Q1

4. Figures

Figure 1: Ligand binding to presynaptic GABA$_B$Rs. A. Soluble APP fragments act as presynaptic GABA$_B$R agonists, by binding to GABA$_{B1a}$ subunits on GABAergic synapses and inhibiting the release of GABA into the synaptic cleft. B. Binding of the antagonist CGP36216 to presynaptic GABA$_{B1a}$ subunits and subsequently allowing the release of GABA. Modified from ref 29.
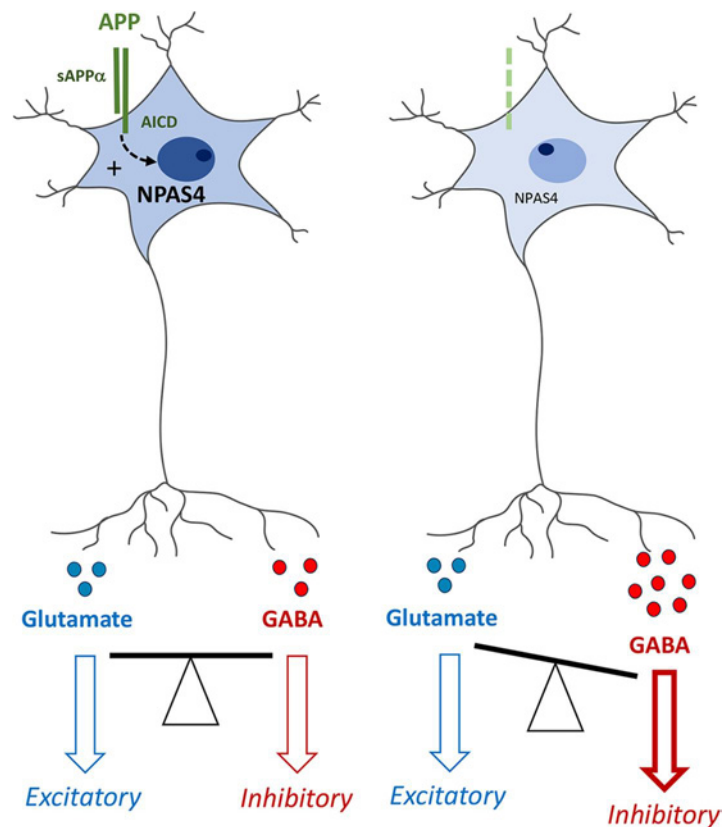

Figure 2: APP-deficient neurons present a downregulation of the activity-dependent transcription factor neuronal PAS domain protein 4 (NPAS4) along with an increase in GABAergic neuron markers and GABA release, but not in excitatory glutamatergic markers.
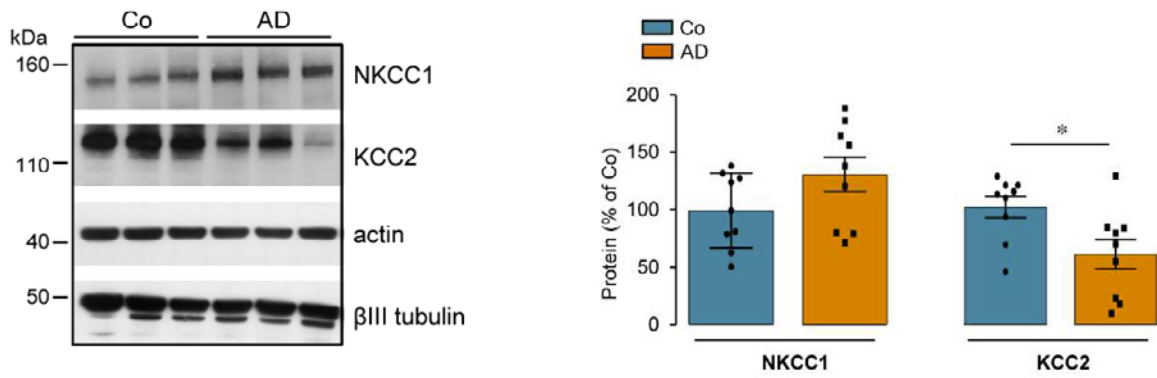
Figure 3: Expression of NKCC1 and KCC2 in late onset AD brains. Representative Western blot of NKCC1 and KCC2 expression in frontal cortex of postmortem human brain tissues from control subjects (Co, n=9) and patients with Alzheimer disease (AD, n=9). Blots were probed using anti-NKCC1, -KCC2, -actin and -βIII tubulin antibodies. Bottom panel: quantification of NKCC1 / actin and KCC2 / βIII tubulin ratios. Results were expressed as percentage (mean ± s.e.m.) of Co, P<0.05, Student's t-test. From our ref 13.
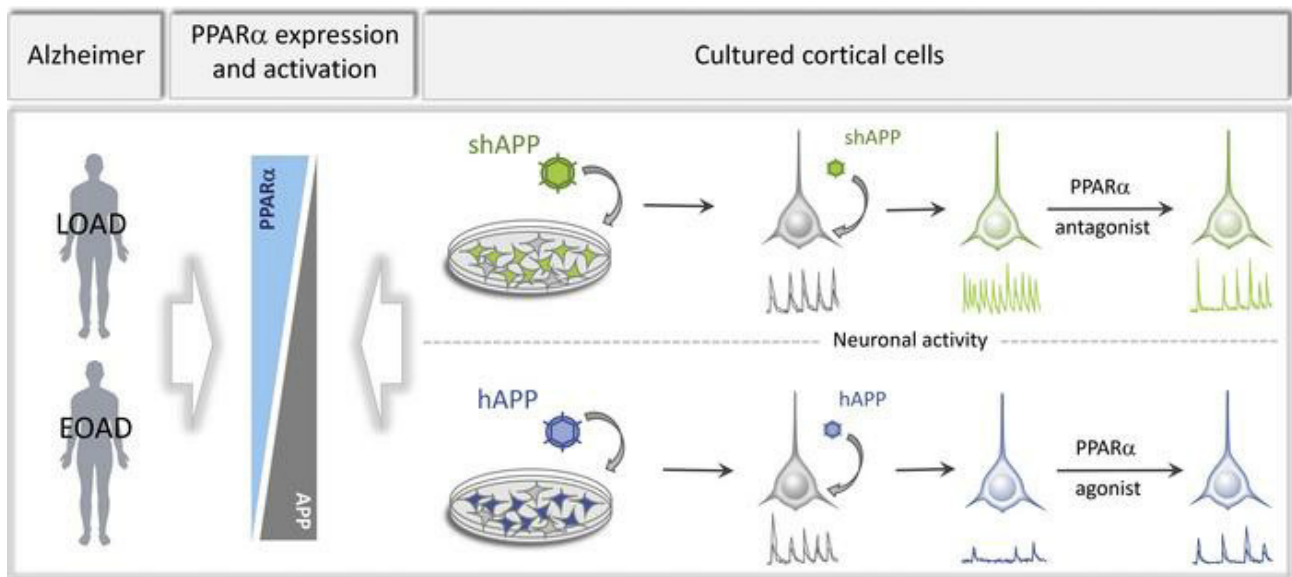
Figure 4: Modulation of APP-induced neuronal activity by PPARα agonists and antagonists.

Effect of WY14663 (40 mg/kg)
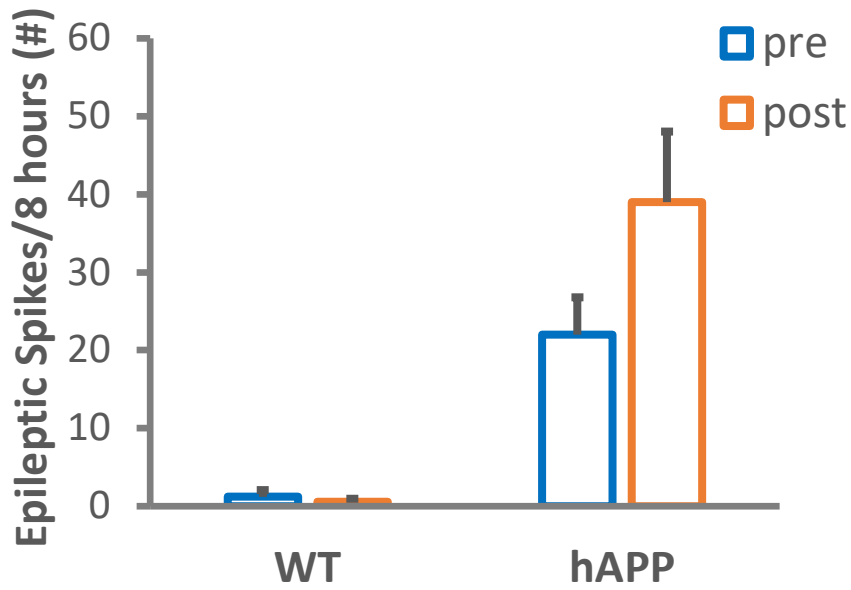
Figure 5: Injection of 40 mg/kg of the PPARa agonist WY14643 increased the number of epileptic spikes only in hAPP mice but did not induce epileptic spikes in WT mice
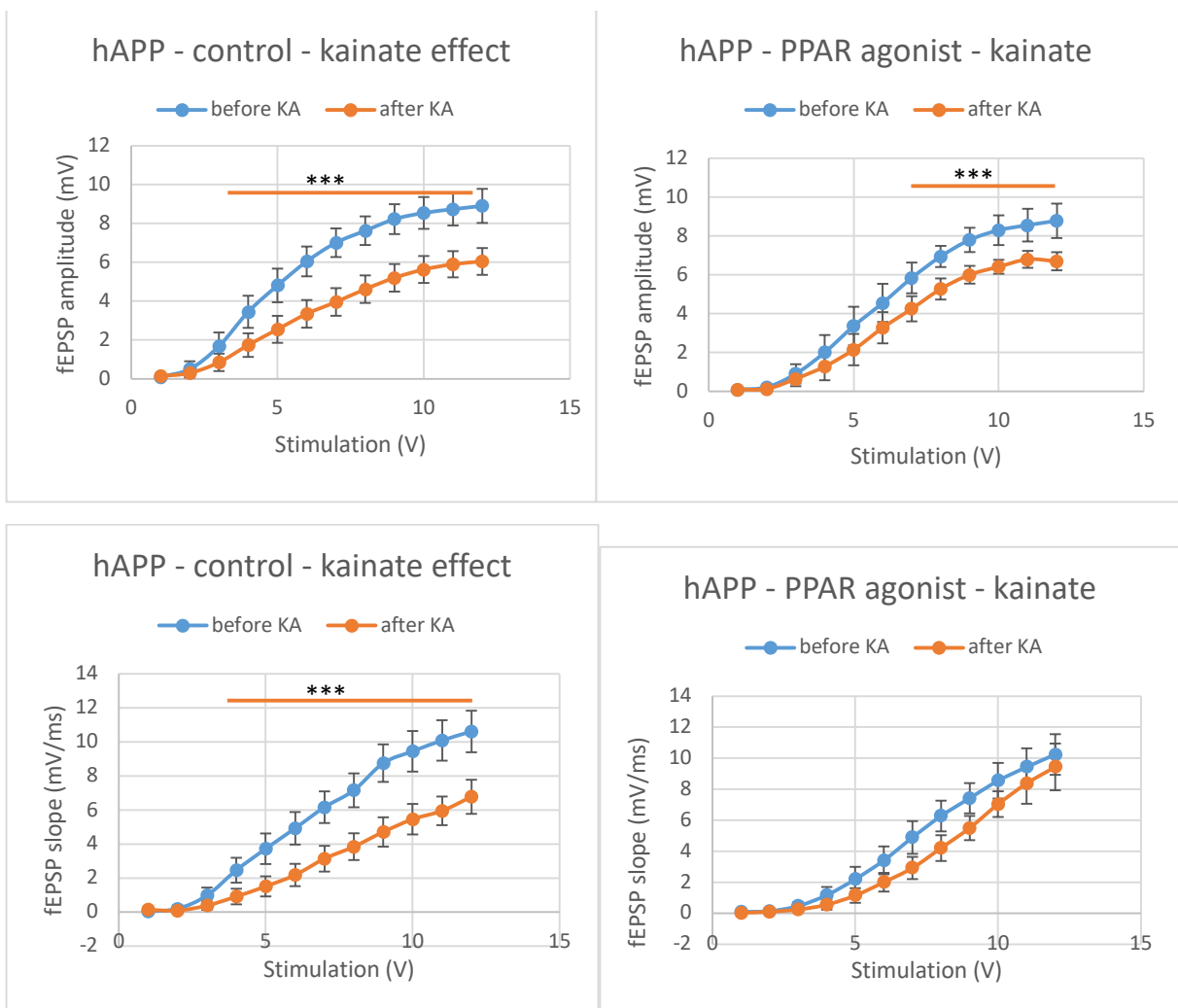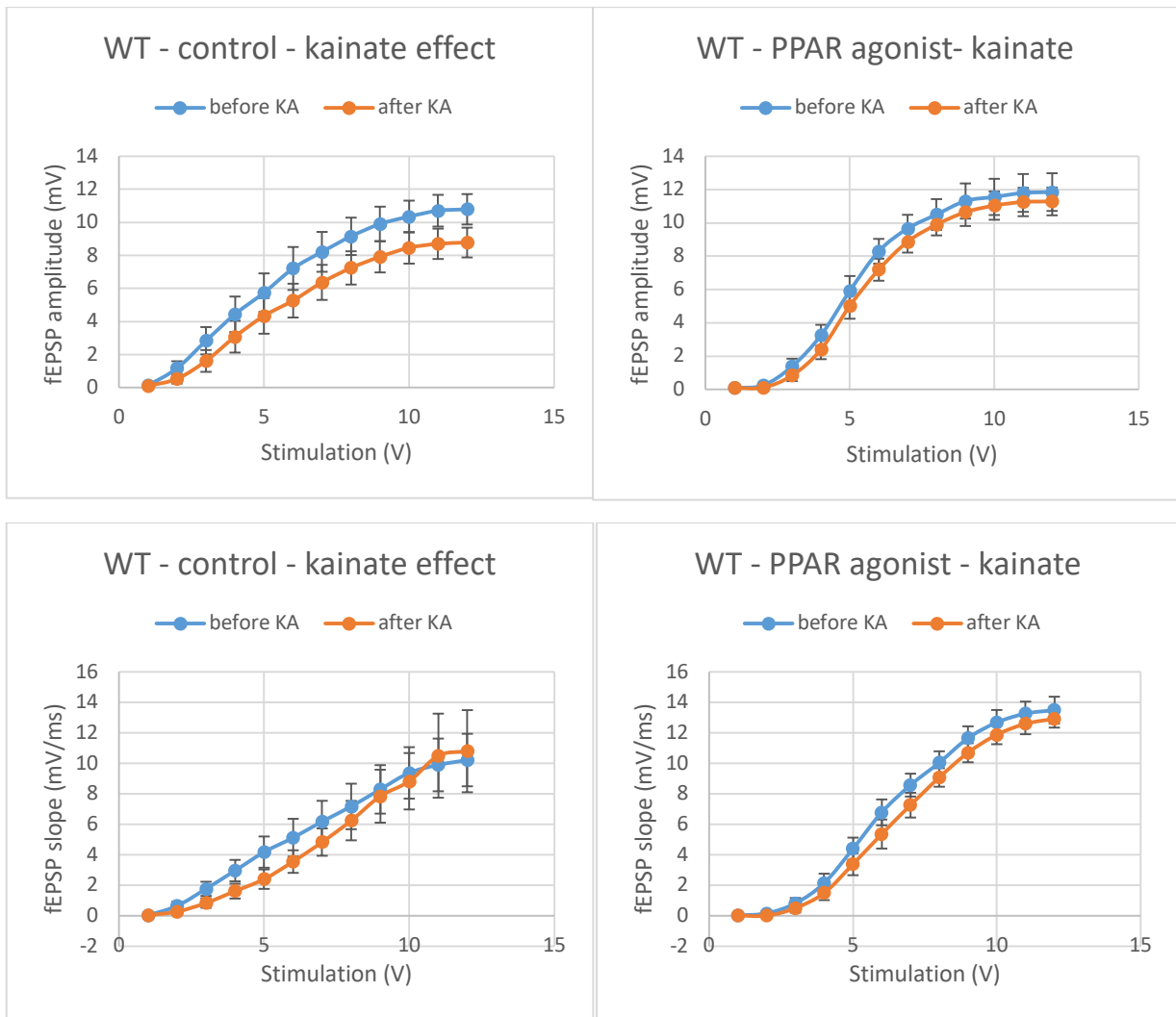
Figure 6: Effect of PPARα agonist WY14643 on the toxic effect of kainate application on hippocampal slices of hAPP mice and WT mice. Input/output curves obtained from the stimulation of Schaeffer Collaterals with incremental intensity. Amplitudes and slopes are presented. Kainate reduced significantly the amplitude and the slope of the fEPSP in hAPP mice (paired t-test, p<0.001) and this effect was significantly reduced by PPARα agonist.

5. References

1. Pearson, R.C., Esiri, M.M., Hiorns, R.W., Wilcock, G.K. & Powell, T.P. Anatomical correlates of the distribution of the pathological changes in the neocortex in Alzheimer disease. *Proc. Natl. Acad. Sci. U. S. A* **82**, 4531-4534 (1985).
2. Uhlhaas, P.J. & Singer, W. Neural synchrony in brain disorders: relevance for cognitive dysfunctions and pathophysiology. *Neuron* **52**, 155-68 (2006).
3. Delbeuck, X., Van der Linden, M. & Collette, F. Alzheimer's disease as a disconnection syndrome? *Neuropsychol Rev* **13**, 79-92 (2003).
4. Martin, L.J., Pardo, C.A., Cork, L.C. & Price, D.L. Synaptic pathology and glial responses to neuronal injury precede the formation of senile plaques and amyloid deposits in the aging cerebral cortex. *Am. J. Pathol* **145**, 1358-1381 (1994).
5. Ponomareva, N.V., Korovaitseva, G.I. & Rogaev, E.I. EEG alterations in non-demented individuals related to apolipoprotein E genotype and to risk of Alzheimer disease. *Neurobiol. Aging* **29**, 819-827 (2008).
6. Sasaguri, H. *et al.* APP mouse models for Alzheimer's disease preclinical studies. *EMBO J* **36**, 2473-2487 (2017).
7. Lustig, C. *et al.* Functional deactivations: change with age and dementia of the Alzheimer type. *Proc. Natl. Acad. Sci. U. S. A* **100**, 14504-14509 (2003).
8. Sperling, R.A. *et al.* Amyloid deposition is associated with impaired default network function in older persons without dementia. *Neuron* **63**, 178-188 (2009).
9. Babiloni, C. *et al.* Brain neural synchronization and functional coupling in Alzheimer's disease as revealed by resting state EEG rhythms. *Int J Psychophysiol* **103**, 88-102 (2016).
10. Bokde, A.L., Ewers, M. & Hampel, H. Assessing neuronal networks: understanding Alzheimer's disease. *Prog Neurobiol* **89**, 125-33 (2009).
11. Santos, S.F. *et al.* Expression of human amyloid precursor protein in rat cortical neurons inhibits calcium oscillations. *J Neurosci* **29**, 4708-18 (2009).
12. Octave, J.N., Pierrot, N., Ferao, S.S., Nalivaeva, N.N. & Turner, A.J. From synaptic spines to nuclear signaling: nuclear and synaptic actions of the amyloid precursor protein. *J. Neurochem* **126**, 183-190 (2013).
13. Doshina, A. *et al.* Cortical cells reveal APP as a new player in the regulation of GABAergic neurotransmission. *Sci Rep* **7**, 370 (2017).
14. Di Battista, A.M., Heinsinger, N.M. & Rebeck, G.W. Alzheimer's Disease Genetic Risk Factor APOE-epsilon4 Also Affects Normal Brain Function. *Curr Alzheimer Res* **13**, 1200-1207 (2016).
15. Pierrot, N. *et al.* Amyloid precursor protein controls cholesterol turnover needed for neuronal activity. *EMBO Mol. Med* **5**, 608-625 (2013).
16. Shimano, H. *et al.* Isoform 1c of sterol regulatory element binding protein is less active than isoform 1a in livers of transgenic mice and in cultured cells. *J. Clin. Invest* **99**, 846-854 (1997).
17. Horton, J.D., Goldstein, J.L. & Brown, M.S. SREBPs: activators of the complete program of cholesterol and fatty acid synthesis in the liver. *J Clin Invest* **109**, 1125-31 (2002).
18. Chang, C.Y., Ke, D.S. & Chen, J.Y. Essential fatty acids and human brain. *Acta Neurol Taiwan* **18**, 231-41 (2009).
19. Luchtman, D.W. & Song, C. Cognitive enhancement by omega-3 fatty acids from child-hood to old age: findings from animal and clinical studies. *Neuropharmacology* **64**, 550-65 (2013).
20. Bazinet, R.P. & Laye, S. Polyunsaturated fatty acids and their metabolites in brain function and disease. *Nat. Rev. Neurosci* **15**, 771-785 (2014).
21. Desvergne, B. RXR: from partnership to leadership in metabolic regulations. *Vitam Horm* **75**, 1-32 (2007).
22. Evans, R.M. & Mangelsdorf, D.J. Nuclear Receptors, RXR, and the Big Bang. *Cell* **157**, 255-266 (2014).
23. Michalik, L. *et al.* International Union of Pharmacology. LXI. Peroxisome proliferator-activated receptors. *Pharmacol. Rev* **58**, 726-741 (2006).
24. Zolezzi, J.M. *et al.* PPARs in the central nervous system: roles in neurodegeneration and neuroinflammation. *Biol. Rev. Camb. Philos. Soc* **92**, 2046-2069 (2017).
25. Moutinho, M. & Landreth, G.E. Therapeutic potential of nuclear receptor agonists in Alzheimer's disease. *J. Lipid Res* **58**, 1937-1949 (2017).
26. Saez-Orellana, F., Octave, J.N. & Pierrot, N. Alzheimer's Disease, a Lipid Story: Involvement of Peroxisome Proliferator-Activated Receptor alpha. *Cells* **9**(2020).
27. D'Orio, B., Fracassi, A., Ceru, M.P. & Moreno, S. Targeting PPARalpha in Alzheimer's Disease. *Curr Alzheimer Res* **15**, 345-354 (2018).
28. Pierrot, N. *et al.* Sex-regulated gene dosage effect of PPARalpha on synaptic plasticity. *Life Sci Alliance* **2**(2019).
29. Rice, H.C. *et al.* Secreted amyloid-beta precursor protein functions as a GABABR1a ligand to modulate synaptic transmission. *Science* **363**(2019).
30. Mucke, L. *et al.* High-level neuronal expression of abeta 1-42 in wild-type human amyloid protein precursor transgenic mice: synaptotoxicity without plaque formation. *J. Neurosci* **20**, 4050-4058 (2000).

31. Johnson, E.C.B. *et al.* Behavioral and neural network abnormalities in human APP transgenic mice resemble those of App knock-in mice and are modulated by familial Alzheimer's disease mutations but not by inhibition of BACE1. *Mol Neurodegener* **15**, 53 (2020).
32. Koch, M. *et al.* Palmitoylethanolamide protects dentate gyrus granule cells via peroxisome proliferator-activated receptor-alpha. *Neurotox Res* **19**, 330-40 (2011).

Progress report of the interuniversity research project of

Prof. dr. Sebastiaan Engelborghs (VUB)
Prof. dr. Chris Baeken (UGent)

Prof. dr. Sebastiaan Engelborghs
Vrije Universiteit Brussel (VUB)
Center for Neurosciences (C4N)
Laarbeeklaan 103, 1090 Brussel

Prof. dr. Chris Baeken
Universiteit Gent
Department of Psychiatry & Neuropsychology
C. Heymanslaan 10, 9000 Gent

Unraveling the link between depression and dementia to improve diagnostic and treatment options

1.   Publications 2022

1. **De Witte, S., De Smet, S., Pulópulos Tripiana, M., & Baeken, C. (2022). Double the dose, double the impact? Effects of iTBS on salivary cortisol in stressed healthy volunteers. COMPREHENSIVE PSYCHONEUROENDOCRINOLOGY, 10**. https://doi.org/10.1016/j.cpnec.2022.100127

Abstract: There is a growing interest in applying double-dose repetitive transcranial Magnetic Stimulation (rTMS) as a therapeutic tool for stress-related psychiatric disorders. Such stimulation protocols may shorten the treatment duration and may result in faster symptom improvement. Currently, theta-burst stimulation (TBS) protocols have gained attention because of their significantly reduced treatment duration, compared to conventional rTMS. However, the effect of one or twice daily rTMS sessions remains unclear in relation to stress. Using a two-period cross-over design, we examined the impact of double-dosed intermittent (TBS) over the left dorsolateral prefrontal cortex on stress responses (salivary cortisol) in thirty-eight healthy participants after being stressed by a validated psychosocial stress task: the Trier Social Stress Test. After the first active iTBS session, as contrasted to sham, no differential effects on salivary output were observed. However, after the second active session, there was a significantly smaller decrease of salivary cortisol concentrations in the active iTBS condition compared to sham. Our results suggest that double-dosed iTBS after being stressed might differently affect stress recovery compared to a single session of iTBS.

2. **Wiels W, Oomens JE, Engelborghs S, Baeken C, Verhey FRJ, Visser PJ, Jansen WJ and the Amyloid Biomarker Study Group. The association between depressive symptoms and amyloid positivity. Abstract submitted to the Alzheimer's Association International Conference in Amsterdam, July 2023.**
    This paper is in a final draft stage.

Background: Amyloid deposition and hippocampal atrophy have been linked to late-life affective disorders, raising concerns for Alzheimer's Disease (AD). However, biomarker and autopsy studies have been inconclusive. It remains unclear if and in what way depressive symptoms imply an increased risk of amyloid positivity. Method: Using data from 49 centers in the Amyloid Biomarker Study, we investigated the association between depressive symptoms and amyloid positivity. We included participants with normal cognition (NC) (n=9776) and MCI (n=2995). Amyloid positivity was defined using standardized CSF (n=5926) and PET (n=6845) measures. Depressive symptoms were obtained through medical history (12%) and various rating scales (88%). Symptoms on rating scales were classified as (1) present/absent using established cut-off values, (2) severity using center-based trichotomisation. We examined associations between depressive symptoms and amyloid positivity using generalized estimating equations and evaluated potential moderation by age and APOE-e4 status. *Result:* Mean age was 69 years and 33.8% were amyloid positive. In NC, no association between the presence or severity of depressive symptoms and amyloid positivity was observed, nor was there when including APOE-e4, sex or education. In MCI, persons with depressive symptoms were ~10% less often amyloid positive than those without depressive symptoms (p=0.001), this was even more pronounced in persons with moderately severe symptoms (p=0.01). We identified an interaction between depressive symptom severity and APOE-e4 status (p=0.034). In APOE-e4 noncarriers with MCI, persons with moderate depressive symptoms were 20% less often amyloid positive than those with no or mild depressive symptoms. In APOE-e4 carriers with MCI, depressive symptom severity was not associated with amyloid positivity. Conclusion: In persons with normal cognition, depressive symptoms are not associated with amyloid positivity.

In MCI patients, however, those with depressive symptoms were ~10% less often amyloid positive. This association increased in persons with moderately severe symptoms and appeared to pertain to APOE-e4 noncarriers. These data suggest that the presence of depressive symptoms in MCI patients is no reliable indicator of amyloid positivity. This may have diagnostic implications for this group.

2. Congresses

Dieter Zeeuws:
- Attended the 5th European Conference of Brain Stimulation in Psychiatry in Zagreb, Croatia (3-4 June 2022). Poster presentation: accelerated dtms in the elderly depressed: preliminary insights on safety, tolerability and applicability. Dieter Zeeuws, Wietse Wiels, Sebastiaan Engelborghs & Chris Baeken.
- Attended the 30th European Congress of Psychiatry (4-7 June 2022). Presented study design. Suicidality during neuromodulation in the elderly depressed: study design. Van Daele, Zeeuws & Baeken.
- Attended conference "communicatie tussen zorgverleners en familieleden van ouderen" (12 may 2022)
- Attended Vormingsavond VUB academiejaar 2022-2023 "Moeilijk te behandelen depressie" (27 october 2022).
- Attended Masterclass by IFCN (5 November 2022): What, Where and How Does TMS Stimulate? Why Is It Relevant to Me?
- Attended lecture on "DBS for Alzheimer's disease": current status (12 january 2022)

Sara De Witte:
- Attended the 5th European Conference of Brain Stimulation in Psychiatry in Zagreb, Croatia (3-4 June 2022). Free communications: Double-dosed non-invasive brain stimulation: is more better? Sara De Witte, Stefanie De Smet, Matias M. Pulopulos, Chris Baeken
- Attended lecture on "DBS for Alzheimer's disease": current status (12 january 2022)

3. Data collection

WP1: Development of a dementia risk score amongst depressed elderly
The data collection and analysis are completed. A research paper is prepared and is scheduled to be published in 2023.

Given the significant delay with patient recruitment (WP2 and WP3) due to the COVID pandemic, there was a budget-neutral prolongation of the project with two years (end date: 31 DEC 2024 instead of 31 DEC 2022).

WP2: Validate the dementia risk score in a prospective longitudinal clinical study
It aims to examine the prognostic relevance of depressive symptoms and amyloid status in the elderly, through a prospective evaluation of cognitively healthy controls, depressed patients, and cognitively impaired patients (all groups >65 years of age). All groups will receive serial clinical, imaging, neuropsychological as well as affective/behavioural, and neurochemical assessment. Furthermore, the added value of plasma-based amyloid tests will be evaluated. Due to the covid-19 pandemic, several aspects of this study were delayed. Recruitment and testing started are still ongoing.

WP3: Evaluate the predictive and clinical effects of non-invasive brain stimulation in the elderly depressed with and without prodromal AD

It will evaluate non-invasive brain stimulation techniques on the elderly depressed, and the impact of this treatment on imaging parameters. Due to the covid-19 pandemic, several aspects of this study were delayed. Recruitment and testing have started in 2022 and are still ongoing.

4.   Budget 2022

From January 2022, Sara De Witte, Ma Psychology and PhD student at UGent, joined the project team as study coordinator. She was paid through the GSKE project budget of UGent.

No expenses were made from the VUB budget.

5.   Future directions for 2022

WP1: Data collection and analyzing data finished. Writing of a research paper is scheduled in 2023.
WP2: Continue recruitment and data collection.
WP3: Continue recruitment and data collection.

Final report of the interuniversity research project of

Prof. dr. Vincent Van Rompaey (UAntwerpen)
Prof. dr. Peter Ponsaerts (UAntwerpen)
Prof. dr. Guy Van Camp (UAntwerpen)
Prof. Rik Gijsbers (KU Leuven)

Prof. dr. Vincent Van Rompaey (UAntwerpen)
Experimental laboratory of Translational Neurosciences Dept. of Translational Neurosciences
University of Antwerp
Universiteitsplein 1
2610 Antwerp, Belgium
vincent.vanrompaey@uantwerpen.be

Prof. dr. Peter Ponsaerts (UAntwerpen)
Laboratory of Experimental Hematology Vaccine and Infectious Disease Institute University of
Antwerp
Universiteitsplein 1
2610 Antwerp, Belgium
Peter.Ponsaerts@uantwerpen.be

Prof. dr. Guy Van Camp (UAntwerpen)
Human Molecular Genetics laboratory
Center of Medical Genetics, University of Antwerp
Universiteitsplein 1
2610 Antwerp, Belgium
guy.vancamp@uantwerpen.be

Prof. Rik Gijsbers (KU Leuven)
Laboratory of Viral Vector Technology and Gene Therapy Department of Pharmaceutical and
Pharmacological Sciences Faculty of Medicine, KU Leuven
RK-Herestraat 49, box 1023
3000 Leuven, Belgium
Rik.Gijsbers@kuleuven.be

Dr. Erwin Van Wijk
Department of Otorhinolaryngology
Radboud University Nijmegen Medical Center Geert Grooteplein 10
6525 GA Nijmegen, The Netherlands
Erwin.vanWyk@radboudumc.nl

Dr. Erik De Vrieze
Departments of Otorhinolaryngology and Human Genetics Radboud University Medical Centre
Geert Grooteplein Zuid 10
P.O. box 9101, 6500 HB
Nijmegen, The Netherlands

Development of allele-specific CRISPR-nuclease gene therapy for late-onset sensorineural hearing impairment in a new humanized DFNA9 mouse model

Work-package 1: the DFNA9 $^{hWT/mWT}$ mice arrived at our animal facility in March 2021. These mice were backcrossed to the C57BL/6 (Cdh23$^{753A>G}$) mice resulting in the generation of DFNA9$^{hWT/hWT}$ C57BL/6 (Cdh23$^{753A>G}$) mice where the mutation in the Cdh23 gene, causing early hearing loss in C57BL/6 mice, is corrected. In October 2021, the DFNA9$^{hP51S/mWT}$ mice arrived at our facility. These mice were bred with our already established DFNA9$^{hWT/hWT}$ C57BL/6 (Cdh23$^{753A>G}$) mice resulting in the generation of DFNA9$^{hP51S/ hP51S}$ C57BL/6 (Cdh23$^{753A>G}$) and DFNA9$^{hWT/hP51S}$ C57BL/6 (Cdh23$^{753A>G}$) mice. We are currently following up all these DNFA9 mouse strains for hearing and vestibular function up to 2 years of age every 3 months. When the phenotyping of the DFNA9 mouse strains is finished, a manuscript will be published and we will acknowledge Q.E.M.F. funding. As this is a long-term experiment the manuscript is expected in early 2025.

We also developed a highly innovative device that is able to measure the Vestibular Ocular Reflex (VOR) which is an objective tool to assess vestibular function in mice. Currently, this device is being optimized and calibrated. We will write a manuscript regarding this new device where we will also acknowledge Q.E.M.F. (manuscript expected in 2023).

Work-package 2: We already injected an AAV2/7 vector, harbouring the luciferase reporter protein next to eGFP, in the inner ear of C57BL/6 (Cdh23$^{753A>G}$) mice by using the posterior semi-circular canal (PSC) approach. Injection through the PSC, using the Nanoliter 2020 device, did not induce sensorineural hearing loss (Figure 1A). Bioluminescence imaging (BLI) revealed a bright signal in the region of the left ear 25 days post-injection (25 DPI) (Figure 1B).
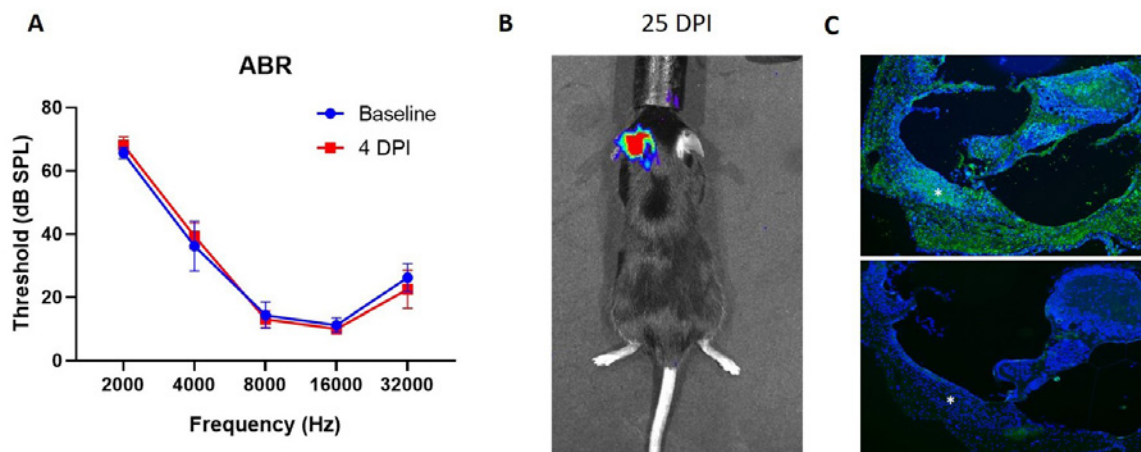
Figure 1. (A) Auditory Brainstem Response (ABR) measurements before and 4 days post Injection (DPI) with AAV2/7. (B) Bioluminescence imaging performed at 25 DPI. (C) eGFP expression in the inner ear at 7 DPI. * indicates the spiral ligament

Currently, we are performing more experiments to investigate inner ear inflammation, and short – and long-term safety of the injection of viral (and non-viral) vectors in the inner ear. Furthermore, we are intensively investigating if these vectors are able to effectively transduce the spiral ligament fibrocytes which are our target region as this is the region of Coch expression. Once we finish the experiment and withhold a vector that is safe and able to efficiently transduce the spiral ligament fibrocytes we will prepare a manuscript mentioning Q.E.M.F. funding (expected end of 2023).

Work-package 3: The strategy to specifically disrupt the mutant *COCH* allele is designed in collaboration with the H&G lab at the Radboud University of Nijmegen. They already designed allele specific ASOs for the targeting of mutant *COCH* (p.P51S allele) demonstrating that the genomic region of the c.151C>T mutation is amenable allele-specific targeting using a base-paring approach. We will proceed with the development of a therapeutic strategy that can be delivered as a single dose to treat DFNA9 by the use of CRISPR/Cas9 to disrupt the mutant COCH allele. To obtain the highest possible specificity for the c.151C>T mutant *COCH* allele, we will employ spCas9-EQR which has a PAM-site preference of "NGAG". The c.151C>T change creates this PAM site on the complementary strand of the mutant *COCH* gene and allows for allele-specific nuclease activity. Upon cleavage of the mutant *COCH* allele, the non-homologous end joining (NHEJ) repair pathway will change the gain-of-function allele into a null allele, effectively creating the situation of heterozygous carriers of *COCH* loss-of-function mutations, which we know exhibit normal inner ear function in human and mice. The PhD student working on this project obtained a grant to visit the H&G lab in Nijmegen in March 2022. During this research stay, she performed several experiments where different gRNAs were tested to assess specific targeting of the mutant Coch allele *in vitro*. Two of these gRNA's demonstrated to effectively disrupt the mutant *Coch* allele. Further *in vitro* experiments to select an optimal gRNA/CRISPR nuclease combination are currently ongoing.

In addition, we will establish cell cultures of embryonic fibroblasts derived from our DFNA9 mouse model. These cell cultures can then be used to assess *in vitro* genome editing efficiency of different gRNA/spCas9-EQR combinations.

Work-package 4: injections with a vector encoding the chosen CRISPR nuclease and suitable gRNA sequences (WP3) will be performed in our new DFNA9$^{hP51S/hWT}$ mouse model. This experiment is expected to start in 2024 when WP2 and WP3 are completed. In WP4 we will look at the genome editing efficiency of the different gRNA's in DFNA9$^{hP51S/hWT}$ C57BL/6 (Cdh23$^{753A>G}$) mice.

Work-package 5: when WP4 is completed we can finally evaluate if the gRNA/CRISPR nuclease can prevent hearing and vestibular loss in our new DFNA9$^{hP51S/hWT}$ mouse model. We expected to inject our DFNA9$^{hP51S/hWT}$ mouse model with the established CRISPR-based gene therapy in the course of 2025.

As this is a long-term project, we didn't publish a related manuscript yet. However, we are planning to publish several manuscripts linked to this project in the future where we will acknowledge Q.E.M.F. funding:
1. Manuscript regarding the generation and phenotyping of the DFNA9 mouse model which is currently ongoing. The manuscript is expected to be published in 2025 (WP1).
2. Manuscript regarding the development of a new device to measure VOR function in mice. The manuscript is expected to be published in 2023 (WP1).
3. Manuscript regarding the selection of an optimal vector that can transduce the spiral ligament fibrocytes in a safe and efficient way. The manuscript is expected to be published at the beginning of 2024 (WP2).
4. Furthermore, manuscripts regarding genome editing efficiency *in vitro* and *in vivo* (WP3 + WP4) and the therapeutic effect of our established gene therapy (WP5) will be prepared in the coming years.

We also want to emphasize that intermediate results regarding this project were already presented at different conferences where Q.E.M.F. funding was mentioned. Below you can find a list of conferences where we acknowledged Q.E.M.F during an oral presentation:
- ARO Midwinter meeting 2021 (February 20-24, online)
- EAONO 2021 (March 6-10, online).
- Radboud Research Round 2021 (September 23, online)
- B-audio conference 2022 (November 25-26, Genk, Belgium)
- Inner ear Biology 2022 (September 10-13, Trieste, Italy)

Also, an abstract regarding the phenotyping of the DFNA9 mouse model where Q.E.M.F funding is acknowledged is accepted for a poster presentation at the ARO Midwinter meeting 2023 (February 11-15, Orlando, Florida, USA).

Final report of the interuniversity research project of

Prof. dr. An Goris (KU Leuven)
Prof. Nathalie Cools (UAntwerpen)

Prof. dr. An Goris (KU Leuven)
Department of Neurosciences
Laboratory for Neuroimmunology
T +32 16 33 07 72
an.goris@kuleuven.be

Prof. Nathalie Cools (UAntwerpen)
Laboratory for Experimental Hematology
University of Antwerp
nathalie.cools@uza.be

Table of contents

Deep sequencing of myelin-reactive T-cells to elucidate new disease mechanisms and identify correlates for treatment responsiveness in multiple sclerosis

1.   Summary and current status of research program

Multiple sclerosis (MS) is one of the most common neurological disorders in young adults, affecting around 13,500 people in Belgium and 2.8 million worldwide. The disease can lead to important physical as well as cognitive disability at a time that is crucial in the personal and professional development of patients. MS is characterized by three hallmarks: inflammation, demyelination and neuronal loss[1]. The exact cause of MS still remains to be elucidated but the past few years have seen exciting progress in the field. Over the last decade, we have – in an international collaborative context as part of the International Multiple Sclerosis Genetics Consortium (IMSGC) – identified >230 genetic risk factors for MS. These include several risk as well as protective variants in the Human Leukocyte Antigen (HLA) region[2], which in combination with the T- and B-cell receptor likely determine the target of the autoimmune reaction[3], and 200 variants throughout the genome, enriched for immunological function and implicating the interplay between B-cells, T-cells, and innate immune cells[4-8]. Hence, the complex interactions between the identified genetic and environmental factors affect the predominantly immune-mediated underlying mechanisms of the disease.

With previous GSKE support (A. Goris, 2017-2019 and Prize Viscountess Valine de Spoelberch), we focused on the role of B-cells and demonstrated an imbalance between pathogenic and immunoregulatory B-cells in MS that is amenable to treatment[9-12]. Besides, it is currently generally accepted that autoimmunity against antigens expressed in the central nervous system (CNS) is mediated by T-cells. Indeed, CD4^{+} T-cells, in particular Th1 and Th17 cells, directed towards various myelin-derived antigens, including myelin basic protein (MBP), proteolipid protein (PLP), myelin oligodendrocyte glycoprotein (MOG) and αB-crystallin have been identified in patients with MS[13-16], and are shown to migrate between blood and CNS[17,18]. Nonetheless, these autoreactive T-cells that are thought to be the culprit in MS form a very small subset in the peripheral blood which has hampered their investigation.

Thanks to the previous and current support of GSKE, we were able to implement state-of-the-art genetic methods that allow to analyze DNA and RNA at the level of single B- or T-cells (single-cell sequencing). This made it now timely to turn our attention to a detailed understanding of their characteristics that make them pathogenic in MS. The combined expertise of our interuniversity team in immunology and characterization of autoreactive T-cells (N. Cools, U Antwerp) on the one hand and in genetics and single-cell sequencing (A. Goris, KU Leuven) on the other made it feasible, timely and innovative to investigate the pathogenic characteristics of autoreactive T-cells in MS. For this, the following three aims were set forth:
1. What is the TCR repertoire of autoreactive T-cells in MS?
2. What are the transcriptional characteristics of autoreactive T-cells?
3. Can the autoreactive T-cell clonotype repertoire be used as a correlate for therapy responsiveness?

Achievements

2. Achievement 1. TCR repertoire of autoreactive T-cells in MS

2.1. Summary

T-cells recognize complexes of specific antigenic peptides and autologous HLA molecules through their TCR. In fact, the TCR sequence functions as a unique fingerprint for each T-cell. Hence, analysis of T-cell clonal expansion can allow the identification of T-cells that are assumed to be involved in the disease process. Since autoreactive T-cells may occur naturally in less than 1 in 300 T-cells[19], clonal expansion by activation and proliferation of antigen-specific T-cells can be provoked by *ex vivo* recognition of an antigen.

2.2. Methodology for the identification of relevant TCR

TCR repertoire sequencing data contain many sequences, originating from naive T-cells, that are unrelated to the underlying immunological condition. Consequently, these sequences do not carry any useful information regarding the condition under investigation. As a primary method for reducing the enormous search space (often exceeding millions of unique TCRs in one dataset), it is paramount to determine the 'functional' T- cell repertoire. In the T-cell repertoire, many different TCRs will respond to the exact same epitope. We can reduce this redundancy by modeling the repertoire as a network in which the nodes represent the TCRs, and edges represent the edit distance (i.e. number of amino acid substitutions, insertions or deletions) between two TCRs. Next, we can determine epitope-specific clusters, based on a similarity criterion linking a group of TCR sequences together. These clusters will subsequently be considered a non-redundant TCR. Next, other filtering strategies will be applied that focus on features derived from the mechanism of V(D)J recombination. One can assume that TCRs that are significantly more common than expected, are under the selective pressure of an immunological driver (e.g. autoantigen in MS). Different models have been developed to estimate the probability for a TCR to be generated. These models are based on the recombination mechanism of the V, D and J gene segments in developing lymphocytes, resulting in a functional TCRβ chain. The Optimized Likelihood estimate of immunoGlobulin Amino-acid sequences (OLGA) algorithm[20] computes generation probabilities (Pgen) from amino acid sequences, whereas the Inference and Generation of Repertoires (IGoR) algorithm[21] infers Pgen from nucleotide sequences. We can hypothesize that CDR3 sequences that are more abundant than determined by their Pgen are under the selective pressure of an immunological driver, either in the past or present. Consequently, T-cells carrying these sequences hold valuable information and can be analyzed in a specific disease context. The main two parameters that will be tested are (i) frequency of the TCR across all samples and (ii) the Pgen of the TCR (Figure 1). Different cut-offs of these parameters will be evaluated in the context of a classification task where we use the area under the receiver operating characteristic curve (AUROC) as a measure for the classification performance. Different machine learning frameworks can be applied to tackle this classification problem. Different candidate frameworks for which in-house experience is available include:

- Ensemble learning methods: These may include Random Forests (RF) or Gradient Tree Boosting (GTB) algorithms. These ensemble techniques provide flexible, yet very powerful methods to solve a classification task.
- Artificial Neural Networks (ANN): One of the most powerful and diversified machine learning methods to achieve high accuracy in a classification task.
- Conditional Random Fields (CRF): This machine learning method has been derived from Hidden Markov Models and has been used in our group for a number of pattern-recognition applications[22-24].

Figure 1 illustrates preliminary results obtained from this procedure on a subset of a well-known TCR repertoire data set by Emerson and colleagues[25].
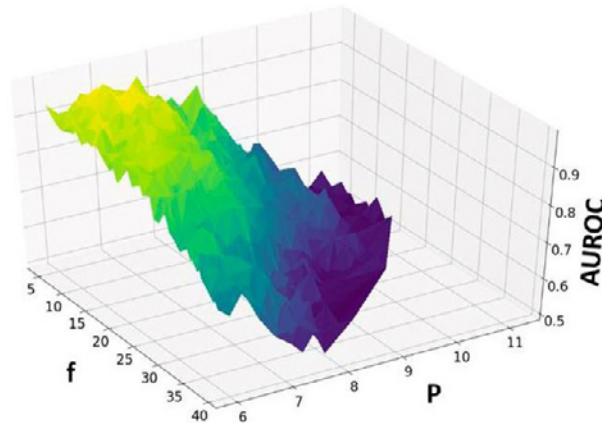

Figure 1. TCR prioritization. Preliminary results of parameter testing in the context of prioritizing relevant TCRs from larger repertoires. A random forest (RF) classifier is trained within a range of cut-offs for f (%) and
P. The data originates from a study of CMV in a large cohort. The procedure was performed on a subset to identify highly predictive TCRs for CMV serostatus. Frequency, f; probability of generation, P; area under the receiver operating characteristic, AUROC.

This analysis can be performed on large rep-seq datasets (such as the one by Emerson et al[25]). The main data sources consist of the immuneACCESS database, NCBI's sequencing read archive (SRA), iReceptor Public Archive and the Pan Immune Repertoire Database (PIRD).

Characterization of MS epitope reacting TCR: One of the main objectives of this project is the characterization of T-cells that react to important MS-derived epitopes. Several of these target epitopes have been described for MS[26-28], but it is still unclear which TCCs are activated by these peptides. To address this question, N. Cools has assembled a unique protocol for enrichment of autoreactive T-cells using a broad antigen panel, and this protocol has been refined in a collaboration between N. Cools and A. Goris so that both sites apply a similar methodology according to (mostly) shared protocols for this project. PBMCs are stimulated *in vitro* in the presence of a selected panel of myelin oligodendrocyte glycoprotein (MOG)-, myelin basic protein (MBP)-, and proteolipid protein (PLP)- derived synthetic peptides that have previously been demonstrated as immunodominant[13-16] and to act in part independently of HLA-DR[14,29,30]. Myelin-reactive T-cells are observed using flow cytometric dual detection of CD71 and CD98 (CD4+ and CD8+) T-cell activation markers following one-week stimulation of T-cells with a pool of myelin-derived peptides (Figure 2). This methodology results in an average of 0.2% of CD4+ and CD8+ T cells in MS patients being characterized as autoreactive. After multiple and some time-consuming adjustments, the lab of N. Cools and A. Goris have established a consistent and reproducible protocol for the generation of myelin-derived T-cells. In addition, we have corroborated the relevance of our myelin peptide selection, which was previously demonstrated by others through a positive T-cell proliferative response to this peptide mix in 74% of RRMS patients compared to 30% of healthy controls[31].
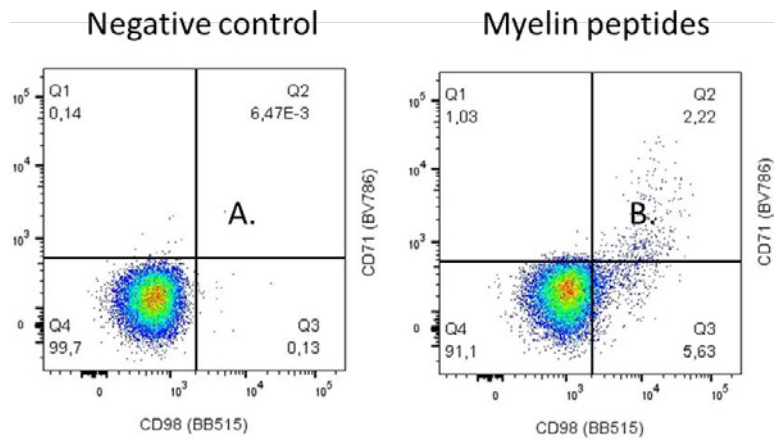
Figure 2. Representative bivariate pseudocolor plots of myelin-reactive CD71- and CD98-positive CD4$^+$ T-cells in a patient with MS. (A) indicates dual-activated CD4$^+$ T- cells from unstimulated cells in quadrant Q2, while (B) depicts dual-activated CD4$^+$ T-cells after myelin-derived peptide stimulation in quadrant Q2.

We will use these sorted autoreactive CD4$^+$ and/or CD8$^+$ T-cells as input for the Chromium Single Cell V(D)J Solution on the 10x Genomics[32] platform available at KU Leuven. We will obtain full- length V(D)J sequences and paired α and β sequences to establish TCR repertoires of autoreactive T- cells on a cell-by-cell basis. For that purpose, we have now implemented the Chromium Single Cell V(D)J Solution on the 10x Genomics[32] platform available at KU Leuven and the bio-informatics pipelines necessary to identify clonal expansions based on identical or highly identical immune cell receptors.

Similarly, patient-derived myelin-specific CD4$^+$ T-cells are single-cell sorted using FACS, followed by an RT-PCR using 76 TCR-primers, by the Antwerp team. The products are used in a second and third PCR reaction, incorporating individual barcodes into each well. Libraries are purified and sequenced using the Illumina MiSeq platform, after which the resulting paired-end raw sequencing reads are assembled and deconvoluted using barcode identifiers at both ends of each sequence. The resulting sequences are then analyzed using the program MiXCR and the CDR3 nucleotide sequences are extracted and translated. First sequencing results were translated into the full functional sequence of a patient-derived MBP$_{85-99}$-specific and MOG$_{97-109}$-specific TCR and the development of their TCR- encoding constructs. Their expression was tested in two TCR-deficient T cell lines (2D3 and SKW-3) by means of TCR-encoding mRNA electroporation. Our preliminary data show a transgene MBP85- 99-TCR expression as high as 90% over the course of 4 days (Figure 3).
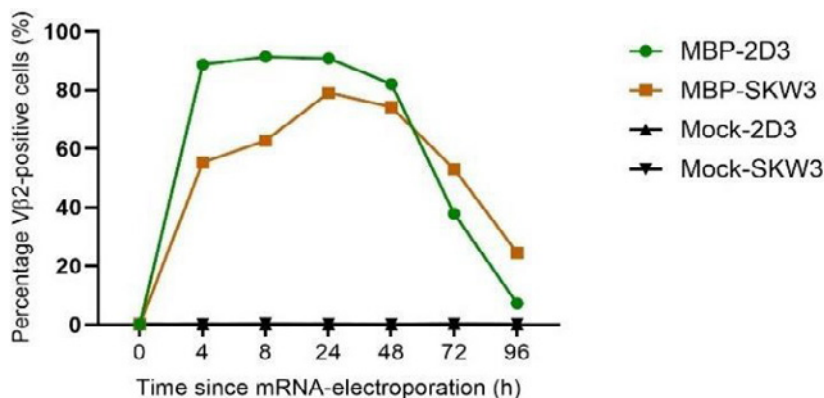

Figure 3. MBP85-99-TCR-encoding mRNA electroporation of TCR- deficient T cell lines. Transgene MBP85-99-TCRexpression is visualized using flow cytometry and a fluorochrome-labeled antibody to Vβ2, binding the variable domain of the newly introduced TCR. As a negative control, a MOCK condition is used, to which no mRNA is added.

Simultaneously, our bio-informatics team has continued the development of a highly performant clustering algorithm, termed ClusTCR, for the detection of groups of TCRs with high sequence similarity. This algorithm can be used to infer common patterns of epitope-reactivity and clonal convergence in TCR repertoires. In doing so, we were able to identify 691 cells with productive V-J spanning pairs recognizing myelin-derived epitopes (Figure 4A and B). In addition, we have manually curated a large, high-quality database of public TCR repertoires from MS patients (n=124), healthy controls (n=75) as well as other diseases related to or mimicking MS (n=33). This database combines the results from 9 independent TCR sequencing studies and constitutes a total of 822 samples. The data is currently being analyzed as part of a large meta-analysis, in which we aim to identify MS-associated TCR patterns through the clustering-based prioritization and annotation of TCRs using the ClusTCR framework described above.
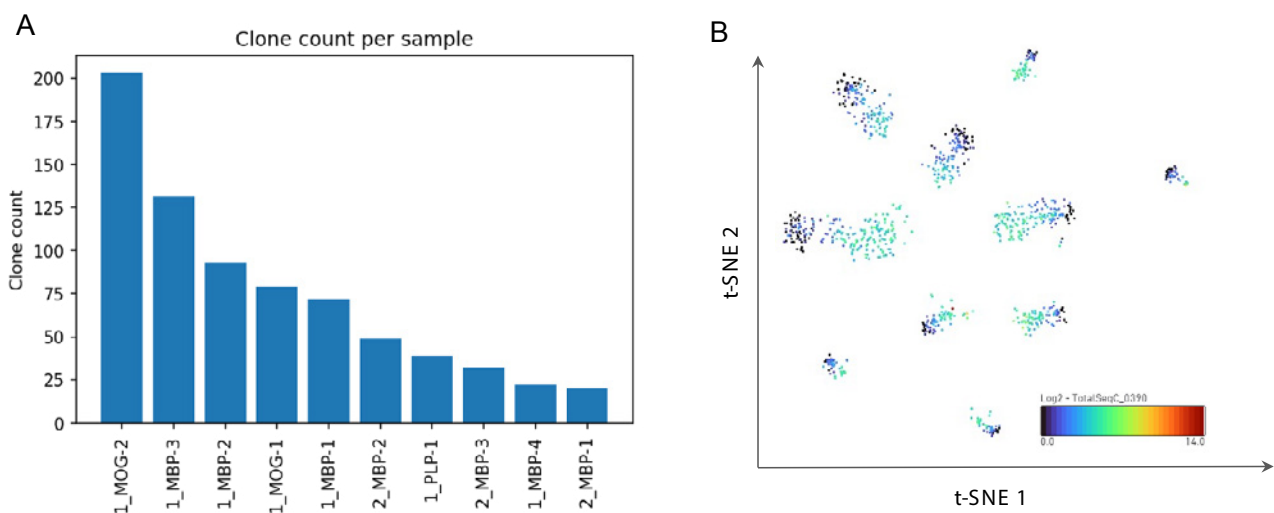

Figure 4. Identification of 691 cells with productive V-J spanning pairs recognizing myelin-derived epitopes. (A) Barplot indicating the number of full αβ-TCR clonotypes identified across different samples. Single-cell profiling was performed on activated T cells following stimulation with different myelin peptides (MBP-1, MBP-2, MBP-3, MBP-4, MOG-1, MOG-2, PLP-1) during a pilot experiment in two donors. (B) log2(CAb) of the TotalSeq™-C0390 anti-human CD127 antibody in ~1000 cells obtained after sorting of activated T cells following stimulation with different myelin peptides (MBP-1, MBP-2, MBP-3, MBP-4, MOG-1, MOG-2, PLP-1) during a pilot experiment in two donors. Low levels of TotalSeq™-C0390 barcodes indicate inadequately low concentrations of the antibody.

2.3.   Future plans

We will finalize our efforts on the integrated meta-analysis done on publicly available MS datasets, in which MS- associated TCRs will be identified. Five MS datasets are available in the immuneACCESS and SRA databases. All datasets originate from a different source, but all have been sequenced by the same provider (Adaptive Biotechnologies). All datasets will be combined into a uniform format. First, the methodology developed and described in 2.1 will be applied to prioritize MS-associated TCRs. In brief, this method focuses on the identification of non-redundant TCR sequences that appear more often than expected by chance.

In addition, we will investigate peripheral blood T-cells from recently diagnosed and untreated patients with MS according to the revised McDonald criteria[33] (N = 15). To this end, we will extend our single- cell sequencing pipelines from B-cell receptor to T-cell receptor repertoires and superimpose identified clonal T-cell expansions on the peripheral blood and cerebrospinal fluid (CSF) T-cell landscape in patients with MS (achievement 2). Access to patient samples is possible by already existing collaborations of both PIs with University Hospitals Leuven (Prof. B. Dubois) and Antwerp (Dr. B. Willekens), respectively.

3.   Achievement 2. Transcriptional characteristics of autoreactive T-cells.

3.1.   Summary

Autoreactive or myelin-reactive T-cells in achievement 1 undergo proliferation and activation as part of the enrichment, which may influence their transcriptome but not their TCR repertoire. We can, however, use the TCR "fingerprint" of autoreactive T-cells established in achievement 1 to superimpose these autoreactive clonal T-cells on the peripheral blood and CSF T-cell landscape in patients with MS. Based on the distribution of these autoreactive T-cells in the T-cell landscape, we can determine the transcriptional phenotype of these autoreactive T-cells in achievement 2.

3.2.   Current status

In a first proof-of-principle experiment, we sampled blood from one treatment-naive MS patient and isolated the peripheral blood mononuclear cells (PBMCs). One sample was used to stimulate these PBMCs *in vitro* using a pool of immunodominant myelin-derived peptides over a 7-day incubation period (as described in achievement 1.2). Next, T-cells that were activated upon myelin peptide stimulation were sorted using FACS (as described in achievement 1.2). Next, single-cell T-cell receptor sequencing (scTCR-seq) to delineate clonal expansions was performed on the isolated myelin-activated T cell population. In order to *in vivo* characterize the transcriptomic profile of these myelin-reactive clonal T-cell expansions, we combined scRNAseq and scTCRseq in another unstimulated PBMC sample from the same MS patient and retraced identical TCRs across the stimulated and unstimulated condition (i.e., TCRs from myelin-reactive T-cells in our autoreactivity assay are projected as a unique "fingerprint" to identify myelin-reactive T-cells in an unstimulated - "as it is" – sample). Via our custom bioinformatics pipeline, we revealed that myelin-reactive clonal T-cell expansions predominantly reside within (terminal) effector memory T cell clusters and are polarized towards a more cytotoxic phenotype, e.g., *GZMA*, *GZMB* and *CCL5* (figure 4). However, when we annotated these myelin-reactive TCRs based on publicly available databases such as VDJdb and McPAS-TCR, we noticed that some TCRs from myelin-reactive clonal T-cell expansions have indeed been described in the context of MS (in other studies) and some others have been associated with infectious agents (e.g., SARS-CoV-2, EBV and influenza type A). Whether these divergent annotations point in the direction of cross-reactivity between TCRs against viruses and myelin components or some non-specificity of our autoreactivity assay, remains a subject for further research (cfr. future plans).

3.3.   Future plans

Based on the above-mentioned results, we will implement tetramer technology to elucidate a potential mechanism of cross-reactivity and to ascertain the antigen specificity of the myelin-reactive clonal T-cell expansions. Afterwards, we will study these myelin-reactive clonal T-cell expansions in our cohort of MS patients with paired CSF-blood samples (N = 10) and non-inflammatory neurological controls (N = 10).
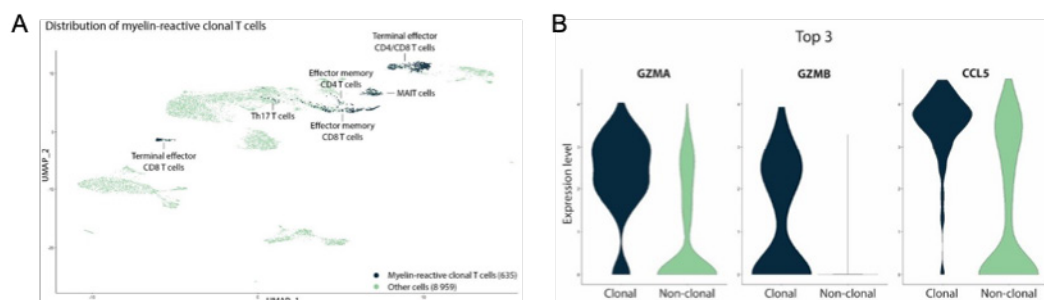

Figure 4. Myelin-reactive clonal T-cell expansions in a never-treated MS patient (A) and the top 3 differentially expressed genes (DEGs) between clonal and non-clonal T cells across clusters (B).

4. Achievement 3. The autoreactive T-cell clonotype repertoire as a correlate for therapy responsiveness.

4.1. Summary

Whereas careful patient monitoring is essential in the development path of novel therapies for MS, conventional outcome measures do not correlate well with long-term disability. Alternatively, immunological assays may provide a valuable alternative as measures of the effect of this and other immunotherapies. In this perspective, the sequences of myelinreactive T-cells from blood could be used to track T-cells from the same clone over time.

4.2. Current status

First, we assessed the kinetics of myelin-specific autoreactive T-cell responses in MS patients. For this, we conducted a prospective cohort study in the MS clinic of the Antwerp University Hospital. PBMC were isolated from 14 MS patients treated with natalizumab at different time points. The mean age of the patients was 41.36 years (SD 10,20, range 24-59). The median EDSS score was 2.0 (range 1-6). Disease duration since first symptoms ranged between 1 year and 20 years (median 8,13 years). Duration of treatment with natalizumab ranged between 6 months and almost 10 years (median 2.25 years). PBMCs were stimulated *in vitro* in the presence of a selected panel of myelin oligodendrocyte glycoprotein (MOG)-, myelin basic protein (MBP)-, and proteolipid protein (PLP)-derived synthetic peptides, as described in WP1. Next, the frequency of myelin-specific autoreactive T cells was determined using IFN-gamma ELISPOT and analysis. We found that T-cell reactivity towards a mixture of myelin-peptides in natalizumab treated MS patients is highly variable. Whereas 80% of patients demonstrate myelin reactivity at baseline, only 30-40% of patients demonstrate myelin- specific autoreactive T cells at every time point that was assessed longitudinally (t=0, t= 8 weeks, t=12 weeks, t= 24 weeks). This underlines that the baseline presence of autoreactive T cells in the peripheral blood of MS patients may be a critical factor when investigating rare cell populations. The observed high intra-patient variability poses some challenges for current project and warrants further investigation.

4.3. Future plans

To date, no comprehensive framework exists to combine and analyze gene expression data and AIRR- seq data in parallel. Some efforts have been made to unite these two levels of organization in the field of cancer research[35,36], but integration remains far from trivial. Using the data from the assay described above, we will develop a comprehensive framework to integrate the immune receptor and transcriptomic data as a means to functionally characterize paired TCR sequences in samples of MS patients. This approach would imply co-clustering of gene expression t-Distributed Stochastic Neighbor Embedding (t-SNE) 60 clusters and TCR clusters (clustered using VDJtools42). Such a framework will provide insight into how a specific functional phenotype (gene expression profile) is associated with the expression of a specific receptor pair. Furthermore, as part of the data curation process described in achievement 1 of this document, we have meticulously collected meta-information of the patients from whom these samples originated. This information includes disease duration and Expanded Disability Status Scale (EDSS) score (clinical outcome measure to quantify the level of disability in MS patients), amongst other clinical and demographic features. This data set will be used to extract signatures of the TCR repertoire that can be linked to disease course. A preliminary model will be built to evaluate the possibility of using these signatures to predict a patient's disease course.

In addition, we will follow the T-cell repertoire fingerprint in MS patients receiving tolDC treatment, as previously described in MS patients treated with stem cell transplantation[37]. For this, paired PBMCs banked in the context of the clinical trial evaluating the feasibility and safety of the

use of tolDC loaded with the selected pool of peptides for the treatment of MS (ClinicalTrials.gov Identifier: NCT02618902), before and after the cell therapy vaccination cycle (N=9x2), will be analyzed as described above.

5. Networking and collaborations

Building on expertise gained with GSKE support (A. Goris, 2017-2019 and Prize Viscountess Valine de Spoelberch), the current GSKE project (2020-2022) was set up in collaboration with Prof. Nathalie Cools (U Antwerpen) and was awarded.

Prof. An Goris is coordinator of the International Multiple Sclerosis Genetics Consortium (www.imsgc.org) since 2018, and her research group is a member of the EU Horizon2020 Consortium MultipleMS (www.multiplems.eu) and EXIMIOUS (https://www.eximious-h2020.eu/).

Prof. Nathalie Cools is the coordinator of the EU H2020 Restore project https://cordis.europa.eu/project/rcn/213047_en.html, promotor of the EU-EFRO Anicells project (1108, https://www.vlaio.be/nl/andere-doelgroepen/europees-fonds-voor-regionale-ontwikkeling- efro/ontdek-efro-vlaanderen/overzicht) and consortium beneficiary of the EU H2020 Marie Curie Training network INsTRuCT, a network of European scientists from academia and industry focused on developing innovative myeloid regulatory cell (MRC)-based immunotherapies.

Over the project duration, members of our research groups attended the online European Conference on the Treatment and Research in Multiple Sclerosis (ECTRIMS) MSVirtual, the online MS Data Alliance Meeting and the online European Charcot Foundation Meeting. Prof. An Goris was invited speaker at ECTRIMS 2021 presenting "Multiple sclerosis genetics: what needs to be done?". Prof. Nathalie Cools was invited speaker at the International workshop on Immune tolerance 2022 and at the annual meeting of the Dutch Society for Immunology (NVVI) 2022, presenting "Using cells to cure disease: development of a cell-based therapy for multiple sclerosis".

PhD student., Ibo Janssens (UA), presented "RNA-based platform for CRISPR/Cas9-mediated disruption of native TCRs and induction of antigen-specificity in regulatory T cells" at the 5th Newcastle International Therapeutic Tolerance Workshop (Newcastle, UK). Poster presentations were given by PhD student, Stijn Swinnen from the Laboratory for Neuroimmunology (KU Leuven), at the Leuven Brain Institute (LBI) scientific meeting in November 2022, and by PhD student, Ibo Janssens at the Translational Immunology meeting organized by the VIB (Ghent, Belgium) in November 2021 and at the International Conference on Lymphocyte Engineering (Munich, Germany) in April 2022.

A collaboration has been initiated by the group of prof. Nathalie Cools and prof. David W. Scott from the Uniformed Services University of the Health Sciences, Bethesda, USA to evaluate the in vivo applicability of TCR-engineered Tregs. For this, Ibo Janssens (PhD student) performed a 3-month research stay at the Scott lab.

6.   Relevance and future perspectives

The relevance of clonal expansions in MS – as recognized in other autoimmune diseases such as rheumatoid arthritis – sprouts, with very recent single-cell sequencing studies demonstrating clonal expansions of both B- and T-cells in MS[38-40]. However, characterization of culprit and favorable clonal expansions is sparse, which is where our approach adds novelty. We anticipate that T-cell repertoire sequencing and transcriptomic profiling of autoreactive T cells will become a critical tool in both biomedical discovery and clinical management of patients.

Moreover, recent advances in TCR and chimeric antigen receptor (CAR) engineering may provide prospects for patient-specific treatment strategies with fewer side effects. Indeed, there is a significant and unmet need for safe and effective therapies for MS that are well-tolerated and target the cause of disease to reduce duration and frequency of therapy and to limit side-effects. A better alternative to systemic treatment of inflammation with generalized immunosuppressants would be specific therapies that target only the detrimental and aberrant immune response against the specific disease-associated antigen(s) involved. This approach is known as antigen-specific therapy. While the antigen-specific activation of pathogenic T-cells is considered essential in the initiation and maintenance of MS, leveraging the body's attempt to prevent autoimmunity, i.e. tolerization, focuses on the underlying cause of the disease and could be the key to solving neuro-inflammation.

Finally, the identification of expanded autoreactive TCRs may allow administration of TCR-specific inhibitors in both acute and chronic autoimmune disease, or eventually a new paradigm of targeted T- cell depletion for these disorders.

7.   Financial report

As foreseen, GSKE project support has been assigned for consumable costs dedicated to this project. The support of the Prize Viscountess Valine de Spoelberch has been used to attract new staff, thereby ensuring continuity of the research group, and consumable costs. The UA and KU Leuven Financial Departments will provide a detailed report.

The Covid-19 pandemic has resulted in continuing restrictions on the number of researchers that are allowed to work in the lab at the same time throughout most of 2020-2021. Ongoing restrictions and stock breaches at - mainly plastics - suppliers further impacted the wet-lab work. Hence, we have had to alter the project time-planning and moved bio-informatics work to earlier in the project. Our universities provided the necessary structure to efficiently carry out bio-informatics work remotely (remote network access, high-throughput computing cluster, …). Hence, despite the pandemic, we have been able to make substantial progress towards completion of this three-year project.

8. Publications under GSKE support

* indicates shared first/senior authors and @ indicates corresponding author

– Janssens I., Van Delen M., Flumens D., Dams A, Roex G., Van den Bos J., Campillo-Davo D., Cools N, (2022). Harnessing the full potential of Regulatory T cells by mRNA-induced antigen specificity. *Submitted for publication.*
– Janssens I@, Campillo-Davo D, Van den Bos J, De Reu H, Berneman ZN, Wens I, Cools N (2022) Engineering of regulatory T cells by means of mRNA electroporation in a GMP-compliant manner. *Cytotherapy*; 24(6). DOI: 10.1016/j.jcyt.2022.01.001. IF 5.414
– Liston A*, Humblet-Baron*, S, Duffy D*, Goris A*@ (2021) Human immune diversity: from evolution to modernity. *Nat Immunol.*; 22:1479-1489. IF 25.606
– Van Horebeek L, Goris A@ (2020) Transcript-specific regulation in T-cells in multiple sclerosis susceptibility. (Invited Comment) *Eur J Hum Genet*; 28:849-850. IF 3.65
– Janssens I@, Cools N (2020) Regulating the regulators: Is introduction of an antigen-specific approach in regulatory T cells the next step to treat autoimmunity? *Cell Immunol*; 358:104236. IF 4.078
– Van Horebeek L, Dubois B, Goris A (2019) A robust pipeline with high replication rate for detection of somatic variants in the adaptive immune system as a source of common genetic variation in autoimmune disease. *Hum Mol Genet*. 28(8):1369-1380. IF 6.150

9. Other scientific output under GSKE support

– Ibo Janssens successfully defended his PhD entitled "Targeted tolerance in multiple sclerosis: Development of transgenic T cell receptor-engineered regulatory T cells recognizing myelin-derived antigens" under the supervision of prof. Nathalie Cools (UA) on January 13, 2023, with the help of this GSKE grant.

10. Team publications

* indicates shared first/senior authors and @ indicates corresponding author

– Van Delen M, Janssens I, Dams A, Roosens L, Ogunjimi B, Berneman ZN, Derdelinckx J, Cools N. (2022). Tolerogenic Dendritic Cells Induce Apoptosis-Independent T Cell Hyporesponsiveness of SARS-CoV-2-Specific T Cells in an Antigen-Specific Manner. Int J Mol Sci.; 23(23):15201. IF 6.208
– Meena M, Vandormael R, De Laere M, Pintelon I, Berneman Z, Watts R, Cools N. (2022) A Microfluidic In Vitro Three-Dimensional Dynamic Model of the Blood-Brain Barrier to Study the Transmigration of Immune Cells. Brain Sci.; 12(10):1293. IF 3.333
– Molenberghs F, Verschuuren M, Barbier M, Bogers JJ, Cools N, Delputte P, Schelhaas M, De Vos WH. (2022) Cells infected with human papilloma pseudovirus display nuclear reorganization and heterogenous infection kinetics. Cytometry A.; 101(12):1035-1048. IF 4.355
– Van den Bos J, Ouaamari YE, Wouters K, Cools N, Wens I. (2022) Are Cell-Based Therapies Safe and Effective in the Treatment of Neurodegenerative Diseases? A Systematic Review with Meta-Analysis. Biomolecules.; 12(2):340. IF 4.569
– Orije MRP, García-Fogeda I, Van Dyck W, Corbière V, Mascart F, Mahieu L, Hens N, Van Damme P, Cools N, Ogunjimi B, Maertens K, Leuridan E. (2022) Impact of Maternal Pertussis Antibodies on the Infants' Cellular Immune Responses. Clin Infect Dis.; 75(3):442-452. IF 20.999
– Derdelinckx J, Cras P, Berneman ZN, Cools N (2021) Antigen-Specific Treatment Modalities in MS: The Past, the Present, and the Future. *Front Immunol*; 12:624685. IF 7.561
– Willekens B, Wens I, Wouters K, Cras P, Cools N (2021) Safety and immunological proof-of-concept following treatment with tolerance-inducing cell products in patients with autoimmune diseases or receiving organ transplantation: A systematic review and meta-analysis of clinical trials. *Autoimmun Rev*; 20(8):102873. IF 9.754
– Wens I, Janssens I, Derdelinckx J, Meena M, Willekens B, Cools N (2021) Made to Measure: Patient- Tailored Treatment of Multiple Sclerosis Using Cell-Based Therapies. *Int J Mol Sci*; 22(14):7536. IF 4.183
– Derdelinckx J, Reynders T, Wens I, Cools N, Willekens B (2021) Cells to the Rescue: Emerging Cell- Based Treatment Approaches for NMOSD and MOGAD. *Int J Mol Sci*; 22(15):7925. IF 4.183

– Meena M, Van Delen M, De Laere M, Sterkens A, Costas Romero C, Berneman Z, <u>Cools N</u> (2021) Transmigration across a Steady-State Blood-Brain Barrie Induces Activation of Circulating Dendritic Cells Partly Mediated by Actin Cytoskeletal Reorganization. *Membranes (Basel)*; 11(9):700. <u>IF 4.106</u>

– Withanage K, De Coster I, <u>Cools N</u>, Viviani S, Tourneur J, Chevandier M, Lambiel M, Willems P, Le Vert A, Nicolas F, Van Damme P (2021) Phase 1 randomized, placebo-controlled, dose-escalating study to evaluate OVX836, a nucleoprotein- based influenza vaccine: intramuscular results. *J Infect Dis*; jiab532. <u>IF 5.226</u>

– Orije MRP, García-Fogeda I, Van Dyck W, Corbière V, Mascart F, Mahieu L, Hens N, Van Damme P, <u>Cools N</u>, Ogunjimi B, Maertens K, Leuridan E (2021) Impact of maternal pertussis antibodies on the infants' cellular immune responses. *Clin Infect Dis*; ciab972. <u>IF 9.079</u>

– Liston A*, Humblet-Baron*, S, Duffy D*, <u>Goris A</u>*@ (2021) Human immune diversity: from evolution to modernity. *Nat Immunol*; 22:1479-1489. <u>IF 25.606</u>

– Smets I, Dubois B, <u>Goris A</u>@ (2021) Treatment-Induced BAFF Expression and B Cell Biology in Multiple Sclerosis. *Front Immunol*; 12:676619. <u>IF 7.561</u>

– Vandebergh M, Dubois B, <u>Goris A</u>@. Genetic Variation in WNT9B Increases Relapse Hazard in Multiple Sclerosis. *Ann Neurol*; 89:884-894. <u>IF 10.422</u>

– Smets, I*, <u>Goris, A</u>*, Vandebergh, M., Demeestere, J., Sunaert, S., Dupont, P., Dubois, B. (2021). Quantitative MRI phenotypes capture biological heterogeneity in multiple sclerosis patients. *Sci Rep*; 11:1573. IF 3.998

– Vandebergh, M., <u>Goris, A</u>@ (2020). Smoking and multiple sclerosis risk: a Mendelian randomization study. *J Neurol*; 267:3083–3091. <u>IF 3.783</u>

– Oldoni, E, Smets, I, Mallants, K, Vandebergh, M, Van Horebeek, L, Poesen, K, Dupont, P, Dubois, B*, <u>Goris, A</u>*@ (2020). CHIT1 at Diagnosis Reflects Long-Term Multiple Sclerosis Disease Activity. *Ann Neurol*; 87:633-645. <u>IF 9.037</u>

– Van Horebeek L, <u>Goris A</u>@ (2020) Transcript-specific regulation in T-cells in multiple sclerosis susceptibility. (Invited Comment) *Eur J Hum Genet*; 28:849-850. <u>IF 3.65</u>

– Derdelinckx J@, Nkansah I, Ooms N, Van Bruggen L, Emonds MP, Daniëls L, Reynders T, Willekens B, Cras P, Berneman ZN, <u>Cools N</u> (2020) HLA Class II Genotype Does Not Affect the Myelin Responsiveness of Multiple Sclerosis Patients. *Cells*; 9: 2703. <u>IF 4.829</u>

– Janssens I@, <u>Cools N</u> (2020) Regulating the regulators: Is introduction of an antigen-specific approach in regulatory T cells the next step to treat autoimmunity? *Cell Immunol*; 358:104236. <u>IF 4.078</u>

– Joossen C, Baán A, Moreno-Cinos C, Joossens J, <u>Cools N</u>, Lanckacker E, Moons L, Lemmens K, Lambeir AM, Fransen E, Delputte P, Caljon G, Van Der Veken P, Maes L, De Meester I, Kiekens F, Augustyns K, Cos P@. (2020) A novel serine protease inhibitor as potential treatment for dry eye syndrome and ocular inflammation. *Sci Rep*; 10: 17268. <u>IF 3.998</u>

– Maes E, <u>Cools N</u>, Willems H, Baggerman G@. (2020) FACS-Based Proteomics Enables Profiling of Proteins in Rare Cell Populations. *Int J Mol Sci*; 21: 6557. <u>IF 4.556</u>

11.   References

1.   Dendrou, C. A., Fugger, L. & Friese, M. A. Immunopathology of multiple sclerosis. *Nat Rev Immunol* **15**, 545-558 (2015).
2.   Moutsianas, L. *et al.* Class II HLA interactions modulate genetic risk for multiple sclerosis.
3.   *Nat Genet* **47**, 1107-1113 (2015).
4.   Goris, A. & Liston, A. The immunogenetic architecture of autoimmune disease. *Cold Spring Harb Perspect Biol* **4**, a007260 (2012).
5.   The International Multiple Sclerosis Genetics Consortium & The Wellcome Trust Case Control Consortium 2. Genetic risk and a primary role for cell-mediated immune mechanisms in multiple sclerosis. *Nature* **476**, 214-219 (2011).
6.   The International Multiple Sclerosis Genetics Consortium. Analysis of immune-related loci identifies 48 new susceptibility variants for multiple sclerosis. *Nat Genet* **45**, 1353-1360 (2013).
7.   The International Multiple Sclerosis Genetics Consortium. Low-Frequency and Rare-Coding Variation Contributes to Multiple Sclerosis Risk. *Cell* **175**, 1679-1687.e1677 (2018).
8.   The International Multiple Sclerosis Genetics Consortium. Multiple sclerosis genomic map implicates peripheral immune cells and microglia in susceptibility. *Science* **365**, eaav7188 (2019).
9.   The International Multiple Sclerosis Genetics Consortium. A systems biology approach uncovers cell-specific gene regulatory effects of genetic associations in multiple sclerosis. *Nat. Commun.* **10**, 2236 (2019).
10.   Smets, I. *et al.* Multiple sclerosis risk variants alter expression of co-stimulatory genes in B cells. *Brain* **141**, 786-796 (2018).
11.   Dooley, J. *et al.* Immunological profiles of multiple sclerosis treatments reveal shared early B cell alterations *Neurol Neuroimmunol Neuroinflamm* **3**, e240 (2016).
12.   Lagou, V. *et al.* Genetic Architecture of Adaptive Immune System Identifies Key Immune Regulators. *Cell Rep* **25**, 798-810 e796 (2018).
13.   Smets, I. *et al.* Quantitative MRI phenotypes capture biological heterogeneity in multiple sclerosis patients. *Sci Rep* **11**, 1573 (2021).
14.   Kerlero de Rosbo, N. *et al.* Predominance of the autoimmune response to myelin oligodendrocyte glycoprotein (MOG) in multiple sclerosis: reactivity to the extracellular domain of MOG is directed against three main regions. *Eur J Immunol* **27**, 3059-3069 (1997).
15.   Hellings, N. *et al.* T-cell reactivity to multiple myelin antigens in multiple sclerosis patients and healthy controls. *J. Neurosci. Res.* **63**, 290-302 (2001).
16.   Wallstrom, E. *et al.* Increased reactivity to myelin oligodendrocyte glycoprotein peptides and epitope mapping in HLA DR2(15)+ multiple sclerosis. *Eur J Immunol* **28**, 3329-3335 (1998).
17.   Jingwu, Z. *et al.* Myelin basic protein-specific T lymphocytes in multiple sclerosis and controls: precursor frequency, fine specificity, and cytotoxicity. *Ann Neurol* **32**, 330-338 (1992).
18.   Battistini, L. *et al.* CD8+ T cells from patients with acute multiple sclerosis display selective increase of adhesiveness in brain venules: a critical role for P-selectin glycoprotein ligand-1. *Blood* **101**, 4775-4782 (2003).
19.   Ifergan, I. *et al.* Central nervous system recruitment of effector memory CD8+ T lymphocytes during neuroinflammation is dependent on alpha4 integrin. *Brain* **134**, 3560-3577 (2011).
20.   Bieganowska, K. D. *et al.* Direct ex vivo analysis of activated, Fas-sensitive autoreactive T cells in human autoimmune disease. *J Exp Med* **185**, 1585-1594 (1997).
21.   Sethna, Z., Elhanati, Y., Callan, C. G., Walczak, A. M. & Mora, T. OLGA: fast computation of generation probabilities of B- and T-cell receptor amino acid sequences and motifs. *Bioinformatics* **35**, 2974-2981 (2019).
22.   Marcou, Q., Mora, T. & Walczak, A. M. High-throughput immune repertoire analysis with IGoR. *Nature communications* **9**, 561 (2018).
23.   Dang, T. H., Van Leemput, K., Verschoren, A. & Laukens, K. Prediction of kinase-specific phosphorylation sites using conditional random fields. *Bioinformatics* **24**, 2857-2864 (2008).
24.   Meysman, P. *et al.* Use of structural DNA properties for the prediction of transcription-factor binding sites in Escherichia coli. *Nucleic Acids Res* **39**, e6 (2011).
25.   Meysman, P. *et al.* Varicella-zoster virus-derived major histocompatibility complex class I- restricted peptide affinity is a determining factor in the HLA risk profile for the development of postherpetic neuralgia. *J Virol* **89**, 962-969 (2015).
26.   Emerson, R. O. *et al.* Immunosequencing identifies signatures of cytomegalovirus exposure history and HLA-mediated effects on the T cell repertoire. *Nat Genet* **49**, 659-665 (2017).
27.   Zamvil, S. S. *et al.* T-cell epitope of the autoantigen myelin basic protein that induces encephalomyelitis. *Nature* **324**, 258-260 (1986).
28.   Kondo, T. *et al.* TCR repertoire to proteolipid protein (PLP) in multiple sclerosis (MS): homologies between PLP-specific T cells and MS-associated T cells in TCR junctional sequences. *Int Immunol* **8**, 123-130 (1996).

29.	Haas, J. *et al.* Reduced suppressive effect of CD4+CD25high regulatory T cells on the T cell immune response against myelin oligodendrocyte glycoprotein in patients with multiple sclerosis. *Eur J Immunol* **35**, 3343-3352 (2005).

30.	Van der Aa, A. *et al.* T cell vaccination in multiple sclerosis patients with autologous CSF- derived activated T cells: results from a pilot study. *Clin Exp Immunol* **131**, 155-168 (2003).

31.	Bielekova, B. *et al.* Expansion and functional relevance of high-avidity myelin-specific CD4+ T cells in multiple sclerosis. *J Immunol* **172**, 3893-3904 (2004).

32.	Grau-Lopez, L. *et al.* Specific T-cell proliferation to myelin peptides in relapsing-remitting multiple sclerosis. *Eur J Neurol* **18**, 1101-1104 (2011).

33.	Zheng, G. X. *et al.* Massively parallel digital transcriptional profiling of single cells. *Nature communications* **8**, 14049 (2017).

34.	Thompson, A. J. *et al.* Diagnosis of multiple sclerosis: 2017 revisions of the McDonald criteria.

35.	*Lancet Neurol* **17**, 162-173 (2018).

36.	Zemmour, D. *et al.* Single-cell gene expression reveals a landscape of regulatory T cell phenotypes shaped by the TCR. *Nat Immunol* **19**, 291-301 (2018).

37.	Azizi, E. *et al.* Single-Cell Map of Diverse Immune Phenotypes in the Breast Tumor Microenvironment. *Cell* **174**, 1293-1308 e1236 (2018).

38.	Li, H. *et al.* Dysfunctional CD8 T Cells Form a Proliferative, Dynamically Regulated Compartment within Human Melanoma. *Cell* **176**, 775-789 e718 (2019).

39.	Muraro, P. A. *et al.* T cell repertoire following autologous stem cell transplantation for multiple sclerosis. *J Clin Invest* **124**, 1168-1172 (2014).

40.	Pappalardo, J. L. *et al.* Transcriptomic and clonal characterization of T cells in the human central nervous system. *Sci Immunol* **5** (2020).

41.	Ramesh, A. *et al.* A pathogenic and clonally expanded B cell transcriptome in active multiple sclerosis. *Proc Natl Acad Sci U S A* **117**, 22932-22943 (2020).

42.	Schafflick, D. *et al.* Integrated single cell analysis of blood and cerebrospinal fluid leukocytes in multiple sclerosis. *Nat. Commun.* **11**, 247 (2020).

Progress report of the interuniversity research project of

Prof. dr. Pascal Kienlen-Campard (UCLouvain)
Prof. dr. Loïc Quinton (ULg)
Prof. dr. Jan Gettemans (UGent)

Partners of the network

UCLouvain :
Prof. dr. Pascal Kienlen-Campard (PI, spokesperson) – partner 1 (P1)
Institute of Neuroscience
IONS-CEMO, Avenue Mounier 53 bte B1.53.02
B-1200 Brussels

Prof. Bernard Hanseeuw, PhD and **Adrian Ivanoiu** (collaborators) – partner 2 (P2)
Cliniques St Luc, UCLouvain
IoNS- NEUR

ULiège
Prof. dr. Loïc Quinton (PI) – partner 3 (P3)
MS-LAB, UR MolSys
Allée du six Aout 11 - Quartier Agora - Liège Université
B4000 -Liège 1

Ghent University
Prof. dr. Jan Gettemans – partner 4 (P4)
Department of Biomolecular Medicine
Faculty of Medicine & Health Sciences
Campus Ardoyen
Technology Lane 75
B-9052 Ghent

New analytical tools to identify and target pathogenic hexameric Aβ assemblies in Alzheimer's disease

1. Context

With an estimated 47 million people affected worldwide, dementia is recognized as the 5th leading cause of death (http://www.who.int). This number is expected to double within the next 20 years as age is identified as being the biggest risk factor of disease. Alzheimer's disease (AD) is the most common form of dementia and accounts for over 60 per cent of diagnoses, with more than 150.000 cases in Belgium.

A major obstacle in developing a treatment for AD has been the lack of reliable diagnostic markers and straightforward target to block the disease onset and progression. It is therefore imperative to (i) develop a reliable and easy-to-use diagnostic (ii) identify efficient therapeutic targets to treat AD. Several clinical trials have focused on targeting either Aβ production or its accumulation, an early event in AD pathogenesis. The high potential interest to target pathologic Aβ forms has for instance been evaluated in passive immunotherapy trials. Unfortunately, they failed so far to improve cognitive function in subjects with mild or moderate AD(Salloway et al., 2014). Indeed, these negative results could stem from two reasons: (i) possibly irrelevant Aβ targets; (ii) therapies targeting amyloid pathologies might be inefficient if administrated in the late phases of the disease.

Recent studies including ours indicate that Aβ neurotoxicity is attributed to oligomers of Aβ(Decock et al., 2016; Marshall et al., 2016). Oligomers are intermediary species formed on the self-assembly pathway of Aβ from monomers to mature amyloid fibrils. With this in mind, we identify the following points as important research objectives:

1. A better identification of the pathologic Aβ forms to be targeted. Our work hypothesis is that toxicity is highly attributed to hexameric assemblies of Aβ found in cellular models.
2. Make available clinical samples to evaluate the relevance of Aβ oligomers (likely hexamers) we identified in cells to the human AD pathology, possibly at very early stages.
3. The improvement and standardization of analytical approaches as reliable tools to measure Aβ oligomers, both in biological models and patient samples.
4. The development of a novel approach to efficiently target Aβ oligomers. We will develop an approach based on nanobodies, which appear much more promising than whole antibodies used so far. Their comparatively low molecular mass leads to a better permeability in tissues and allows them to bind to hidden epitopes that are not accessible to whole antibodies. In addition, they do not show complement system triggered cytotoxicity as they lack an Fc region.

2. Progress in the different objectives

2.1. Identification of the pathogenic Aβ oligomers

As stated in the year 2020, with the support of the FMRE, we finalized a first project aimed at identifying the molecular conformations of the Amyloid precursor protein (APP) triggering the production of pathological Aβ assemblies. We demonstrated that dimeric orientations of amyloidogenic APP C-terminal fragments (C99) regulate the precise cleavage by -secretase that releases Aβ. We found that one precise orientation of C99 favored processing to Aβ43/40 forms, promoting formation of SDS oligomers, reminiscent of Aβ peptide oligomers. (See Figure on the right, from Perrin et al., 2020). This work has been published in iScience, December 2020 (Perrin et al., 2020). An erratum is associated to clarify the display and calculation in a figure (Perrin et al., 2021). **This work involved P1.**

We further investigated the nature and the properties of Aβ assemblies that we identified in cellular models. The misfolding of Aβ leads to subsequent amyloid fibril formation by nucleated polymerization. This requires an initial and critical nucleus for self-assembly. We identified and characterized the composition and self-assembly properties of cell-derived hexameric Aβ42 and showed its assembly enhancing properties which are dependent on the Aβ monomer availability. Identification of nucleating assemblies that contribute to self-assembly in this way may serve as therapeutic targets to prevent the formation of toxic oligomers. **This work involved P1 and P3 and has been published in 2021(Vadukul et al., 2021)**. We isolated these hexameric Aβ assemblies from a cellular model and assessed its effect on primary neuron viability *in vitro*, and its contribution to amyloid deposition in vivo. In 5xFAD mice, where human Aβ species are pre-existing, the hippocampal injection of cell-derived Aβ hexamers aggravated Aβ deposition, in agreement with its previously described nucleation properties. Finally, by editing human cell lines, we investigated the respective contribution of Presenilin 1 (PS1) and 2 (PS2)-dependent -secretases, which are responsible for the release of monomeric Aβ, to this process. We found experimental evidence suggesting a direct link between PS2-dependent activity and the release of hexameric Aβ in extracellular vesicles. **This work involved P1, P2 and P3 and has been published in 2021(Vrancx et al., 2021).**
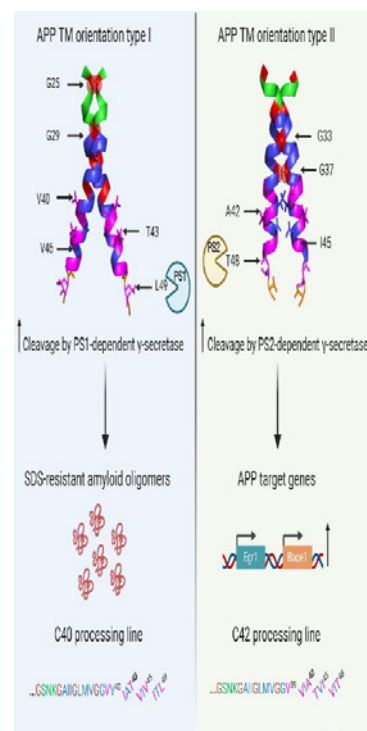
2.2. Patient cohort and clinical samples workflow

P1 together with P2 built up a cohort of around 300 individuals. All patients with clinical symptoms have been genotyped for ApoE4.

2.3. Standardization of analytical approaches

The plasma samples from the UCLouvain/St Luc Hospital cohort is currently formed by AD patients (N=20), age-matched controls (N around 160), non-inflammatory neurological disease (NIND) with dementia (N=16) and non-demented NIND (N=16).

The workflow has been set up to isolate blood exosomes and particularly Neurally-derived blood exosomes (NDBEs) from plasma samples. Standard AD biomarkers are currently evaluated for each patient sample (Aβ42:40 ratio, cognitive assays and amyloid PET imaging when possible). Biomarkers are measured in blood samples through the newly acquired (2021) ultra-sensitive

SIMOA® immunoassay technology by using multiplex assays. Our next aim (2002) is to establish the profile of standard AD biomarkers in blood samples (controls and patients). The content of NDBEs is currently under analysis. We expect Aβ oligomers (hexamers) to be enriched in these fractions. Our aim is to establish to check whether Aβ hexamers are present in CSF, in case to concentrate them for further analysis by mass spectrometry (**P3**) the Aβ isoforms composing them. A correlation with other amyloid biomarkers will be estimated (**P2**). This work is mainly conducted by a PhD student (Emilien Boyer, MD. **P1** supervisor, **P2** co-supervisor). He also plans to evaluate the ability of some nanobodies (**P4**) to detect oligomeric Aβ in biological models (cell lines); in order to test them eventually in human samples.

2.4. Development of nanobodies targeting Aβ hexamers and other AD related targets.

The team at Ghent university (**P4**) obtained single domain antibodies (nanobodies) against serum amyloid P component or SAP from human or murine origin. SAP interacts with amyloid fibrils and strengthens them. **P4** is keen to understand which proteins interact with SAP and towards this end anti-human SAP nanobodies were derivatized with a C-terminal azido-Phe residue that allows oriented coupling onto alkyn-activated magnetic beads. The beads were used for SAP immunoprecipitation from human plasma and a SAP interactome map has been set up using mass spectrometry together with **P3**. In anticipation of Abeta hexamers for immunization and nanobody generation, we are developing nanobodies against ApoE4. Two *apoE4* alleles constitute a high risk for developing late onset AD. The protein differs by only one amino acid from its two close isoforms, ApoE3 and ApoE2, but it has a distinct tertiary structure. ApoE4-specific nanobodies could be instrumental in development of a diagnostic test or to understand more about the damaging intracellular effects of this protein. After a first immunization we generated a VHH library and panned this library with ApoE4. The resulting nanobodies were cross-reactive with human ApoE3, but do not cross-react with mouse ApoE. More recently we immunized two animals with a peptide from ApoE4 that was previously used for obtaining ApoE4 conventional antibodies and we aim to identify unique E4 nanobodies from the VHH libraries. Such nanobodies could also be used by **P2**. In addition, we have generated nanobodies against RgpA, a bacterial protease believed to be tightly associated with AD, and these are currently being characterized.

Dissemination

The restrictions related to the COVID pandemic have again prevented the organization of research meeting/symposia on the topic in 2021 but the network organized remote meetings (Teams) to ensure the exchange of materials and the monitoring of information necessary for the progress of the project. In 2022, attendance to international meetings allowed oral presentations (publications 1-3, 10 in the list below).

Main achievements:

- Validation of blood biomarkers (Aβ ad Tau) that can be monitored by highly sensitive techniques (SIMOA, Mass spectrometry) to diagnose early stages of Alzheimer's disease. This work is finalized and will be submitted for publication (Spring 2023) (**P1-P2-P3**).
- Building of a unique cohort of blood samples (up to 300 at the moment) from control individuals and patients with dementia (with paired clinical data). Plasma samples are available to the community (**P1-P2**).
- A new technique to isolate Neurally Derived Blood Exosomes has been set up to identify with high accuracy biomarkers of neurodegenerative disorders present in the blood (**P1-P3**)
- New techniques for labeling and delivery of nanobodies into living cells (**P4**).
- Generation of pathological assemblies of Aβ in cell models (**P1**) to further develop nanobodies (**P4**) for clinical approaches (**P2**).

3.   Reference List

– Decock, M., Stanga, S., Octave, J.N., Dewachter, I., Smith, S.O., Constantinescu, S.N., and Kienlen-Campard, P. (2016). Glycines from the APP GXXXG/GXXXA Transmembrane Motifs Promote Formation of Pathogenic Abeta Oligomers in Cells. Front Aging Neurosci *8*, 107. 10.3389/fnagi.2016.00107 [doi].
– Marshall, K.E., Vadukul, D.M., Dahal, L., Theisen, A., Fowler, M.W., Al-Hilaly, Y., Ford, L., Kemenes, G., Day, I.J., Staras, K., and Serpell, L.C. (2016). A critical role for the self-assembly of Amyloid-beta1-42 in neurodegeneration. Sci. Rep *6*, 30182. srep30182 [pii];10.1038/srep30182 [doi].
– Perrin, F., Papadopoulos, N., Suelves, N., Opsomer, R., Vadukul, D.M., Vrancx, C., Smith, S.O., Vertommen, D., Kienlen-Campard, P., and Constantinescu, S.N. (2021). Erratum: Dimeric Transmembrane Orientations of APP/C99 Regulate gamma-Secretase Processing Line Impacting Signaling and Oligomerization. iScience *24*, 102057. 10.1016/j.isci.2021.102057 [doi];S2589-0042(21)00025-0 [pii].
– Salloway, S., Sperling, R., Fox, N.C., Blennow, K., Klunk, W., Raskind, M., Sabbagh, M., Honig, L.S., Porsteinsson, A.P., Ferris, S., et al. (2014). Two phase 3 trials of bapineuzumab in mild-to-moderate Alzheimer's disease. N Engl J Med *370*, 322-333. 10.1056/NEJMoa1304839.
– Vadukul, D.M., Vrancx, C., Burguet, P., Contino, S., Suelves, N., Serpell, L.C., Quinton, L., and Kienlen-Campard, P. (2021). An evaluation of the self-assembly enhancing properties of cell-derived hexameric amyloid-beta. Sci. Rep *11*, 11570. 10.1038/s41598-021-90680-y [doi];10.1038/s41598-021-90680-y [pii].
– Vrancx, C., Vadukul, D.M., Suelves, N., Contino, S., D'Auria, L., Perrin, F., van Pesch, V., Hanseeuw, B., Quinton, L., and Kienlen-Campard, P. (2021). Mechanism of Cellular Formation and In Vivo Seeding Effects of Hexameric beta-Amyloid Assemblies. Mol Neurobiol *58*, 6647-6669. 10.1007/s12035-021-02567-8.

4.   Work published in 2020 2022 acknowledging FMRE

1. Perrin F, Papadopoulos N, Suelves N, et al. Erratum: Dimeric Transmembrane Orientations of APP/C99 Regulate gamma-Secretase Processing Line Impacting Signaling and Oligomerization. iScience 2021; 24(2): 102057. (IF 5.08)
2. Vadukul DM, Vrancx C, Burguet P, et al. An evaluation of the self-assembly enhancing properties of cell-derived hexameric amyloid-beta. Sci Rep 2021; 11(1): 11570. (IF4.13)
3. Vrancx C, Vadukul DM, Suelves N, et al. Mechanism of Cellular Formation and In Vivo Seeding Effects of Hexameric beta-Amyloid Assemblies. Mol Neurobiol 2021; 58(12): 6647-69. (IF4.95)
4. Kreis A, Desloovere J, Suelves N, et al. Overexpression of wild-type human amyloid precursor protein alters GABAergic transmission. Sci Rep 2021; 11(1): 17600 (IF 4.13)
5. Papadopoulos, N., Suelves, N., Perrin, F., Vadukul, D.M., Vrancx, C., Constantinescu, S.N., and Kienlen-Campard, P. (2022). Structural Determinant of beta-Amyloid Formation: From Transmembrane Protein Dimerization to beta-Amyloid Aggregates. Biomedicines 10. 10.3390/biomedicines10112753 (IF 4.76).
6. Gettemans J. Site-Specific Fluorescent Labeling, Single-Step Immunocytochemistry and Delivery of Nanobodies into Living Cells. Method in Molecular Biology vol 2246. *In press.*
7. Decoene, K.W., K. Unal, A. Staes, O. Zwaenepoel, J. Gettemans, K. Gevaert, J.M. Winne, and A. Madder. 2022. Triazolinedione protein modification: from an overlooked off-target effect to a tryptophan-based bioconjugation strategy. Chem Sci. 13:5390-5397 (IF=9,825).
8. Gettemans, J. 2022. Site-Specific Fluorescent Labeling, Single-Step Immunocytochemistry, and Delivery of Nanobodies into Living Cells. Methods Mol Biol. 2446:373-393 (IF=1,37)
9. Gettemans, J., and B. De Dobbelaer. 2021. Transforming nanobodies into high-precision tools for protein function analysis. Am J Physiol Cell Physiol. 320:C195-C215 (IF=4,249)
10. Grobler, C., M. van Tongeren, J. Gettemans, D.B. Kell, and E. Pretorius. 2023. Alzheimer's Disease: A Systems View Provides a Unifying Explanation of Its Development. J Alzheimers Dis. 91:43-70 (IF=4,472).
11. Malotaux V, Dricot L, Quenon L, Lhommel R, Ivanoiu A, Hanseeuw B. (2022) Default-Mode Network Connectivity Changes During the Progression Toward Alzheimer's Dementia: A Longitudinal Functional Magnetic Resonance Imaging Study. Brain Connectivity. IF = 2.7
12. Lebrun L; Hanseeuw B; Van Pesch V ; Ivanoiu A. (2022) Alzheimer disease's cerebrospinal fluid biomarkers differences between immigrants and natives in a Belgian memory clinic. Acta Neurologica Belgica. IF = 2.4
13. Hanseeuw, B. J., Malotaux, V., Dricot, L., Quenon, L., Sznajer, Y., Cerman, J., Woodard, J. L., Buckley, C., Farrar, G., Ivanoiu, A., & Lhommel, R. (2021). Defining a Centiloid scale threshold predicting long-term progression to dementia in patients attending the memory clinic : An [18F] flutemetamol amyloid PET study. European Journal of Nuclear Medicine and Molecular Imaging. IF = 10.1

14. Mormont, E., Bier, J.-C., Bruffaerts, R., Cras, P., De Deyn, P., Deryck, O., Engelborghs, S., Petrovic, M., Picard, G., Segers, K., Thiery, E., Versijpt, J., & Hanseeuw, B. (2020). Practices and opinions about disclosure of the diagnosis of Alzheimer's disease to patients with MCI or dementia : A survey among Belgian medical experts in the field of dementia. Acta Neurologica Belgica. IF = 2.4

15. Hanseeuw, B. J., Scott, M. R., Sikkes, S. A. M., Properzi, M., Gatchel, J. R., Salmon, E., Marshall, G. A., & Vannini, P. (2020). Evolution of anosognosia in alzheimer's disease and its relationship to amyloid. Annals of Neurology, 87(2), 267 280. IF = 10.4

Universitaire onderzoeksprojecten 2020-2022 gefinancierd door de G.S.K.E.

Projets de recherche universitaire 2020-2022 subventionnés par la F.M.R.E.

University research projects 2020-2022 funded by the Q.E.M.F.

Universiteiten met onderzoeksprogramma's die gesteund worden door de G.S.K.E.

Universités ayant des programmes de recherche subventionnés par la F.M.R.E.

Universities having research programs supported by the Q.E.M.F.

→ Universiteit Antwerpen (UAntwerpen)

→ Kulak, de Kortrijkse campus van de KU Leuven (KULAK)

→ Katholieke Universiteit Leuven (KU Leuven)

Brussel/Bruxelles/Brussels

België
Belgique
Belgium

Europa
Europe

Universitaire onderzoeksprojecten 2020-2022 gefinancierd door de G.S.K.E.

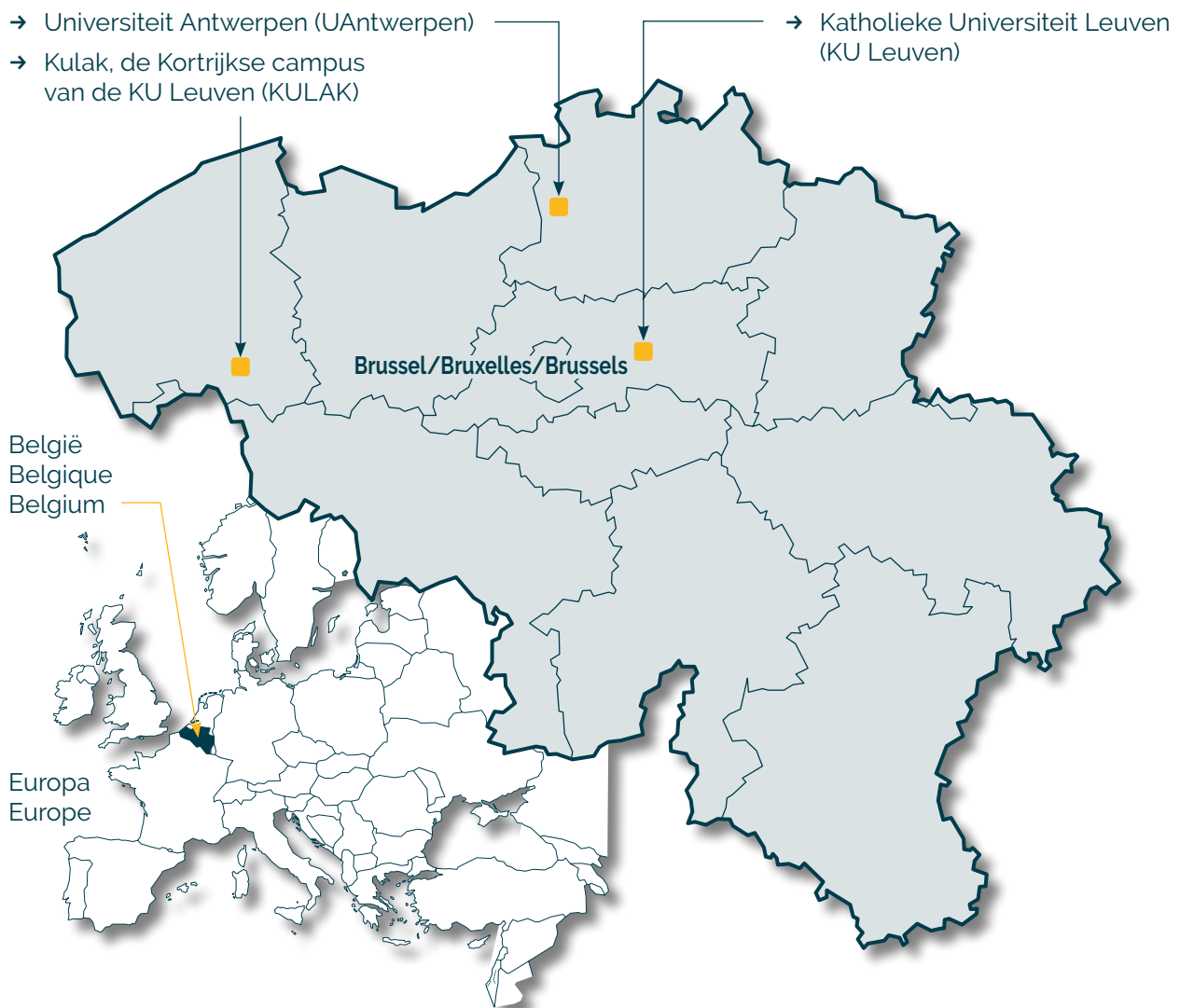# Projets de recherche universitaire 2020-2022 subventionnés par la F.M.R.E.

University research projects 2020-2022 funded by the Q.E.M.F.

UAntwerpen

Prof. dr. Sarah Weckhuysen, MD, PhD
Study and targeted treatment development for epileptic encephalopathies using 2D and 3D human induced plupripotent stem cell-derived neuronal cultures

KU Leuven

Prof. Pierre Vanderhaeghen, MD, PhD (VIB)
Deciphering the mechanisms underlying intellectual deficiency and autism spectrum disorders by cellular modelling in human neurons in vivo

Prof. dr. Lieve Moons & dr. Lies De Groef
Oligodendrocytes in Wolfram syndrome: bystanders or partners in crime?

Prof. dr. Thomas Voets (VIB)
Unraveling the cellular and molecular basis of noxious cold sensing

KULAK

Prof. dr. ir. Simon De Meyer
Unravelling the thrombo-inflammatory role of von Willebrand factor in neurodegeneration after ischemic stroke

Final report of the university research project of

Prof. dr. ir. Simon De Meyer
Kulak, de Kortrijkse campus van de
KU Leuven (KULAK)

Prof. dr. ir. Simon De Meyer
Professor, Dept. of Cardiovascular Sciences
Laboratory for Thrombosis Research
KU Leuven Campus Kulak Kortrijk
E. Sabbelaan 53
8500 Kortrijk
Belgium
Tel: +32 56 246232
simon.demeyer@kuleuven.be
www.kuleuven-kulak.be/irf/thrombosis

Unravelling the thrombo-inflammatory role of von Willebrand factor in neurodegeneration after ischemic stroke

1.   Summary of the project

Ischemic stroke is one of the leading causes of death and sustained disability worldwide. Blockade of blood flow to the brain by an occlusive thrombus leads to irreversible damage of the associated brain tissue. The enormous clinical, economic and social burden of ischemic stroke is in strong contrast with the limited treatment options that are currently available. In acute ischemic stroke, the mainstay of acute treatment is rapid recanalization of the occluded blood vessel, either via pharmacological thrombolysis or via mechanical thrombectomy.

In recent years, it has become clear that rapid recanalization of the occluded blood vessel is not sufficient to fully salvage the threatened brain tissue. Novel insights show that cerebral ischemia and subsequent reperfusion elicit a thrombo-inflammatory cascade that promotes progressive brain damage in stroke patients.[1] This problem does not only occur after successful thrombolysis but also often complicates stroke outcome after successful mechanical thrombectomy.[2] This so-called ischemia/reperfusion injury (I/R injury) is a complex process that interrelates thrombosis with inflammation, leading to several pathophysiological effects in the neuro-vascular unit. The exact mechanisms of how cerebral I/R injury accelerates neurodegeneration are still poorly understood. Yet, such insights will be crucial to develop effective strategies to promote neuroprotection in stroke management. One of our major findings in the last decade is our discovery that von Willebrand factor (VWF) plays a crucial role in cerebral I/R injury. [1,3-6] VWF is a large multimeric plasma glycoprotein that recruits platelets at sites of vascular injury and that promotes both thrombosis and inflammation. Remarkably, we found that initial VWF-mediated platelet adhesion rather than subsequent platelet aggregation contributes to cerebral I/R injury with a prominent role for the interaction between the VWF A1 domain and platelet glycoprotein (GP)Ib.[4,6-8] At present we do not know exactly how VWF contributes to thrombo-inflammation in the (post-)ischemic brain. Our hypothesis is that VWF, after release by activated (hypoxic) endothelial cells recruits and activates both platelets and leukocytes, leading to obstruction of the microvasculature and local inflammation.

The general objective of this research project was to elucidate the mechanisms by which VWF mediates cerebral I/R injury in ischemic stroke. More specifically, we are aiming at (i) unravelling the inflammatory component of VWF-mediated I/R injury and (ii) at visualizing the molecular and cellular interactions of VWF-mediated thrombo-inflammation in the brain via advanced 3D microscopy.

In order to successfully complete this project, two delineated work packages (WP) were defined:

- WP1: Elucidating the inflammatory component of VWF in cerebral I/R injury
- WP2: Advanced 3D microscopy to map VWF-mediated thrombo-inflammation in the brain

The 2-year progress for each work package is detailed, as well as the planned next steps for the following years.

WP 1: Elucidating the inflammatory component of VWF in cerebral I/R injury

OBSERVATION 1: VWF-deficiency reduces immune cell recruitment to the brain after ischemic stroke

To examine the cerebral immune cell response mediated by VWF, we performed flow cytometric analysis of single cell suspensions prepared from brain tissue isolated from WT and VWF KO mice subjected to stroke. After stroke, mice were perfused, their brains harvested and subsequently divided into ipsilateral (affected by stroke) and contralateral (unaffected) hemispheres. Interestingly, we observed significantly reduced cerebral infarcts in VWF KO mice, compared to WT mice ($p < 0.01$, Figure 1A). Twenty-four hours after stroke, the ipsilateral hemisphere showed an increased amount of infiltrated white blood cells (WBCs) compared to the contralateral hemisphere in both the WT ($p < 0.005$) and VWF KO mice ($p < 0.05$). However, averaged recruitment of WBC in the ipsilateral hemisphere of VWF KO mice was two-fold lower than in WT mice (5596 ± 1644 vs. 12435 ± 2083, respectively; $p < 0.05$, Figure 1B). Both the amount of myeloid and lymphoid white blood cells was significantly reduced in the brains of VWF KO mice compared to WT mice ($p < 0.05$, Figure 1C-D).

OBSERVATION 2: VWF deficiency leads to reduced recruitment of inflammatory monocytes, neutrophils and T-cells

To better determine which inflammatory cells were potentially recruited by VWF to the affected brain tissue during stroke, we used two antibody cocktails that allowed discrimination and quantification of recruited inflammatory monocytes, neutrophils, T-cells and CD3^{neg} lymphocytes (B cells and NK cells) (Table 1).

As shown in figure 1E-H, all four subsets of immune cells were significantly increased in the ipsilateral brain of WT mice 24 hours after stroke, compared to the unaffected contralateral hemisphere. However, despite the presence of an infarct core in the affected ipsilateral hemisphere of VWF KO mice, the numbers of neutrophils and T-cells did not increase and remained similar to the baseline values of the contralateral hemisphere (Figure 1E and 1F). Hence, the absolute numbers of recruited neutrophils and T- cells was significantly higher in the ischemic brain of WT mice compared to VWF KO mice (2017 ± 733 vs 512 ± 203, $p < 0.05$ and 974 ± 184 vs 244 ± 44, $p < 0.01$ respectively). These results suggest an important role for VWF in recruiting both neutrophils and T-cells to the affected brain tissue during ischemic stroke.

A similar, yet less outspoken, trend was observed for inflammatory monocytes (Figure 1G). In VWF KO mice, the ischemic hemisphere contained significantly more inflammatory monocytes than the unaffected hemisphere, but this was still significantly lower than the number of inflammatory monocytes that were recruited in the ischemic brain of WT mice (2466 ± 955 vs 6760 ± 1414; $p < 0.05$).

No differences regarding CD3^{neg} lymphocytes were observed between WT and VWF KO mice as similar numbers were recruited in the ischemic hemisphere of both groups (1162 ± 245 vs 585 ± 188 respectively, $p > 0.05$, Figure 1H). Leukocyte blood counts and circulating platelet-leukocyte complexes were similar between VWF KO and VWF WT mice 24 hours after stroke (data not shown).

Table 1. Antibodies cocktails used to discriminate between different white blood cell subtypes.

|	antigen	supplier
Antibody cocktail 1	CD45 APC-Cy7	Biolegend
	CD11b PE-Cy7	eBioscience
	Ly6G BV510	Biolegend
	Ly6C FITC	Biolegend
	CD16/CD32 (Fc-block)	eBioscience
	Live/Death Fixable Violet Dead Cell Stain Kit	ThermoFisher
Antibody cocktail 2	CD45-APC-Cy7	Biolegend
	CD11b PE-Cy7	eBioscience
	CD11c PerCp-Cy5	eBioscience
	CD3e FITC	eBioscience
	CD16/CD32 (Fc-block)	eBioscience
	Live/Death Fixable Violet Dead Cell Stain Kit	ThermoFisher
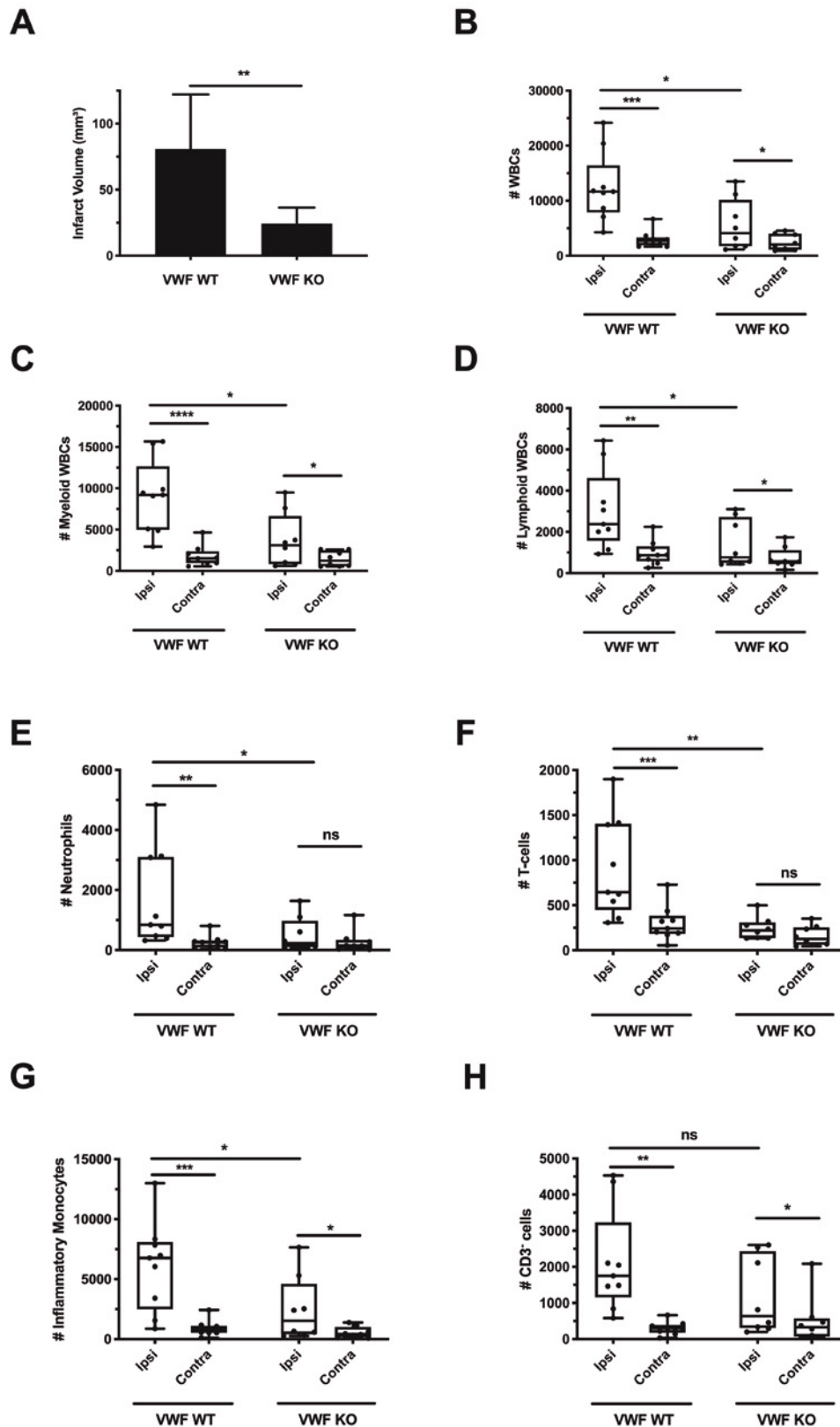
Figure 1 (see next page): VWF deficiency leads to a reduction of the number of monocytes, neutrophils and T-cells to the brain after acute ischemic stroke. *Transient focal cerebral ischemia was induced by 60 minutes occlusion of the right middle cerebral artery (tMCAO), followed by 23 hours of reperfusion in WT and VWF KO mice, after which edema-corrected brain infarct volumes were quantified by planimetric analysis (A) and WBC recruitment to each hemisphere was determined by flow cytometry. Total amount of white blood cells (CD45^{high}) was analyzed (B) as well as the myeloid (CD45^{high}; CD11b$^+$) (C) and lymphoid white blood cells (CD45^{high}; CD11b$^-$; CD11c$^-$) (D). More specifically: Neutrophils (CD45^{high}; CD11b$^+$; Ly6G$^+$) (E); T-cells (CD45^{high}; CD11b$^-$; CD11c$^-$; CD3e$^+$) (F); Inflammatory Monocytes (CD45^{high}; CD11b$^+$; Ly6C$^+$; Ly6G$^-$) (G); CD3^{neg} lymphocytes (CD45^{high}; CD11b$^-$; CD11c$^-$; CD3e$^-$) (H) were quantified. Data are represented as box plots showing all data points and the median value, except for infarct size which is shown as mean ± standard deviation. * p < 0.05; **, p<0.01; ***: p < 0.005; ****, p<0.001. (n = 8-9)*

OBSERVATION 3: VWF-mediated thromboinflammation in the ischemic stroke brain via fluorescence microscopy

For visualization of VWF-mediated thromboinflammation, immunofluorescent staining of platelets and leukocytes was performed on brains obtained from VWF WT and KO mice 24 hours after stroke (Figures 2 and 3). In VWF KO mice, very few platelet accumulations were found within the ipsilateral brain (Figure 2A). In contrast, platelet/VWF-rich microthrombi were found frequently throughout the ipsilateral brain of VWF WT mice, underscoring the importance of VWF-mediated platelet adhesion in the ischemic stroke brain (Figure 2B-D). Platelet/VWF-rich microthrombi were absent in the contralateral hemisphere of both WT and VWF KO mice (data not shown).

Next, we visualized immune cell recruitment in VWF WT and KO mice. Since previous studies found no major role for monocytes, but an important detrimental role for both T-cells[9] and neutrophils[10] in the acute phase of ischemic stroke, we focused on visualizing neutrophils and T-cells in the stroke brain. To stain the vasculature in both VWF WT and KO mice, a sensitive lectin staining of the endothelium was performed (Figure 3). Using a specific histological marker for neutrophils (Ly6G), we observed that neutrophils were more frequently present within the ipsilateral side of the brain of VWF WT mice compared to VWF KO mice (Figure 3A-B). Since the smaller infarct sizes observed in VWF KO mice might bias neutrophil quantification by flow cytometry, we also quantified neutrophil recruitment in the ischemic infarct core in both VWF KO and WT mice by histology. Importantly, analysis of fixed areas of 1 mm^2 in the infarct core corroborated our flow cytometric data, arguing against a nonspecific effect related to smaller infarct sizes. Quantification of neutrophil recruitment to the infarct core revealed a two-fold reduction of neutrophil density in VWF KO brains compared to WT mice (Figure 3C). Intriguingly, neutrophils were frequently observed within the microcirculation (Figure 3A-B). To investigate this further, intra – and extravascular neutrophils were counted in brain sections of VWF WT mice. On average, 66 ± 4% of neutrophils were found within the vasculature of the ischemic hemisphere, while the remaining neutrophils were already extravasated (Figure 3D). A comparable observation was made when we stained for T-cells, which were also occasionally found within the microvasculature of VWF WT mice (Figure 3E). Due to the low number of T-cells within the ischemic brain, quantification of T-cells was not feasible. Lastly, T-cells were virtually absent in the ipsilateral brain hemisphere of VWF KO mice (Figure 3F), confirming our flow cytometric data.
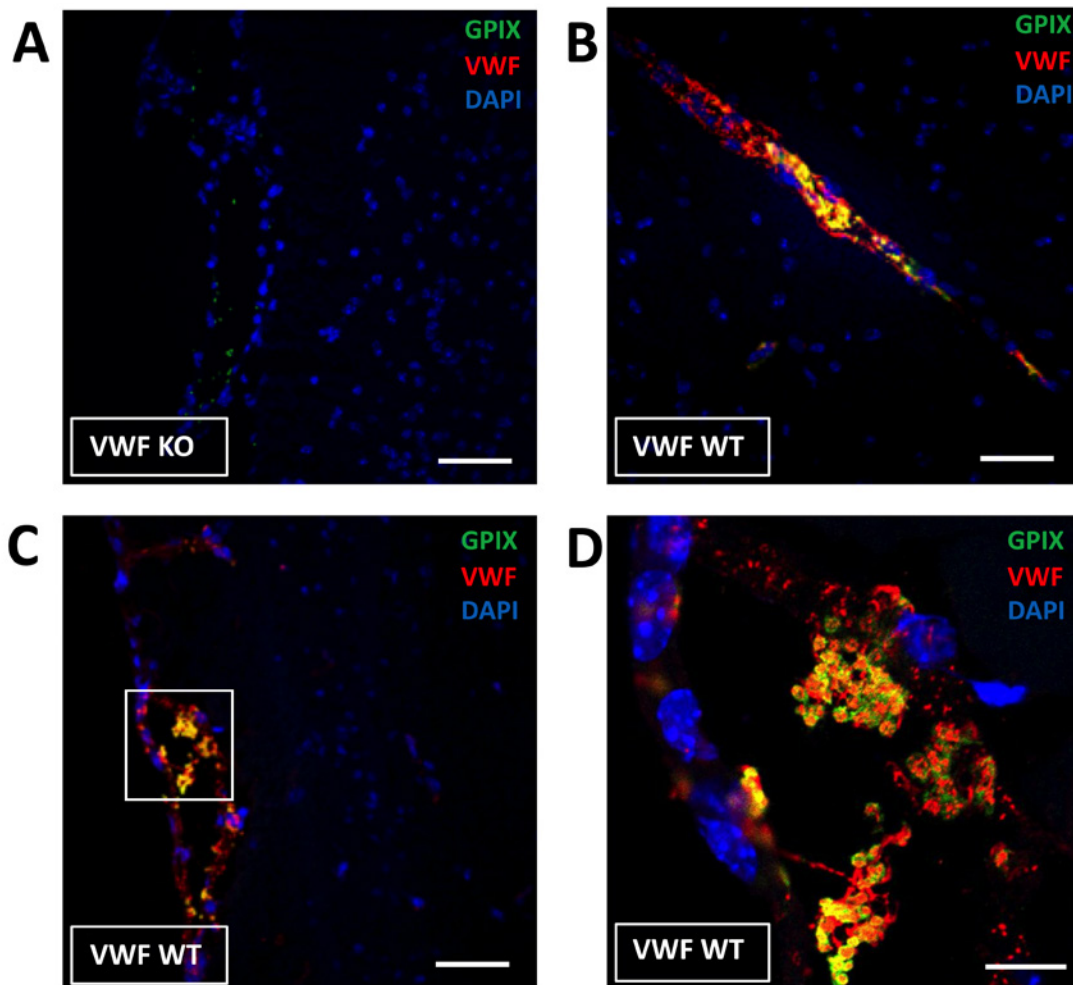
Figure 2: Immunofluorescent visualization of thromboinflammation in the ipsilateral hemisphere of mice 24 hours after ischemic stroke brain injury. *Transient focal cerebral ischemia was induced by 60 minutes occlusion of the right middle cerebral artery (tMCAO), followed by 23 hours of reperfusion in VWF WT or KO mice, after which, brain-sections were stained for VWF (red), platelets (green) and nuclei (blue). **A.** Only a few platelets are found within the ischemic brain of VWF KO mice. **B-D.** Clumps of VWF together with platelets were frequently found attached to the vessel wall within the ipsilateral hemisphere. Panel D is a magnification of the white box in panel C. Scale bars are 50μm except for panel D where the scale bar is 25μm. Images are representative for n = 3 per genotype.*
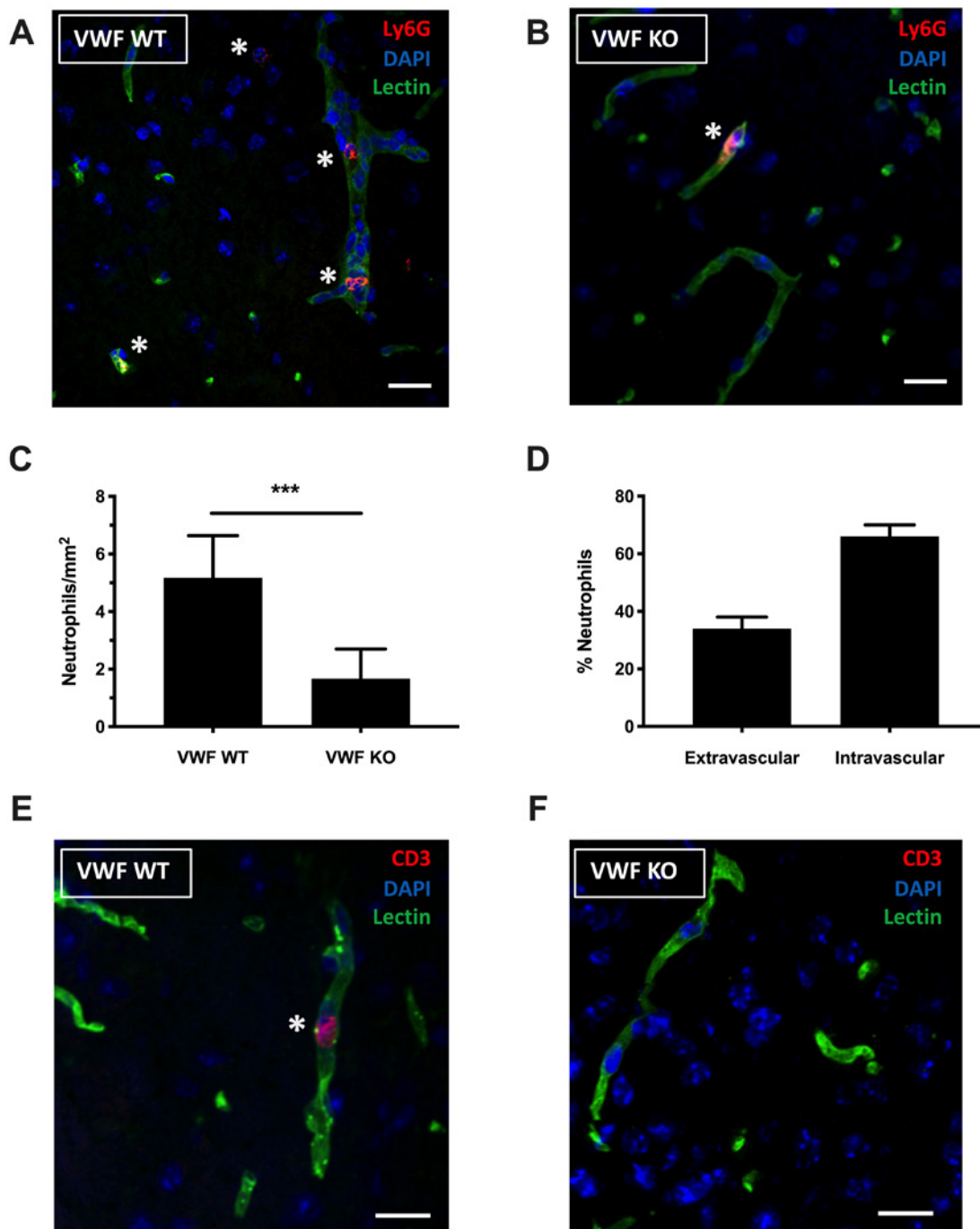
Figure 3: Immunofluorescent visualization of neutrophils and T-cells in the ipsilateral hemisphere of mice 24 hours after ischemic stroke brain injury. *Transient focal cerebral ischemia was induced by 60 minutes occlusion of the right middle cerebral artery (tMCAO), followed by 23 hours of reperfusion in VWF WT and KO mice, after which, brain-sections were stained for blood vessels and neutrophils or T-cells.* **A-B.** *Neutrophils were stained with a marker for Ly6G (red) and blood vessels with a lectin staining (green). Neutrophils are marked with a *.* **C.** *Quantification of the number of neutrophils/mm^2 in the infarct core of WT and VWF KO mice. (n = 3) Data is represented as mean ± standard deviation.* **D.** *The number of neutrophils within and outside the vasculature (n = 3). Data is represented as mean ± standard deviation.* **E and F.** *T-cells were stained with a marker for CD3 (red) and blood vessels with a lectin staining (green). T-cells are marked with a *. Scale bars are 20µm. Images are representative for n = 3 per genotype.*

OBSERVATION 4: Inhibition of the VWF A1 domain limits ischemic stroke brain injury

Given the central role of the VWF A1 domain in cerebral ischemia/reperfusion injury[4], we next wanted to unravel its potential inflammatory contribution in ischemic stroke. To this end, we used a nanobody (KB-VWF-006bv) that specifically binds the VWF A1 domain, inhibiting its interaction with the platelet receptor GPIbα.[11] Intravenous treatment with 10mg/kg of the nanobody was

started immediately after establishment of reperfusion. Mean residence time of the nanobody is 3.5 hours and this allows blocking of the VWF-A1 domain during the acute reperfusion phase. As a control, a nonspecific nanobody (KB-VWF-004bv) was administered. Twenty-four hours after stroke, mice treated with the anti-VWF A1 nanobody KB-VWF-006bv had significantly less ischemic stroke brain damage compared to control-treated mice (Figure 4A and B). This translated in an improved motor score (Figure 4C) and neurological behavior (Figure 4D), although this difference was only statistically significant for the latter. Of note, no intracranial bleedings were observed in any of the mice treated with the VWF A1 nanobody. These data further corroborate the crucial involvement of the VWF-GPIbα axis in cerebral ischemia/reperfusion injury.[6,7,12,13]

OBSERVATION 5: Inhibition of the VWF A1 domain reduces the recruitment of neutrophils, monocytes and T-cells

Targeting the VWF A1 domain also significantly reduced inflammatory cell recruitment to the ischemic brain (Figure 5). Indeed, similar to our results in VWF KO mice, flow cytometric analysis revealed that inhibition of VWF A1 also leads to a 2-fold reduction of immune cell recruitment in the brains of treated mice compared to control mice (7095 ± 2550 vs 16310 ± 3980; $p < 0.005$; Fig. 5A). Both myeloid (5195 ± 2259 vs 11978 ± 3322; $p < 0.05$; Fig. 5B) and lymphoid WBCs (1529 ± 269 vs 3017 ± 514; $p < 0.05$; Fig. 5C) were reduced in the ipsilateral hemispheres of VWF A1 nanobody treated mice. Specifically, inhibition of the VWF A1 domain reduced the amount of infiltrated inflammatory monocytes (3726 ± 1824 vs 8266 ± 2651; $p < 0.05$; Fig. 5D), neutrophils (304 ± 94 vs 1557 ± 317; $p < 0.0005$; Fig. 5E) and T-cells (487 ± 93 vs 1111 ± 248; $p < 0.05$; Fig. 5F) in the ipsilateral hemisphere of the brain, 24 hours after stroke. These data suggest that the inflammatory effect of VWF in ischemic stroke is mediated through the VWF A1 domain.
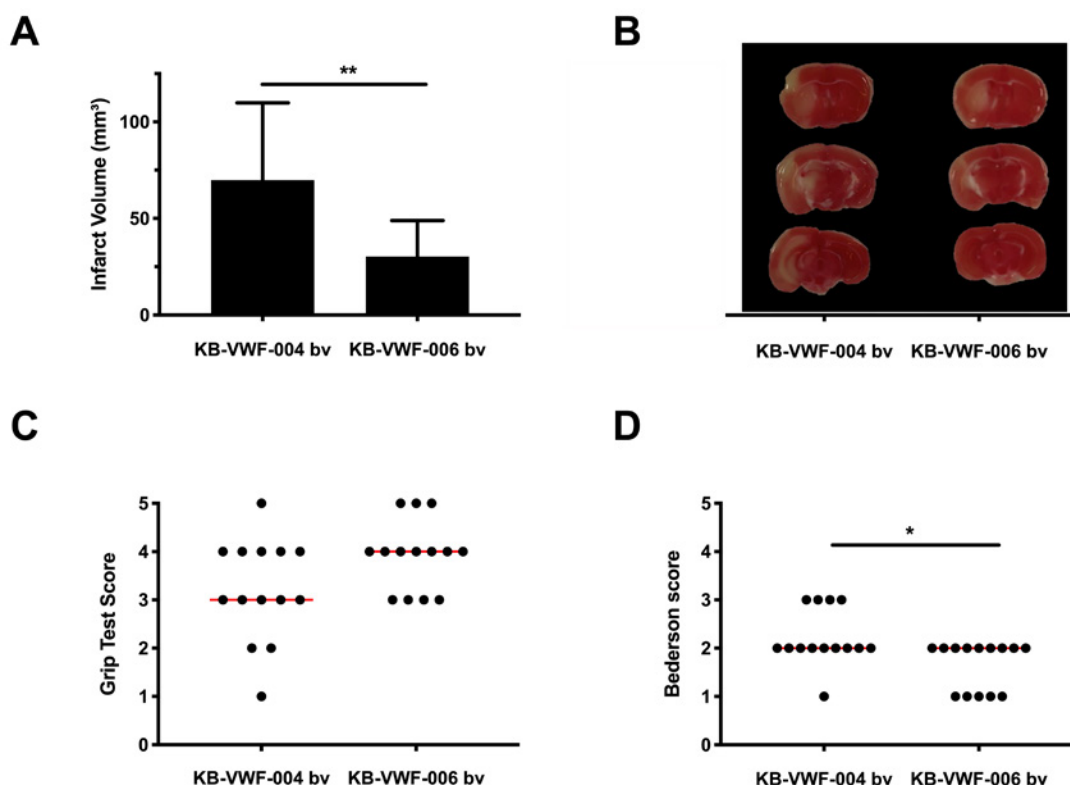

Figure 4: Inhibition of the VWF-A1 domain protects mice from acute ischemic stroke. *Transient focal cerebral ischemia was induced by 60 minutes occlusion of the right middle cerebral artery (tMCAO), followed by 23 hours of reperfusion. Immediately at the start of reperfusion, mice were intravenously treated with 10 mg/kg of either control (KB-VWF-004 bv) or inhibitory anti-VWF A1 nanobody (KB-VWF-006 bv). **A.** Edema-corrected brain infarct volumes were quantified by planimetric analysis 24 hours after stroke. **B.** Representative TTC staining of 3 consecutive brain sections. **C.** Motor function was examined using the grip test. **D.** Neurological outcome 24 h after stroke was assessed using the Bederson test. Data are represented as scatter plots showing all data points and the median value, except for infarct size which is shown as mean ± standard deviation. *, p<0.05; **, p<0.01. (n = 10-11)*
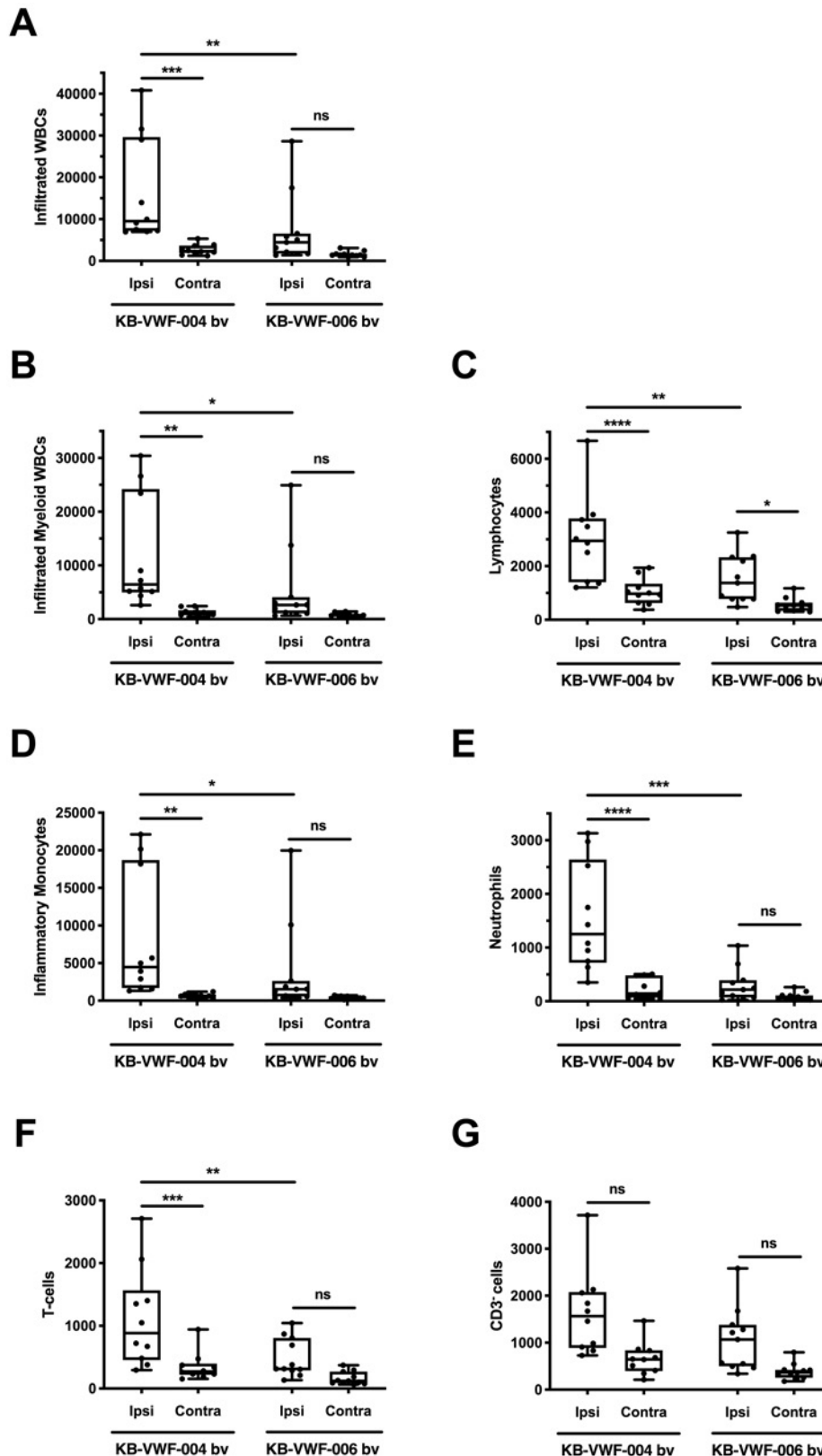
Figure 5: The VWF-A1 domain recruits monocytes, neutrophils and T-cells to the brain after acute ischemic stroke. *Transient focal cerebral ischemia was induced by 60 minutes occlusion of the right middle cerebral artery (tMCAO), followed by 23 hours of reperfusion. Immediately at the start of reperfusion, mice were intravenously treated with 10 mg/kg of either control (KB-VWF-004 bv) or inhibitory anti-VWF A1 nanobody (KB-VWF-006 bv). Twenty-four hours after tMCAO, recruitment of specific subsets of WBC to each hemisphere was determined by flow cytometry. **A.** White blood cells (CD45^{high}). **B.** Myeloid white blood cells (CD45^{high}; CD11b$^+$). **C.** Lymphoid white blood cells (CD45^{high}; CD11b$^-$; CD11c$^-$). **D.** Inflammatory Monocytes (CD45^{high}; CD11b$^+$; Ly6C$^+$; Ly6G$^-$). **E.** Neutrophils (CD45^{high}; CD11b$^+$; Ly6G$^-$). **F.** T-cells (CD45^{high}; CD11b$^-$; CD11c$^-$; CD3e$^+$). **G.** CD3^{neg} lymphocytes (CD45^{high}; CD11b$^-$; CD11c$^-$; CD3e$^-$). * p < 0.05; **, p<0.01; ***: p < 0.005; ****, p<0.001. (n = 10-11)*

OBSERVATION 6: Neutrophil extracellular traps form during cerebral ischemia/reperfusion injury

To examine the formation of neutrophil extracellular traps (NETs) in cerebral ischemia/reperfusion injury in ischemic stroke, we performed an immunofluorescent staining for neutrophils (Ly6G), citrullinated histones (H3Cit) and DNA (DAPI) on brain slices of WT mice subjected to stroke (Figure 6A). NETs could be identified in the ipsilateral brain hemisphere 24 hours post-ischemia (Figure 6B). To quantify these NETs, tile scans were obtained of three different brain sections per mouse (Figure 6C). NET formation mainly occurred in the ipsilateral (affected by stroke) hemisphere and were virtually absent in the contralateral (unaffected) hemisphere (Figure 6D). Moreover, the number of NETs is correlated with the infarct size (Spearman r = 0.8322; p < 0.01; Figure 6E).

To study the temporal characteristics of NET formation, NETs were identified at different timepoints post-ischemia (1 hour, 2 hours, 6 hours, 12 hours, 24 hours, 48 hours) in WT mice subjected to stroke using quantitative immunofluorescence microscopy. Interestingly, quantification of NETs at these different timepoints, revealed that no NETs were present at 1 hour and 2 hours post-ischemia in the affected mouse brain. NETs could be detected in the ipsilateral hemisphere at 6 hours, increased at 12 hours, peak around 24 hours and started to disappear again 48 hours after induction of ischemia (Figure 7).

OBSERVATION 7: NETS are predominantly localized intravascularly

To better understand the involvement of neutrophil extracellular DNA traps in the thrombo-inflammatory processes that contribute to progressive stroke brain damage in the reperfused tissue, NETs (Ly6G, H3Cit, DNA) were visualized together with the brain vasculature (lectin), thereby enabling the visualization of intra- or extravascular NETs. Remarkably, NETs were predominantly localized within the brain vasculature at 12 hours, 24 hours and 48 hours post-ischemia and to a lesser extent in the brain parenchyma (Figure 8). These data suggest that NETs might play a role in secondary microthrombotic events leading to an exacerbation of brain tissue damage after ischemic stroke.
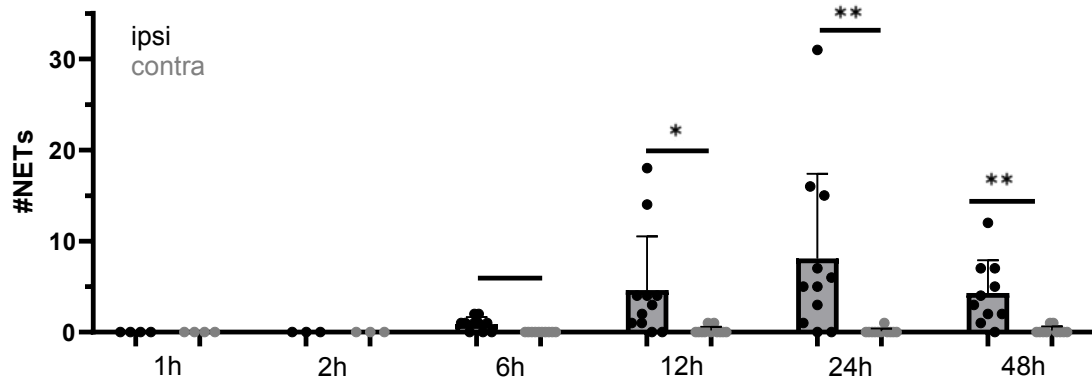
Figure 6: Neutrophil extracellular trap formation in affected mouse brain tissue 24 hours after induction of ischemic stroke. *Transient focal cerebral ischemia was induced by 60 minutes occlusion of the right middle cerebral artery (tMCAO) followed by 23 hours of reperfusion in WT mice. Mouse brains were harvested, and infarct volumes were measured. To identify neutrophil extracellular traps (NETs), an immunofluorescent staining for neutrophils, citrullinated histones and DNA was performed on three brain sections per mouse (A). NETs were visualized via 2D fluorescent microscopy in WT mice, 24 hours after induction of ischemia. Neutrophils (LyG6) are stained in red, citrullinated histones (H3Cit) in green and nuclei (DAPI) are depicted in blue. Scale bars are 10μm (B). To quantify these NETs, tile scans of three different brain sections per mouse were made (C). NETs are indicated with white arrows, showing that NETs were found within the affected hemisphere. The orange rectangle depicts an example of a NET. Magnifications are 40x and 100x. Scale bars are 10μm (C). NET formation (sum of three sections) predominantly occurred in the ipsilateral hemisphere compared to the contralateral hemisphere. Moreover, the mean number of NETs is related to the infarct size of the mouse brain (D).*

Figure 7: Temporal characteristics of neutrophil extracellular trap formation during ischemic stroke. Transient focal cerebral ischemia was induced in wild-type (WT) mice by 60 minutes occlusion of the right middle cerebral artery (tMCAO), followed by reperfusion. At different timepoints postischemia (1 hour, 2 hours, 6 hours, 12 hours, 24 hours and 48 hours), mice brain sections were stained for neutrophils (Ly6G), citrullinated histones (H3Cit) and DNA (DAPI), after which, neutrophil extracellular traps (NETs) were counted as described above. Data are presented as the sum of NETs on three different brain sections per mouse ± standard deviation. No NETs are present in the ischemic mouse brain at 1 hour and 2 hours postischemia. NETs were detected in the ipsilateral hemisphere at 6 hours after induction of ischemia, increased at 12 hours, peak around 24 hours and start to decrease again at 48 hours postischemia (*: p < 0,05; ** p<0,01).
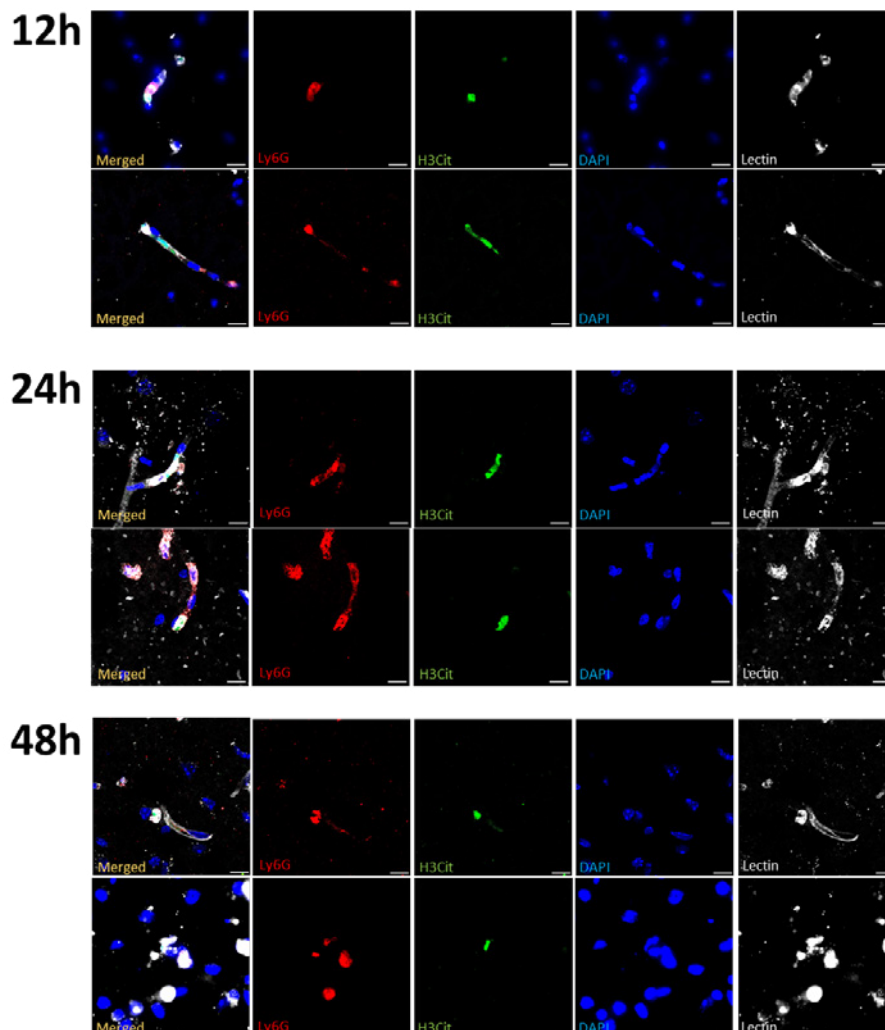

Figure 8: Immunofluorescent visualization of intravascular neutrophil extracellular traps in cerebral ischemia/reperfusion injury in ischemic stroke. Transient focal cerebral ischemia was induced in wild-type (WT) mice by 60 minutes occlusion of the right middle cerebral artery (tMCAO), followed by reperfusion. At different timepoints postischemia (12 hours, 24 hours and 48 hours), mice brain sections were stained for neutrophils (Ly6G, red), citrullinated histones (H3Cit, green), DNA (DAPI, blue) and brain vasculature (lectin, white). Two-dimensional fluorescent images of intravascular neutrophil extracellular traps (NETs) are shown at 12 hours, 24 hours and 48 hours postischemia. Scale bars are 10μm.

OBSERVATION 8: Deficiency of VWF is associated with significantly reduced formation of NETs in the ischemic brain

Given the central role of VWF in cerebral ischemia/reperfusion injury in ischemic stroke, further unraveling of the VWF-neutrophil interaction would give more insights into thrombo-inflammatory processes contributing to the aggravation of stroke brain injury. To investigate the potential regulation of NETosis by VWF, brain sections of VWF WT and littermate KO mice subjected to stroke were stained for the presence of NETs (Ly6G, H3Cit, DNA), after which, NETs were quantified in three different brain sections per mouse (Figure 9). A significantly reduced cerebral infarct was observed in VWF KO mice compared to VWF WT mice, 24 hours postischemia (p<0.05, data not shown). NETs were visualized in VWF WT and littermate KO mice 24 hours after induction of ischemia (Figure 9A-B). Strikingly, quantification of these NETs revealed that a significantly lower number of NETs was present in VWF KO mice compared to WT mice 24 hours post-ischemia (p < 0.001, figure 9C). To confirm that NET formation was not merely a consequence of the larger infarct sizes observed in VWF WT mice, the number of NETs was normalized for the infarct size of the mouse brain. After normalization, a significant decrease in NET formation was still identified in VWF KO mice compared to WT mice 24 hours post-ischemia (p<0.01, figure 9D). Hence these data suggest that VWF promotes the formation of NETs in the ischemic brain, most likely by recruiting neutrophils to the vascular wall of the ischemic brain.

OBSERVATION 9: Deficiency of VWF is associated with lower blood brain barrier permeability after ischemic stroke

To examine whether VWF mediates BBB disruption in ischemic stroke, WT and littermate VWF KO mice were subjected to a transient occlusion of the MCA, followed by 23 hours of reperfusion. One hour prior to euthanasia, mice were intravenously injected with 4mg/kg EBD. Following transcardial perfusion, mouse brains were harvested and subsequently divided into an ipsilateral and contralateral part, after which leakage of EBD was determined based on a standard curve. Extravasation of EBD was observed in all affected brain hemispheres and was as good as absent in the unaffected contralateral hemispheres (Figure 10). This increase in EBD leakage in the affected hemispheres is specific for ischemic conditions, as no leakage was observed in sham-operated mice (not shown). Interestingly, the amount of EBD found in the affected hemisphere of WT mice (1.69 + 1.13 µg/g) 24 hours poststroke was nearly double the amount of EBD observed in VWF KO mice (0.92 + 0.70 µg/g), indicating a significantly increased dysfunctional BBB in VWF WT mice (p=0.0431) (Figure 10). As a control, we also assessed the presence of EBD in mice not subjected to surgery and no difference in leakage of EBD into the brain was observed in both hemispheres of WT and VWF KO mice in these control experiments (not shown). Our results indicate that VWF may play a role for VWF in the disruption of the BBB during cerebral ischemia and reperfusion. This opens up opportunities for further research on how VWF can control BBB permeability and the possibility of targeting VWF to preserve BBB stability.
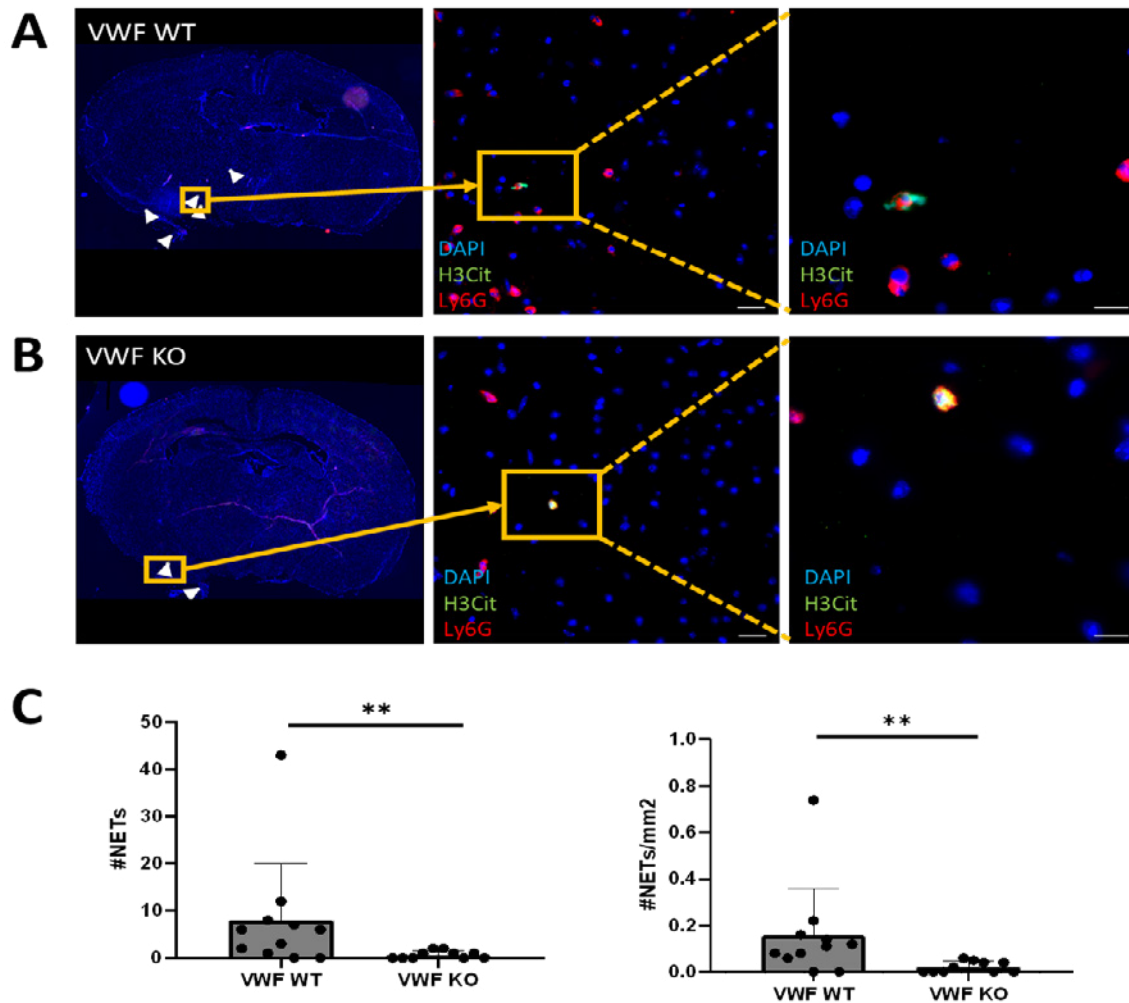
Figure 9: Deficiency of VWF is associated with significantly reduced formation of NETs in the ischemic brain. Transient focal cerebral ischemia was induced in wild-type (WT) and littermate VWF-knockout (KO) mice by 60 minutes occlusion of the right middle cerebral artery (tMCAO), followed by 23 hours of reperfusion. Mice brain sections were stained for neutrophils (Ly6G, red), citrullinated histones (H3Cit, green) and DNA (DAPI, blue). NETs were quantified afterwards in three different brain sections per mouse. A. Representative tile scan of a VWF WT mouse with white arrows pointing towards NETs. Two-dimensional fluorescent pictures (40x, 100x) of a NET found within the infarct core. Scale bars are 20μm (40x) and 10μm (100x). B. Representative tile scan of a VWF KO mouse with white arrows pointing towards NETs. Two-dimensionam fluorescent pictures (40x, 100x) of a NET found within the infarct core. Scale bars are 20μm (40x) and 10μm (100x). C. A Significant lower number of NETs was observed in VWF KO mice compared to WT mice 24 hours post-ischemia (p < 0.01). D. Number of NETs corrected for infarct size was also significantly lower in VWF KO mice compared to VWF WT mice 24 hours after induction of ischemia (p < 0.01).
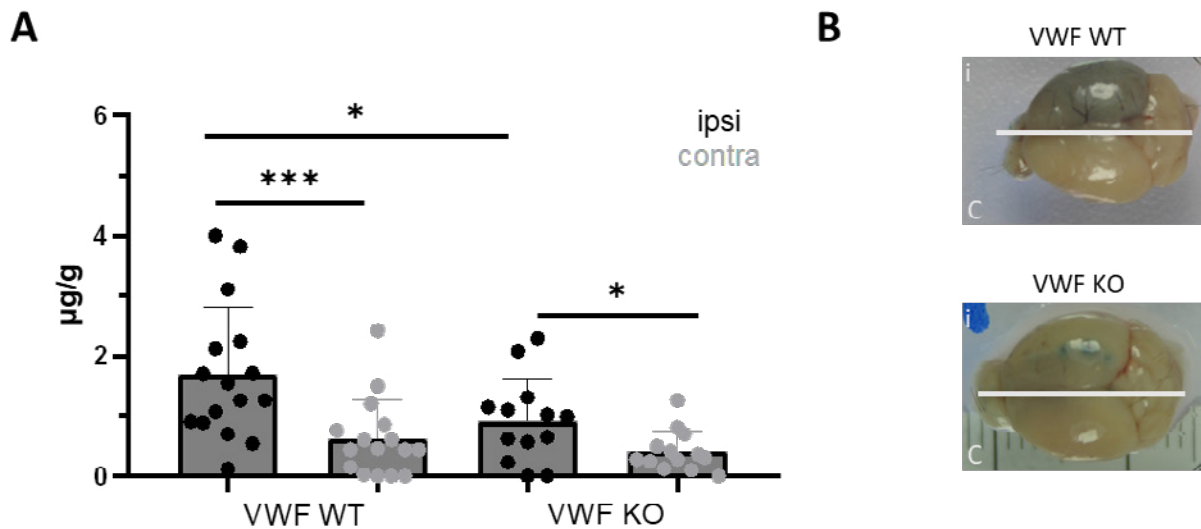
Figure 10: The absence of von Willebrand factor decreases blood-brain barrier permeability poststroke. *Transient focal cerebral ischemia was induced in wild-type (WT) and littermate VWF-knockout (KO) mice by 60 minutes occlusion of the right middle cerebral artery (tMCAO), followed by 23 hours of reperfusion. The extent of blood-brain barrier (BBB) disruption was assessed via the leakage of Evans blue dye (EBD) into the ischemic mouse brain and expressed as µg EBD/g mouse brain tissue. (A) Leakage of EBD could be observed in the affected hemispheres (black dots) of both WT and VWF KO mice compared to the unaffected contralateral hemispheres (grey dots) 24 hours poststroke. The ischemic ipsilateral hemispheres of WT mice were significantly more permeable to EBD compared to those of VWF KO mice . (B) Representative pictures of a WT and VWF KO mouse brain, 24 hours after induction of cerebral ischemia, showing a leakage of EBD into the affected ipsilateral (i) hemisphere, but not in the contralateral hemisphere (c).(WT: n=16, VWF KO: n=13) (*p<0.05, ***p<0.001)*

WP 2: 3D-microscopy to map VWF-mediated thrombo-inflammation in the brain

A light sheet microscope was installed November 2023. 3D-analyses of the mouse brain after stroke are currently ongoing.

2. Output

2.1. Papers with GSKE acknowledgement (2020-2023):

– Dewilde M, Desender L, Tersteeg C, Vanhoorelbeke K, De Meyer SF, Spatiotemporal profile of neutrophil extracellular trap formation in a mouse model of ischemic stroke, RESEARCH AND PRACTICE IN THROMBOSIS AND HAEMOSTASIS,2023 – in press (Impact factor: 5.95)

– Staessens, S., Moussa, M.D., Pierache, A., Rauch, A., Rousse, N., Boulleaux, E., Ung, A., Desender, L., Pradines, B., Vincentelli, A., Mercier, O., Labreuche, J., Duhamel, A., Van Belle, E., Vincent, F., Dupont, A., Vanhoorelbeke, K., Corseaux, D., De Meyer, S.F., Susen, S. with Susen, S. (corresp. author) (2022). Thrombus formation during ECMO: Insights from a detailed histological analysis of thrombus composition. JOURNAL OF THROMBOSIS AND HAEMOSTASIS, 20 (9), 2058-2069. (Impact factor: 16.04)

– Aspegren, O., Staessens, S., Vandelanotte, S., Desender, L., Cordonnier, C., Puy, L., Bricout, N., De Meyer, S.F., Andersson, T., Arnberg, F. with Aspegren, O. (corresp. author) (2022). Unusual Histopathological Findings in Mechanically Removed Stroke Thrombi - A Multicenter Experience. FRONTIERS IN NEUROLOGY, 13, Art.No. ARTN 846293. (Impact factor: 4.09)

– De De Meyer, S.F., Langhauser, F., Haupeltshofer, S., Kleinschnitz, C., Casas, A. with Casas, A. (corresp. author) (2022). Thromboinflammation in Brain Ischemia: Recent Updates and Future Perspectives. STROKE, 53 (5), 1487-1499. (Impact factor: 10.17)

– Staessens, S., Francois, O., Brinjikji, W., Doyle, K.M., Vanacker, P., Andersson, T., De Meyer, S.F. (2021). Studying Stroke Thrombus Composition After Thrombectomy What Can We Learn? *STROKE*, *52* (11), 3718-3727. (Impact factor: 10.17)

– Siddiqui, A.H., Waqas, M., Brinjikji, W., De Meyer, S.F., Doyle, K., Fiehler, J., Hacke, W., Hanel, R.A., Jovin, T.G., Liebeskind, D.S., Yoo, A.J., Zaidat, O.O., Andersson, T., Nogueira, R.G. (2021). Embotrap Extraction & Clot Evaluation & Lesion Evaluation for NeuroThrombectomy (EXCELLENT) Registry design and methods. *JOURNAL OF NEUROINTERVENTIONAL SURGERY*. (Impact factor: 8.57)

– Boodt, N., van Schauburg, P.R W S., Hund, H.M., Fereidoonnezhad, B., McGarry, J.P., Akyildiz, A.C., van Es, A.C G M., De Meyer, S.F., Dippel, D.W J., Lingsma, H.F., van Beusekom, H.M M., van der Lugt, A., Gijsen, F.J H. (2021). Mechanical Characterization of Thrombi Retrieved With Endovascular Thrombectomy in Patients With Acute Ischemic Stroke. STROKE, 52 (8), 2510-2517. (Impact factor: 10.17)

– Denorme, F., Martinod, K., Vandenbulcke, A., Denis, C.V., Lenting, P.J., Deckmyn, H., Vanhoorelbeke, K., De Meyer, S.F. (2021). The von Willebrand factor A1 domain mediates thromboinflammation, aggravating ischemic stroke outcome in mice. HAEMATOLOGICA, 106 (3), 819-828. (Impact factor: 11.05)

– Staessens, S., Francois, O., Desender, L., Vanacker, P., Dewaele, T., Sciot, R., Vanhoorelbeke, K., Andersson, T., De Meyer, S.F. (2021). Detailed histological analysis of a thrombectomy-resistant ischemic stroke thrombus: a case report. THROMBOSIS JOURNAL, 19 (1), Art.No. ARTN 11 (Impact factor: 5.51)

– Staessens, S., De Meyer, S.F. (2020). Thrombus heterogeneity in ischemic stroke. PLATELETS, 32 (3), 331-339. (Impact factor: 4.24)

– Staessens, S., Denorme, F., François, O., Desender, L., Dewaele, T., Vanacker, P., Deckmyn, H., Vanhoorelbeke, K., Andersson, T., De Meyer, S. (2020). Structural analysis of ischemic stroke thrombi: histological indications for therapy resistance. HAEMATOLOGICA, 105 (2), 498-507. (Impact factor: 11.05) Staessens S, Fitzgerald S, Andersson T, Clarençon F, Denorme F, Gounis MJ, Hacke W, Liebeskind DS, Szikora I, van Es A, Brinjikji W, Doyle KM, **De Meyer SF.** (2020). Histological stroke clot analysis after thrombectomy: Technical aspects and recommendations. *INTERNATIONAL JOURNAL OF STROKE*, 2020 Jul;15(5):467-476 (Impact factor: 6.95)

3.   References

1. De Meyer SF, Denorme F, Langhauser F, et al. Thromboinflammation in Stroke Brain Damage. *Stroke*. 2016;47(4):1165–1172.
2. Mizuma A, You JS, Yenari MA. Targeting Reperfusion Injury in the Age of Mechanical Thrombectomy. *Stroke*. 2018;49(7):1796–1802.
3. De Meyer SF, Stoll G, Wagner DD, Kleinschnitz C. von Willebrand factor: an emerging target in stroke therapy. *Stroke*. 2012;43(2):599–606.
4. Denorme F, De Meyer SF. The VWF-GPIb axis in ischaemic stroke: lessons from animal models. *Thromb. Haemost.* 2016;116(4):597–604.
5. Kleinschnitz C, De Meyer SF, Schwarz T, et al. Deficiency of von Willebrand factor protects mice from ischemic stroke. *Blood*. 2009;113(15):3600–3603.
6. De Meyer SF, Schwarz T, Deckmyn H, et al. Binding of von Willebrand factor to collagen and glycoprotein Ibalpha, but not to glycoprotein IIb/IIIa, contributes to ischemic stroke in mice--brief report. *Arteriosclerosis, Thrombosis, and Vascular Biology*. 2010;30(10):1949–1951.
7. De Meyer SF, Schwarz T, Schatzberg D, Wagner DD. Platelet glycoprotein Ibα is an important mediator of ischemic stroke in mice. *Exp Transl Stroke Med*. 2011;3(1):9.
8. Verhenne S, Denorme F, Libbrecht S, et al. Platelet-derived VWF is not essential for normal thrombosis and hemostasis but fosters ischemic stroke injury in mice. *Blood*. 2015;126(14):1715–1722.
9. Kleinschnitz C, Schwab N, Kraft P, et al. Early detrimental T-cell effects in experimental cerebral ischemia are neither related to adaptive immunity nor thrombus formation. *Blood*. 2010;115(18):3835–3842.
10. Jickling GC, Liu D, Ander BP, et al. Targeting neutrophils in ischemic stroke: translational insights from experimental studies. *J. Cereb. Blood Flow Metab.* 2015;35(6):888–901.
11. Aymé G, Adam F, Legendre P, et al. A Novel Single-Domain Antibody Against von Willebrand Factor A1 Domain Resolves Leukocyte Recruitment and Vascular Leakage During Inflammation-Brief Report. *Arteriosclerosis, Thrombosis, and Vascular Biology*. 2017;37(9):1736–1740.
12. Kleinschnitz C, Pozgajova M, Pham M, et al. Targeting platelets in acute experimental stroke: impact of glycoprotein Ib, VI, and IIb/IIIa blockade on infarct size, functional outcome, and intracranial bleeding. *Circulation*. 2007;115(17):2323–2330.
13. Li T-T, Fan M-L, Hou S-X, et al. A novel snake venom-derived GPIb antagonist, anfibatide, protects mice from acute experimental ischaemic stroke and reperfusion injury. *Br. J. Pharmacol.* 2015;172(15):3904–3916.
14. Scully M, Cataland SR, Peyvandi F, et al. Caplacizumab Treatment for Acquired Thrombotic Thrombocytopenic Purpura. *N. Engl. J. Med.* 2019;380(4):335–346.
15. Scully M, Knöbl P, Kentouche K, et al. Recombinant ADAMTS-13: first-in-human pharmacokinetics and safety in congenital thrombotic thrombocytopenic purpura. *Blood*. 2017;130(19):2055–2063.
16. Denorme F, Martinod K, Vandenbulcke A, et al. The von Willebrand Factor A1 domain mediates thromboinflammation, aggravating ischemic stroke outcome in mice. *Haematologica*. 2020;haematologica, 106 (3), 819-828

Final report of the university research project of

Prof. dr. Lieve Moons &
Lies De Groef, MSc, PhD
Katholieke Universiteit Leuven (KU Leuven)

Prof. dr. Lieve Moons
Head Division Animal Physiology and Neurobiology (APN)
Head RU Neural Circuit Development and Regeneration (http://bio.kuleuven.be/df/LM/)
Department of Biology, KU Leuven
Zoological Institute, Naamsestraat 61, bus 2464
3000 Leuven

Phone: 32-16-32 39 91
E-mail: lieve.moons@kuleuven.be

Lies De Groef, MSc, PhD
Onderzoeksgroep neurale ontwikkeling en regeneratie premonstreit college
Naamsestraat 61 bus 2464 b-
3000 leuven
lies.degroef@kuleuven.be

Oligodendrocytes in Wolfram syndrome: bystanders or partners in crime?

1.   Project aims

Wolfram syndrome (WS) is a rare hereditary disease, causing diabetes, blindness, deafness and other neurological problems in infants and young adults, and results in death around the age of 30 years. WS is mainly caused by autosomal recessive mutations in the *WFS1* gene (and rarely in the *WFS2* gene), that result in loss of function of wolframin (WFS1), an endoplasmatic reticulum (ER) transmembrane glycoprotein. Deficiency of WFS1 has been shown to result in ER stress, dysregulated Ca^{2+} homeostasis and mitochondrial dysfunction, but its exact pathophysiological role(s) remain unknown. Some of the clinical manifestations can be managed, but for its most severe one, the neurodegenerative pathology, there are currently no treatments available, in part due to the limited understanding of the underlying cellular mechanisms. In particular, it is still unclear which cell type(s) to focus on in the CNS (CNS). Neuroscience research in general is increasingly moving away from the neuron-centric approach to neurodegenerative diseases, and it is becoming increasingly clear that –although neurons eventually die– there is a central role for glial cell types in most CNS disorders. Consequently, it is essential to determine which of these cell types is the catalyst of the disease processes leading to WS, so that future therapies can be targeted to this cell type. Recent evidence suggests that the neurodegenerative component of WS could be driven by an oligodendrocyte rather than a neuronal pathology[1]. Remarkably, MRI studies in Wolfram patients found white matter changes and volume loss in different brain regions, most prominently in the brainstem, cerebellum and optic radiations, already early in the disease pathogenesis[2,3]. Combining this with the observation that myelinating oligodendrocytes are especially sensitive to ER stress, we hypothesized that oligodendrocytes play an important role in the neurodegeneration seen in Wolfram patients. Therefore, in this project, we aimed to investigate what the effect of these 'diseased' oligodendrocytes is on the function of 'healthy' neurons, focusing on ER stress, mitochondria and cell metabolism as potential underlying mechanisms. In addition, we studied the interplay between oligodendrocyte/myelin loss and neurodegeneration in a *Wfs1* knockout (KO) mouse model. Originally, we also planned to further unravel the function of the WFS1 protein by identifying its binding partners and aimed to provide evidence that interfering with the studied cellular processes and WFS1 binding partners could rescue the disease phenotype. Here, however, we shifted gears to follow a more novel approach and focused on gene replacement therapy for WS, by investigating the possibility to use base editing of the diseased neural cells.

The concrete goals of this project thus slightly modified and can currently be summarized as follows:

I.   To develop methods to correct *WFS1* mutations by exploring the efficiency of base editing *in vitro* using human pluripotent stem cell (iPSC)-derived non-dividing neural cells, being either neurons or oligodendrocytes.

II.   To study *in vitro* which cellular processes are affected in induced iPSC-derived oligodendroglia from WS patients, thereby focusing on ER stress, mitochondrial function and metabolism; studying the effect of 'diseased' oligodendroglia on wild-type 'healthy' neurons by using 2D neuron-oligodendrocyte coculture on multielectrode arrays, as well as their tendency for neuron myelination by using a 3D iPSC derived neuron-oligodendrocyte coculture model.

III. To study *in vivo* the changes in oligodendrocytes and neurons in a *Wfs1* KO mouse model, to compose a timeline of neuronal *versus* oligodendrocyte pathology and to investigate the possibility to rescue the neurodegenerative WS phenotype in *Wfs1* mutant mice using *in vivo* base editing approaches.

2.   Progress report

During the past three years –and as planned in the original Gantt chart of the proposal– we have been focusing on all envisioned goals. Unfortunately, our studies have been delayed, largely by COVID-19 restrictions, but also because of prolonged medical leaves of both the PhD student and a senior investigator involved in the research. As such, we did not yet publish the data gathered within this GSKE project. We are now preparing a manuscript and foresee a first paper being published by June 2023[4], and two more to follow later. In short, we are finalizing the *in vitro* study of the effects of WFS1 deficiency in iPSC-derived oligodendroglia (WPII-task II.1) and have been setting up a continuation of these experiments in neuron-oligodendrocyte 2D- and 3D- cocultures (WPII-task II.2&3). Furthermore, we have concluded the morphological (WPIII-task III.1) as well as a functional characterization (WPIII-task III.2) of the CNS integrity in *Wfs1* KO mice. Experiments related to the study of the WFS1 binding partners (original WPI) were dropped and instead more resources were invested into the functional characterization of CNS integrity in the *Wfs1* KO mice, as well as in the generation of an additional mouse line, harvesting a patient-specific point mutation and allowing us to test the *in vivo* efficacy of base editing for gene replacement in non-dividing neural cells. We deemed this to be more impactful and more likely to allow us to progress faster to a deeper understanding of the pathological processes underlying WS as well as to develop a therapy to treat the neurodegenerative phenotype in the patients. Of note, the choices for making these changes were based on interactions with the WS community and the explicit question of the WS patient organizations to investigate the potential of CRISPR-base editing as a curative therapy for the neurodegenerative problems in WS children.

Work package I

Homology directed repair following induction of a double strand DNA break by CRISPR/Cas has been the common method for genome editing in monogenic disease, but is inefficient in non-dividing terminally differentiated cells. The recently developed DNA base-editors, including cytosine base-editors (CBEs) and adenine base-editors (ABEs) –although based on CRISPR/Cas building blocks– circumvent this issue and –definitely ABE– have fewer off-target effects than conventional CRISPR/Cas9[5]. The research group of our collaborator Prof. Catherine Verfaillie, and specifically the work of Dr. Arefe Nami (Stem Cell Institute Leuven (SCIL), Dept. Development and Regeneration, KU Leuven), recently demonstrated that ABE is a very efficient tool (>80% of cells edited) to correct point mutations in *WFS1* and other mutant iPSCs, that are still dividing[6]. A first prove that ABEs can also correct mutations in non-dividing neural cells was recently delivered. Indeed, using human iPSC-derived astrocytes[7], we demonstrated that CRISPR base editing can edit 100% of cells when it is stably expressed in the cells for 18 days (Figure 1). To further prove that ABE in non-dividing cells is possible, we are/have been creating post-mitotic retinal ganglion cells and oligodendrocytes from iPSCs from three *WFS1^(Mu/Mu)* patient lines (see below), and will test its efficacy and safety in these cells using an intein-split ABE viral vector[8] to transduce the cells. Patient and isogenic control iPSC cell lines and protocols for iPSC differentiation are available (see below, unpublished information and [7,9]), and the split-intein constructs are ready to use. Correct gene editing will be assessed by sequencing. Off-target genomic loci associated with the specific guide RNAs will be identified by full genome (or exome) sequencing, RNA sequencing and EndoV-seq, a method developed to evaluate ABE off target sites[5]. Finally, we will demonstrate that the WFS1 protein is restored following base editing via Western blot.
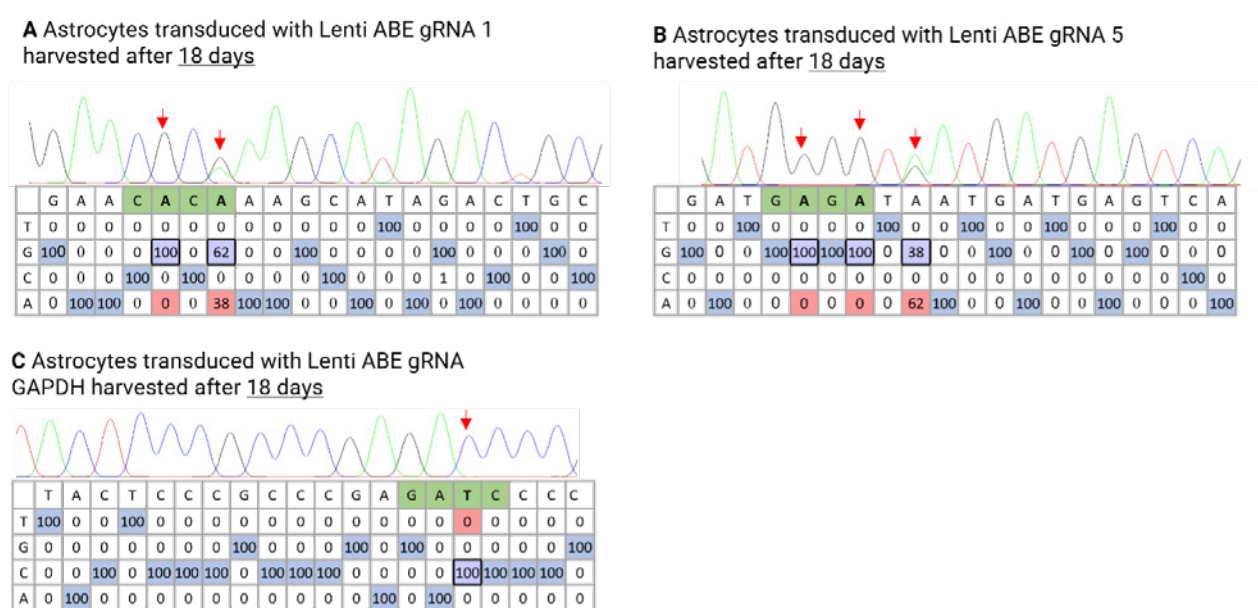
A Astrocytes transduced with Lenti ABE gRNA 1 harvested after 18 days

	G	A	A	C	A	C	A	A	A	G	C	A	T	A	G	A	C	T	G	C
T	0	0	0	0	0	0	0	0	0	0	0	0	0	100	0	0	0	0	100	0
G	100	0	0	0	100	0	62	0	0	100	0	0	0	0	100	0	0	0	100	0
C	0	0	0	100	0	100	0	0	0	0	100	0	0	0	1	0	100	0	0	100
A	0	100	100	0	0	0	38	100	100	0	0	100	0	100	0	100	0	0	0	0

B Astrocytes transduced with Lenti ABE gRNA 5 harvested after 18 days

	G	A	T	G	A	G	A	T	A	A	T	G	A	T	G	A	G	T	C	A
T	0	0	100	0	0	0	0	100	0	0	100	0	0	100	0	0	0	100	0	0
G	100	0	0	100	100	100	100	0	38	0	0	100	0	0	100	0	100	0	0	0
C	0	0	0	0	0	0	0	0	0	0	0	0	0	0	0	0	0	0	100	0
A	0	100	0	0	0	0	0	0	62	100	0	0	100	0	0	100	0	0	0	100

C Astrocytes transduced with Lenti ABE gRNA GAPDH harvested after 18 days

	T	A	C	T	C	C	C	G	C	C	C	G	A	G	A	T	C	C	C
T	100	0	0	100	0	0	0	0	0	0	0	0	0	0	0	0	0	0	0
G	0	0	0	0	0	0	0	100	0	0	0	100	0	100	0	0	0	0	100
C	0	0	100	0	100	100	100	0	100	100	100	0	0	0	0	100	100	100	0
A	0	100	0	0	0	0	0	0	0	0	0	0	100	0	100	0	0	0	0

Figure 1. Base editing in iPSC-derived astrocytes. *After 50 days of differentiation, human iPSC-derived astrocytes were transduced with a lentiviral vector carrying ABE and gRNA targeting Hek site 1[10] (A), Hek site 5[10] (B) or the GAPDH gene (C). Cells were harvested after 18 days, and their DNA was sequenced by Sanger sequencing. Using the Edit R program to analyze Sanger sequencing results, BE was observed in all the target sites. An efficiency of 100% was observed when the target base is at position 5 (A, B and C), an efficiency of 62-100% when the target base is at position 7 (A and B), and even 38% for position 9 (B) –which is outside of activity window and often not amenable to BE. Protospacer adjacent motif (PAM) bases were counted as positions 21-23. Activity windows are shown in green; desired base edits are presented by a purple square with a thick black border; non-edited bases are shown in pink squares; base edits are indicated with red arrows.*

Work package II

Task II.1 *In vitro* study of the effects of WFS1 deficiency in iPSC-derived oligodendroglia

At the start of the project, two WS patient iPSC lines, one isogenic control line and two commercially available control lines were available in house. Using the protocol published by García-León *et al.*[11] these iPSC lines were differentiated into O4+ oligodendrocytes. A first series of experiments with these iPSC-derived oligodendrocytes, however, revealed that differentiation into iPSC is suboptimal. Hence we switched to a newly developed protocol[2] which can subsequently myelinate neurons, both *in vitro* and in vivo. To date, OPCs have been derived from eight different hPSC lines including those derived from patients with spontaneous and familial forms of MS and ALS, respectively. hPSCs, fated for 8 d toward neural progenitors, are transduced with an inducible lentiviral vector encoding for SOX10. The addition of doxycycline for 10 d results in >60% of cells being O4-expressing OPCs, of which 20% co-express the mature OL marker myelin basic protein (MBP that uses genome engineering to deliver SOX10, the 'master' transcriptional regulator of the oligodendrocyte lineage, to iPSCs. We found that iPSC-derived oligodendrocytes from this protocol show a better morphology, survival and tremendously increased oligodendrocyte maturation. Therefore, three *WFS1^Mu/Mu* patient and three control isogenic iPSC lines were genome engineered according to this protocol, using adenine base editing.

These engineered iPSC lines were next differentiated into oligodendrocytes, which were then further characterized to study *in vitro* the pathological processes that have been linked to WS. A first series of experiments using two of the three pairs of iPSC lines shows that patient iPSC-derived oligodendrocytes are more vulnerable to tunicamycin- or thapsigargin-induced ER stress compared to controls, as evident from qPCR for C/-EBP homologous protein (CHOP) (Figure 2A), an X-box binding protein 1 (XBP1) splicing assay (Figure 2B), and Western blot for Binding immunoglobulin protein (BiP) (Figure 2C). RNA sequencing of these cell lines revealed many differentially expressed genes in Wolfram patient-derived oligodendrocytes vs their corresponding isogenic cells (Figure 2D-E) with a higher number of transcripts per

unit of markers related to ER stress and unfolded protein response pathway in the diseased oligodendrocytes (Figure 2F). In addition, we also observed signs of metabolic abnormalities linked to mitochondrial dysfunction in the patient iPSC-derived oligodendrocytes compared to isogenic controls, namely reduced mitochondrial respiration (Figure 2G-H) and mitochondrial membrane depolarization (Figure 2I). Finally, Western blot for Monocarboxylate transporter 1 (MCT1) pointed towards dysfunction of the metabolic coupling of oligodendrocytes with axons in cells derived from Wolfram patients (Figure 2J).
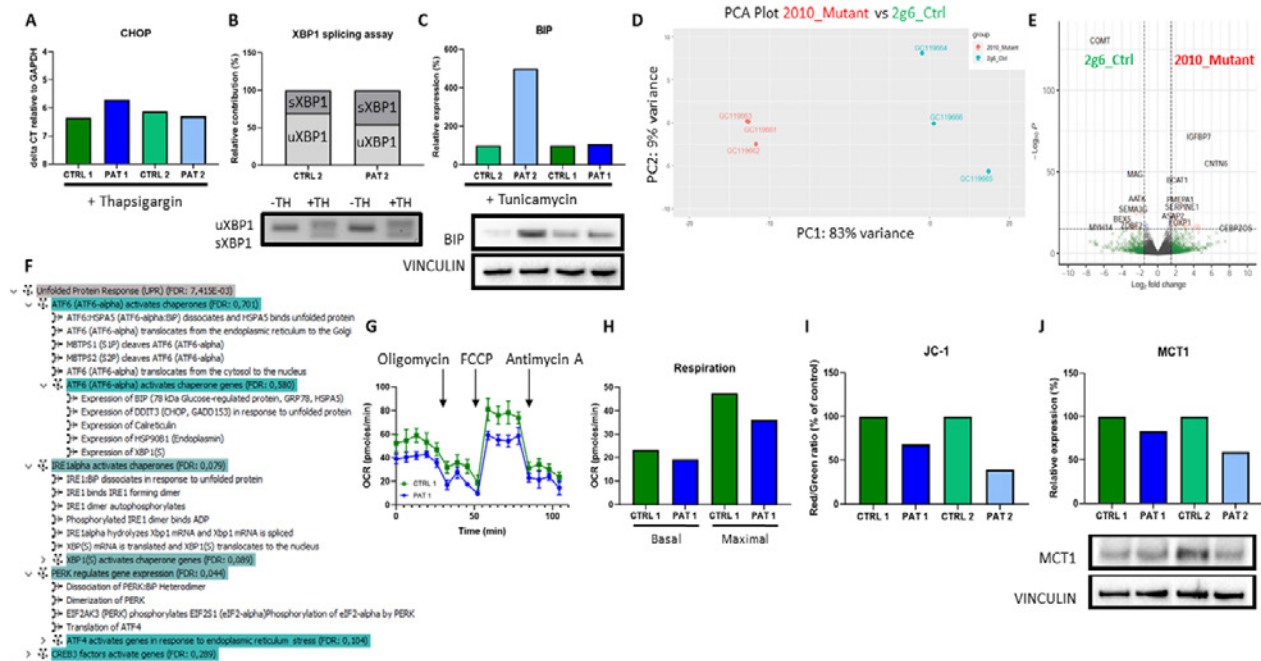
Figure 2. iPSC-derived oligodendrocytes from Wolfram patients are more vulnerable to ER stress, mitochondrial and metabolic dysfunction. (A-C) ER stress assays for different ER stress markers, including qPCR for CHOP (A), a splicing assay and western blot of XBP1 (B), and qPCR and Western blot for BiP (C), suggest that iPSC-derived oligodendrocytes from Wolfram patients are more vulnerable to tunicamycin- or thapsigargin-induced ER stress compared to isogenic controls. (D, E) PCA and volcano plots for differentially expressed genes for Wolfram patient-derived oligodendrocytes (in red) vs their corresponding isogenic cells (in green), (F) A high number of transcripts per unit of markers related to ER stress and unfolded protein response pathway confirm more vulnerability of Wolfram patient oligodendrocyte to ER stress. (G-I) Mitochondrial dysfunction was observed in iPSC-derived oligodendrocytes from Wolfram patients. Seahorse analysis of the oxygen consumption rate in these cells showed reduced mitochondrial respiration (G-H) and staining with the mitochondrial membrane potential probe JC-1 revealed mitochondrial membrane depolarization in patient iPSC-derived oligodendrocytes compared to isogenic controls (I). (J) Reduced expression of MCT1 by patient iPSC-derived oligodendrocytes, as evident from Western blot analysis, suggests that the metabolic coupling of these cells with axons may be compromised. PAT & CTRL: Wolfram patient-derived & isogenic control cell lines.

Altogether these data suggest that iPSC-derived oligodendrocytes from WS patients may be more vulnerable to ER stress and display signs of mitochondrial dysfunction. This, together with their seemingly reduced capacity to transfer metabolites and thereby support axons, suggests that oligodendrocyte dysfunction may, at least partially, be underlying the neurodegenerative component of WS. Replicate experiments and additional studies are ongoing to confirm these findings. Unfortunately, the PhD student, Marjan Vandenabeele (paid by an FWO PhD fellowship; supervisors L. Moons, L. De Groef & C. Verfaillie), decided to stop her PhD training, and left the team end of January 2022. The studies have been on hold for a while but were taken over recently by another PhD student, Karan Ahuja (FWO SB PhD fellowship; supervisors L. Moons, L. De Groef & C. Verfaillie).

Task II.2. *In vitro* study of WFS1 deficiency in iPSC-derived 2D cocultures of oligodendroglia and neurons

As our findings point towards a crucial role for non-neuronal cells (i.e., oligodendrocytes, but maybe also other glial cells) in the neurodegeneration phenotype of WS patients (and animal models), we believe that it is essential to elucidate the role of oligodendrocytes *versus* neurons, and even *versus* astrocytes, in this disease. Thereto, we have created a 2D bi-/tri- coculture system containing hiPSCs derived Dual SMAD cortical neurons, astrocytes and oligodendrocytes (Figure 3A). We have accessed this coculture system by multi-electrode array to determine the effect of glial cells (astrocytes/oligodendrocytes or both) on maturation of cortical neurons in terms of their functional output/electrophysiology. Primarily, we found that the presence of glial cells, especially oligodendrocytes, enhances the electrophysiological property of Dual SMAD cortical neurons even in shorter culture duration (from week 4-5 onwards) (Figure 3B). Therefore, we are currently using a neuron-oligodendrocyte bi-culture system to check the effect of *WFS1* oligodendrocytes on healthy cortical neurons in comparison to their corresponding isogenic lines.
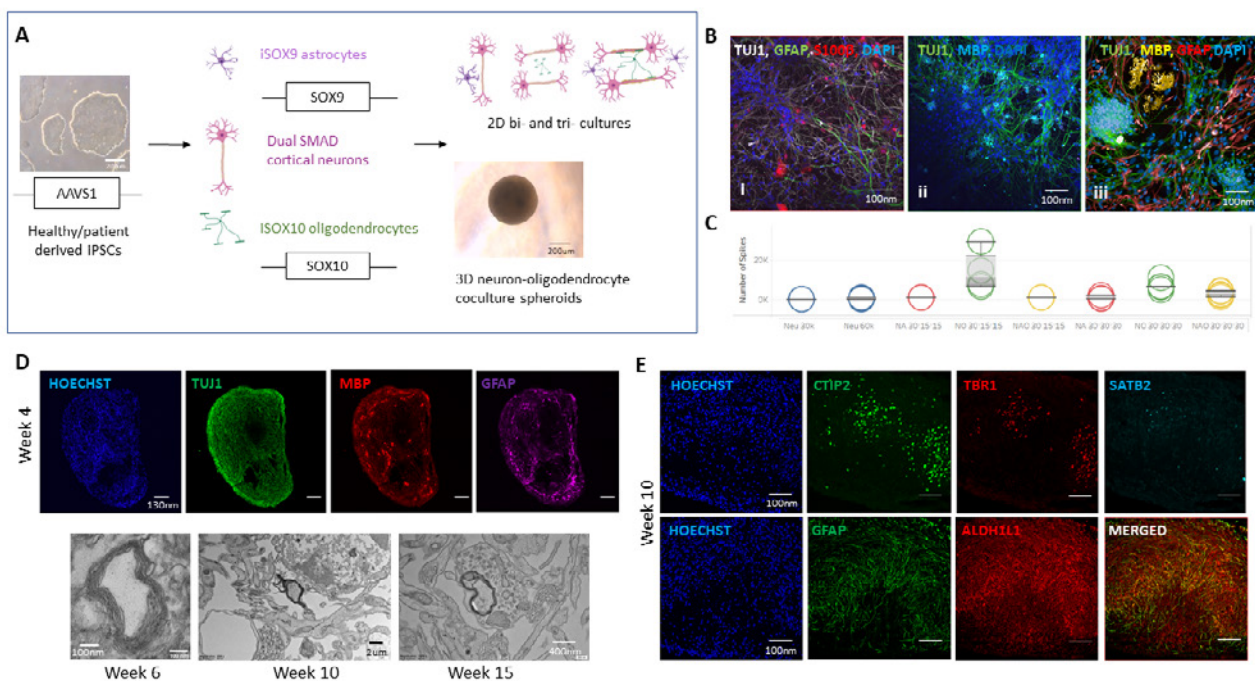
Figure 3. Glial cells promote maturation and myelination of neurons in human iPSC derived 2D and 3D neuron-glia cocultures. (A) Schematic representation for the development of *in vitro* 2D neuron-astrocyte and/or oligodendrocyte bi- and tri-cultures; and 3D neuron-oligodendrocyte coculture model from control and patient derived iPSCs. (B) Representative fluorescent images of 2D neuron-astrocyte coculture (TUJ1+ neurons, GFAP+ and S100β+ astrocytes (i)); neuron-oligodendrocyte coculture (TUJ1+ neurons and MBP+ oligodendrocytes (ii)) and neuron-astrocyte-oligodendrocyte triculture (TUJ1+ neurons, MBP+ oligodendrocytes and GFAP+ astrocytes (iii)). (C) Improvement in neuron electrophysiology (MEA system) of neurons in presence of astrocytes and/or oligodendrocytes compared to neuron monoculture. (D-E) Representative fluorescence images of 3D neuron-oligodendrocytes spheroid cryosections (30 μm): Four-week old spheroid cryosections after immunostaining for TUJ1 (green), MBP (red) and GFAP (violet) scale bars = 200 μm (D(i)); and electron microscopic images of 6-, 10- and 15-weeks old 3D neuron-oligodendrocytes spheroid showing myelinated axons (D(ii)). Ten-week old 3D neuron-oligodendrocyte spheroid cryosections showing the presence of cortical neuron markers CTIP2 (green), TBR1 (red), and SATB2 (light blue) (E(i)); and astrocytes markers GFAP (green), ALDH1L1 (red) (E(ii)). Data by Karan Ahuja, in collaboration with Prof. C. Verfaillie (SCIL, KU Leuven).

Task II.3.: *In vitro* study of WFS1 deficiency on neuron myelination using a human iPSC derived 3D neuron-oligodendrocyte coculture model.

As the main functions of oligodendrocytes are to support neuron growth and facilitating their action potential conduction by myelinating their axons; investigating the role of *WFS1* deficiency on neuron myelination is crucial. We have developed a 3D neuron-oligodendrocyte coculture

model consisting of human iPSC derived cortical neurons and oligodendrocytes and have shown the presence of myelinated axons (Figure 3 C,D). Oligodendrocytes in this system started forming loose myelin sheaths from week 6 on, that later got compacted from week 10-15. Of note, such myelination can only be seen in conventional brain organoids after more than 150-200 days in culture[12]. In long term cultures of these 3D neuron-oligodendrocyte coculture spheroids (week 12-15), also the presence of neurons with different cortical layer markers (*CTIP2, TBR1 and SATB2*) and astrocytes (ALDH1L1+ and GFAP+) have been confirmed (Figure 3E). Therefore, we believe that the 3D neuron-oligodendrocyte coculture model can be used to study the effect of *WFS1* mutant oligodendrocytes on neuron-glia interactions. To test this hypothesis, experiments including electron microscopy and transcriptomics are currently being performed. Funding to support these latter tasks has been secured (FWO SB PhD fellowship to Karan Ahuja).

Work package III

Task III.1&2. Morphological and functional characterization of CNS integrity in Wfs1 KO mice

Within WP III, we have been characterizing the neurodegenerative phenotype of the *Wfs1Δexon8* deletion (*Wfs1* KO) mouse[13]. The eye, optic nerve and brain phenotype of *Wfs1* KO mice and corresponding wild-type (WT) littermates was studied at 3, 4.5, 6 and 7.5 months of age, largely using previously established technologies[14-17].

We first characterized the ocular phenotype of the Wfs1 KO animals. Even at 7.5 months of age, no overt structural thinning of retinal layers, probed with non-invasive OCT imaging, was apparent (data not shown). This suggests that, at least on a structural level, synapse and cell density are maintained. We next studied structural changes of RGC somas and axons on a single cell level. In accordance, counts on retinal wholemounts after immunohistochemistry with the pan-RGC marker, RPBMS revealed no changes in RGC density and quantitative analysis of EM images of optic nerve transections did not reveal loss of RGC axons (see below, Figure 5). Subsequent functional analysis, however, revealed that *Wfs1* KO mice display abnormal electrophysiological responses of their retinal ganglion cells and reduced action potential conduction in the optic nerve, from respectively 3 and 4,5 months of age on (Figure 4A,B). They also show reduced visual acuity from 6 months on, with even a diminished contrast sensitivity from 3 months of age (Figure 4C,D). These functional deficits are accompanied by both gliosis and neuroinflammation in retina and optic nerve, as apparent from increased expression levels of glial fibrillary acidic protein (GFAP), S100 calcium-binding protein B (S100B) and Ionized calcium binding adaptor molecule 1 (IBA1) in mice of all ages, determined by both immunohistochemistry and western blotting (data not shown). All in all, these data clearly show that functional and glial cell alterations precede structural neuronal changes.
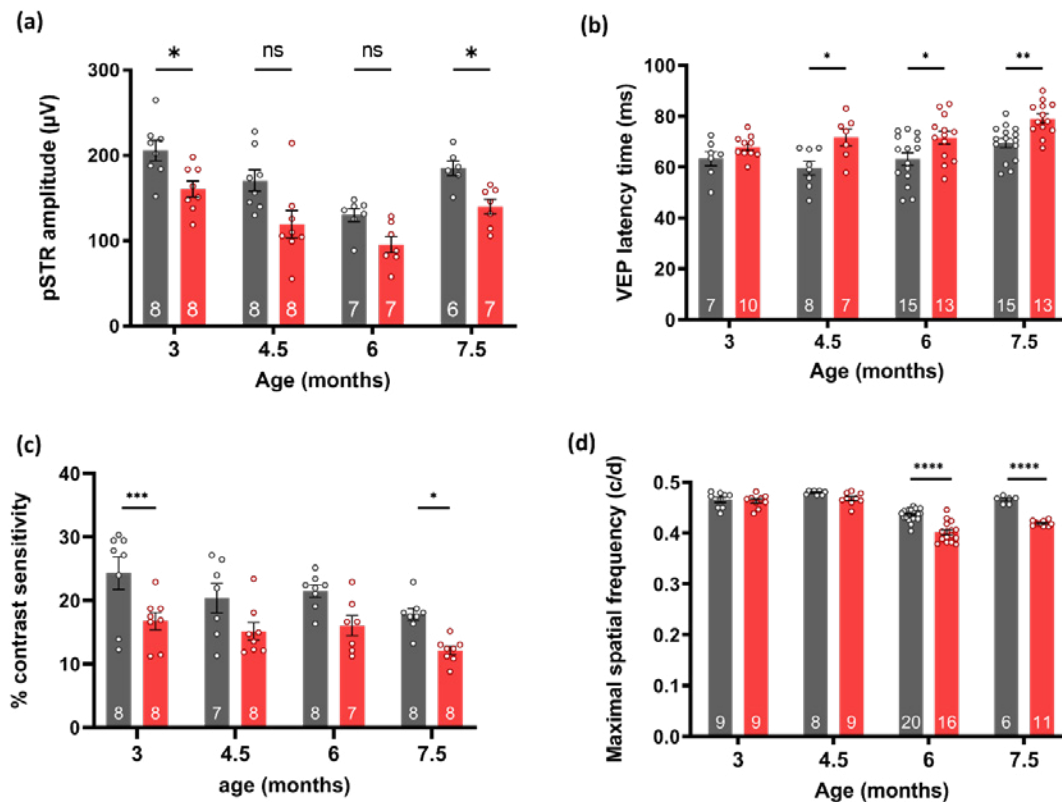
Figure 4. Functional deficits are apparent in the visual system of the Wfs1 KO model. (*A*) *The amplitude of the pSTR was significantly lower in the KO animals as compared to age-matched WT mice at all ages examined. (B) Axonal conduction, as measured by VEP latency, was slower in KO mice from 4,5 months on. (C-D) Probing post-retinal processing revealed that contrast sensitivity was declined in KO mice, already at young age (C), and visual acuity, as measured by maximal spatial frequency, was diminished from 6 months on (D), all as compared to littermate controls. Two-way ANOVA, Sidak's post-hoc test; *, $p<0.05$; **, $p<0.01$; ***, $p<0.001$; ****, $p<0.0001$; the number of biological repeats/mice is included in the graphic. WT mice: black bars; Wfs1 KO mice: red bars.*

Since these functional abnormalities point to optic nerve atrophy, and given the defects seen in oligodendrocytes derived from Wolfram patients in our *in vitro* work (*cfr.* above), we further investigated the optic nerve of *Wfs1* KO mice via transmission electron microscopy (in collaboration with Prof. E. Wolfs, U Hasselt). We were able to find an accelerated appearance of subtle signs of degradation in *Wfs1* KO mice over time (data not shown). This coincided with a higher g-ratio in the nerve of *Wfs1* KO animals at 7,5 months of age, probably due to degeneration of the myelin sheet. However, no difference was noted in myelin coverage or white space (Figure 5A-C, data shown for 7,5 months of age only). The g-ratio and percentage myelin coverage specifically inform us about the myelin sheet thickness relative to the axon diameter and total myelin differences between *Wfs1* KO and wild-type animals. As both myelination and metabolic support are depending on axonal activity, we also looked at axonal parameters. We did not observe differences in axon density or inner axon diameter between the genotypes at any age studied (Figure 5D-F).

Next, we evaluated the overall number of cells of the oligodendroglial lineage, and performed immunostainings for oligodendrocytes and oligodendrocyte precursor cells. However, cell counting of mature oligodendrocytes, all oligodendrocytes and oligodendrocyte precursors, using immunolabelings for respectively CC1, Olig2 and Pdgfra, only showed a reduced number of oligodendrocyte precursor cells in the optic nerve of 6 and 7,5-month-old *Wfs1* KO mice (data shown for 7,5 months-old mice only, Figure 6). Still, no difference was seen in the number of oligodendrocytes at that age and Western blots on optic nerve samples of mice at 7,5 months of age revealed no differences in the expression of the myelin component MBP (data not shown).
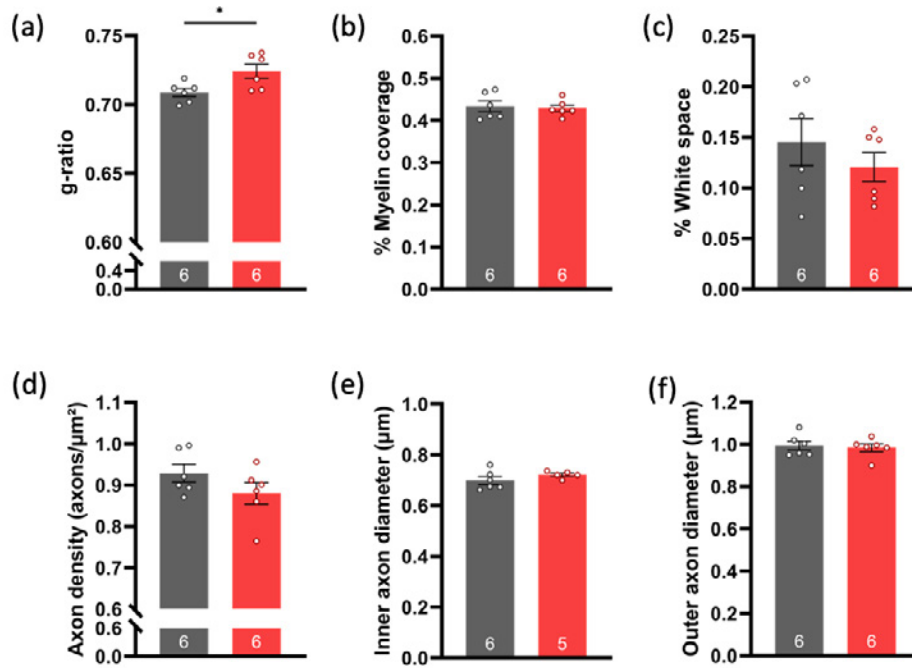
Figure 5: Structural analysis of axonal integrity in the optic nerve shows a higher g-ratio and thus a thinner myelin sheet of RGC axons in Wfs1 KO mice at 7.5 months of age. (A-F) Electron microscopic images were made of optic nerves of 7.5 months of age. Four images were analyzed per optic nerve, from which the mean value was obtained for the analysis of each parameter. A significant higher g-ratio (A) was found for Wfs1 KO optic nerve axons, meaning that they have a thinner myelin sheet compared to wild-type axons at that age. The myelin coverage (B) and white space (C) were found to be similar for Wfs1 KO and wild-type optic nerves. Also, the axon density (D) did not differ between optic nerves of wild-type and Wfs1 KO mice at 7.5 months of age, neither did the inner (without myelin sheet) (E) and outer (with myelin sheet) (F) axon diameter. Statistical significance was tested with an unpaired student t-test; data are illustrated as mean + SEM; * = $p < 0.05$; the number of biological repeats is indicated in the graphs. WT mice: black bars; Wfs1 KO mice: red bars.
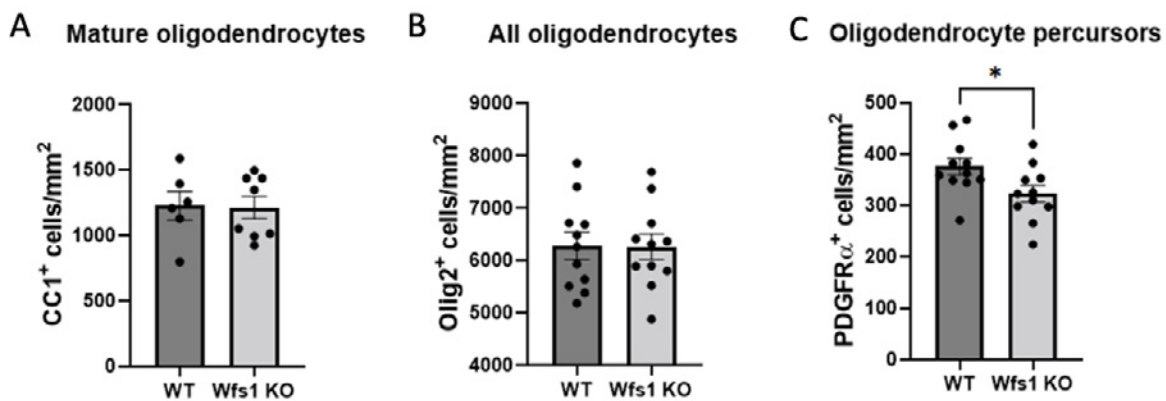
Figure 6: Quantification of oligodendrocyte lineage cells point to oligodendrocyte abnormalities in Wfs1 KO mice at 7.5 months of age. *Cell countings on immunohistologically stained longitudinal sections of the optic nerve of 7.5-month-old animals disclosed equal cell numbers for mature (A) and all (B) oligodendrocytes yet a reduced number of oligodendrocyte precursor cells (C) in Wfs1 KO mice. Statistical significance was tested with an unpaired student t-test; data are illustrated as mean + SEM; * = $p < 0.05$.*

In a next step, we tried to determine the underlying molecular mechanisms. First, we were able to show ER stress in both the retina and optic nerve using Western blotting for the early and late ER stress markers BIP and CHOP respectively in mice of 7.5 months old (data not shown). Western blots on optic nerve samples of mice at 7.5 months of age, however, did not reveal differences in the expression of the MCT1 oligodendrocyte lactate transporter between genotypes. Nevertheless, although these first pilot experiments failed to show a different expression of metabolic transporter MCT1 in optic nerves of *Wfs1* KO mice, we can for now not exclude problems or changes in metabolic support of oligodendrocytes towards axons in *Wfs1*

KO mice. Further studies in both retina and optic nerve are ongoing.

In summary, our results point towards problems with the oligodendrocyte cell lineage, leading to a decreased OPC number, a thinner myelin sheet and more signs of axon degradation in the *Wfs*1 KO animals. Based on these data it is tempting to speculate that the white matter changes and neuron loss observed in WS patients is at least partly caused by problems with the supportive functions of oligodendrocytes: signal transduction via myelination and metabolic support of axons.

Finally, to confirm the above findings, zoom in on the brain phenotype and expand our analysis to other brain regions, we assessed the neurodegeneration phenotype of the *Wfs1* KO mouse via magnetic resonance imaging (MRI) (in collaboration with Prof. U. Himmelreich, moSAIC, KU Leuven). Anatomical, T2-weighted and diffusion tensor images, as well as manganese-enhanced MRI images, were collected at 3, 4.5, 6 and 7.5 months of age in *Wfs1* KO and WT mice (Figure 7). Analysis reveals that the total brain volume as well as the volume of several brain regions is reduced, including the cerebellum and brainstem (Figure 7A, B, C) – regions also affected in Wolfram patients –, pointing towards neurodegeneration. Furthermore, manganese-enhanced MRI scans show that the diameter of the optic nerve is reduced (Figure 5D) and that the innervated area in the superior colliculus (*i.e.* where the optic nerve axons synapse) is smaller (Figure 5E). Notably, the corpus callosum, which is almost entirely made up by white matter, is also reduced in the Wfs1 KO mice (Figure 7F). In addition, we also observed changes in the apparent diffusion coefficient in several of these regions (data not shown). Analyses of the fractional anisotropy are currently being performed to elucidate whether these structural changes may reflect changes in myelination. Notably, ongoing analyses investigating brain inflammation, BIP/CHOP and MCT1 expression, etc., already point out that what we see in the eye also reflects pathological signs in the brain, indicating that the eye can be seen as a window to the brain.

In conclusion, a pathological phenotype was observed in the retina, optic nerve and brain of *Wfs1* KO mice. This phenotype comprises axonal degeneration, neuronal dysfunction, neuroinflammation and oligodendrocyte abnormalities. These findings are now being prepared for publication[4]. While we originally planned to use this settled *Wfs1* KO phenotype, the established timeline and read-outs to next evaluate the effect of a disease-modifying therapy (original task III.3), we face the problem that this mouse model harbors a full deletion of exon 8, and cannot be used for testing the *in vivo* efficiency and safety of base editing therapy in WS, the more novel approach we shifted to. Thereto, we started with the (generation) and phenotyping of novel transgenic knock-in mice with point mutations that have been found in WS patients.
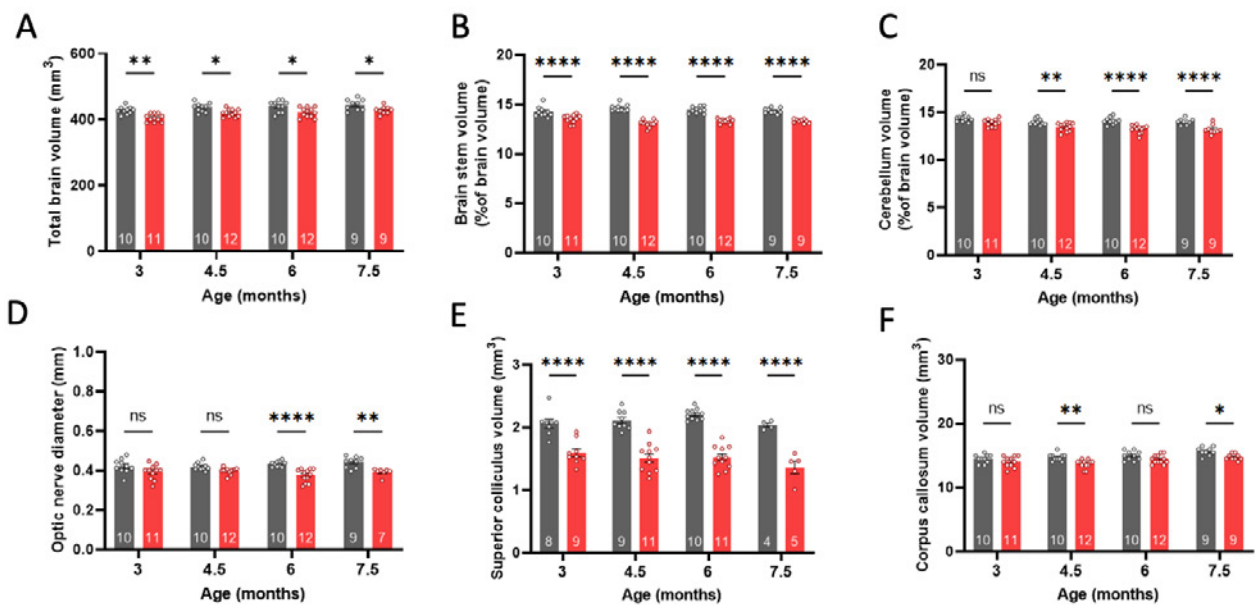
Figure 7. MRI data in Wfs1 KO mice confirm neurodegeneration in several brain areas that are also affected in Wolfram syndrome patients. *(A-C) The volume total brain volume (A) as well as the volume of several brain areas, including the cerebellum (B) and brainstem (C) is smaller in Wfs1 KO mice. (D-E) Detailed analysis of the optical projection via manganese-enhanced MRI shows a reduced innervation of the primary visual target area, the superior colliculus (C), and a smaller optic nerve diameter (D) in Wfs1 KO animals. (F) Also the white matter corpus callosum (F) is reduced in the Wfs1 KO brains. Two-way ANOVA, Sidak's post-hoc test; *, p<0.05; **, p<0.01; ***, p<0.001; ****, p<0.0001; the number of biological repeats/mice is included in the graphic. WT mice: black bars; Wfs1 KO mice: red bars.*

Task III.3. Rescue the WS phenotype in *Wfs1* mutant mice using *in vivo* base editing approaches

Since WS results from a genetic defect in the *WFS1* gene, genetic correction seems the most effective way to treat the disease. This can be done via genome editing methods, in which the mutation in the gene is corrected using CRISPR/Cas technology. Based on the promising *in vitro* data gathered by Prof. C. Verfaillie and Dr. A. Nami (SCIL, KU Leuven) using adenine base editing (see above), we now envision a further translation to in vivo animal models to evaluate the applicability of this base editing therapy in the clinic. However, this requires relevant animal models that contain point mutations in the *WFS1* gene that replicate the genetic cause of the disease.

As such, we initiated the creation of a novel knock-in mouse model for WS, characterized by a point mutation in the *Wfs1* gene, i.e., the Wfs1Q669* (c.2002C>T) mouse. This *Wfs1* mutant mouse has been generated by Taconic-Cyagen and the colony is currently being expanded. The start of phenotyping is planned for May 2023. Retinal/optic nerve structure and function will be evaluated via electron microscopy and histology, *in vivo* optical coherence tomography imaging and electrophysiology and visual behavioral studies. Particular attention will be paid to the role of neurons versus glial cells in WS, and the appropriate time point/time window for therapy will be determined. Once this mouse model is fully characterized, we will take advantage of another ongoing research line, not explained in detail here, in which we will work on a tailored delivery of the CRISPR BE tools *in vivo* in the mouse visual system. Selection of neuronal *versus* glial cells will be based on the results obtained. Besides testing the *in vivo* safety of this therapeutic approach, we will assess its efficiency via morphological and functional evaluations of visual system integrity.

3. Conclusions and future planning

The data gathered within this project, in WS patient iPSC-derived oligodendrocytes and a WS mouse model, point towards a critical role for oligodendrocytes in this neurodegenerative pathology. This supports the central hypothesis of the project, *i.e.* that oligodendrocytes rather than neurons might be the drivers of the disease processes that lead to neurodegeneration in WS, and confirms that we are on track with the proposed research.

Despite some delays due a less efficient working time during the first and second COVID-19 period, and prolonged medical leaves of both the PhD student and senior investigator involved in this project, we can state that the work was largely performed according to the original plans and the goals set for the 3 years of the project were largely reached. Many experiments and analyses were carried out as planned, and some additional research activities were developed. We remain convinced of the successful completion of the project and publication of the data in the coming year.

Notably, the novel mouse model, that we will be characterizing, also provides a new tool for the development of WS therapies that is relevant to the entire WS research community. Indeed, WS preclinical research in mice has so far been based almost entirely on the Wfs1exon8 mouse. However, given that this genetic model contains a complete deletion of exon 8, it does not reflect the point mutations in the WFS1 gene that underlie WS in patients nor is this mouse amenable to gene editing therapy. The latter is an important limitation and leads to the ultimate goal of the WS research at KU Leuven, namely testing the in vivo safety and efficacy of the base editing therapy developed by the Verfaillie lab in this mouse. Indeed, in a complementary multidisciplinary project, the teams of Profs. L. De Groef, L. Moons, C. Verfaillie and S. Soenen are further developing a base editing therapy for WS. However, the in vivo validation of this treatment requires a suitable mouse model, and thus research performed within this GSKE project is an essential step in this larger research program. The overall goal of the latter is the implementation of CRISPR base editing in clinical practice, by (i) providing a first *in vitro* and *in vivo* proof-of-concept that CRISPR base editing can be efficiently and safely used to correct the *Wfs1* gene in cells of the retina; (ii) developing a tailored non-viral delivery method to administer CRISPR base editing to the relevant retinal cell types. Upon successful completion, the project's results will aid preventing blindness/neurodegeneration in WS patients, and pave the way for genome editing as a therapy for other sight-threatening monogenetic diseases and for the entire CNS as a whole. In summary, the GSKE project was extremely valuable for us, as it provided a strong backbone for integrated and multidisciplinary research on a focused theme – investigating the role of glial cells and develop novel therapies to combat blindness and the neurodegenerative pathology in Wolfram patients. It helped us structuring and further expanding this research theme and was critical for successful grant and fellowship applications (see below). As such, it helped to ensure the continuity of our research in this field.

4.   References

1. Samara, A.*, et al.* Developmental hypomyelination in Wolfram syndrome: new insights from neuroimaging and gene expression analyses. *Orphanet J Rare Dis* **14**, 279 (2019).
2. Lugar, H.M.*, et al.* Neuroimaging evidence of deficient axon myelination in Wolfram syndrome. *Sci Rep* **6**, 21167 (2016).
3. Hershey, T.*, et al.* Early brain vulnerability in Wolfram syndrome. *PLoS One* **7**, e40604 (2012).
4. Ahuja, K.*, et al.* Oligodendrocytes in Wolfram syndrome: bystanders or partners in crime? . *Acta Neuropathologica, in preparation* (2023).
5. Liang, P.*, et al.* Genome-wide profiling of adenine base editor specificity by EndoV-seq. *Nature communications* **10**, 67 (2019).
6. Nami, F.*, et al.* Fast and Efficient Generation of Isogenic Induced Pluripotent Stem Cell Lines Using Adenine Base Editing. *CRISPR J* **4**, 502-518 (2021).
7. Neyrinck, K.*, et al.* SOX9-induced Generation of Functional Astrocytes Supporting Neuronal Maturation in an All-human System. *Stem Cell Rev Rep* (2021).
8. Villiger, L.*, et al.* Treatment of a metabolic liver disease by in vivo genome base editing in adult mice. *Nat Med* **24**, 1519-1525 (2018).
9. Garcia-Leon, J.A.*, et al.* Generation of oligodendrocytes and establishment of an all-human myelinating platform from human pluripotent stem cells. *Nat Protoc* **15**, 3716-3744 (2020).
10. Gaudelli, N.M.*, et al.* Programmable base editing of A*T to G*C in genomic DNA without DNA cleavage. *Nature* **551**, 464-471 (2017).
11. Garcia-Leon, J.A.*, et al.* SOX10 Single Transcription Factor-Based Fast and Efficient Generation of Oligodendrocytes from Human Pluripotent Stem Cells. *Stem Cell Reports* **10**, 655-672 (2018).
12. Marton, R.M.*, et al.* Differentiation and maturation of oligodendrocytes in human three-dimensional neural cultures. *Nat Neurosci* **22**, 484-491 (2019).
13. Luuk, H.*, et al.* Wfs1-deficient mice display impaired behavioural adaptation in stressful environment. *Behav Brain Res* **198**, 334-345 (2009).
14. Vandenabeele, M.*, et al.* The App(NL-G-F) mouse retina is a site for preclinical Alzheimer's disease diagnosis and research. *Acta Neuropathol Commun* **9**, 6 (2021).
15. Moons, L. & De Groef, L. Multimodal retinal imaging to detect and understand Alzheimer's and Parkinson's disease. *Curr Opin Neurobiol* **72**, 1-7 (2022).
16. Jagomae, T.*, et al.* Early Intervention and Lifelong Treatment with GLP1 Receptor Agonist Liraglutide in a Wolfram Syndrome Rat Model with an Emphasis on Visual Neurodegeneration, Sensorineural Hearing Loss and Diabetic Phenotype. *Cells* **10**(2021).
17. Claes, M. & Moons, L. Retinal Ganglion Cells: Global Number, Density and Vulnerability to Glaucomatous Injury in Common Laboratory Mice. *Cells* **11**(2022).

5.   Papers and presentations related to the GSKE project:

1. Vandenabeele, M., Lefevere, E., Van hoecke, J., Veys, L., Himmelreich, U., Looser, Z., . . .De Groef, L. (2021). Characterization of the visual system of the Wfs1 Δexon8 knockout mouse model. In LBI Scientific meeting, Leuven, November 23, 2021. Virtual meeting.
2. Ahuja, K., Chin Chai Y., Lemeitre A., Neyrinck K., De Groef L., Moons L., Verfaillie C. (2022) Development of multicellular 3D human induced pluripotent stem cell derived brain model to study *in vitro* Neuron Myelination. Hydra Summer School, Greece, September 13-19 2022.
3. Jagomäe, T., Seppa, K., Reimets, R., Pastak, M., Plaas, M., Hickey, M., . . . Plaas, M. (2021). Early Intervention and Lifelong Treatment with GLP1 Receptor Agonist Liraglutide in a Wolfram Syndrome Rat Model with an Emphasis on Visual Neurodegeneration, Sensorineural Hearing Loss and Diabetic Phenotype. Cells, 10(11). doi:10.3390/cells10113193
4. Punapart, M., Seppa, K., Jagomäe, T., Liiv, M., Reimets, R., Kirilov, S., . . . Plaas, M. (2021). The Expression of RAAS Key Receptors, Agtr2 and Bdkrb1, Is Downregulated at an Early Stage in a Rat Model of Wolfram Syndrome. Genes, 12(11). doi: 10.3390/genes12111717

6. Granted fellowships and projects related to the GSKE project:

1. FWO fellowship to Drs. Marjan Vandenabeele (2019 – 2023) - "*Unraveling the importance of oligodendrocytes in neurodegeneration: a new look on Wolfram syndrome.*"
   Goal: Study the differential contribution of neurons *versus* oligodendrocytes to Wolfram syndrome pathogenesis in iPSC and mouse models
2. FWO SB fellowship to Drs. Karan Ahuja (2021 – 2025) - "*Unravelling neuron-glia interactions in Wolfram syndrome through optic nerve-on-chip and in vivo base editing*"
   Goal: Understand the differential contribution of neurons versus glia to Wolfram syndrome and develop a gene therapy
3. Central Europe Leuven Strategic Alliance (CELSA) grant (2020 – 2022) - "*Ferroptosis: a novel paradigm in the neurodegenerative pathology of Wolfram syndrome*"
   Goal: Study ferroptosis as a disease mechanism underlying Wolfram syndrome, with a focus on the visual system
4. Life Sciences Research Partners VZW (LSRP) and Eye Hope VZW funding (2022-2023) - "*Developing a base editing therapy to treat ocular degeneration in Wolfram syndrome*"
   Goal: Study the in vivo efficiency and safety of base editing in a novel wolfram syndrome mouse model - creation and characterization of the model

Final report of the university research project of

Prof. Pierre Vanderhaeghen, MD, PhD (VIB)
Katholieke Universiteit Leuven (KU Leuven)

Prof. Pierre Vanderhaeghen, MD, PhD
Stem Cell and Developmental Neurobiology
Lab VIB-KU Leuven Center for Brain & Disease Research Department of Neurosciences,
Leuven Brain Institute IRIBHM / ULB Neuroscience Institute
pierre.vanderhaeghen@kuleuven.be

Deciphering the mechanisms underlying intellectual deficiency and autism spectrum disorders by cellular modelling in human neurons in vivo.

1. State of the art and objectives

Neurodevelopmental disorders (NDDs), including intellectual disability (ID) and autism spectrum disorders (ASD) present a major challenge in clinical genetics and medicine (Klingler et al., 2021; Marín, 2016). The advent of novel genomic technologies has led to the identification of many underlying genetic defects. However, before tailored therapies can be developed, one needs to decipher the exact underlying pathophysiology.

To this aim, most of the studies on NDD have relied on animal models, which has led to substantial progress thanks to the evolutionary conservation of many signaling pathways. However there are also important evolutionary differences in brain development, so that the exact impact of NDD mutations in human neurons remains unknown, as well as the translatability of preclinical findings. This is particularly relevant for ID and ASD, which are mostly linked to alterations of the cerebral neocortex, the most evolutionary divergent structure in the human brain.

Given the the difficulty to study the brain of patients at the cellular level, the advent of human pluripotent stem cell (PSC) has offered new opportunities. While *in vitro* PSC-based models have been used successfully to model several NDD, *in vivo* elements are crucially missing from these approaches, which thus display serious limitations to model faithfully all aspects of ID/ASD. For this reason we have started to develop models of xenotransplantation, where PSC-derived human neurons are transplanted into the mouse cortex. Following transplantation in the mouse neonatal cortex, the PSC-derived pyramidal neurons develop like endogenous cortical neurons, and integrate functionally in the host brain, following their species-speciifc time-line (Linaro et al., 2019; Vermaercke et al., 2022).

In this project we aim to determine the pathophysiological mechanisms of ID/ASD conditions through the *in vivo* study of human neurons displaying clinically relevant mutations. The project is based on the following objectives:
Aim1. **Development of fully validated *in vitro* PSC models for *ID/ASD* related disorders.**
Aim2. **Characterization of ID/ASD in human cortical neurons *in vivo*.**

2. Results

This project relied a recently optimized experimental model to study NDD with xenotransplanted cortical neurons (Linaro, Neuron 2019; reviewed in Vermaercke et al. Cell 2022); the characterization of the development of MECP2 duplicated human neurons in vivo (Merckx et al., unpublished data); the first demonstration of disrupted developmental timing in human cortical neurons in vivo following SYNGAP1 mutations (Vermaercke et al. 2023, ms. submitted to Neuron), and the discovery of a species-specific molecular mechanism of SYNGAP1 regulation in human neurons (Libé-Philippot et al. 2023, ms. submitted to Cell). Collectively these data point to ID/ASD gene mutations that lead to acceleration of neuronal development, which has important implications for our understanding of human brain evolution and diseases (Libé-Philippot and Vanderhaeghen, 2021; Vanderhaeghen

and Polleux, 2023). In this frame, we also obtained recent results indicating that mitochondria genes play an essential role in the regulation of developmental timing of human cortical neurons (Iwata et al. Science 2023).

We first generated isogenic PSC lines displaying specific heterozygote and homozygote mutations using directed genomic engineering. We thus validated the generation of mutant neurons for each gene and genotype.
We next started to study SYNGAP1 mutant (both het and homo) neurons in the xenotransplantation model. Remarkably, we discovered a greatly accelerated pattern of maturation of the mutant neurons, morphologically, but also functionally, combining *ex vivo* slice analyses and *in vivo* multiphoton imaging (Vermaercke et al., 2023). This work constitutes the first demonstration of the consequences of an NDD gene mutation in human cortical neurons *in vivo*, and demonstrate that SYNGAP1 deficient human neurons display accelerated development *in vivo*, even at the neural circuit level, with important implications for the pathophysiology and future treatments of these conditions.

Moreover, while performing these experiments we discovered a surprising and important molecular link between SYNGAP1 and the human-specific genes SRGAP2B/C, thought to be involved in neuronal neoteny. SRGAP2B/C were found to act by upregulating the levels of SYNGAP1 at the synapse, thus revealing a direct link between a human-specific gene and an important ID/ASD gene (Libé-Philippot et al., 2023).

Finally and importantly, thanks to the models and methods that we developed we discovered a new mechanism of regulation of the speed of neuronal development involving mitochondria dynamics and metabolism (Iwata et al., 2023). This new line of investigation will be pursued in our next GSKE/FMRE project, focusing on the impact of mittchondria diseases on developmental timing.

3. References

– Iwata, R., Casimir, P., Erkol, E., Boubakar, L., Planque, M., Gallego, I.M., Ditkowska, M., Gaspariunaite, V., Beckers, S., Remans, D., et al. (2023). Mitochondria Metabolism Sets the Species-Specific Tempo of Neuronal Development. Science 379, eabn4705.
– Klingler, E., Francis, F., Jabaudon, D., and Cappello, S. (2021). Mapping the molecular and cellular complexity of cortical malformations. Science (80-.). 371, eaba4517.
– Libé-Philippot, B., and Vanderhaeghen, P. (2021). Cellular and Molecular Mechanisms Linking Human Cortical Development and Evolution. Annu. Rev. Genet. 55, 555–581.
– Libé-Philippot, B., Iwata, R., Recupero, A.J., Benedikt, V., Ditkowska, M., Gaspariunaite, V., Wierda, K., Remans, D., Polleux, F., and Vanderhaeghen, P. (2023). Human synaptic neoteny requires species-specific balancing of SRGAP2-SYNGAP1 cross-inhibition. Submitted to Cell.
– Linaro, D., Vermaercke, B., Iwata, R., Ramaswamy, A., Libé-Philippot, B., Boubakar, L., Davis, B.A.B.A., Wierda, K., Davie, K., Poovathingal, S., et al. (2019). Xenotransplanted Human Cortical Neurons Reveal Species-Specific Development and Functional Integration into Mouse Visual Circuits. Neuron 104, 972-986.e6.
– Marín, O. (2016). Developmental timing and critical windows for the treatment of psychiatric disorders. Nat. Med. 22, 1229–1238.
– Vanderhaeghen, P., and Polleux, F. (2023). Developmental mechanisms underlying the evolution of human cortical circuits. Nat. Rev. Neurosci. in press.
– Vermaercke, B., Bonin, V., and Vanderhaeghen, P. (2022). Studying human neural function in vivo at the cellular level: Chasing chimeras? Cell 185, 4869–4872.
– Vermaercke, B., Iwata, R., Weirda, K., Rodriguez, P., Ditkowska, M., Bonin, V., and Vanderhaeghen, P. (2023). SYNGAP1 deficiency disrupts neoteny in human cortical neurons in vivo. BioRxiv https://doi.org/10.1101/2023.01.14.524054. Submitted to Neuron.

4. Publications 2020-2022

- Developmental mechanisms underlying the evolution of human cortical circuits.
  Vanderhaeghen P, Franck Polleux.
  Nature Rev. Neurosci. 2023*, in press.* *IF: 39*
- Mitochondria Metabolism Sets the Species-Specific Tempo of Neuronal Development.
  Iwata, R., Casimir, P., Erkol, E., Boubakar, L., Planque, M., Ditkowska, M., Vints, K., Gaspariunaite, V., Bird, M., Corthout, N., Vermeersch, P., Davie, K., Gounko, V., Aerts, S., Ghesquière, B., Fendt, S-M, **Vanderhaeghen P.**
  Science (2023) 379, eabn4705 DOI: 10.1126/science.abn4705. *IF: 41*
- CROCCP2 acts as a human-specific modifier of cilia dynamics and mTOR signalling to promote expansion of cortical progenitors
  Van Heurck R, Wojno M, Suzuki IK, Velez-Bravo FD, Bonnefont J, Erkol E, Nguyen DT, Herpoel A, Bilheu A, Ledent C, **Vanderhaeghen P.**
  Neuron (2022):S0896-6273(22)00947-3. *IF: 18*
- Studying human neural function in vivo at the cellular level: Chasing chimeras?
  Vermaercke B, Bonin V, **Vanderhaeghen P**.
  Cell (2022)185(26):4869-4872. *IF: 38*
- Cellular and molecular mechanisms linking human cortical development and evolution. Libé-Philippot B, **Vanderhaeghen P.** *Annu. Rev. Genetics. 2021. 55:555-581.* *IF: 16.8*
- Mitochondria dynamics in postmitotic cells regulate neurogenesis.
  Iwata R, Casimir P, and **Vanderhaeghen P**.
  Science (2020), 369(6505):858-862. *IF: 38*

Final report of the
university research project of

Prof. dr. Thomas Voets (VIB)
Katholieke Universiteit Leuven (KU Leuven)

Prof. dr. Thomas Voets

Laboratory of Ion Channel Research

VIB-KU Leuven Center for Brain & Disease Research

KU Leuven, Department of Cellular and Molecular Medicine

Herestraat 49 bus 801

3000 Leuven

Tel: +32 16 33 02 17

Thomas.voets@kuleuven.vib.be

Table of contents

Unraveling the cellular and molecular basis of noxious cold sensing

1. Background

Noxious cold and noxious heat have detrimental effects on key biological macromolecules, and thus on the integrity of cells, tissues and organisms[1]. Thanks to the action of a subset of somatosensory neurons, mammals can swiftly detect noxiously cold or hot objects or environments. These temperature-sensitive nociceptor neurons become activated when the temperature at their free endings in the skin or mucosae reaches noxious levels, provoking acute pain and initiating avoidance reflexes[2].

In the last two decades, several ion channels of the transient receptor potential (TRP) superfamily have been put forward as key molecular sensors in somatosensory neurons, involved in various aspects of temperature sensing and pain[1-3]. In a recent key paper from our research group, with the support of the Queen Elisabeth Medical Foundation, we uncovered the molecular basis of noxious heat detection, by showing that acute heat-induced pain depends on three TRP channels (TRPV1, TRPM3 and TRPA1), acting as redundant heat sensors in nociceptor neurons[4]. We found that simultaneous elimination of all three TRP channels fully eliminates heat responses in isolated sensory neurons, and completely abolishes heat-induced pain responses in mice[4].

In contrast, the molecular basis of noxious cold sensing remains unresolved[1]. Several studies, including work from our research group, have revealed that TRPM8 and TRPA1 act as molecular cold sensors involved in different aspects of innocuous and noxious cold sensing[5-13] . However, a subset of sensory neurons remains cold sensitive after combined elimination of both channels, and $Trpm8^{-/-}/Trpa1^{-/-}$ double knockout mice still exhibit a robust pain response to noxious cold[11, 14]. Thus, the cellular and molecular basis of noxious cold sensing remains essentially unknown[1]. The aim of the proposed research is therefore to unravel the cellular and molecular mechanisms underlying cold-induced pain, by identifying the mechanisms underlying TRPM8- and TRPA1-independent cold sensing.

Elucidating the basis of cold-induced pain not only addresses a fundamental question in sensory neurobiology, but may also have important medical applications. About one in five of adult Europeans suffer from moderate-to-severe chronic pain, and despite the fact that access to adequate pain management is considered a Fundamental Human Right[15], half of these chronic pain sufferers report inadequate pain control with available analgesic treatments[16, 17]. Cold allodynia, the condition where non-noxious cool stimuli evoke pain, is a frequent aspect of chronic pain and represents one of the hallmarks of neuropathic pain following nerve injury or chemotherapy[18]. Unfortunately, there are currently no safe and efficient therapies to treat cold allodynia. We anticipate that novel insights into the mechanisms of cold-induced pain may fuel the development of novel targeted pain therapies.

2. Scientific objective

In earlier work, we and others identified a subset sensory neurons exhibiting robust TRPM8- and TRPA1-independent Ca^{2+}-influx in response to cold[11, 19, 20]. As the origin of their cold sensitivity is unknown, we will name this subset of sensory neurons **O**rphan **C**old **N**eurons (OCNs).

We hypothesize that these OCNs play a central role in cold pain, and express at least one type of cold sensor of unknown molecular identity. We intend to characterize these OCNs and identify the molecular basis of their cold sensitivity.

3. Results

3.1. Functional characterization and transcriptome analysis of cold-sensitive sensory neurons

A number of recent studies have reported RNA-seq-based single-cell transcriptome analyses of mouse DRG neurons, leading to hierarchical clustering of neurons into 11-18 subtypes[21-23]. However, how this transcriptome-based classification relates to the functional properties of sensory neurons is poorly understood. By performing Fura-2-based Ca^{2+}-imaging experiments followed by single-cell sequencing, we generated an approach that combines functional information with the cell's transcriptional fingerprint.

Our published and unpublished results indicate that approximately 8% of DRG neurons can be classified as M8-CNs and approximately 15% as A1-CNs; between 3 and 7% of all DRG neurons are OCNs[11]. In order to properly identify OCNs and exclude TRPA1 and TRPM8-cold mediated responses, we used $TRPA1^{-/-}$ knockout mice and excluded all neurons that reacted to the cooling agent menthol (TRPM8 agonist). Therefore, all DRG neurons that responded to cooling but failed to react to menthol (200 µM) stimulation were identified as OCNs. Once we identified by Ca^{2+}-imaging all OCNs, menthol-sensitive neurons and neurons that did not respond to colling, we individually harvested the neurons of interest. For this, we used microcapillary pipettes connected to a micromanipulator to aspirate single cells under visual control. Individually harvested neurons had their transcriptome profile unraveled by Smart-seq 2 technology. Smart-seq2 is the preferred approach as it provides good coverage of the transcriptome, including rarer transcripts and splice variants [24]. To date, we collected and fully sequenced a total of 46 cells (20 OCNs, 4 menthol sensitive cells and 22 cells that do not respond to cooling). An average of approximately 8.000 genes was identified per cell. The marker genes used to identify cell types were: neurons = Rbfox3, endothelial = Cldn5, macrophages = Mrc1, glia = Mbp and fibroblasts = Mgp. All the collected samples presented a high expression of the neuronal marker Rbfox3 (Figure 1A), indicating that we successfully harvested sensory neurons. Some samples showed high expression of the glial cell marker Mbp (Figure 1A). DRGs contain a unique type of glial cells, known as satellite glial cells, which form a sheath around the cell body of DRG neurons (generally, one neuron is wrapped by several SGCs), which may explain the high expression of the glial marker in a few neuronal samples (Figure 1A-B).
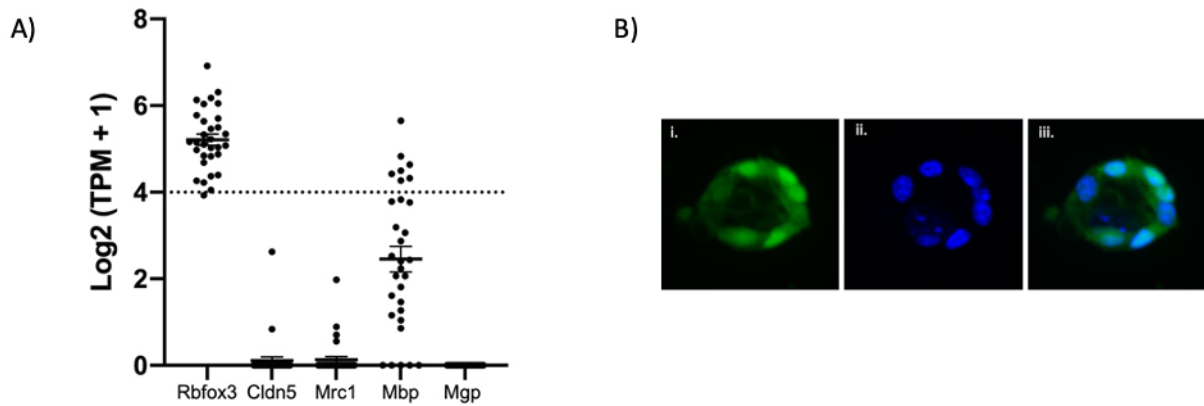
Figure 1: Cell subtype identification in DRG culture. (A) RNA seq data showing DRG cell subtype marker gene expression. Marker genes: Rbfox3 = neurons, Cldn5 = endothelial, Mrc1 = macrophages, Mbp = glia and Mgp = fibroblasts. (B) Satellite glial cells wrapping DRG neurons in a standard DRG culture. Cells were loaded with the calcium indicator Fluo-4 AM (green) and cell nuclei were stained with Hoechst® 33342 dye (blue). Images were made using a confocal microscope. i. Fluo-4 AM, ii. Hoechst® 33342 and iii. overlay of the two channels.

The functional data obtained by Fura-2-based Ca^{2+}-imaging experiments indicate that an average of 8.5% of the measured sensory neurons (isolated from $TRPA1^{-/-}$ knockout mice) are identified as OCNs (Figure 2A). In addition, there is a good correlation between our functional and transcriptome data (Figure 2B-C). The collected neurons that were sensitive to both menthol (TRPM8 agonist) and cooling stimulation turned out to have high expression levels of TRPM8 ion channels (Figure 2B-C). On the other hand, no reads corresponding to TRPM8 transcripts were identified in neurons that did not respond to menthol stimulation (Figure 2B-C).
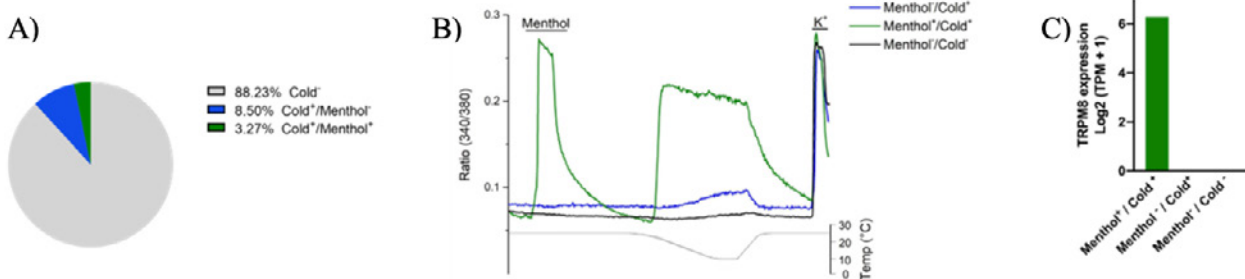
Figure 2: Functional and molecular characterization of DRG neurons. (A) Percentage of neurons that are not sensitive to cold (Cold⁻), neurons that are sensitive do cold and not sensitive to menthol(Cold⁺/Menthol⁻) and neurons that are sensitive to both cold and menthol (Cold⁺/Menthol⁺). (B) Ratiometric measurement of changes in intracellular Ca^{2+} in response to menthol (200 μM) and cooling stimulation. The traces represent individual responses of 3 distinct neurons. (C) RNA seq data showing TRPM8 transcript expression levels of the cells functionally characterized in panel B. Gene expression is given as log2(TPM+1).

3.2.   Identification of candidate genes underlying cold responses in OCNs

For further characterization of OCNs and identification of genes that may underlie their cold sensitivity, we compared the transcriptomes of the identified OCNs and those from cells insensitive to cooling stimulation. Our data revealed that 315 genes are differentially expressed between the two groups of cells (Figure 3A). Of these 315 genes, 170 are significantly upregulated in OCNs and thus may contribute to their "orphan" cold sensitivity. Among the upregulated genes found in OCNs, 99 are identified as plasma membrane proteins (Figure 3B). As ion channels and membrane receptors represent prime candidate cold sensors, we initially focused on genes that encode proteins with at least one transmembrane domain and select either proteins with unknown function or known ion channels. Among the plasma membrane candidates that are upregulated in OCNs, 7 are members of the G-protein coupled receptor family and 11 correspond

to ion channels (Figure 3B-C). For example, these possible candidates include ion channels permeable for sodium, potassium and calcium ions (Figure 4).
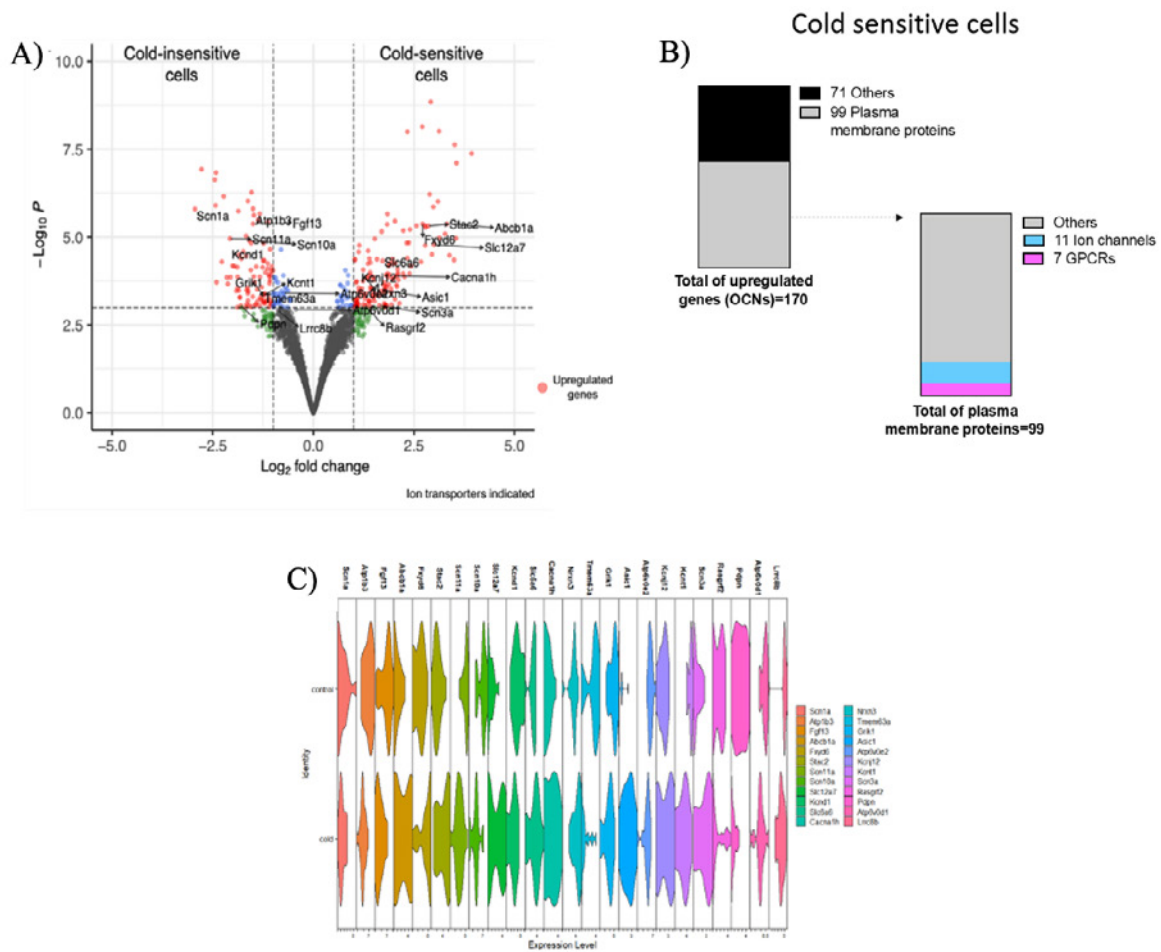

Figure 3: Gene expression analysis of scRNA-seq data. (A) Volcano plot displaying differentially expressed genes of cold-sensitive and insensitive cells. Genes with a P-value smaller than 0.05 and an absolute log (fold change) larger than 1 are considered significant. Upregulated genes in cold-sensitive and insensitive cells are colored in red. Significantly upregulated ion transporters are indicated. (B) General overview of the upregulated genes corresponding to proteins located at the plasma membrane. (C) Summary of the expression levels of ion channel transporters between the 2 groups: Control (cold-insensitive cells) and cold (cold-sensitive cells).

3.3. Cold-mediated modulation of Asic ion channels

Interestingly, our data suggest the acid-sensing ion channel (Asic1) as one of the top candidates for cold sensing in sensory neurons (Figure 4). These channels are members of the epithelial Na^+ channel (ENaC)/degenerin (Deg) family. Asic channels are proton-gated cation channels widely expressed in the central and peripheral nervous systems. They are modulated by a broad range of pH ranges during physiological and pathological conditions. Asics are trimeric channels and their subunits are encoded by four genes: Asic1, Asic2, Asic3 and Asic4 [25].

We performed whole-cell patch-clamp recordings to investigate the effect of cold temperature on Asic1 channel kinetics. At pH 7.4, cold stimulation could not directly evoke any currents in HEK293T cells expressing Asic1 channels (data not shown). On the other hand, currents induced by low pH were tremendously potentiated at cold temperatures. Cold stimulation not only potentiates current amplitude but also slows channel desensitization (Fig. 5A-B). In order to confirm that the resulting H^+-gated currents at low temperatures were induced via Asic1 activation, we tested whether the Asic channel inhibitor (amiloride) could impair channel activation. Amiloride could fully inhibit H^+-gated currents potentiated by cold temperature (Figure 5C).
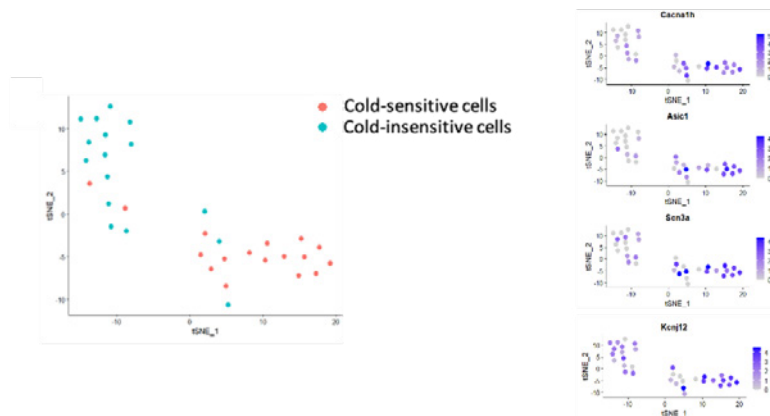
Figure 4: t-SNE plot of the 2 distinct cell clusters: Cold-sensitive and Cold-insensitive cells. In detail: Expression levels of the upregulated calcium (Cacna1h), Asic (Asic1), sodium (Scn3a) and potassium (Kcnj12) ion channels found in OCNs indicated per cell.
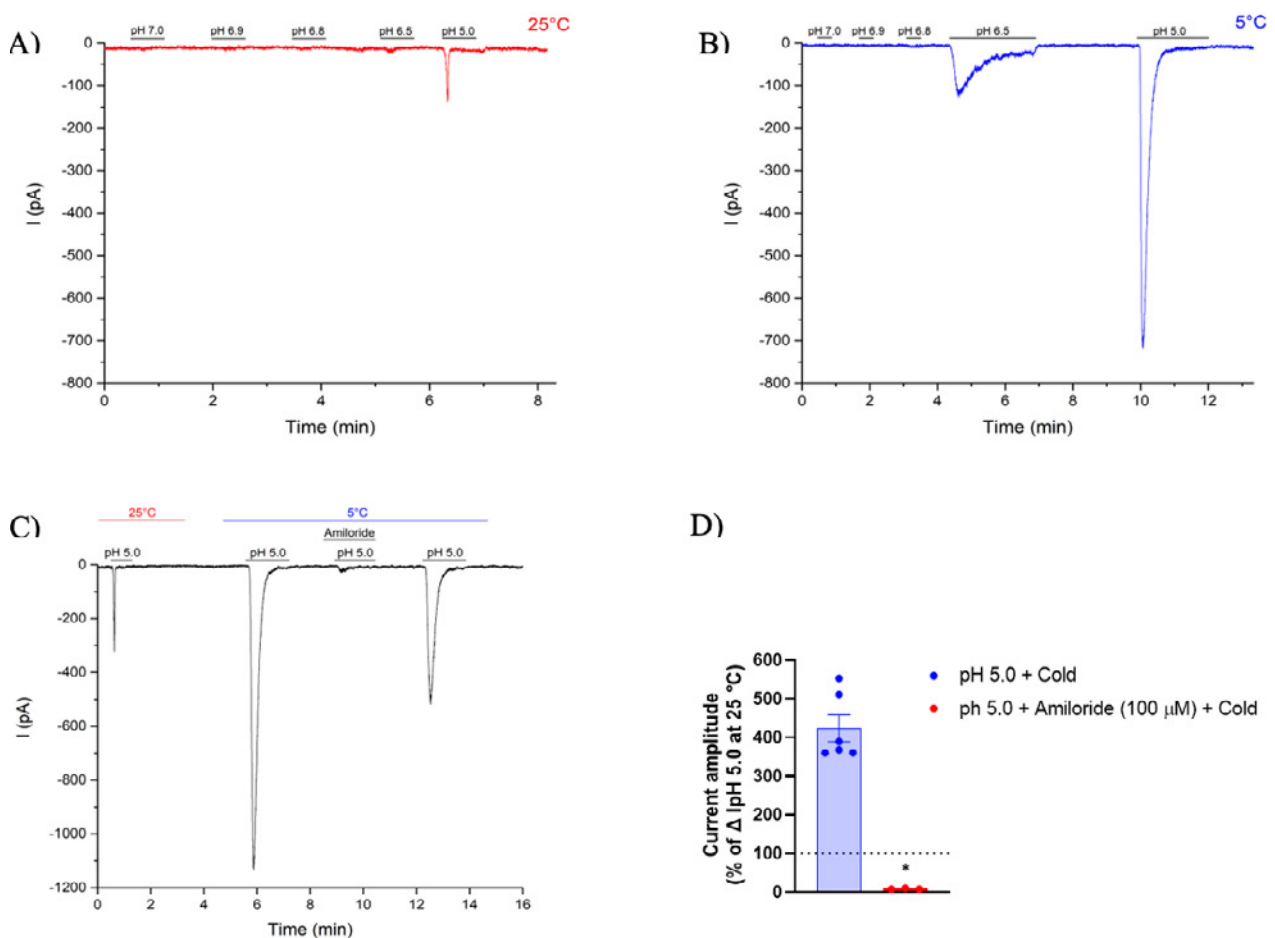

Figure 5: Cold-induced potentiation of H⁺-gated currents of Asic1 channels. Representative currents evoked by stepping from pH 7 to pH 5 solutions recorded from HEK293T expressing Asic1 ion channels at 25 °C (A) and 5 °C(B). Effect of the Asic inhibitor amiloride on potentiated H⁺-gated currents at cold temperature (C-D). (D) Each point represents mean ± S.E.M. from 3-6 cells. *p <0.05 with Student's two-tailed unpaired t-test.

Since Asic3 is primarily and widely expressed in sensory neurons, we decided to test whether this ion channel is also modulated by cold stimulus [26, 27]. Similar to Asic1, cold temperatures do not directly induce Asic3-mediated currents. However, low temperature potentiates both the outward and inward Asic3 H+-gated currents (Figure 6A-B). Additionally, cold stimulus significantly potentiates Asic3 currents at different pH ranges (Figure 6C). The potentiation of

Asic H+-gated currents by cold has already been described in the literature [28]. However, the gating mechanisms modulated by temperature are not fully understood. Likewise, the impact of temperature on Asic channels in pathological conditions where there is extracellular acidification, for example, during inflammation, has never been explored.

Although amiloride is a well-known Asic inhibitor, it has a paradoxical effect on Asic3 ion channels. This compound blocks the activation of the channel at certain pH ranges. However, amiloride induces a stimulatory effect at a more modest pH fluctuation (such as pH 7). Besides that, at higher concentrations, amiloride induces a sustained current at neutral pH [29]. The way by which amiloride modulates the Asic3 channel has been proven to be quite complex. It has been demonstrated that this compound binds to a non-proton ligand-sensing domain of the channel to induce the observed sustained currents [30, 31]. However, it has been suggested that amiloride may have multiple distinct binding sites that may impact channels gating mechanisms in different ways [29]. Therefore, we wanted to investigate whether cold stimulus would modulate amiloride-induced currents. Our results suggest that cold temperature potentiates the outward amiloride-induced current. Interestingly, holding the cell at negative voltages induced a voltage-depended component to the amiloride-induced current. The mechanism by which temperature influences Asic activity stimulated by non-proton ligands is yet to be investigated. The impact of that on cell physiology should also be further studied.
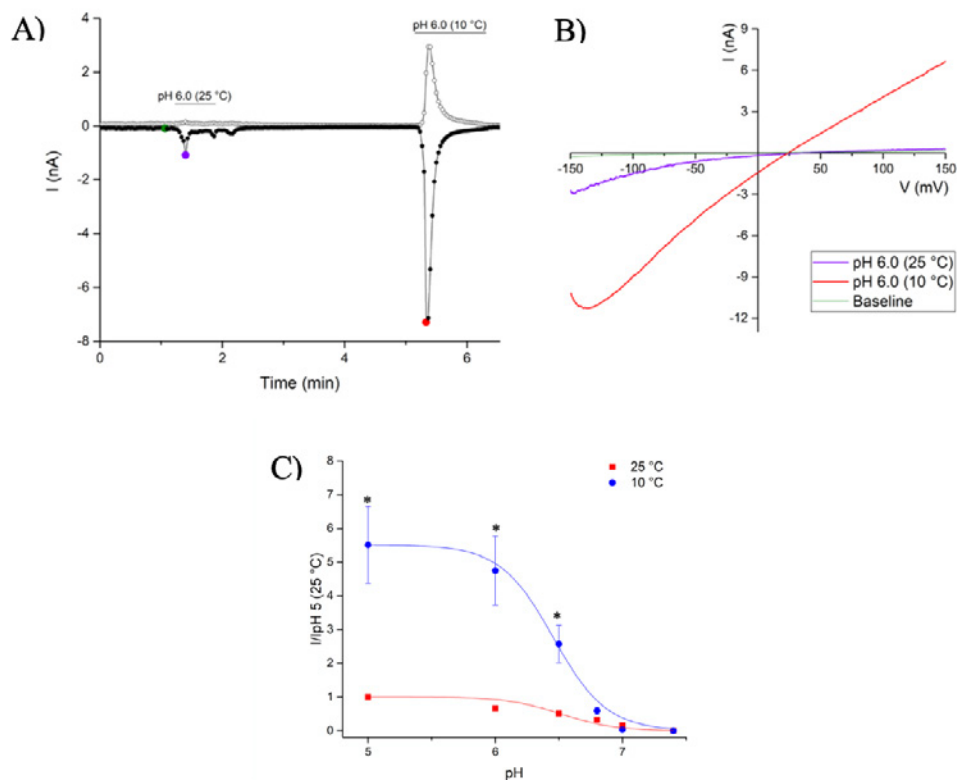

Figure 6: Cold-induced potentiation of H+-gated currents of Asic3 channels. (A) Time course of whole-cell patch-clamp recording at holding potentials of +80 mV (open circles) and –80 mV (closed circles) of Asic3 expressed in HEK293T cells during application of pH 6 solution at 25 °C and at 10 °C. (B) Current-voltage relationship (I–V) of time points indicated in panel (A). (C) pH dose-response curves were measured at 25 °C and 10 °C (whole-cell patch-clamp recording at holding potential of -60 mV). Each point represents mean ± S.E.M. from 5-7 cells. Two-way ANOVA with Šidák's multiple comparisons test showing *p < 0.05.
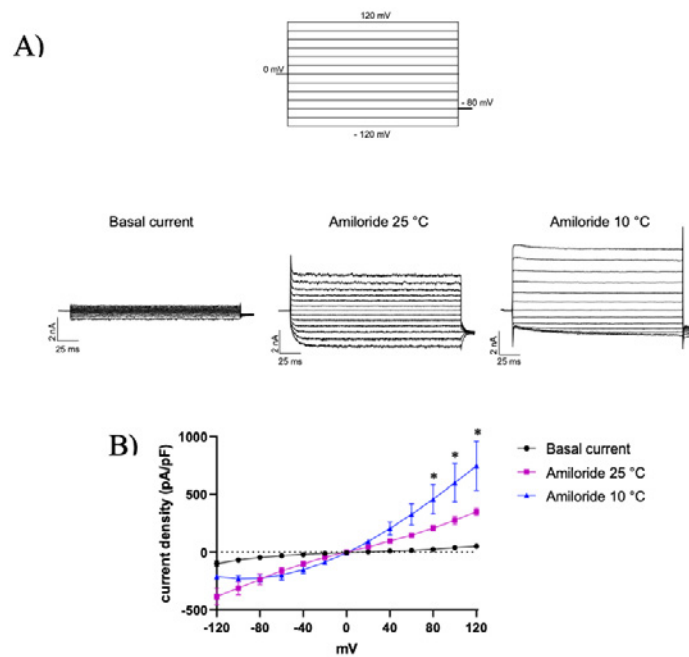
Figure 7: Amiloride-induced currents of Asic3 channels. (A) Representative current traces of HEK293T expressing Asic3 in response to amiloride (100 μM) at voltage steps measured at 25 ˚C and 10 ˚C. (B) Current-voltage relationship of Asic3 channels in the presence of amiloride (100 μM) at 25 ˚C and 10 ˚C. Each point represents mean ± S.E.M. from 2 cells. Two-way ANOVA with Tukey's multiple comparisons showing *$p < 0.05$ for amiloride 25 ˚C vs. amiloride 10 ˚C

3.4. The impact of extracellular acidification on OCNs activity

Protons positively or negatively modulate a significant number of ion channels and receptors. For example, while low pH may stimulate the heat sensor TRPV1, extracellular acidification may suppress currents of the cold sensor TRPM8 [32]. Therefore, modulation of OCNs activity by low pH is an interesting tool to shed light on the functional characteristics of the cold sensors present in these cells. In addition to that, our data suggest that OCNs express proton-gated channels (Asic1) and that temperature greatly influences this ion channel kinetics. Therefore, we tested whether acidification of the extracellular environment would impact OCNs cold-mediated activity. Three different OCN profiles were identified (Figure 8A). Surprisingly, most OCNs (~80%) were inhibited by low pH, around 14% were not modulated by extracellular acidification and only ~7% were stimulated by protons. These data suggest that OCNs comprise a heterogeneous population and that more than one cold sensor may be present in these cells. To further look into OCNs transcriptome information, we have now collected 123 new samples: 11 single cells that respond to menthol and cold stimulation, 48 cold insensitive cells and a total of 64 OCNs. We hope that these additional samples will provide us with better insights into the molecular fingerprint of these poorly understood temperature-sensitive sensory neurons.
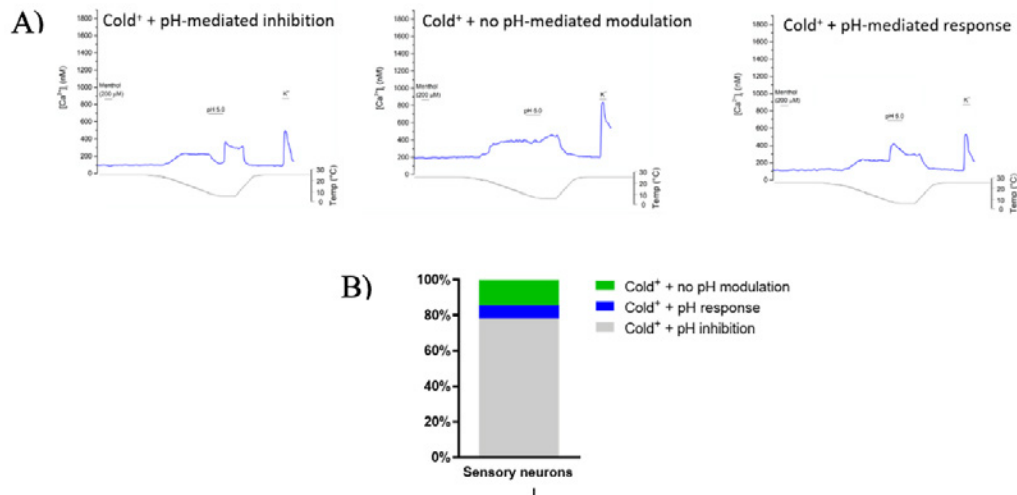
Figure 8: Effect of low pH on cold sensitivity of sensory neurons. (A) Ratiometric measurement of changes in intracellular Ca^{2+} of sensory neurons in response to cooling stimulation and simultaneous application of pH 5.0 solution. (B) Percentage of cold-sensitive neurons corresponding to each profile identified in panel (A).

4.   Outlook and budget

With the financial support of the GSKE, we have been able to establish an approach to obtain a detailed transcriptome analysis of functionally characterized sensory neurons and provide part of the salary of a dedicated postdoctoral researcher, Dr. Ana Freitas. This has allowed us to identify a set of candidate genes that may contribute to "orphan" cold responses. We are currently refining the candidate selection based on functional characterization and single-cell sequencing of new samples. Additionally, we are conducting further electrophysiological characterization of OCNs, combining Fura-2-based Ca^{2+}-imaging experiments with whole-cell patch-clamp recordings. The financial support to Dr. Ana Freitas has enabled her to obtain important preliminary data and technical skills, which lie at the basis of a successful application for a senior postdoctoral fellowship from the FWO.

Interestingly, amongst the top candidates is ASIC1, well known as an acid-activated ion channel. Our preliminary data suggest that it may contribute to cold responses in sensory neurons. However, our study also identified several other candidate genes of unknown function, which may contribute to cold sensing. Further characterisation of some of these candidates is currently ongoing, beyond the duration of this project.

Moreover, the research in this project has also tapped into other ongoing lines of research in the team, aimed at understanding the action of known drugs on cold-sensitive ion channels. This has led tot he important discovery that the urinary tract analgesic phenazopyridine directly acts on cold-sensitive sensory neuronal endings in the bladder, which likely underlies the analgesic effects of this drug (Luyts et al. 2023). The innovative single-cell approaches developed within this project are also now widely used in the team, for the molecular characterisation of functionally specific sensory neurons innervating specific organs and body parts.
Finally, we would like to thank GSKE for their generous support.

5. Recent papers (published in 2020-23) mentioning financial support of GSKE

– Burglen, L., Van Hoeymissen, E., Qebibo, L., Barth, M., Belnap, N., Boschann, F., Depienne, C., De Clercq, K., Douglas, A.G.L., Fitzgerald, M.P., Foulds, N., Garel, C., Helbig, I., Held, K., Horn, D., Janssen, A., Kaindl, A.M., Narayanan, V., Prager, C., Rupin-Mas, M., Afenjar, A., Zhao, S., Ramaekers, V.T., Ruggiero, S.M., Thomas, S., Valence, S., Van Maldergem, L., Rohacs, T., Rodriguez, D., Dyment, D., Voets, T., Vriens, J., 2023. Gain-of-function variants in the ion channel gene TRPM3 underlie a spectrum of neurodevelopmental disorders. Elife 12. https://doi.org/10.7554/eLife.81032

– De Bruyn, H., Corthout, N., Munck, S., Everaerts, W., Voets, T., 2022. Machine learning-assisted fluoroscopy of bladder function in awake mice. Elife 11. https://doi.org/10.7554/eLife.79378

– Freitas, A.C.N., Voets, T., 2020. Why the emperor penguin reigns where elephants shiver. Cell Calcium 91, 102263. https://doi.org/10.1016/j.ceca.2020.102263

– Held, K., Aloi, V.D., Freitas, A.C.N., Janssens, A., Segal, A., Przibilla, J., Philipp, S.E., Wang, Y.T., Voets, T., Vriens, J., 2022. Pharmacological properties of TRPM3 isoforms are determined by the length of the pore loop. Br J Pharmacol 179, 3560-3575. https://doi.org/10.1111/bph.15223

– Kelemen, B., Pinto, S., Kim, N., Lisztes, E., Hanyicska, M., Vladar, A., Olah, A., Penzes, Z., Shu, B., Vriens, J., Biro, T., Rohacs, T., Voets, T., Toth, B.I., 2021. The TRPM3 ion channel mediates nociception but not itch evoked by endogenous pruritogenic mediators. Biochem Pharmacol 183, 114310. https://doi.org/10.1016/j.bcp.2020.114310

– Luyts, N., Daniluk, J., Freitas, A.C.N., Bazeli, B., Janssens, A., Mulier, M., Everaerts, W., Voets, T., 2023. Inhibition of TRPM8 by the urinary tract analgesic drug phenazopyridine. Eur J Pharmacol 942, 175512. https://doi.org/10.1016/j.ejphar.2023.175512

– Mulier, M., Van Ranst, N., Corthout, N., Munck, S., Vanden Berghe, P., Vriens, J., Voets, T., Moilanen, L., 2020. Upregulation of TRPM3 in nociceptors innervating inflamed tissue. Elife 9. https://doi.org/10.7554/eLife.61103

– Mulier, M., Vandewauw, I., Vriens, J., Voets, T., 2020. Reply to: Heat detection by the TRPM2 ion channel. Nature 584, E13-E15. https://doi.org/10.1038/s41586-020-2511-6

– Persoons, E., De Clercq, K., Van den Eynde, C., Pinto, S., Luyten, K., Van Bree, R., Tomassetti, C., Voets, T., Vriens, J., 2020. Mimicking Sampson's Retrograde Menstrual Theory in Rats: A New Rat Model for Ongoing Endometriosis-Associated Pain. Int J Mol Sci 21. https://doi.org/10.3390/ijms21072326

– Vangeel, L., Benoit, M., Miron, Y., Miller, P.E., De Clercq, K., Chaltin, P., Verfaillie, C., Vriens, J., Voets, T., 2020. Functional expression and pharmacological modulation of TRPM3 in human sensory neurons. Br J Pharmacol 177, 2683-2695. https://doi.org/10.1111/bph.14994

6. References

1. Viana, F. and T. Voets, *Heat Pain and Cold Pain*, in *The Oxford Handbook of the Neurobiology of Pain*, J.N. Wood, Editor. 2019, Oxford University Press: Oxford.
2. Vriens, J., B. Nilius, and T. Voets, *Peripheral thermosensation in mammals.* Nat Rev Neurosci, 2014. **15**(9): p. 573-89.
3. Caterina, M.J., et al., *The capsaicin receptor: a heat-activated ion channel in the pain pathway.* Nature, 1997. **389**(6653): p. 816-24.
4. Vandewauw, I., et al., *A TRP channel trio mediates acute noxious heat sensing.* Nature, 2018. **555**(7698): p. 662-666.
5. McKemy, D.D., W.M. Neuhausser, and D. Julius, *Identification of a cold receptor reveals a general role for TRP channels in thermosensation.* Nature, 2002. **416**(6876): p. 52-8.
6. Peier, A.M., et al., *A TRP channel that senses cold stimuli and menthol.* Cell, 2002. **108**(5): p. 705-15.
7. Obata, K., et al., *TRPA1 induced in sensory neurons contributes to cold hyperalgesia after inflammation and nerve injury.* J Clin Invest, 2005. **115**(9): p. 2393-401.
8. Bautista, D.M., et al., *TRPA1 mediates the inflammatory actions of environmental irritants and proalgesic agents.* Cell, 2006. **124**(6): p. 1269-82.
9. Colburn, R.W., et al., *Attenuated cold sensitivity in TRPM8 null mice.* Neuron, 2007. **54**(3): p. 379-86.
10. Dhaka, A., et al., *TRPM8 is required for cold sensation in mice.* Neuron, 2007. **54**(3): p. 371-8.
11. Karashima, Y., et al., *TRPA1 acts as a cold sensor in vitro and in vivo.* Proc Natl Acad Sci U S A, 2009. **106**(4): p. 1273-8.
12. Gentry, C., et al., *The roles of iPLA2, TRPM8 and TRPA1 in chemically induced cold hypersensitivity.* Mol Pain, 2010. **6**: p. 4.
13. Uvin, P., et al., *Essential role of transient receptor potential M8 (TRPM8) in a model of acute cold-induced urinary urgency.* Eur Urol, 2015. **68**(4): p. 655-61.
14. Knowlton, W.M., et al., *TRPM8, but not TRPA1, is required for neural and behavioral responses to acute noxious cold temperatures and cold-mimetics in vivo.* Pain, 2010. **150**(2): p. 340-50.

15. Lohman, D., R. Schleifer, and J.J. Amon, *Access to pain treatment as a human right.* BMC Med, 2010. **8**: p. 8.

16. Reid, K.J., et al., *Epidemiology of chronic non-cancer pain in Europe: narrative review of prevalence, pain treatments and pain impact.* Curr Med Res Opin, 2011. **27**(2): p. 449-62.

17. Colloca, L., et al., *Neuropathic pain.* Nat Rev Dis Primers, 2017. **3**: p. 17002.

18. Jensen, T.S. and N.B. Finnerup, *Allodynia and hyperalgesia in neuropathic pain: clinical manifestations and mechanisms.* Lancet Neurol, 2014. **13**(9): p. 924-35.

19. Munns, C., M. AlQatari, and M. Koltzenburg, *Many cold sensitive peripheral neurons of the mouse do not express TRPM8 or TRPA1.* Cell Calcium, 2007. **41**(4): p. 331-42.

20. Memon, T., et al., *TRPA1 expression levels and excitability brake by KV channels influence cold sensitivity of TRPA1-expressing neurons.* Neuroscience, 2017. **353**: p. 76-86.

21. Li, C.L., et al., *Somatosensory neuron types identified by high-coverage single-cell RNA-sequencing and functional heterogeneity.* Cell Res, 2016. **26**(8): p. 967.

22. Usoskin, D., et al., *Unbiased classification of sensory neuron types by large-scale single-cell RNA sequencing.* Nat Neurosci, 2015. **18**(1): p. 145-53.

23. Zeisel, A., et al., *Molecular Architecture of the Mouse Nervous System.* Cell, 2018. **174**(4): p. 999-1014 e22.

24. Picelli, S., et al., *Full-length RNA-seq from single cells using Smart-seq2.* Nat Protoc, 2014. **9**(1): p. 171-81.

25. Carattino, M.D. and N. Montalbetti, *Acid-sensing ion channels in sensory signaling.* Am J Physiol Renal Physiol, 2020. **318**(3): p. F531-F543.

26. Babinski, K., K.T. Le, and P. Seguela, *Molecular cloning and regional distribution of a human proton receptor subunit with biphasic functional properties.* J Neurochem, 1999. **72**(1): p. 51-7.

27. Waldmann, R., et al., *Molecular cloning of a non-inactivating proton-gated Na+ channel specific for sensory neurons.* J Biol Chem, 1997. **272**(34): p. 20975-8.

28. Askwith, C.C., et al., *DEG/ENaC ion channels involved in sensory transduction are modulated by cold temperature.* Proc Natl Acad Sci U S A, 2001. **98**(11): p. 6459-63.

29. Matasic, D.S., et al., *Paradoxical Potentiation of Acid-Sensing Ion Channel 3 (ASIC3) by Amiloride via Multiple Mechanisms and Sites Within the Channel.* Front Physiol, 2021. **12**: p. 750696.

30. Li, W.G., et al., *Nonproton ligand sensing domain is required for paradoxical stimulation of acid-sensing ion channel 3 (ASIC3) channels by amiloride.* J Biol Chem, 2011. **286**(49): p. 42635-42646.

31. Yu, Y., et al., *A non-proton ligand sensor in the acid-sensing ion channel.* Neuron, 2010. **68**(1): p. 61-72.

32. Behrendt, H.J., et al., *Characterization of the mouse cold-menthol receptor TRPM8 and vanilloid receptor type-1 VR1 using a fluorometric imaging plate reader (FLIPR) assay.* Br J Pharmacol, 2004. **141**(4): p. 737-45.

Final report of the university research project of

Prof. dr. Sarah Weckhuysen, MD, PhD
Universiteit Antwerpen (UAntwerpen)

Prof. dr. Sarah Weckhuysen, MD, PhD
Applied&Translational Neurogenomics Group
VIB-UAntwerp Center for Molecular Neurology
UAntwerp-CDE
Parking P4, Building V
Universiteitsplein 1, 2610 Antwerpen
Belgium
uantwerpen.vib.be

Neurology Department
Antwerp University Hospital
Drie Eikenstraat 655, 2650 Edegem
Belgium
www.uza.be/neurologie

Study and targeted treatment development for epileptic encephalopathies using 2D and 3D human induced plupripotent stem cell-derived neuronal cultures

1. Background

The developmental and epileptic encephalopathies (DEEs) are a debilitating subgroup of the epilepsies, characterized by frequent and often treatment resistant seizures with early onset, and developmental delay. The majority of patients have a genetic cause. Current treatments for DEE focus on seizure control using anti-epileptic drugs. However, even though some patients do become seizure free, most patients with genetic DEEs still suffer from severe developmental delay. Many lines of evidence suggest that the developmental and the epileptic features are both, at least partially, an independent result of the underlying genetic defect. There is thus a strong need for new therapies that not only treat seizures, but also target the developmental aspects of DEEs. The prototype and most common genetic form of neonatal DEE, illustrating many of the characteristics of genetic DEEs, is *KCNQ2* encephalopathy (KCNQ2-E). This disorder, described by our group in 2012, is caused by *de novo* missense mutations in the gene *KCNQ2* encoding the Kv7.2 subunit of the tetrameric M-channel, a voltage-gated potassium channel that is widely expressed throughout the brain, in excitatory and inhibitory neurons at the axon initial segment (AIS), nodes of Ranvier, presynaptic terminals and the soma, as well as in astrocytes. The M-current is responsible for repolarization of the membrane, dampening of repetitive firing and controlling neuronal excitability. Both a severe lack and excess of channel function can result in the development of KCNQ-E, due to heterozygous dominant negative (DN) or gain of function (GOF) mutations respectively. Seizures in children with KCNQ-E often respond poorly to anti-epileptic drugs, and more importantly, therapies for the developmental problems are currently unavailable.

With the financial support of the GSKE, we have developed human induced Pluripotent Stem Cell (hIPSC)-derived neuronal cultures starting from patient peripheral blood mononuclear cells, as a model of KCNQ2-E. Using electrophysiology and (high-content) microscopy we have performed multimodal characterization of these cultures and identified feature identifiers unique to DN and GOF genotypes. Furthermore drug screens in our model have produced promising results that push mutant-specific electrophysiological readouts toward wild-type.

2. Summary of achievements

2.1. Generation of patient-derived hIPSC-derived excitatory neurons and isogenic lines

We have now generated a total of 11 hIPSC-derived excitatory neuronal lines comprised of: 3 DN mutations (G290D, A294V, R560W), 2 less severe, self-limiting neonatal epilepsy (SeLNE) mutations (K327Q, R547W), 2 GOF mutations (R201C, R201H), and 4 control lines; including 1 healhy sibling, 1 commericial line and 2 isogenic lines (isoG290D, isoR201C). iPSCs-derived neuronal cultures were generated using inducible overexpression of human Neurogenin1 (hNGN1) and Neurogenin2 (hNGN2), a popular method to generate cortical excitatory neurons that mature significantly faster than neurons generated via small-molecules. TALEN targeting the CLYBL locus was used to stably integrate the construct containing hNGN1 and hNGN2 under a doxycycline inducible promoter, as well as an EF-1 promoter driving expression of mCherry in the hIPSC lines (Fig1A). After nucleofection with the TALEN and the donor construct, hIPSC lines were sorted using the mCherry signal to enrich for successfully engineered hIPSCs (Fig1A).

Subsequently, clonal lines were generated and only clones with a homozygous insertion of the donor construct were used in further experiments. The clones showed no genomic abnormalities tested by single-nucleotide polymorphism chip microarray analyses and showed pluripotency marker expression tested by qPCR.

For neuronal differentiation, hIPSCs were pre-differentiated for 3 days to become post mitotic (Day3 Neurons). Day 3 neurons were then co-cultured with primary mouse astrocytes for the final differentiation (Fig1B left). Using immunocytochemistry, we show that hIPSC-derived neurons grown to 28 days *in vitro* (DIV) are positive for the neuronal marker MAP2 and synaptic markers Homer and Bassoon (Fig1B, right).

A
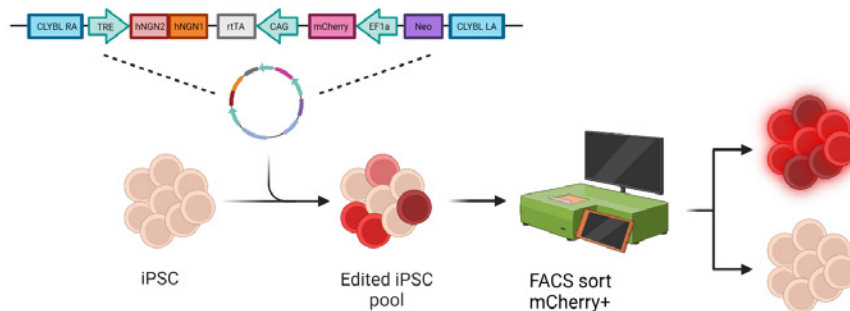
B
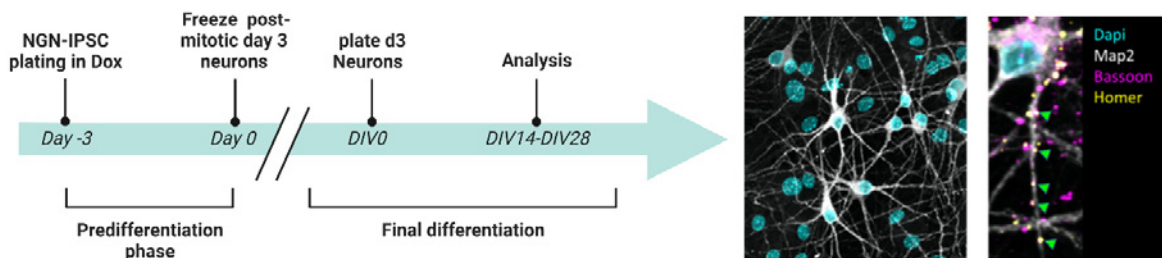
Figure 1: *A. Graphical overview of the generation of NGN-stable iPSC lines using Facs sorting of mCherry positive cells. B Left). Workflow for neuronal differenitation. B Right) Immunostaining of pre- and post-synaptic marker Bassoon (magenta) and Homer (yellow) at DIV 28, respectively. Synapses are shown by co-localization of the two markers (green arrow).*

To increase our number of control lines, we generated isogenic corrected lines for a DN and GOF variant. The isogenic DN line was out sourced, whereas the isogenic of the GOF line was generated by ourselves using the novel Crispr prime editing (PE) technology, which significantly decreased risks of off target effects.

We optimized the Crispr PE technology by generating novel all-in-one, nick RNA-independent, PE plasmids driven by a tissue-broad EF-1alpha promoter which is especially suitable for human hIPSC disease models. The PE construct was inserted in the cells using nucleofection, and by using an additional GFP cell sorting step (Figure 2), we could increase edit efficiencies up to 50% of cell clones (Figure 3). Quality control of the edited cell lines verified expression of pluripotency markers Oct4, Nanog and Sox2, and the absence of the recurrent chr20q11.21 duplication. Whole genome sequencing of the mother line and two edited lines confirmed the absence of PE mediated off-target effects. A paper describing the methods in more detail (including comparison of different versions of the PE system) is accepted for publication (https://pubmed.ncbi.nlm.nih.gov/37443005/).
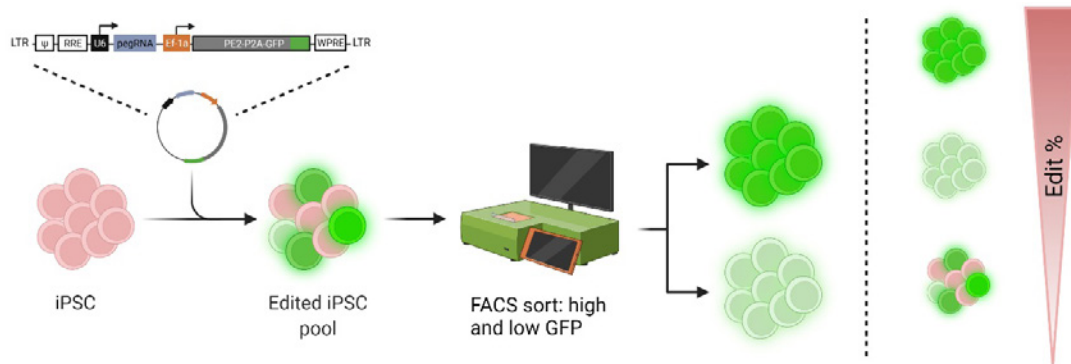
Figure 2: Graphical overview of the prime editing workflow to increase editing efficiency.
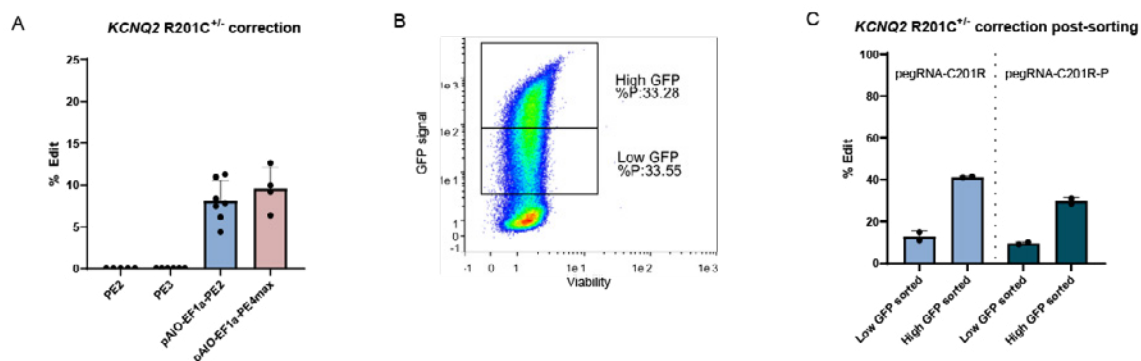

Figure 3: Patient-derived hIPSC editing using pAIO-PE2-GFP and pAIO-PE4max. (A) Comparison of the editing efficiency when correcting the heterozygous KCNQ2 R201C mutation using CMV-PE2-GFP and CMV-PE3-GFP versus pAIO-PE2-GFP and pAIO-PE4max. (B) FACS showing the two GFP-positive fractions that were separated when sorting the GFP populations. (C) Editing efficiency of pAIO-PE2-GFP after sorting on the high and low GFP expressing fractions using pegRNA-C201R and pegRNA-C201R-P.

2.2.   2. Characterization of hIPSC-neurons
a) Morphology

Four-week-old neuronal cultures were morphologically characterized using a high-throughput microscopy pipeline optimized by the group of Prof. W. De Vos at the University of Antwerp. Cultures are immunocytochemically labelled with neuronal specific pre- and post-synaptic markers Bassoon and Homer, and dendrite marker MAP2 (as the mCherry signal faints after PFA fixation). Confocal images are acquired with an automated Opera Phenix High Content Screening System (PerkinElmer) using a 40x water immersion lens (numerical aperture 1.1), enabling the fast generation of high-quality data (Figure 4). The images are processed and analyzed using the Acapella® software. The strength of this approach lies in the fact that it can account for a number of potential sources of bias. For example, differences in the number of synapses could have many origins such as alterations in cell density, dendrite density or pre- and/or post-synaptic density. We could show that both the DN and LOF neurons show alterations in synaptic density, namely a significant reduction in presynaptic density (puncta/neurite area) for all KCNQ2 lines and a significant increase of postsynaptic density (puncta/neurite area) for G290D and K327Q
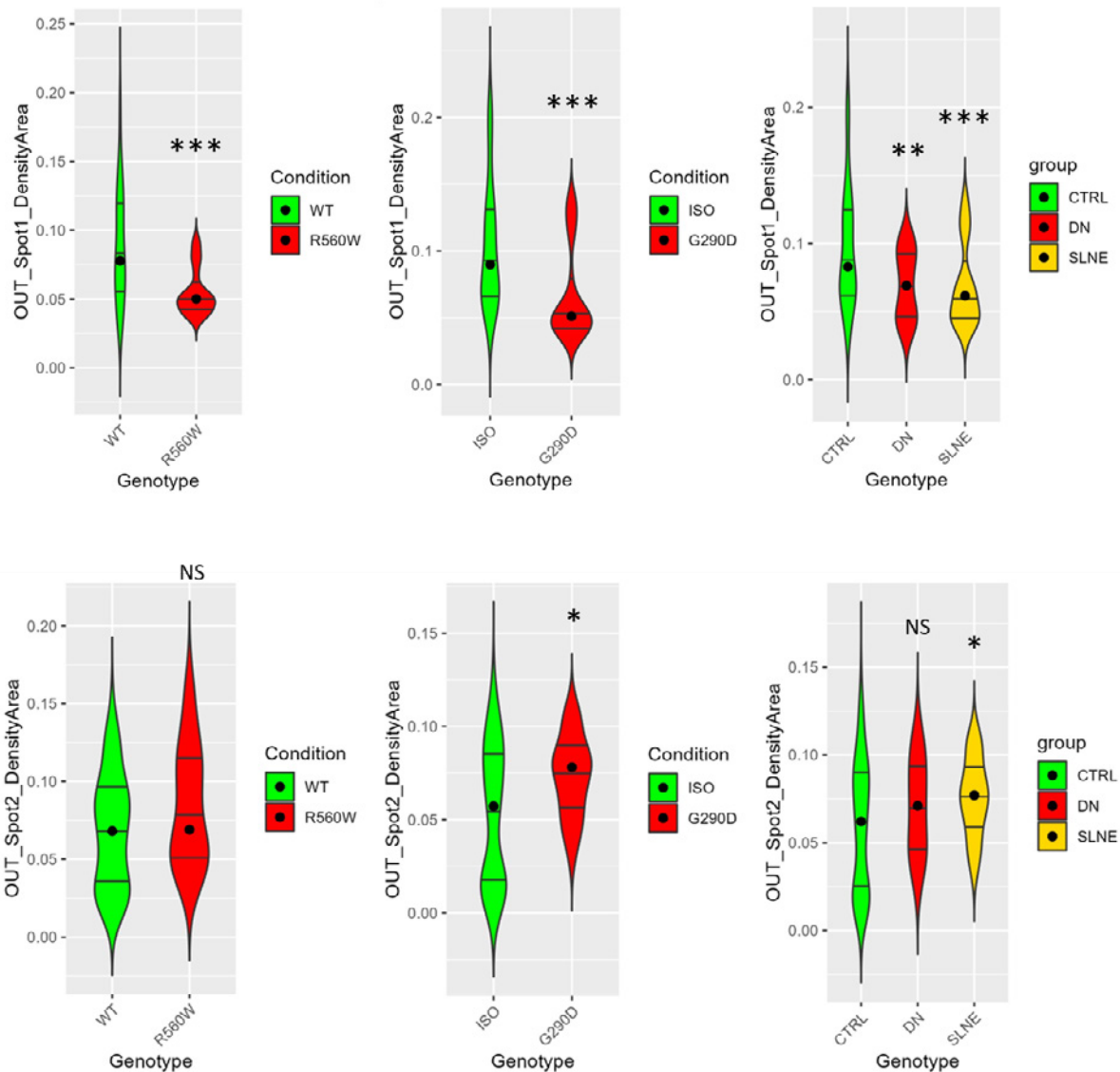
Figure 4: Morphological profile of KCNQ2-E hIPSC derived neurons at week 4.

The axonal initial segment (AIS) has the ability to change its length, as well as its distance to the soma as a response to hyperexcitability. To investigate if this was also the case for in our mutant lines, we stained 7 week old cultures using AnkG and MAP2. We chose this late stage timepoint to increase the chance for the occurrence of (dis)homeostatic plasticity events. AIS length remained unchanged in all the KCNQ2 mutant lines, except for a significant reduction observed in the length of AIS in the DN A294V variant. Distance to the soma was increased for all mutant lines (Figure 5).
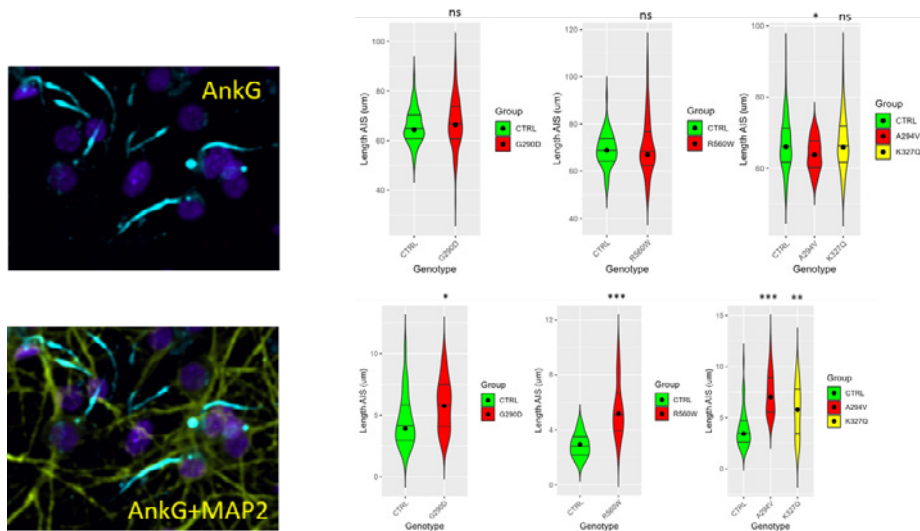
Figure 5: Length measurements of the AIS in iPSC-derived neuronal cultures. Left, Close up of AnkerinG (light blue) and MAP2 (yellow) staining in week 7 neuronal cultures. Right, Average length of AIS and distance of the AIS to the soma in healthy and mutant lines.

b) Functional characterization – Ca2+ imaging

During the optimization of the MEA seeding, we started optimizing fluo4AM calcium imaging experiments as an additional, more high-throughput, electrophysiological read out. In our initial experimental set up, 4-week-old hIPSC-derived neuronal cultures rarely presented spontaneous bursting during ca-imaging experiments, likely because during the procedure of fluo4AM experiments, frequent and total media changes are required, which are not well tolerated by neuronal cultures. Therefore, to stimulate neuronal bursting activity we added 10 μM of Forskolin, a compound known to increase cAMP, resulting in synchronous bursting of the neuronal networks. Preliminary data showed significant hyperactive bursting shortly after forskolin stimulation in the DN lines, whereas the SeLNE lines do not differ statistically from the control (Figure 6).
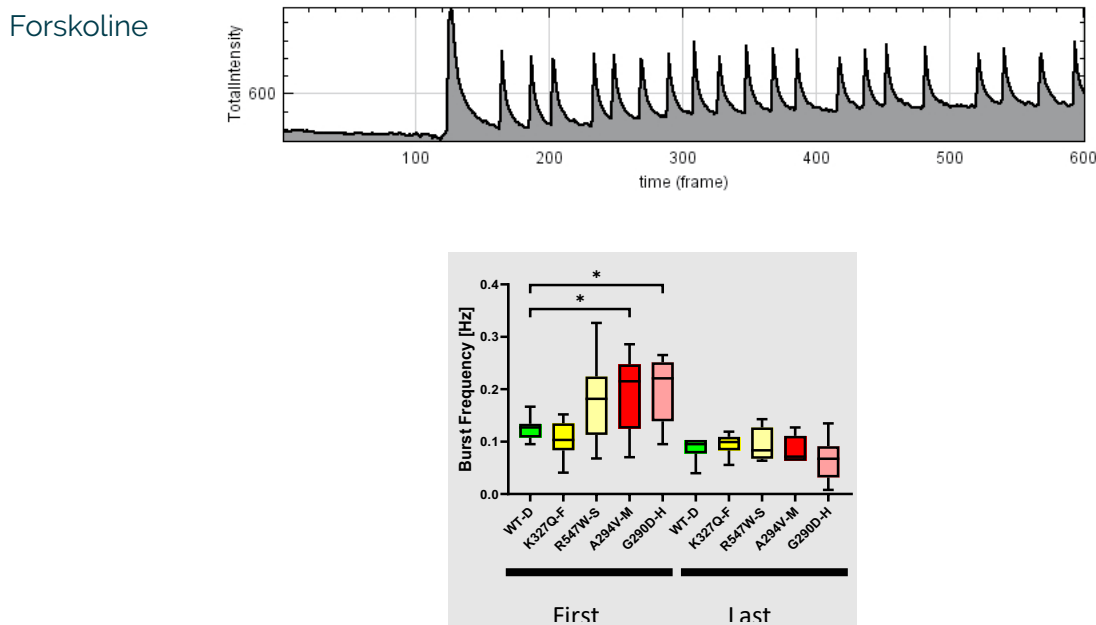

Figure 6: Ca²⁺ traces of iPSC-derived neuronal cultures after forskolin treatment. Top, total fluorescent signal over time shows no network activity before forskolin stimulation, and synchronous, repetitive bursting after stimulation. Bottom, separating burst frequency in early phase and a late phase, demonstrates significant hyperactivity in the early phase for the DN lines vs the control.

As opening the plate for addition of forskolin disrupts control over temperature and CO2 and induces variability, we have also generated a robust and simple method protocol that allows the recording of spontaneous network bursting in 95 to 100% of our hIPSC-derived neuronal cultures using Fluo4AM Ca-imaging (Figure 7). This method is very valuable for researchers that do not have access to a MEA system, or when spatial information is of interest.
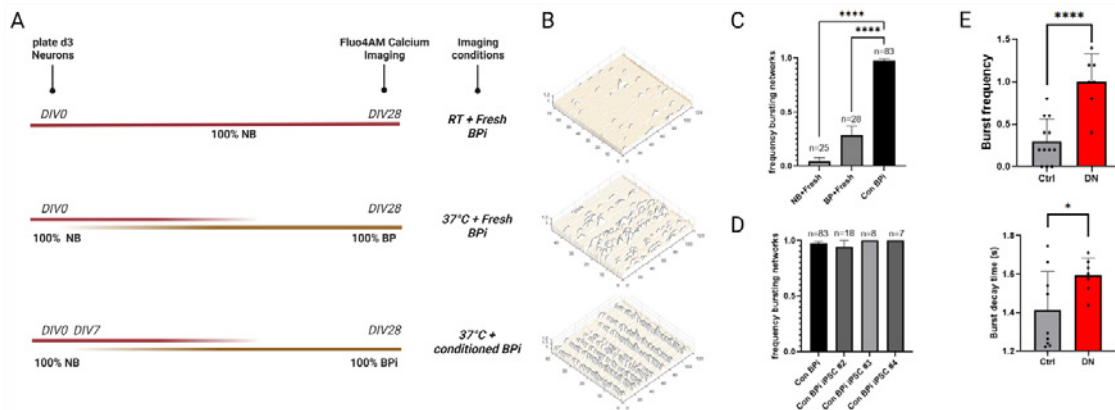

Figure 7: Overview of the bursting behaviour of iPSC-derived neuronal cultures in 3 different experimental setups. *A. Schematic representation of the 3 different experimental setups tested to detect network bursting using Ca2+ imaging. B. Representative Ca2+ imaging traces show absence of bursting and low, unsynchronized spiking for setup 1 (top), a more active network with mainly unsynchronized spiking in setup 2 (middle), and spontaneous synchronized bursting in setup 3 (bottom). C. Bar plot representing average network bursting frequency shows a significant increase for setup 3 compared to setup 1 and 2. D. Validation of setup 3 in three different hIPSC lines shows nearly 100% efficiency. E. Using setup 3, neurons carrying the KCNQ2-DN mutations parallel MEA bursting characteristics (see subsequent section), showing an increased burst frequency and burst decay times compared to controls. NB: Neurobasal, BP: Brainphys, BPi: Brainphys optimized for imaging, RT: Room temperature,*

c) Functional characterization – high-density cMOS-MEA

Over the past years, we have optimized the high-density cMOS-MEA plate preparation and seeding of the neurons for recording on the Max Two system of Maxwell Biosystems. We have now recorded neuronal cultures every week for 10 minutes, up to 7 weeks long. We have seen statistical significant differences between the electrophysiological characteristics of the mutant and isogenic cultures, and have seen opposite changes in DN versus GOF lines. Neuronal electrical activity increased as a function of time, with GOF displaying slower development and lower overall activity (Figure 8).
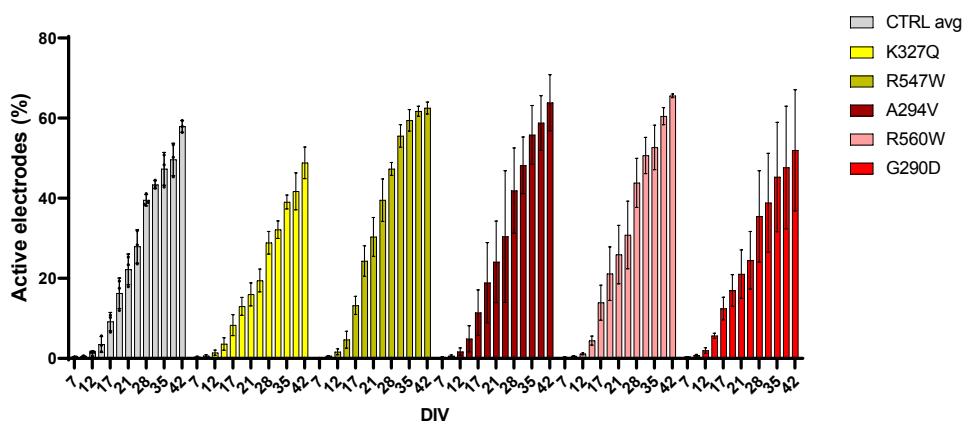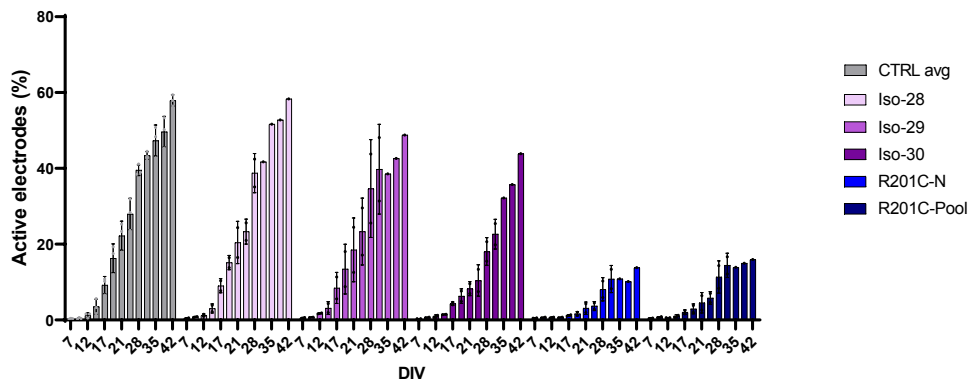
Figure 8: Development of electrically active neurons grown on high-desnsity cMOS MEA plates. *Percentage of electrodes that detect neuronal electrical activity in DN (red) and SeLNE (yellow) (top), and GOF (bottom) sampled across day in vitro 7 to 42. Three individual isogenic R201C clones (purple) are shown for comparison with one R201C clone as well as a pool of GOF clones.*

Electrophysiological activity is measured as individual spontaneous extracellular action potentials (spikes), and synchronized plate-wide bursts of activity. Cultures of DN *KCNQ2* genotypes display a greater rate of individual spiking, and duration of synchronized burst events, whereas GOF display reduced rate of individual spiking in mature cultures and reduced burst duration (Figure 9).
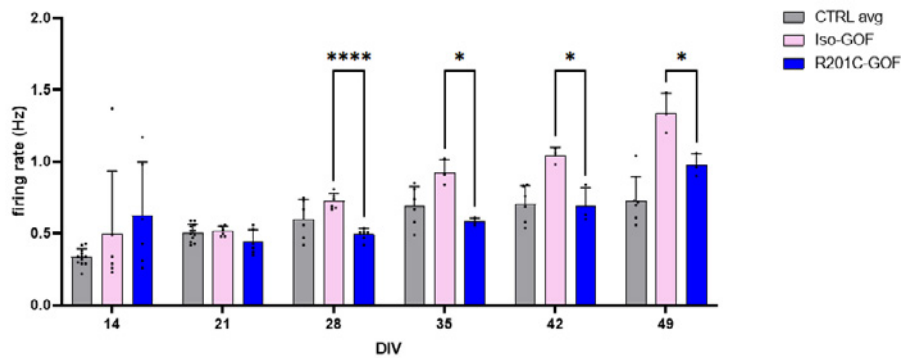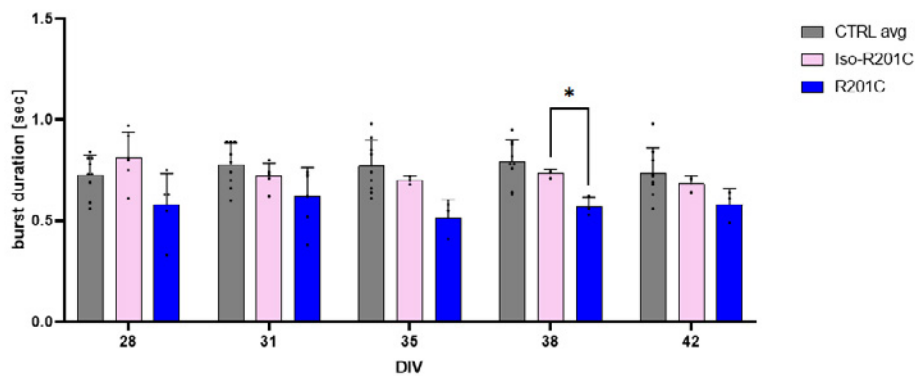
A
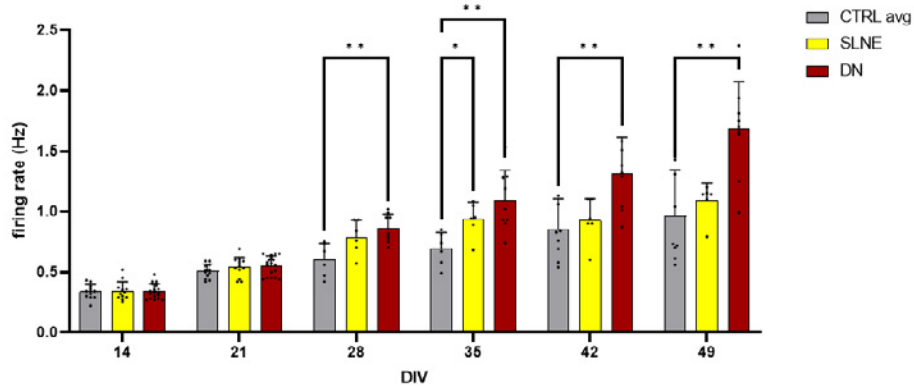
B
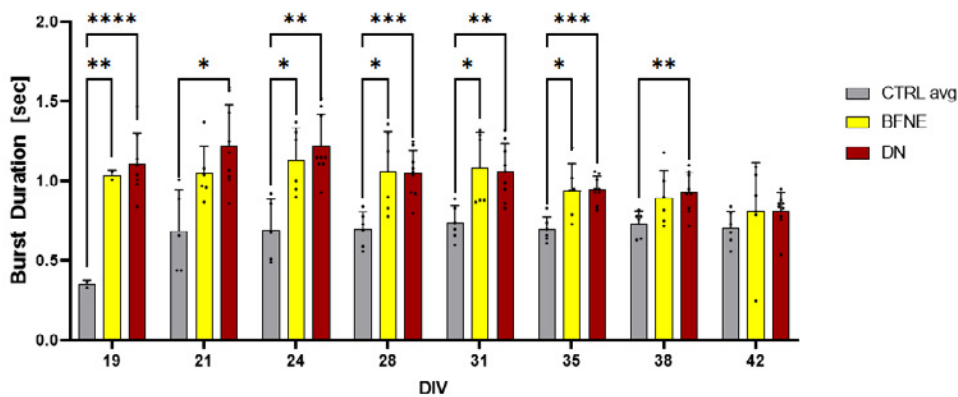
C

D

Figure 9: Development of spike firing rate and synchronized burst duration differ between DN/LOF, GOF and wildtype KCNQ2 control (CTRL) neurons. *DN (red) and SeLNE (yellow) KCNQ2 neurons develop networks with greater spike firing rates(A), and duration of synchronized bursts (B) compared to controls (grey). In contrast, GOF KCNQ2 neurons developed reduced firing rates at later stages of network development (C), and show a trend towards shorter synchronized bursting events (D) compared to pooled control data and isogenic controls.*

Statistical analysis of all the data is still ongoing, and heat maps are being generated to identify the most consistent and robust parameters that are impacted by the different mutant types.

d) Treatment development

Having identified features of mutant *KCNQ2* networks, we assayed the ability Kv7.2 channel agonists to pharmacologically rescue wildtype control network behaviours in a DN *KCNQ2* background. For these experiments we compared the classical Kv7.2 activator, retigabine (RTG), with a retigabine analog (Compound 60) developed by a collaborator within the TreatKCNQ consortium with the aim to validate improved pharmacology. We found that a maximal concentration of 10 µM RTG was required to silence network activity, in comparison to 0.3-1 µM RTG-A. In chronic exposure, treatment experiments with 100 nM of Compound 60 beginning from DIV1, reduced network activity of DN G290D *KCNQ2* mutants (Figure 10), whereas RTG had no effect at this concentration.
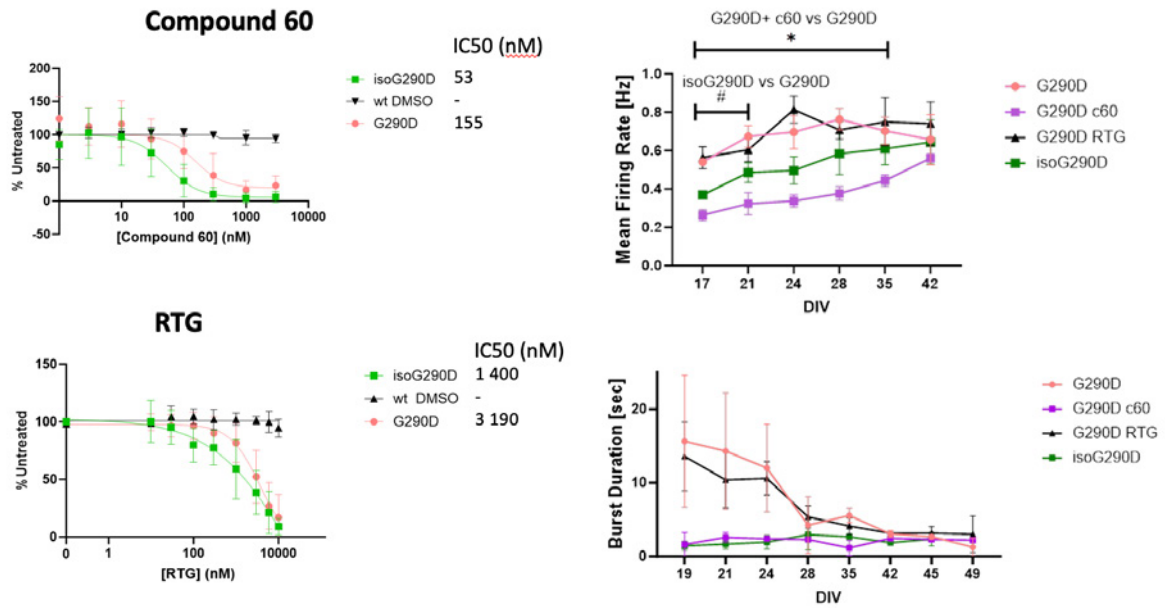
Figure 10: Effect of Compound 60 versus RTG treatment on DN and isogenic networks. *Compound 60 reduced burst duration, firing rate with a much larger potency than RTG.*

We also developed antisense oligonucleotides (ASOs) designed to knockdown general expression of *KCNQ2* with the aim of rescuing wildtype network function in GOF mutations. One lead design generated knockdown of *KCNQ2* mRNA transcript levels in GOF-R201C and wt control lines, and was chosen to test chronic treatment on GOF-R201C cultures grown on the cMOS-MEA. All MEA ASO experiments were performed alongside wells treated with Xe-991, a Kv7 channel blocker to compare the effects of channel knockdown (Figure 11). Both channel blocker and ASO treatment increased the total active electrodes and spike firing rate, pushing these parameters towards wt controls seen in Figure 11. ASO treatment in particular produced reliably longer synchronized burst with greater overall spiking activity within the bursts in comparison to vehicle or channel blocker wells.
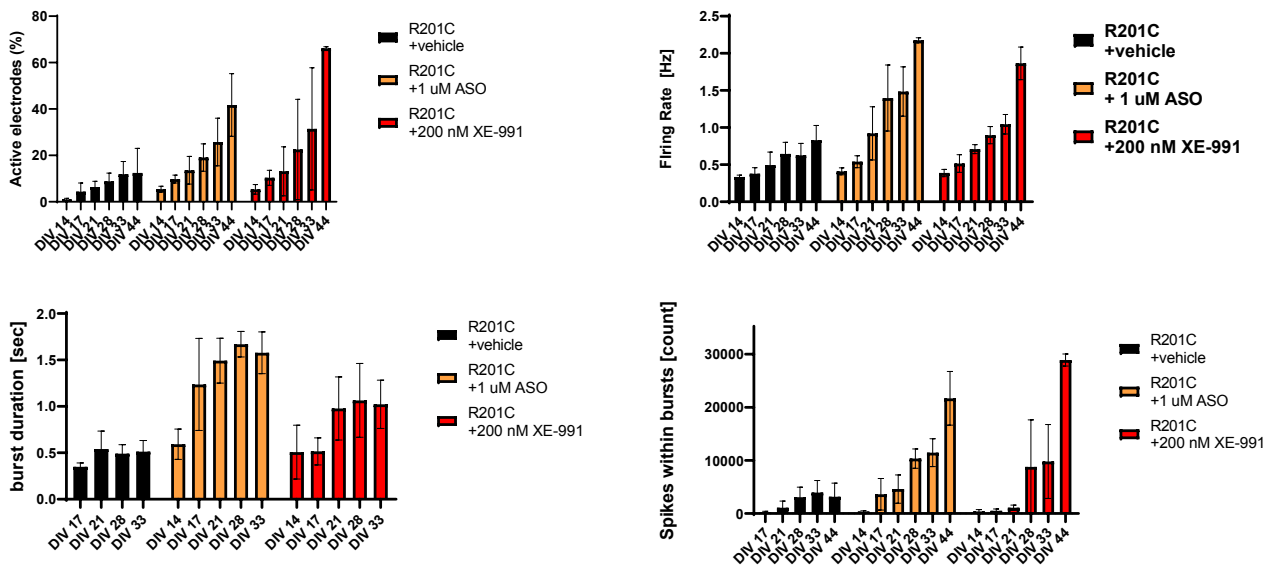

Figure 11: Chronic ASO treatment rescues wildtype network function and development in a GOF KCNQ2 background. *1 uM treatment with a KCNQ2-targeted ASO knockdown increased GOF-R201C spiking (top) and bursting (bottom) features compared to vehicle controls. Chronic treatment with Kv7.2 channel blocker, Xe-991, included for comparison.*

d) Transcriptome analysis
We have already generated pellets for RNA extraction of all the hIPSC-derived neuronal lines at week 2 and week 4. Short read RNA sequencing of RNA of 4 weeks old hIPSC-derived neuronal lines has been performed for evaluation of differential gene expression between genotypes. Analysis is currently ongoing.

3. Further planning

We are currently analysing all final data. In the next 6 months, we plan to submit at least 2 additional manuscript describing 1. the results of experiments on our SeLNE and DN patient lines, and 2. the results of experiments on our GoF patient lines.

4. Additional funding acquired

The GSKE funding allowed us to generate the necessary preliminary data and expertise (as described above) to acquire additional funding for the work on neurodevelopmental and epileptic encephalopathies in our research group. As already mentioned in our previous project report, in 2021 we received funding from the European EJP-RD program to coordinate the international "TreatKCNQ" project. This allowed us among other to recruit a new bright Canadian postdoc (Mark Kaji) who is helping us to expand our work with hIPSC derived neuronal models. In 2021 we also received project funding from FWO to use hIPSC derived neuronal cultures to better understand the mechanisms of KCNQ2 related epilepsies. In addition, in December 2021 we received the good news that we were granted a second FWO project to support our research line that uses advanced genomics techniques to unravel the genetics of the developmental and epileptic encephalopathies. Also in this project, we will use hIPSC derived neuronal cultures to validate genetic findings. So also here, the expertise we established with the help of GSKE was instrumental in receiving this funding. Finally, from 02/2023, we receive funding for the PhD salary of our new PhD student Noortje Zonnekein, who will use iPSC-derived neuronal and microglial cultures and organoids to study the mechanisms underlying KCNQ3 related encephalopathy.

Projecten jonge onderzoekers 2020-2022 gefinancierd door de G.S.K.E.

Projets de recherche de jeunes chercheurs 2020-2022 subventionnés par la F.M.R.E.

Research projects of young researchers 2020-2022 funded by the Q.E.M.F.

Universiteiten met onderzoeksprogramma's die gesteund worden door de G.S.K.E.

Universités ayant des programmes de recherche subventionnés par la F.M.R.E.

Universities having research programs supported by the Q.E.M.F.

→ Universiteit Antwerpen (UAntwerpen)
→ Universiteit Gent (UGent)

→ Katholieke Universiteit Leuven (KU Leuven)

Brussel/Bruxelles/Brussels

België
Belgique
Belgium

Europa
Europe

→ Université Catholique de Louvain (UCLouvain)

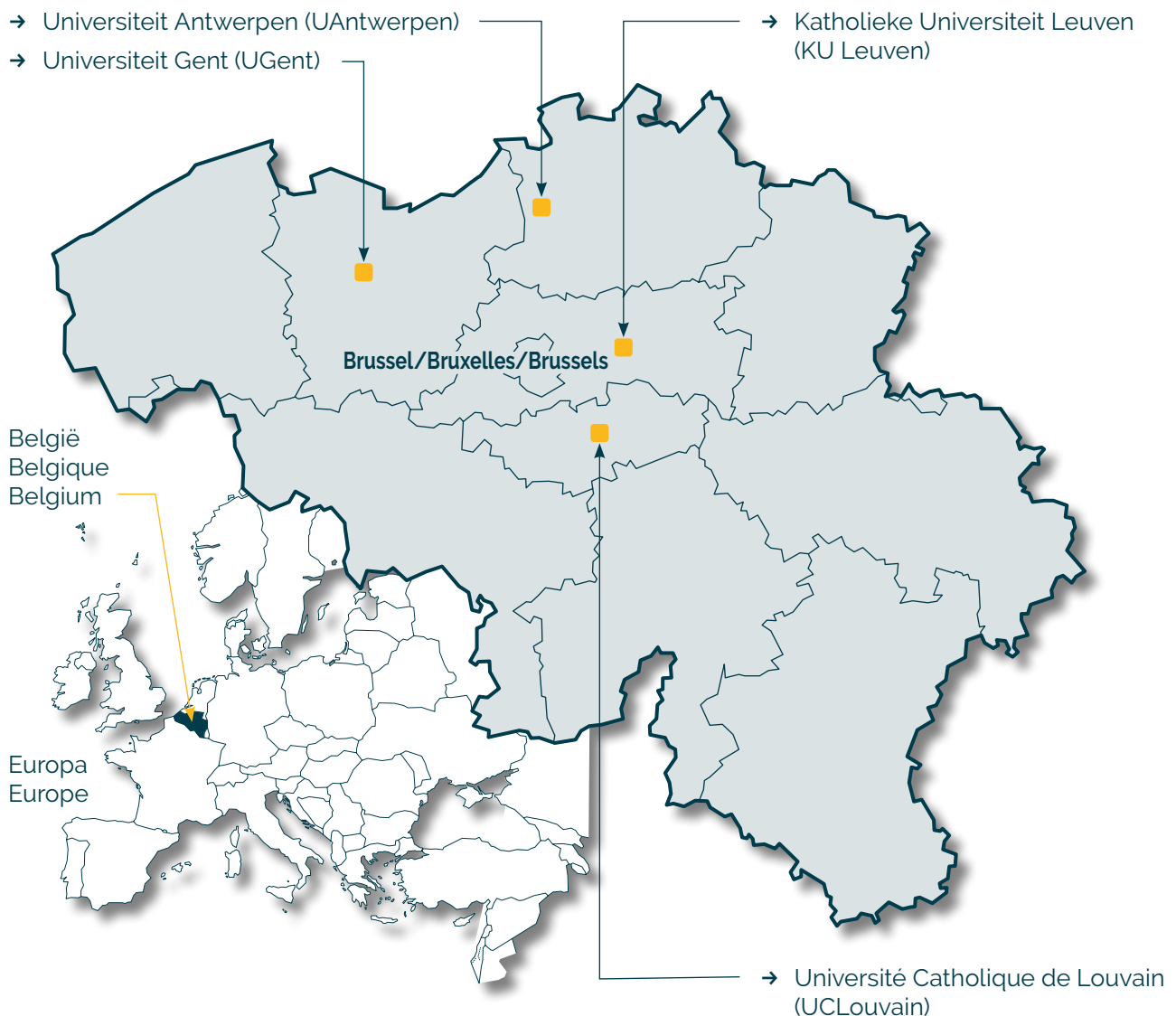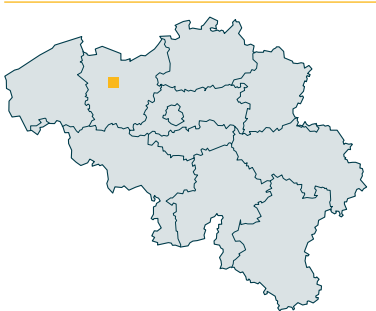# Projecten jonge onderzoekers 2020-2022 gefinancierd door de G.S.K.E.

Projets de recherche de jeunes chercheurs 2020-2022 subventionnés par la F.M.R.E.

Research projects of young researchers 2020-2022 funded by the Q.E.M.F.

UGent

Dr. Lars Emil Larsen, PhD
Closed loop precision therapy for epilepsy using photopharmacology

Prof. dr. Evelien Carrette (UZ Gent)
Novel interventions for patients with drug resistant epilepsy and cognitive decline: neuromodulatory effects of combined transcutaneous vagal nerve stimulation and cognitive therapy

UAntwerpen

Eline Wauters, PhD (VIB)
Onset age variability in GRN-associated frontotemporal lobar degeneration: identification of a functional onset age modifier

KU Leuven

Dr. Valerie Uytterhoeven
Molecular mechanisms and inducers of chaperone mediated Tau autophagy in Alzheimer's Disease

Aya Takeoka, PhD (IMEC)
Learning to walk without the brain: Determining cellular signatures underlying age-dependent spinal cord plasticity

UCLouvain

Prof. Bernard Hanseeuw, PhD
Biochemical mechanisms of regional tau protein aggregation in the human brain

Dr. Emanuel van den Broeke
The involvement of top-down facilitatory serotonergic pathways in nocebo- induced pain hypersensitivity

Prof. Riëm El Tahry, MD, PhD
Optimization Vagus nerve stimulation for refractory epilepsy

Final report of the research project of the young researcher

Prof. dr. Evelien Carrette
(UZ Gent)

Prof. dr. Evelien Carrette
Beleidsmedewerker
Neurologie | Neuroscience@U(Z)Gent

Universitair Ziekenhuis Gent | C. Heymanslaan 10 | 9000 Gent
T +32 9 332 45 40
evelien.carrette@uzgent.be
Skype eveliencarrette
Ingang 12 | Route 1556 | uzgent.be |

Novel interventions for patients with drug resistant epilepsy and cognitive decline: neuromodulatory effects of combined transcutenaous vagal nerve stimulation and cognitive therapy.

Our goal was to investigate the efficacy and underlying mechanism of action of transcutaneous vagal nerve stimulation (t-VNS), a non-invasive neurostimulation approach for patients with DRE and memory problems in a collaborative setting of the Reference Center for Refractory Epilepsy at Ghent University Hospital.
We hypothesize that combined tVNS-CT is able to improve the memory performance of these patients better than CT alone by affecting neuronal cortical plasticity networks and aim to demonstrate this by electrophysiological co-registration.

Based on the results of our initial studies that we already reported on in our previous progress reports, we have slightly adjusted the scope of the research towards further investigation of the mechanism of action and effects of tVNS and other non-invasive neuromodulatory interventions on epilepsy and cognitive decline using both behavioral and electrophysiological outcome parameters.

1.   Achieved results

In the past years we have evaluated the effects of tVNS in depth both in healthy subjects and in patients. We have reported on the results of some of these studies in last years' progress reports and have added new results from additional analyses and studies completed in 2022.
We have initiated new collaborations to further study the potential of neurostimulation in cognitive decline with both studies in healthy volunteers and in patients but also initiated research on others forms on non-invasive neuromodulatory interventions.

Please find below the full report of the research performed in this context over the previous years (2020-2022).

1.1.   Studies in healthy volunteers

1. investigating the effect of tVNS on verbal memory in young and old healthy volunteers.
As reported on before we performed a randomized, controlled, crossover study, to investigate the effect of tVNS on verbal memory using a word-recognition paradigm in healthy volunteers (n=48, younger and older group) as a basis for investigating the potential of tVNS to improve cognitive decline. While VNS using an implanted device was previously shown to improve performance on memory paradigms in epilepsy patients, in this study we did not find a significant effect of tVNS, the non-invasive approach to target vagal fibers, on verbal memory performance in a group of young and older healthy participants.
Further research to investigate the potential of targeting vagus nerve fibers noninvasively to improve cognitive function is required. As optimal stimulation parameters have not been elucidated, future research should focus on the effect of different stimulation settings in an individualized way in order to define the most efficient stimulation parameters.

Mertens A, Naert L, Miatton M, Poppa T, Carrette E, Gadeyne S, Raedt R, Boon P, Vonck K. Transcutaneous Vagus Nerve Stimulation Does Not Affect Verbal Memory Performance in Healthy Volunteers. Front Psychol. 2020, 15;11:551 (IF 2,9) (attachment 1)

2. Investigating the effect of tVNS on the cognitive evoked potential in healthy volunteers

The objective of this study was to investigate whether tVNS is able to modulate the P3b component of the P300, a cognitive event related potential (ERP) reflecting noradrenaline (NA) brain activation under control of the Locus Coeruleus (LC) that could serve as a (bio)marker for non-invasive LC activation via tVNS. In this study we demonstrated that targeting vagal nerve fibers via a transcutaneous approach did not alter the P3b in healthy participants. The stimulation parameters used during a relative short period of time may have been insufficient to adequately modulate the LC-NE system. A dysfunctional locus coeruleus - norepinephrine system in patients may be more prone for improvement in contrast to the normal system in healthy volunteers investigated in this study

Gadeyne S, Mertens A, Carrette E, Van den Bossche F, Boon P, Raedt R, Vonck K (2021). Transcutaneous auricular vagus nerve stimulation cannot modulate the P3b event-related potential in healthy volunteers. Clin Neurophysiol. 2022. 135:22-29(IF 3,7) (attachment 2)

3. Investigating the effect of tVNS on cortical excitability in healthy volunteers

By combining transcranial magnetic stimulation (TMS) with EMG and EEG, we can study the modulation of Motor Evoked Potentials (MEPs) and TMS Evoked Potentials (TEPs). As these MEPs and TEPS are reproducible within subjects, they can be useful to study the effect of neuromodulatory interventions, like tVNS, on cortical excitability. These findings are expected to provide insight in the mechanism of action and help identify more optimal stimulation paradigms to be used in treatment of various neurological disorders such as epilepsy and cognitive decline. Like reported last year, we performed a prospective single-blind cross-over study in which 15 healthy male subjects underwent 2 sessions, at least one week apart. During each session, tVNS or sham stimulation was delivered at the maximum tolerated amplitude during one hour. The resting motor threshold, MEPs and TEPs were measured before and after the intervention. For these measurements, 120 single TMS pulses, 120 paired TMS pulses with a short interstimulus interval and 120 paired TMS pulses with a long interstimulus interval, were delivered over the motor hotspot. To assess the effect of tVNS on MEP morphology, we measured the average latency and amplitude of all MEPs for each condition and each pulse type. Intracortical inhibition after paired pulses was assessed by expressing the amplitude of the paired pulse response as a percentage of the amplitude of the single pulse response. MEP latency, amplitude and percentage were then compared at the single subject level before and after each intervention. Statistical analysis was conducted by means of a two-way repeated measures ANOVA. TEP data was preprocessed offline using the TESA toolbox in Matlab. A cluster-based permutation statistical analysis was conducted.

In the overall group of patients, MEP and TEP measurements were not affected by tVNS in this study. We did find an association between tVNS stimulation output current and MEP outcome measures indicating a decrease in cortical excitability in participants who tolerated higher tVNS currents. A subanalysis of participants (n = 8) who tolerated a tVNS current above 2.5 mA showed a significant increase in the resting motor threshold, a decrease in MEP amplitude and modulation of the P60 and P180 TEP components.

In this study it was shown that tVNS did not affect cortical excitability measurements in the overall population in this study. However, tVNS has the potential to modulate specific markers of cortical excitability in participants who tolerate higher stimulation levels. These findings further support the development of appropriate stimulation protocols for future studies investigating the effect of tVNS in epilepsy patients based on the recording of objective outcome parameters.

Mertens A, Carrette S, Klooster D, Lescrauwaet E, Delbeke J, Wadman WJ, Carrette E, Raedt R, Boon P, Vonck K (2021). Investigating the Effect of Transcutaneous Auricular Vagus Nerve Stimulation on Cortical Excitability in Healthy Males. Neuromodulation. 2022. 25:395-406. (IF 4,0) (attachment 3)

4. Investigating tVNS modulation of the heart-evoked potential

In collaboration with our colleagues from the UGent Ghep-lab we investigated the effects of tVNS on the so-called "heart-evoked potential". Accumulating evidence suggests that tVNS influences activity in the brainstem solitary and parabrachial nuclei, the primary relays for the transmission of visceral sensory afferents to the insula. The insula mediates interoception, which concerns the representation and regulation of homeostatic bodily states. Consequently, interoceptive pathways may be relevant to the mechanisms of action of tVNS.

For this study it was hypothesized that tVNS modulates an EEG-derived marker of interoceptive processing known as the heart-evoked potential (HEP) and that tVNS-induced HEP effects would be localizable to the insula. Like reported in our previous progress report we have performed a within-subject, sham-controlled study and we recorded EEG and ECG concurrent to tVNS in 43 healthy adults. Using ECG and EEG data, we extracted HEPs. Estimation of the cortical sources of the tVNS-dependent HEP responses observed at the scalp were computed using the Boundary Element Method and weighted Minimum Norm Estimation. Statistics were calculated using cluster-based permutation methods.

We demonstrated that tVNS altered HEP amplitudes at frontocentral and centroparietal electrode sites at various latencies. The tVNS-dependent HEP effect was localized to the insula, operculum, somatosensory cortex, and orbital and ventromedial prefrontal regions.

These results support the hypothesis that tVNS can access the insula as well as functionally and anatomically connected brain regions and that HEPs may serve as an objective, non-invasive outcome parameter for the cortical effects of tVNS.

Poppa T, Benschop L, Horczak P, Vanderhasselt MA, Carrette E, Bechara A, Baeken C, Vonck K. Auricular transcutaneous vagus nerve stimulation modulates the heart-evoked potential. Brain Stimul. 2022. 15(1):260-269. (IF 8,9) (attachment 4).

In conclusion we found that tVNS is not able to affect verbal memory in healthy volunteers, nor does it affect the cognitive evoked potential. The stimulation parameters used and the relatively short-term delivery of tVNS may have been insufficient to activate vagal fibres and adequately modulate the LC. In this study in healthy volunteers, normal functioning memory and LC-NE system in healthy volunteers may simply not be receptive for modulation, in contrast to diseased states in patients with epilepsy, memory problems or depression, in whom a disbalanced LC-NA system may be more prone for improvement.

We did find **effects on cortical excitability** in a subgroup of patients treated when relatively high output currents were applied, further demonstrating the importance of identifying optimal stimulation parameters to target the vagal nerve fibers in a non-invasive way in individual patients. We also identified a cortical evoked potential reflective of vagal nerve fiber targeting, the HEP, that may be used in the future as a biomarker in studies investigating tVNS effects on interoceptive pathways.

1.2. Studies in patients

<u>1. The potential of invasive and non-invasive vagus nerve stimulation to improve verbal memory performance in epilepsy patients</u>

As described higher (study 1), we were unable to confirm the beneficial effects of invasive VNS on verbal memory shown previously in epilepsy patients with non-invasive tVNS in healthy subjects. We therefore performed a prospective randomized cross-over study in epilepsy patients who received both tVNS and VNS with the implanted device. We aimed to replicate the effects shown with invasive VNS in 15 drug-resistant epilepsy patients and in the same patients investigated the effects of non-invasive tVNS.

All patients conducted a word recognition memory paradigm in 3 conditions: VNS ON, VNS OFF and tVNS (3-period 3-treatment cross-over study design). For each condition, patients memorized 21 highlighted words from text paragraphs. Afterwards, the intervention was delivered for 30 s. Immediate recall and delayed recognition scores were obtained for each condition. This memory paradigm was repeated after 6 weeks of invasive VNS therapy in 2 conditions: VNS ON and VNS OFF (2-period 2-treatment cross-over study design).

Recent analysis has demonstrated that acute invasive VNS and non-invasive tVNS did not improve verbal memory performance however immediate recall and delayed recognition scores were significantly improved after 6 weeks of invasive VNS treatment irrespective of the acute intervention.

In this study we were unable to demonstrate effects on verbal memory after short term invasive or non-invasive VNS in epilepsy patients. We did find for the first time in a prospective study an improved verbal memory performance after 6 weeks of VNS treatment, suggesting that longer and more repetitive stimulation of the vagal pathway is required to modulate verbal memory performance.

Mertens A, Gadeyne S, Lescrauwaet E, Carrette E, Meurs A, De Herdt V, Dewaele F, Raedt R, Miatton M, Boon P, Vonck K (2022). The potential of invasive and non-invasive vagus nerve stimulation to improve verbal memory performance in epilepsy patients. Scientific Reports 2022. 12(1):1984 (see attachment 5)

<u>2. Laryngeal Muscle-Evoked Potential Recording as an Indicator of Vagal Nerve Fiber Activation</u>

In the sideline of the ongoing research above a seperate study has been set-up to establish a objective read-out for effective stimulation of the vagus nerve with vagus nerve stimulation.

Noninvasive evoked potential recordings in laryngeal muscles (LMEPs) innervated by vagal branches may provide this marker to assess effective vagal nerve fiber activation. We investigated VNS-induced LMEPs in patients with epilepsy implanted with an (invasive) stimulator, in acute and chronic settings. A total of 17 of 25 patients underwent LMEP recordings at initiation of therapy (acute group); 15 of 25 patients after one year of VNS (chronic group); and 7 of 25 patients were tested at both time points (acute + chronic group). VNS-induced LMEPs were recorded following different pulse widths and output currents using six surface laryngeal EMG electrodes to calculate input/output curves and estimate LMEP latency, threshold current for minimal (Ithreshold), half-maximal (I50), and 95% of maximal (I95) response induction and amplitude of maximal response (Vmax). Without presenting the detailed results here we could conclude that noninvasive VNS-induced LMEP recording is feasible both at initiation of VNS therapy and after one year. Low output currents (0.25–1.00 mA) may be sufficient to activate vagal Aα-motor fibers. Maximal LMEP amplitudes seemed to decrease after chronic VNS therapy in patients.

Bouckaert C, Raedt R, Larsen LE, El Tahry R, Gadeyne S, Carrette E, Proesmans S, Dewaele F, Delbeke J, De Herdt V, Meurs A, Mertens A, Boon P, Vonck K. Laryngeal Muscle-Evoked Potential Recording as an Indicator of Vagal Nerve Fiber Activation. Neuromodulation. 2022 Apr;25(3):461-470. doi: 10.1016/j.neurom.2022.01.014. Epub 2022 Feb 15. PMID: 35177376. (attachment 8).

2.   Established collaborations and future lines of research in this field

Based on the results of the ongoing research with tVNS we have initiated new research projects:

- <u>The potential of non-invasive vagus nerve stimulation to enhance cognitive emotion regulation.</u>
Based on studies that have demonstrated that non-invasive VNS is able to enhance cognitive control, it has been suggested as a potential new tool in the treatment of major depressive disorder. In collaboration with our colleagues of the GHEP-lab we have conducted a between-subject study involving 83 healthy subjects who underwent a single session of active transcutaneous auricular (Ta)-VNS or sham stimulation after which cognitive reappraisal was examined. Our results indicate that participants receiving active taVNS, compared to sham, were better at using cognitive reappraisal and rated their response to emotion-eliciting pictures as less intense. Yet, even though we found significant differences in behavioral measures of cognitive emotion regulation, no differences between groups were found in terms of physiological responses to the emotional stimuli. Overall, these findings suggest a positive effect of taVNS on the cognitive reappraisal of emotions, but future studies assessing objective measures of neural activity during cognitive emotion regulation following taVNS are warranted.

De Smet S, Baeken C, Seminck N, Tilleman J, Carrette E, Vonck K, Vanderhasselt MA. Non-invasive vagal nerve stimulation enhances cognitive emotion regulation. Behav Res Ther. 2021 145 (see attachment 7).

- <u>Early detection of cognitive decline from EEG responses in AD risk group</u>
Via a collaboration with Prof. Van Hulle (KU Leuven) a study in individuals with high and low risk of Alzheimer Disease (AD) development will start.
In this study it will be determined which Event Related Potential (ERP) components differ between healthy controls, subjective cognitive decline (SCD) individuals at high and low risk of AD development, MCI and early-AD patients (research question 1). Candidate ERP components were already identified in a pilot study on healthy individuals. We will use the known risk factors (e.g., APOE 4 genotype) and the collected structural and molecular neuroimaging data (PET/ MR) from all participants as our ground truth when assessing which ERP components differ between the mentioned subject groups.
For our second objective, we reverse research question 1 and want to show that we can differentiate between the tested groups based on the ERP components we identified (research question 2). We will conduct the ROC analysis, as well as evaluate positive and negative predictive values for studied ERP components. We will do this by using the latest statistical techniques of classification.

Inclusion is now open for patients and will continue throughout 2023.

- <u>Non-pharmacological interventions to promote sleep and memory in ageing: a multimodal approach</u>
Via a collaboration with Prof. Peigneux and Dr. Alison Mary (ULB) a project will be set-up combining our expertise on tVNS with their expertise on sleep and memory. Understanding how cognitive functions can be maintained at old age is an increasingly important societal issue. Indeed, substantial changes in cognitive functions occur with age, memory decline being the most frequent complaint in the elderly. In this project the goal is to evaluate the effect of <u>tVNS in healthy ageing</u> to induce neuroplastic changes in brain regions that have been shown to play a crucial role on memory processes. These effects will be investigated via a multimodal approach, combining high-density electroencephalography (hdEEG), functional magnetic resonance imaging (fMRI) and diffusion-weighted magnetic resonance imaging (DWI). This

multimodal project will shed light on the brain mechanisms of induced-memory enhancement and may offer new therapeutic interventions to restore sleep and improve memory that may reduce the risk of cognitive impairment in ageing.

In 2022 this project was started in collaboration with 4BRAIN.

- <u>Continuation of the successful in-house methodology (described higher) beyond tVNS</u>
We believe to have established and developed a very interesting approach in our hands to study the effect of neuromodulatory interventions on the cortical excitability using MEP's and TEPs. We have reported higher and published our results with this approach on tVNS however we have in the meanwhile also established studies evaluating the effect of other non-invasive neuromodulatory interventions like transcranial Direct Current Stimulation (tDCS), Transcranial Magnetic Stimulation (TMS) and Focused Ultrasound (FUS) on cortical excitability both in patients and in healthy subjects.
The TMS and tDCS studies have been set-up, approved by the ethical committee and data-collection and analysis is ongoing. A first safety study by Carrette et al. with TMS in epilepsy patients has been published already.

Carrette S, Boon P, Klooster D, Van Dycke A, Carrette E, Miatton M, Raedt R, Delbeke J, Meurs A, Vonck K. Continuous theta burst stimulation for drug-resistant epilepsy. Front Neurosci. 2022 Aug 17;16:885905. doi: 10.3389/fnins.2022.885905. PMID: 36061598; PMCID: PMC9433314 (attachment 8).

Other publications on TMS and tDCS will follow in the months to come.
In addition, based on the gained expertise within these studies so far and the interest in the field in general, we will elaborate further in the future on the effect of exact timing of our neurostimulation (millisecond level) taking into account the so-called brain-state at the exact moment of performing neurostimulation. To do this we have recently received additional funding via a granted FWO-project "*Senior research projects fundamental research - G0D3323N* - entitled "*The crucial importance of timing of brain stimulation: Towards brain-oscillation-synchronized transcranial magnetic stimulation for the treatment of epilepsy*" 2023 - 2028).

- <u>International collaborations and networks</u>
Scientific Research Network (WOG) on Transcutenous Vagus Nerve Stimulation
Prof. Evelien Carrette is part of the core group of the Scientific Research Network (WOG) on Transcutenous Vagus Nerve Stimulation supported by FWO-Flanders. This research network offers the unique opportunity to consolidate and intensify collaborations between internationally renowned research groups, to create a truly multidisciplinary research consortium. The Flemish research groups in the network offer internationally renowned expertise on VNS, both from a clinical standpoint using invasive VNS (UGent) and from a fundamental research standpoint. The non-Flemish research groups of the proposed network have critically contributed to researching the fundamental questions underlying tVNS research, and will provide complementary expertise on psychophysiology, neuro-gastroenterology, (autonomic) neuroscience, anesthesiology, and clinical psychology. While there are already strong collaborations between some of these groups, as attested by several publications and joint symposia, collaborative efforts are currently hampered by the lack of a communicational infrastructure to facilitate communication, data- and methods sharing, or even shared research projects. Evelien Carrette has organized and moderated international meetings of this consortium. Follow-up meetings are planned during the 3 coming years.

3.   All publications (with acknowledgment GSKE funding)

1. Mertens A, Naert L, Miatton M, Poppa T, Carrette E, Gadeyne S, Raedt R, Boon P, Vonck K. Transcutaneous Vagus Nerve Stimulation Does Not Affect Verbal Memory Performance in Healthy Volunteers. Front Psychol. 2020, 15;11:551 (IF 2,9) (attachment 1)
2. Gadeyne S, Mertens A, Carrette E, Van den Bossche F, Boon P, Raedt R, Vonck K (2021). Transcutaneous auricular vagus nerve stimulation cannot modulate the P3b event-related potential in healthy volunteers. Clin Neurophysiol. 2022. 135:22-29(IF 3,7) (attachment 2)
3. Mertens A, Carrette S, Klooster D, Lescrauwaet E, Delbeke J, Wadman WJ, Carrette E, Raedt R, Boon P, Vonck K (2021). Investigating the Effect of Transcutaneous Auricular Vagus Nerve Stimulation on Cortical Excitability in Healthy Males. Neuromodulation. 2022. 25:395-406. (IF 4,0) (attachment 3)
4. Poppa T, Benschop L, Horczak P, Vanderhasselt MA, Carrette E, Bechara A, Baeken C, Vonck K. Auricular transcutaneous vagus nerve stimulation modulates the heart-evoked potential. Brain Stimul. 2022. 15(1):260-269. (IF 8,9) (attachment 4).
5. Mertens A, Gadeyne S, Lescrauwaet E, Carrette E, Meurs A, De Herdt V, Dewaele F, Raedt R, Miatton M, Boon P, Vonck K (2022). The potential of invasive and non-invasive vagus nerve stimulation to improve verbal memory performance in epilepsy patients. Scientific Reports 2022. 12(1):1984 (attachment 5)
6. Bouckaert C, Raedt R, Larsen LE, El Tahry R, Gadeyne S, Carrette E, Proesmans S, Dewaele F, Delbeke J, De Herdt V, Meurs A, Mertens A, Boon P, Vonck K. Laryngeal Muscle-Evoked Potential Recording as an Indicator of Vagal Nerve Fiber Activation. Neuromodulation. 2022 Apr;25(3):461-470. doi: 10.1016/j.neurom.2022.01.014. Epub 2022 Feb 15. PMID: 35177376. (attachment 8).
7. De Smet S, Baeken C, Seminck N, Tilleman J, Carrette E, Vonck K, Vanderhasselt MA. Non-invasive vagal nerve stimulation enhances cognitive emotion regulation. Behav Res Ther. 2021 145 (see attachment 6).
8. Carrette S, Boon P, Klooster D, Van Dycke A, Carrette E, Miatton M, Raedt R, Delbeke J, Meurs A, Vonck K. Continuous theta burst stimulation for drug-resistant epilepsy. Front Neurosci. 2022 Aug 17;16:885905. doi: 10.3389/fnins.2022.885905. PMID: 36061598; PMCID: PMC9433314 (attachment 7).

4. Financial Report 2022

Here you can find an overview of the financial status so far.

	A	B	C	D	E	F	G
	Naam v. kostensoort ▼	Boekingsda ▼	Omschrijving ▼	Waarde var./versl.val ▼	Naam van tegenrekening ▼	Boekjai ▼	Documentdatui ▼
1							
2	INDUSTRIËLE INKOMST	7/02/2020		-5.000,00	G.S.K.E.	2020	7/02/2020
3	INDUSTRIËLE INKOMST	31/03/2020		-5.000,00	G.S.K.E.	2020	31/03/2020
4	INDUSTRIËLE INKOMST	22/06/2020		-5.000,00	G.S.K.E.	2020	22/06/2020
5	INDUSTRIËLE INKOMST	22/09/2020		-5.000,00	G.S.K.E.	2020	22/09/2020
6	INDUSTRIËLE INKOMST	15/01/2021		-5.000,00	G.S.K.E.	2021	15/01/2021
7	INDUSTRIËLE INKOMST	23/03/2021		-5.000,00	G.S.K.E.	2021	23/03/2021
8	INDUSTRIËLE INKOMST	23/06/2021		-5.000,00	G.S.K.E.	2021	23/06/2021
9	INDUSTRIËLE INKOMST	30/09/2021		-5.000,00	G.S.K.E.	2021	30/09/2021
10	INDUSTRIËLE INKOMST	28/12/2021		-5.000,00	G.S.K.E.	2021	28/12/2021
11	INDUSTRIËLE INKOMST	5/04/2022		-5.000,00	G.S.K.E.	2022	5/04/2022
12	INDUSTRIËLE INKOMST	23/06/2022		-5.000,00	G.S.K.E.	2022	23/06/2022
13	INDUSTRIËLE INKOMST	29/09/2022		-5.000,00	G.S.K.E.	2022	29/09/2022
14	CONS VER UZIII WR	7/02/2020		726,50	INDUSTRIËLE INKOMST	2020	7/02/2020
15	CONS VER UZIII WR	31/03/2020		726,50	INDUSTRIËLE INKOMST	2020	31/03/2020
16	CONS VER UZIII WR	22/06/2020		726,50	INDUSTRIËLE INKOMST	2020	22/06/2020
17	CONS VER UZIII WR	22/09/2020		726,50	INDUSTRIËLE INKOMST	2020	22/09/2020
18	CONS VER UZIII WR	15/01/2021		726,50	INDUSTRIËLE INKOMST	2021	15/01/2021
19	CONS VER UZIII WR	23/03/2021		726,50	INDUSTRIËLE INKOMST	2021	23/03/2021
20	CONS VER UZIII WR	23/06/2021		726,50	INDUSTRIËLE INKOMST	2021	23/06/2021
21	CONS VER UZIII WR	30/09/2021		726,50	INDUSTRIËLE INKOMST	2021	30/09/2021
22	CONS VER UZIII WR	28/12/2021		726,50	INDUSTRIËLE INKOMST	2021	28/12/2021
23	CONS VER UZIII WR	5/04/2022		726,50	INDUSTRIËLE INKOMST	2022	5/04/2022
24	CONS VER UZIII WR	23/06/2022		726,50	INDUSTRIËLE INKOMST	2022	23/06/2022
25	CONS VER UZIII WR	29/09/2022		726,50	INDUSTRIËLE INKOMST	2022	29/09/2022
26	ANDERE UITGAVEN ADM	1/04/2020	article processing fee:transcutaneous vagus ne	2.664,91	FRONTIERS MEDIA SA	2020	9/03/2020
27	VORMING BUIT UZ FACT	1/10/2020	Neuroscan school Evelien Carette	300,00	COMPUMEDICS EUROPE GMBH	2020	9/09/2020
28	BIJDR&LIDGELD&ONLINE	1/02/2022	The potential of invasive…	1.790,00	SPRINGER NATURE / MACMILLAN SUBSCRI	2022	19/01/2022
29	BIJDR&LIDGELD&ONLINE	1/06/2022	article Evelien Carette	2.791,31	FRONTIERS MEDIA SA	2022	30/05/2022
30	BIJDR&LIDGELD&ONLINE	11/07/2022	Article: Continuos thetaburst stimulator for drug	2.789,86	FRONTIERS MEDIA SA	2022	11/07/2022
31	VERPLAATSING WAGEN	9/11/2022	- Strategische Namiddag Epilepsie Liga	64,17	Carette Evelien	2022	14/10/2022
32				-40.881,75			
33							

In 2022 a year extension of the budget was granted (see the printscreens below).

ED **Erik Ludovicus Dhondt**   26 september 2022 om 09:51
Antw: Extension bursary
Aan: Carrette Evelien,   Kopie: FMRE,   Jean-Marie Maloteaux   Details

Prof.
Uw aanvraag en het overzicht van het reeds gebruikte krediet is goed ontvangen
De wetenschappelijk directeur en ikzelf gaan akkoord om het gebruik van het krediet Jonge Onderzoeker 2020-2022 te verlengen
tot **eind 2023**
Op die datum wensen wij een definitief overzicht van de uitgaven te ontvangen.
Gelieve eveneens de financiële dienst van de Universiteit Gent op de hoogte te brengen
Met de meeste hoogachting
Hartelijke groet
Erik

G.S.K.E.
F.M.R.E.

Erik Dhondt
Secretaris-Secrétaire
+32 2 478 35 56
fmre.gske@skynet.be
www.fmre-gske.be
www.fmre-gske.eu
www.fmre-gske.com

Final report of the research project of the young researcher

Prof. Riëm El Tahry, MD, PhD
Université Catholique de Louvain (UCLouvain)

Prof. Riëm El Tahry, MD, PhD
Chef de Clinique Adjointe
Neurologie, Centre de référence pour l'épilepsie réfractaire
Tel.: +32 2 764 28 55

Secrétariat:
Tel.: +32 2 764 10 82 / +32 2 764 33 09
Fax: +32 2 764 36 79

Avenue Hippocrate 10
1200 Brussels
Belgium
Tel.: +32 2 764 11 11
www.saintluc.be

Optimization Vagus nerve stimulation for refractory epilepsy

1.   Final report

Dear Pr Jean-Marie Maloteaux, dear President of the Scientific committee,

As requested, we are sending you a report of our scientific activities performed in 2022. We previously have asked permission to postpone the use of the grant by November 2022 and extend its use until 30 September 2024.

2.   The following manuscripts were published/accepted as last author:

1. Vespa, Simone ; Stumpp, Lars ; Liberati, Giulia ; Delbeke, Jean ; Nonclercq, Antoine ; Mouraux, André ; El Tahry, Riëm. Characterization of vagus nerve stimulation-induced pupillary responses in epileptic patients. In: Brain stimulation, (2022). IF : 9, cited :0
2. Fahoum, Firas ; Boffini, Massimiliano ; Kann, Lennart ; Faini, Silvia ; Gordon, Charles ; Tzadok, Michal ; El Tahry, Riëm. VNS parameters for clinical response in Epilepsy. In: Brain stimulation, Vol. 15, no.3, p. 814-821 (2022). IF :9, cited :0
3. Alexandre Berger, Evelina Carapancea, Simone Vespa, Venethia Danthine, Jean Delbeke, Antoine Nonclercq, Riëm El Tahry. Vagus Nerve Stimulation-Induced Laryngeal Motor Evoked Potentials : A Possible Tool for Response Assessment and Therapy Titration. Accepted for publication in Clinical Neurophysiology. IF : 4, cited :NA
4. M. Dumoulin, S. Vespa, G. Liberati, A Mouraux, J.Delbeke, A.Nonclercq, R. El Tahry. Effects of acute Transcutaneous Auricular Vagus Nerve Stimulation on EEG oscillations and synchronicity in healthy subjects. Submitted to Clinical neurophysiology. IF :4, cited : NA
5. Clinical added value of interictal automated electrical source imaging in the presurgical evaluation of MRI-negative epileptic patients: A monocentric prospective study. Roberto Santalucia, Evelina Carapancea , Simone vespa, Pascal Vrielynck, Alexane Fierain, Vincent Joris, Christian Raftopoulos, Susana Ferrao Santos, Riëm El Tahry. Submitted to Epilepsy and Behaviour. IF : 3, cited : NA

3.   The following manuscripts were published as co-author:

1. Fierain, A ; Gaspard, N ; Lejeune, Nicolas ; El Tahry, Riëm ; Speybroeck, Niko ; Dermauw, V ; Ferrao Santos, Susana. Beware of nonconvulsive seizures in prolonged disorders of consciousness: Long-term EEG monitoring is the key. In: Clinical Neurophysiology., Vol. 136, p. 228-234 (2022). IF : 4, cited : 1
2. Smets, Hugo ; Stumpp, Lars ; Chavez, Javier ; Cury, Joaquin ; Vande Perre, Louis ; Doguet, Pascal ; Vanhoestenberghe, Anne ; Delbeke, Jean ; El Tahry, Riëm ; Nonclercq, Antoine. Chronic recording of the vagus nerve to analyze modulations by the light-dark cycle.. In: Journal of Neural Engineering, Vol. 19, no.4 (2022). IF : 5, cited : 0
3. Goel, Keshav ; Pek, Valérie ; Shlobin, Nathan A. ; Chen, JiaShu ; Wang, Andrew ; Ibrahim, George M. ; Hadjinicolaou, Aristides ; Roessler, Karl ; Dudley, Roy W. ; Nguyen, Dang K. ; El Tahry, Riëm ; Fallah, Aria ; Weil, Alexander G.. Clinical Utility of Intraoperative Electrocorticography for Epilepsy Surgery: A Systematic Review and MetaAnalysis. In: Epilepsia, (2022). IF : 7, cited : 0
4. De Borman, Aurélie ; Vespa, Simone ; Absil, Pierre-Antoine ; El Tahry, Riëm. Estimation of seizure onset zone from ictal scalp EEG using independent component analysis in extratemporal lobe epilepsy. In: Journal of neural engineering, Vol. 19 (2022). IF : 5, cited : 0
5. Bouckaert, Charlotte ; Raedt, Robrecht ; Larsen, Lars Emil ; El Tahry, Riëm ; Gadeyne, Stefanie ; Carrette, Evelien ; Proesmans, Silke ; Dewaele, Frank ; Delbeke, Jean ; De Herdt, Veerle ; Meurs, Alfred ; Mertens, Ann ; Boon, Paul ; Vonck, Kristl. Laryngeal Muscle-Evoked Potential Recording as an Indicator of Vagal Nerve Fiber Activation. In: Neuromodulation, p. 1-10 (2022). IF : 5, cited : 2
6. Cury, Joaquín ; Smets, Hugo ; Bouzin, Caroline ; Doguet, Pascal ; Vanhoestenberghe, Anne ; Delbeke, Jean ; El Tahry, Riëm ; Nonclercq, Antoine ; Gorza, SimonPierre. Optical birefringence changes in myelinated and unmyelinated nerves: A comparative study. In: Journal of Biophotonics, (2022). IF : 3, cited : 1

7. Tzadok, Michal ; Verner, Ryan ; Kann, Lennart ; Tungala, Deepika ; Gordon, Charles ; El Tahry, Riëm ; Fahoum, Firas. Rapid titration of VNS therapy reduces time-to-response in epilepsy.. In: Epilepsy & Behavior, Vol. 134, p. 108861 (2022). IF : 3, cited : 0
8. Vitello, Marie M. ; Briand, Marie-Michèle ; Ledoux, Didier ; Annen, Jitka ; El Tahry, Riëm ; Laureys, Steven ; Martin,Didier ; Gosseries, Olivia ; Thibaut, Aurore. Transcutaneous vagal nerve stimulation to treat disorders of consciousness: protocol for a double-blind randomized controlled trial. In: International Journal of Clinical and Health Psychology, (2022) IF : 5, cited : 0

4.   Abstracts and poster presentations

European Congress Epileptology, Geneva Zwitserland, 9-12/7/2022
Poster presentation selected for oral presentation:

The objective of the study was to record Laryngeal Motor Evoked Potentials (LMEPs) in Vagus Nerve Stimulation (VNS)-implanted patients suffering from Drug-Resistant Epilepsy (DRE). Based on these recordings, LMEPs characteristics were evaluated and compared between responders (R) and non-responders (NR). Finally, possible under- or over-stimulation was assessed based on a physiological indicator of fiber engagement.

Methods: Mean dose-response curves were compared between R and NR. A Support Vector Machine (SVM) model was built based on both LMEP and dose-response curves features, to discriminate R from NR. For the exploration of possible under- or overstimulation, a ratio between the clinically applied stimulation intensity and the intensity
yielding to LMEP saturation was computed for each patient.

Results: A trend towards a greater excitability of the nerve was observed in R compared to NR. The SVM classifier discriminated R and NR with an accuracy of 80%. An ineffective attempt to overstimulate at current levels above what is usually necessary to obtain clinical benefits was suggested in NR.

Conclusions: The SVM model built emphasizes a possible link between vagus nerve recruitment characteristics and treatment effectiveness. Most of the clinically responding patients receive VNS at a stimulation intensity 1-fold and 2-fold the intensity inducing LMEP saturation.

Significance: LMEP saturation could be a practical help in guiding the titration of the stimulation parameters using a physiological indicator of fiber engagement.

IEEE Biomedical Circuits and Systems Conference (BioCAS), Tapei Taiwan, 13-15/10/2022
Raffoul, R ; Chavez-Cerda, Javier ; Acedo Reina, Elena ; Smets, Hugo ; Verstraeten, Maxime ; Vande Perre, Louis ; Taheri, R ; Doguet, P ; Delbeke, Jean ; El Tahry, Riëm ; Deviere, J ; Nonclercq, Antoine. Action Potential Detection Algorithm Adaptable to Individual Nerve and Recording Setup. In: IEEE Biomedical Circuits and Systems Conference (BioCAS), p. 655-659.

Chavez-Cerda, Javier ; Acedo Reina, Elena ; Smets,H. ; Verstraeten, M. ; Vande Perre, L. ; Diaz Cortés, M. ; Doguet, P. ; Delbeke, Jean ; El Tahry, Riëm ; Nonclercq, Antoine. Chronic Setup System for Continuous Monitoring of Epileptic Rats. In: IEEE Biomedical Circuits and Systems Conference (BioCAS), p. 591-594.

Chavez-Cerda, Javier ; Acedo Reina, Elena ; Stumpp, Lars ; Raffoul, R. ; Vande Perre, L. ; Díaz Cortés, Macarena ; Doguet, P. ; Delbeke, Jean ; El Tahry, Riëm ; Nonclercq, Antoine. Micro Cuff Electrode Manufacture for Vagus Nerve Monitoring in Rats (Soumis).

5. New obtained fundings

We have been able to successfully obtain the welbio starting grant (800K over 4 years, with intermediate evaluation after 2 years) and Innoviris funding (348K). Both projects will further permit to expand our VNS research to develop new tools for seizure detection, understand pathophysiology for sudden unexpected death in epilepsy and develop new biomarkers of clinical efficacy and dosing in patients implanted with a vagal nerve stimulator for refractory epilepsy.

6. Laboratory personnel and funding

Elena Aceido Reina, PhD student: FMRE and Fondation St Luc
Elise Collard, PhD student: Welbio starting grant
Inci Cakiroglu, PhD student: Welbio starting grant
Enrique Germany, postdoc: Welbio starting grant
Alexandre Berger, PhD student: Doctorat en Entreprise Synergia medical- Walloon region
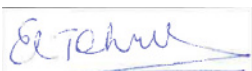Vénéthia Danthine, PhD student: FRIA –FNRS
Andres Torres, PhD student: Innoviris
Roberto Santalucia, neuropediatrician, resident CUSL, PhD student : Fond de recherche clinique
Vincent Joris : neurosurgeon, resident CUSL, PhD student : Fond de recherche clinique

Finally, we would like to thank the Queen Elisabeth Medical Fondation for the support given over the past years.

Sincerely yours,

Riëm El Tahry

Final report of the research project of the young researcher

Prof. Bernard Hanseeuw, PhD
Université Catholique de Louvain (UCLouvain)

Principal Investigator
Bernard Hanseeuw, MD, PhD

Postdocs
Lisa Quenon

PhD students
Imaging
- Vincent Malotaux
- Lise Colmant
- Thomas Gérard
- Yasmine Salman
- Lara Huyghe
- Melina Regy

Biological analyses (CSF)
- Nathalie Nyalu Ngoie
- Emilien Boyer

Main collaborators
Adrian Ivanoiu, MD PhD (Neurology)
Renaud Lhommel, MD (Nuclear Medicine)
Laurence Dricot, Ir PhD (Radiology)
Vincent van Pesch, MD PhD (Neurochemistry)
Yves Sznajer, MD (Neurogenetics)
Didier Vertommen, PhD (Mass Spectrometry)

Website
https://uclouvain.be/fr/instituts-recherche/ions/neur/the-louvain-aging-brain-lab.html

Contact
recherche-alzheimer@uclouvain.be
bernard.hanseeuw@uclouvain.be

The Human Tau study

The **Human Tau study** evaluates the manifestations related to pathological aging, such as that caused by Alzheimer's disease (AD) and related disorders, called tauopathies. These disorders all involve biochemical alterations in the tau protein. We relate brain damage disclosed by imaging techniques (MRI, tau-PET using [18F]-MK6240) and biological changes observed in post-mortem brain samples or in-vivo cerebrospinal fluid (CSF) and plasma samples to cognitive changes measured using neuropsychological testing. Our research targets are patients with mild cognitive impairment who consult the Memory Clinic, normal subjects at family risk for developing Alzheimer's disease and healthy control subjects, young and old.

In 2019, we have acquired the first tau-PET images in French-speaking Belgium. Since then, more than 150 patients benefited from the technique (as of late 2022). Four imaging PhD students are funded by the FNRS, and one by the WELBIO fund. We developed a classification of the tau-PET images inspired by the post-mortem neuropathological stages of Heiko Braak (Fig.1). The support of the Queen Elisabeth Medical Foundation has allowed me to expand this research program, and also to hire a biochemical PhD student and cover the high costs of mass spectrometry experiments to characterize the post-translational modifications (PTM) of the tau protein in brain samples and CSF.

__Fig.1 Tau-PET image of patients with various levels of tau pathology:__ In Braak stage 1 or 2, the pathology is restricted to the medial temporal lobe and CSF is most often normal. In Braak stage 3 or 4, the temporal lobe is strongly affected by tau pathology, but the frontal and occipital lobes are still largely preserved, consistent with the preservation of executive and visuospatial functions observed in patients with mild cognitive impairment. Tau is most often abnormal in the CSF. Braak stage 5 and 6 are mostly observed in patients with AD dementia.
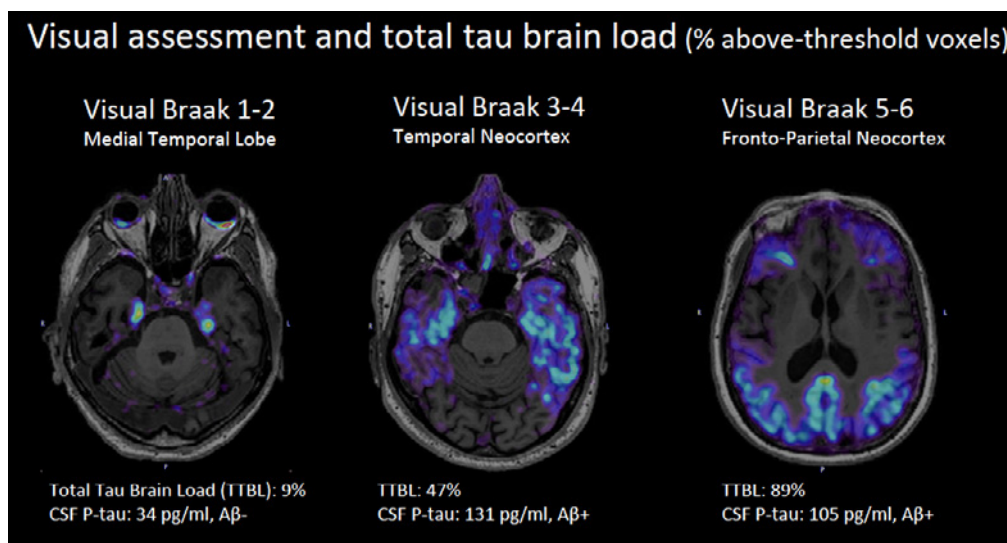
Results accepted for an oral presentatiton by Thomas Gérard, PhD student at the European Conference on Clinical Neuroimaging in Geneva (March 14-15, 2022).

Nathalie Kyalu Ngoie (4th year PhD student in 2022-2023) was supported by the FMRE funding. She first developed an immuno-precipitating protocol isolating the tau protein from the CSF and brain samples. She then analyzed the protein with mass spectrometry from patients with different tauopathies, such as AD, but also fronto-temporal lobe degeneration (FTLD) or cortico-basal degeneration (CBD). She achieved to identify tau isoforms (3R vs 4R) in tau aggregates and in the soluble fraction of the brain. Whereas tau isoforms followed the expected distribution in the aggregated (4R in CBD, 3R in Pick disease, 3R and 4R in AD), this distribution was not observed in soluble tau, explaining the difficulties of conducting tau isoform measurements in CSF. We then searched for differences in post-translational modifications (PTMs) in soluble tau and CSF (Fig.2).
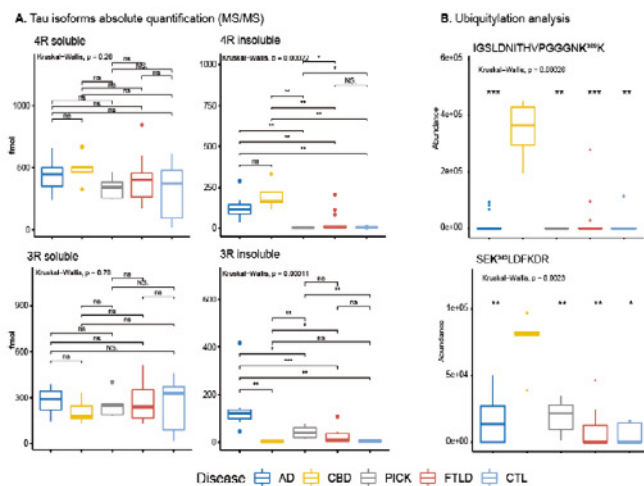
In preliminary work (Fig.2), we could demonstrate that differences in tau PTMs were observable in soluble brain fractions, and in post-mortem cerebrospinal fluid (CSF), making these PTMs good candidates to develop *in-vivo* biomarkers distinguishing between tauopathies.

Fig.2: Mass Spectrometry (MS) analyses of (A) tau isoforms and (B) post-translational modifications (PTMs) in soluble and insoluble brain extracts. Tau^{K369} ubiquitination is observed in 4R-taupathies: *CBD and three FTLD cases with predominant 4R-tau in the aggregates*. This illustrates our ability to conduct biochemical studies, in addition to brain imaging studies. *Data presented at EuroTau 2021.*

The first imaging publication supported by the Foundation has been published in September 2022 in the journal Brain Connectivity. A biochemical publication is currently under revision in Nature Communications. Vincent Malotaux and Nathalie Kyalu will both defend their PhD thesis in 2023.

Finally, the support of the Foundation has allowed me to start collaboration with the lab of Pascal Kienlen-Campard who used CSF that I collected to demonstrate the in-vivo seeding effect of hexameric amyloid assemblies and with Vincent van Pesch and Adrian Ivanoiu who investigated CSF differences between immigrants and native Belgians.

1.   Key publications in 2020-2022.

– *Malotaux V, Dricot L, Quenon L, Lhommel R, Ivanoiu A,* **Hanseeuw B***. (2022) Default-Mode Network Connectivity Changes During the Progression Toward Alzheimer's Dementia: A Longitudinal Functional Magnetic Resonance Imaging Study.* **Brain Connectivity***.*

– *Lebrun L;* **Hanseeuw B***; Van Pesch V ; Ivanoiu A. (2022) Alzheimer disease's cerebrospinal fluid biomarkers differences between immigrants and natives in a Belgian memory clinic.* **Acta Neurologica Belgica.**

– *Vrancx C, Vadukul DM, Suelves N, Contino S, D'Auria L, Perrin F, van Pesch V,* **Hanseeuw B***, Quinton L, Kienlen-Campard P. (2021). Mechanism of Cellular Formation and In Vivo Seeding Effects of Hexameric β-Amyloid Assemblies.* **Molecular Neurobiology***.*

– **Hanseeuw, B. J.***, Malotaux, V., Dricot, L., Quenon, L., Sznajer, Y., Cerman, J., Woodard, J. L., Buckley, C., Farrar, G., Ivanoiu, A., & Lhommel, R. (2021). Defining a Centiloid scale threshold predicting long-term progression to dementia in patients attending the memory clinic : An [18F] flutemetamol amyloid PET study.* **European Journal of Nuclear Medicine and Molecular Imaging***.*

– *Mormont, E., Bier, J.-C., Bruffaerts, R., Cras, P., De Deyn, P., Deryck, O., Engelborghs, S., Petrovic, M., Picard, G., Segers, K., Thiery, E., Versijpt, J., &* **Hanseeuw, B***. (2020). Practices and opinions about disclosure of the diagnosis of Alzheimer's disease to patients with MCI or dementia : A survey among Belgian medical experts in the field of dementia.* **Acta Neurologica Belgica***.*

– **Hanseeuw, B. J.***, Scott, M. R., Sikkes, S. A. M., Properzi, M., Gatchel, J. R., Salmon, E., Marshall, G. A., & Vannini, P. (2020). Evolution of anosognosia in alzheimer's disease and its relationship to amyloid.* **Annals of Neurology***, 87(2), 267280.*

– **Hanseeuw, B. J.***, Betensky, R. A., Jacobs, H. I. L., Schultz, A. P., Sepulcre, J., Becker, J. A., Cosio, D. M. O., Farrell, M., Quiroz, Y. T., Mormino, E. C., Buckley, R. F., Papp, K. V., Amariglio, R. A., Dewachter, I., Ivanoiu, A., Huijbers, W., Hedden, T., Marshall, G. A., Chhatwal, J. P., … Johnson, K. (2019). Association of Amyloid and Tau With Cognition in Preclinical Alzheimer Disease : A Longitudinal Study.* **JAMA Neurology***, 76(8), 915.*

→ *This last publication received the FMRE CBC Prize in 2021.*

Final report of the research project of the young researcher

Dr. Lars Emil Larsen, PhD
Universiteit Gent (UGent)

Dr. Lars Emil Larsen, PhD
Postdoctoral Researcher
4Brain/MEDISIP
Ghent University

Campus UZ
Corneel Heymanslaan 10,
Entrance 36 - Ground floor
9000 Gent
Belgium

Closed loop precision therapy for epilepsy using photopharmacology

1. Summary of progress

Following a 6-month extension of the budget of this project, I hereby provide a final project report on this project. The 6-month extension allowed a PhD student of the 4Brain lab to perform additional experiments and provide *in vivo* proof of concept of photopharmacology for seizure suppression in a mouse epilepsy model. In summary, we achieved the following with financial support from the Queen Elisabeth Medical Foundation (GSKE):

- Provided *in vitro* and *in vivo* proof of concept of photopharmacology for seizure suppression
- Provided *in vitro* proof of concept for closed loop seizure suppression with photopharamcology
- Published 4 A1 manuscripts with 3 additional A1 manuscripts still in preparation. Two are to be submitted in Q3 2023 and the other in Q4 2023.

2. Project overview

The principal goal of this project is to develop and provide proof of concept for closed loop precision therapy for epilepsy using photopharmacology in a mouse model for temporal lobe epilepsy. In the previous reports, I described the identification of DEACM-CPA (cCPA), a coumarin-caged adenosine A_1 (A_1) receptor agonist, which is uncaged and activated by purple light (405 nm). The cCPA compound gains unique access to the potent seizure suppressing efficacy of the A_1 receptor signaling system, without inducing the side effects, such as cardiac and respiratory suppression, that are otherwise associated with systemic activation. I further described how an initial shift towards studying closed-loop photopharmacology at an *ex vivo* level, rather than *in vivo* level, was motivated by delays in delivery of crucial electronic equipment (covid-19 related). In the previous report from 2021, I presented initial data from our *ex vivo* and *in vivo* experiments with cCPA and recently a first manuscript was published on this work in the *International Journal of Molecular Sciences*. The budget in relation to this grant was recently extended for 6 months in order to finish a series of final experiments to provide *in vivo* proof of concept of photopharmacology for seizure suppression, the data of which we expect to prepare for publication towards Q4 2023. At this moment we are in the process of finalizing three additional manuscripts, all which are supported by this GSKE grant. Before outlining these manuscripts, I will first briefly outline already published work in relation to this grant.

2.1. Already published work with support of this grant

1. Acharya AR, Larsen LE, Van Lysebettens W, Wadman WJ, Delbeke J, Vonck K, Meurs A, Boon P, Raedt R. Attenuation of hippocampal evoked potentials in-vivo by activation of GtACR2, an optogenetic chloride-channel. Frontiers in Neuroscience. 29 March 2021 https://doi.org/10.3389/fnins.2021.653844.
   Peer Reviewed, Impact factor (2021) = 5.152, Category: Neurosciences, Rank 88/275, Q2

In this paper, we showed the utility of the GtACR2 opsin, a blue light gated chloride channel, for inhibition of evoked hippocampal activity. Opsins, such as GtACR2 is a powerful alternative to photopharmacology for closed-loop applications.

2. *Acharya AR, Vandekerckhove B, Larsen LE, Delbeke J, Wadman WJ, Vonck K, Carette E, Meurs A, Vanfleteren J, Boon P, Missinne J, Raedt R. In vivo blue light illumination for optogenetic inhibition: effect on local temperature and excitability of the rat hippocampus. Journal of Neural Engineering, 2021 Dec 24;18(6) doi: 10.1088/1741-2552/ac3ef4.*
    Peer Reviewed, Impact factor (2021, most recent) = 5.043, Category: Engineering, Biomedical, Rank 32/98, Q2

In this paper, effects of blue light on local temperature was explored through modeling and simulations and subsequently validated with experimental recordings from the rat brain. The models constructed and validated in this paper will be of great value in the *ex vivo* to *in vivo* translation of our photopharmacology work.

3. *Acharya AR, Larsen LE, Delbeke J, Wadman WJ, Vonck K, Meurs A, Boon P, Raedt R. In vivo inhibition of epileptiform afterdischarges in rat hippocampus by light-activated chloride channel, stGtACR2. CNS Neuroscience Therapeutics, 2022 Dec 8.doi: 10.1111/cns.14029.*
    Peer reviewed, Impact Factor (2021, most recent) = 7.035, Category: Pharmacology & Pharmacy, Rank 31/279, Q1

In this paper, we showed the utility of the GtACR2 opsin, a blue light gated chloride channel, for inhibition of evoked hippocampal seizures. Opsins, such as GtACR2 is a powerful alternative to photopharmacology for closed-loop applications. A pdf of this manuscript was attached to the report.

4. *Craey E, Hulpia F, Spanoghe J, Manzella S, Larsen LE, Sprengers M, De Bundel D, Smolders I, Carrette E, Delbeke J, Vonck K, Boon P, Van Calenbergh S, Wadman WJ, Raedt R. Ex Vivo Feedback Control of Neurotransmission Using a Photocaged Adenosine A1 Receptor Agonist.*
    Peer Reviewed, Impact factor (2021, most recent) = 6.208, Category: Biochemistry & Molecular Biology, Rank 69/297, Q1

In this paper, we characterized the cCPA compound and showed its initial application for control of feedback control of neurotransmission, i.e. hippocampal evoked potentials, in a brain slice model. A pdf of this manuscript was attached to the report.

Manuscript in preparation: Closed-loop photopharmacology for *ex vivo* control of hyperexcitability: a proof of concept

In this manuscript, we explore the use of the concept developed in the previous manuscript for control of excitability under hyperexcitable conditions. The data for this manuscript is encouraging and we are currently in the process of collecting the final data and finalizing the manuscript. Submission of this manuscript is anticipated for Q3 2023. The setup for these experiments is similar to the previous manuscript and includes the use of the same type of 64-channel multi-electrode-array (MEA) for *ex vivo* slice electrophysiology. In this study, however, we induce epileptiform burst by elevating extracellular potassium concentrations from 3.25 mM to 8.5 mM. while simultaneously being able to record evoked field potentials in the CA1 following electrical stimulation of afferent Schaeffer collaterals (**Figure 1**).
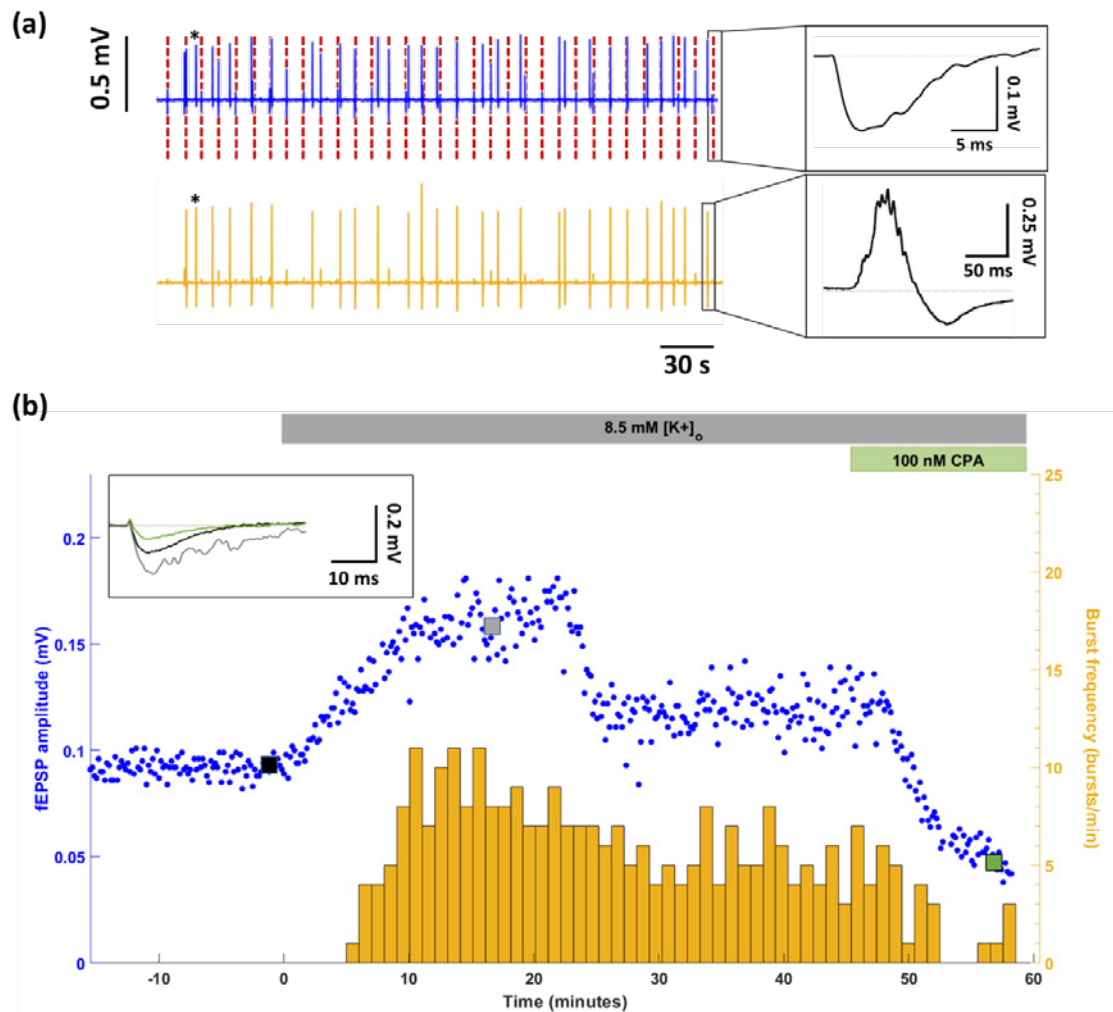
Figure 1: Effects of elevated [K⁺]ₒ on epileptiform bursting activity and evoked field potentials. (**a**) Continuous traces recorded with a selected electrode in the stratum radiatum for CA1 fEPSPs (blue) with corresponding stimulation artefacts (dashed red lines) and a second electrode in the proximity of the CA3 region (yellow) for burst detection (asterisk). Insets display a representative fEPSP trace (upper panel) and an epileptiform burst (lower panel). (**b**) Time course of the effects of elevating [K⁺]ₒ on the fEPSP amplitude (blue) and burst frequency (yellow) in a representative slice. Inset displays fEPSP traces at three different timepoints as indicated by square markers: baseline (black), near the maximum of the fEPSP amplitude increase (grey) and after incubation with 100 nM CPA (green).

The idea of this concept is to use evoked potentials as an index for excitability, which is closely related to the probability for epileptic tissue to generate epileptic activity. Indeed, what we observed as we elevated potassium concentrations was an initial increase in the amplitude of evoked potentials, which precedes the onset of spontaneous epileptiform bursts or spikes. We then designed a closed-loop paradigm, as in the previously published paper, where we use inhibitory photopharmacology, with cCPA, to prevent elevation of the amplitude of evoked potentials and by doing so try to prevent hyperexcitability and the generation of epileptiform activity. This is indeed what our experiments show (**Figure 2**) and this exciting data is to be published imminently.
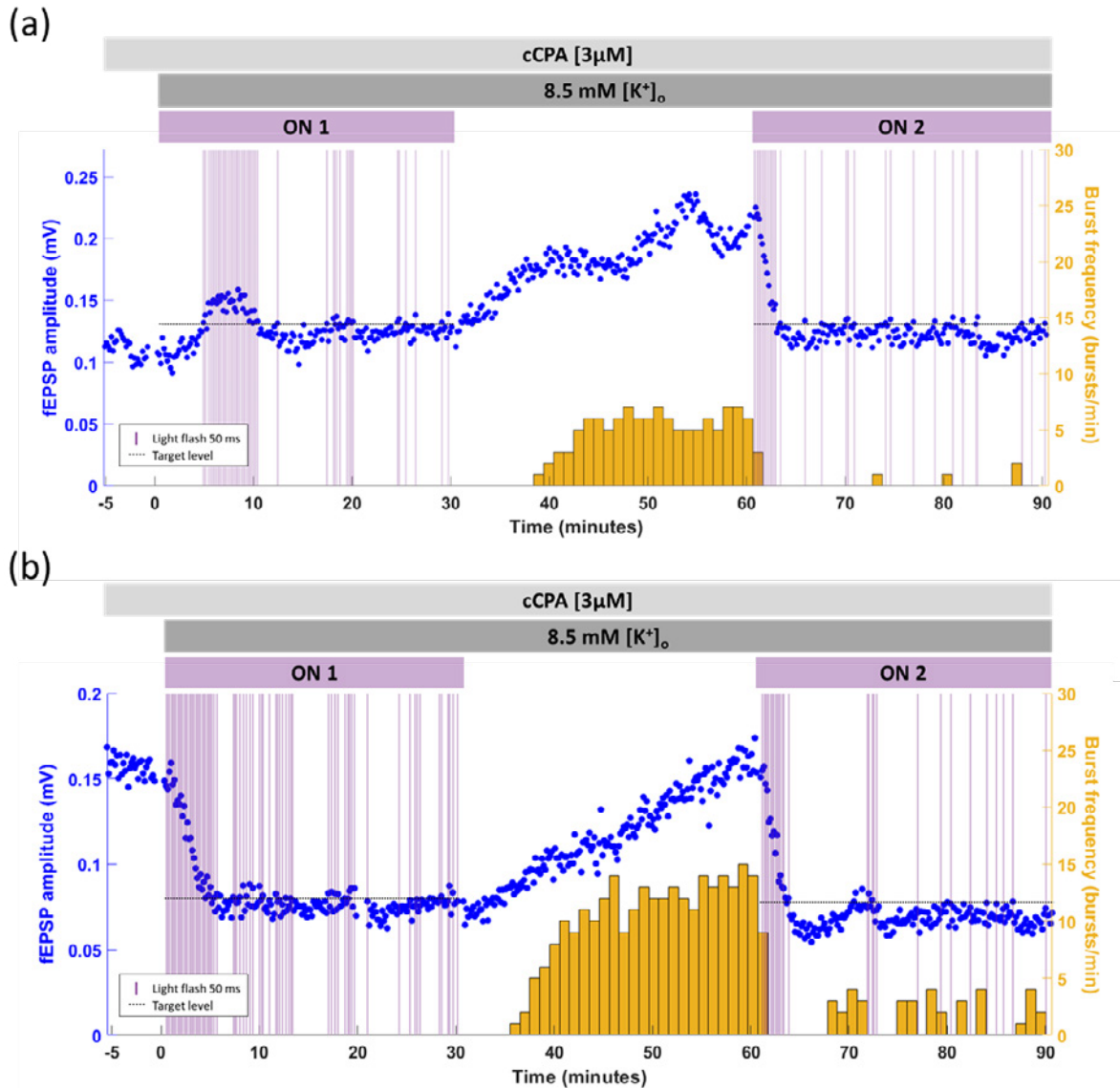
Figure 2: Closed-loop CPA-mediated photopharmacological control of neurotransmission in the elevated [K⁺]ₒ slice model. (**a**) Time course of the fEPSP amplitude (blue) and the epileptiform burst frequency (yellow) in a representative slice, incubated with 3 μM cCPA and 8.5 mM $[K^+]_o$. Following baseline, the feedback loop was closed (ON 1) at zero minutes. A light flash of 50 ms was triggered whenever the amplitude crossed the target level, set at 110 % in this slice. At 30 min, the loop was disconnected (OFF) and closed again at 60 min (ON 2). (**b**) A similar closed-loop paradigm was used as in (**a**) with a target level of 50 %.

Manuscript in preparation: 'Photopharmacological suppression of increased dentate gyrus excitability in acute hippocampal slices from chronically epileptic mice using a photocaged adenosine A₁ receptor agonist'

The previous manuscripts concern the study of cCPA and its utility for closed-loop application in healthy tissue. In this manuscript, however, we turn to a commonly used model for chronic temporal lobe epilepsy, the intrahippocampal kainic acid (IHKA) model in mice. In this model, kainic acid is initially injected intrahippocampally to evoke a status epilepticus, resulting in several histopathological changes common to human temporal lobe epilepsy, and the occurrence of spontaneous seizures. We thus aim to adapt the concept of closed-loop photopharmacology with cCPA for control of (hyper)excitability in this model of chronic temporal lobe epilepsy, bringing us one step closer to translation to a realistic epilepsy model. This manuscript is currently under internal revision and is envisioned to be submitted in Q3 2023.

The experimental setup is similar, although in addition to studying the CA1, we also look at another subregion of the hippocampal formation, the dentate gyrus (DG). Evoked potentials can be studied in the DG by electrically stimulating perforant path afferents originating from the entorhinal cortex. As a first objective of this manuscript, we describe changes in excitability in tissue of epileptic mice vs. healthy control mice. In this case we observed hyperexcitability only in the dentate gyrus, reflected by an elevation of the fEPSP component and an increased prevalence of population spikes in epileptic vs. healthy slices (**Figure 3** and **Figure 4**).
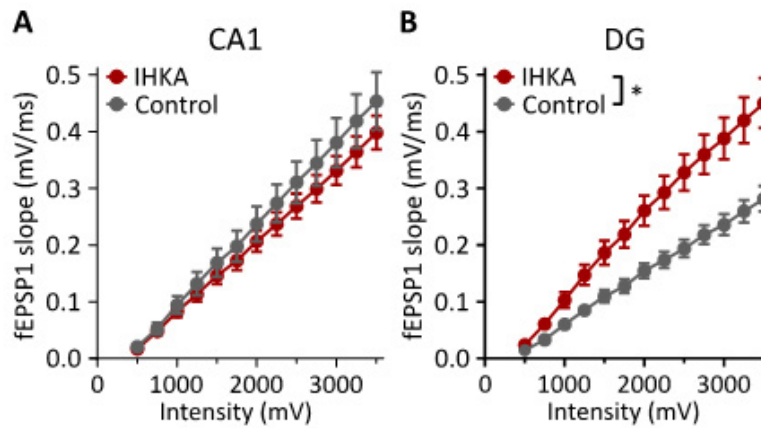
Figure 3: Evoked potentials were recorded in both the CA1 and dentate gyrus (DG) of healthy and epileptic mice. The plots show the fEPSP slope recorded over a range of varying stimulation intensities and show clear signs of elevated excitability in the DG of epileptic mice.
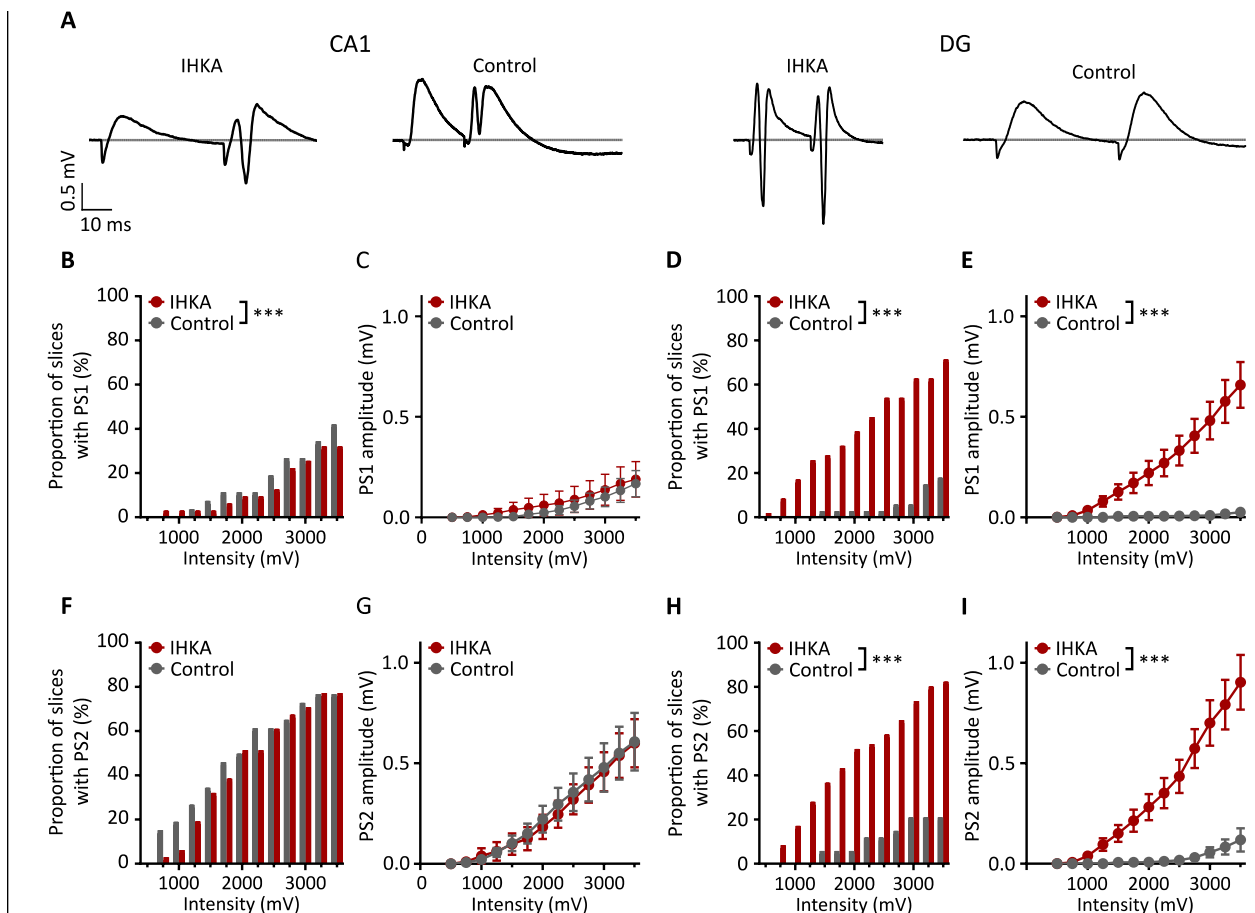
Figure 4: Differences in postsynaptic activation, which the population spike reflects, between IHKA and control animals. A. Representative examples of EPs in IHKA and control slices measured in the CA1 and DG region, respectively, after maximal stimulation (3500 mV). B-C/F-G. Input-output curves of the proportion of slices with a PS and amplitude of the PS after the first and second stimulation, respectively, in the CA1 region. D-E/H-I. Input-output curves of the proportion of slices with a PS and amplitude of the PS after the first and second stimulation, respectively, in the DG region. The proportion of slices data are shown as the effective proportion over all slices in our sample group, the PS amplitude data are shown as mean ± SEM; ***$p < 0.001$.

Beyond assessing changes in baseline excitability between healthy and epileptic slices, we further wanted to assess any potential changes in the potency of A_1 receptor signaling between these conditions. This was motivated by previous reports that have indicated compromised adenosine signaling under epileptic conditions, which could decrease efficacy of our photopharmacological approach. We thus studied effects of varying concentrations of the native CPA compound on evoked potentials in both the CA1 and DG recorded in slices of healthy and epileptic mice (**Figure 5**). CPA induced a dose-dependent suppression of fEPSP in both the CA1 and DG. There was a tendency for a stronger suppression of the fEPSP slope in healthy vs. epileptic slices in the DG over the concentrations studied. Population spikes were only studied in the DG of epileptic slices due to a low prevalence in healthy slices. In this case, CPA was observed to induce a potent suppression of the population spikes at doses much lower than those needed to suppress the fEPSP component (**Figure 6**). This suggests that targeting A_1 receptor signaling may be an effective strategy to suppress neuronal excitability even in epileptic tissue.
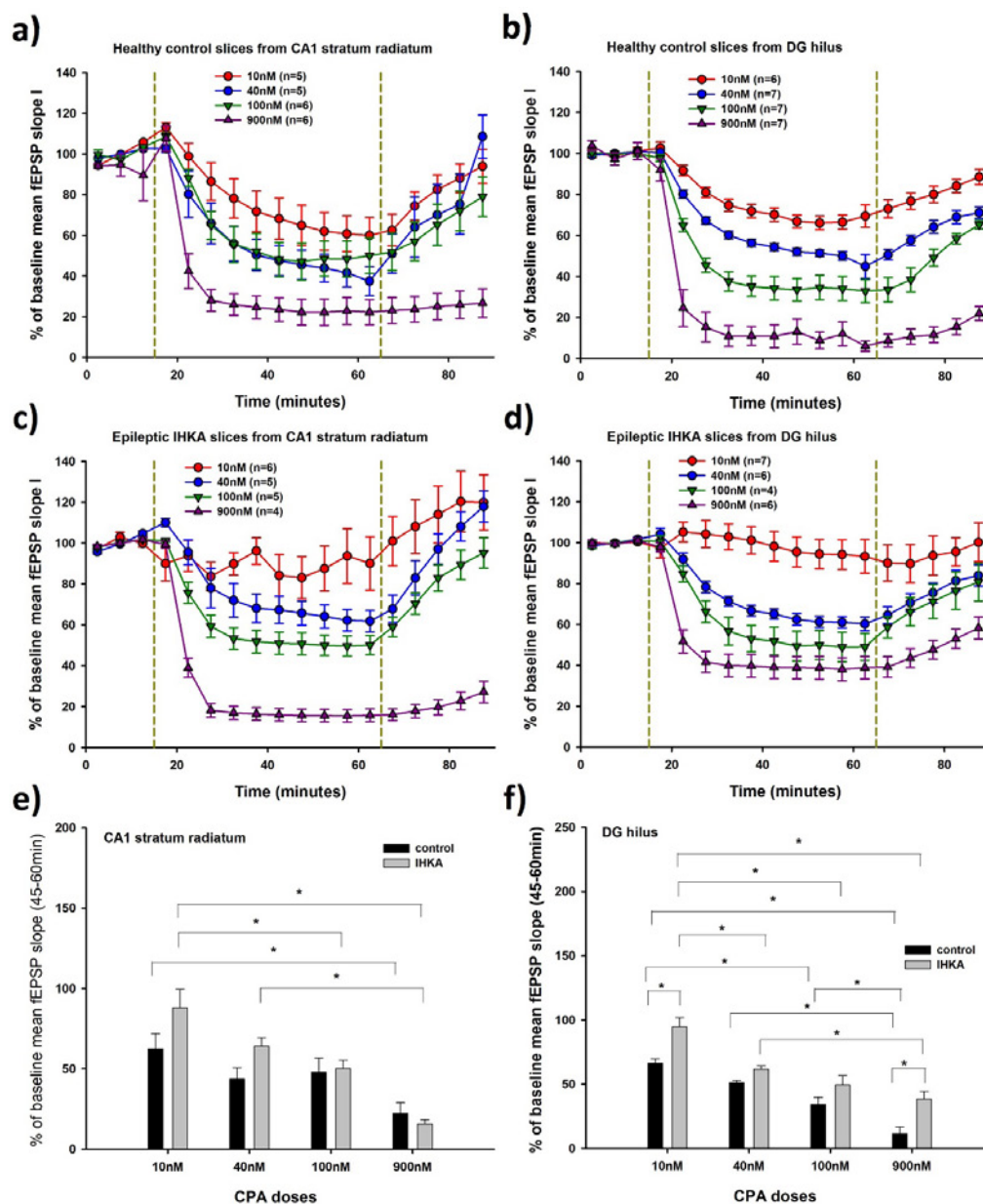

Figure 5: Effects of CPA on the fEPSP slope of evoked potentials recorded in the CA1 and dentate gyrus (DG) in both healthy and epileptic slices. CPA induces an equipotent dose dependent suppression of the fEPSP slope in both the CA1 (a, c, e) and DG (b, d, f) of both healthy and epileptic slices.
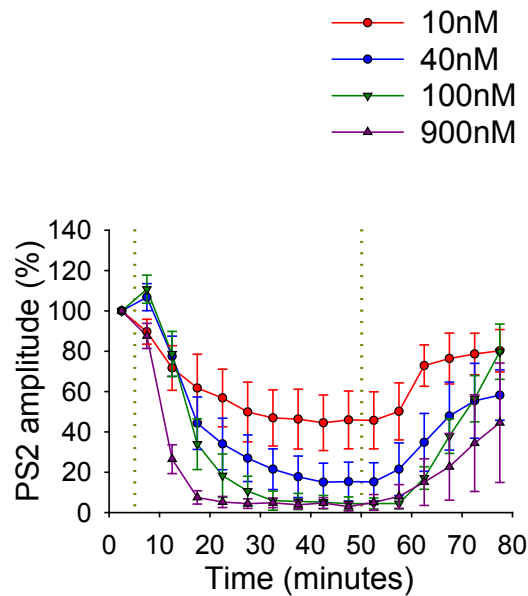
Figure 6: Effects of CPA on population spike amplitude of evoked potentials recorded in the DG.

In a final experiment, we adapted the previously designed closed loop algorithm with cCPA to control excitability in the epileptic DG. Here we have shown that we are consistently able to reduce excitability in the dentate gyrus by triggering the delivery of light to uncage cCPA upon the population spike of DG evoked potentials exceeding a specified threshold value (**Figure 1**). We therefore feel confident that we are ready to test this concept to suppress spontaneous seizures *in vivo*.
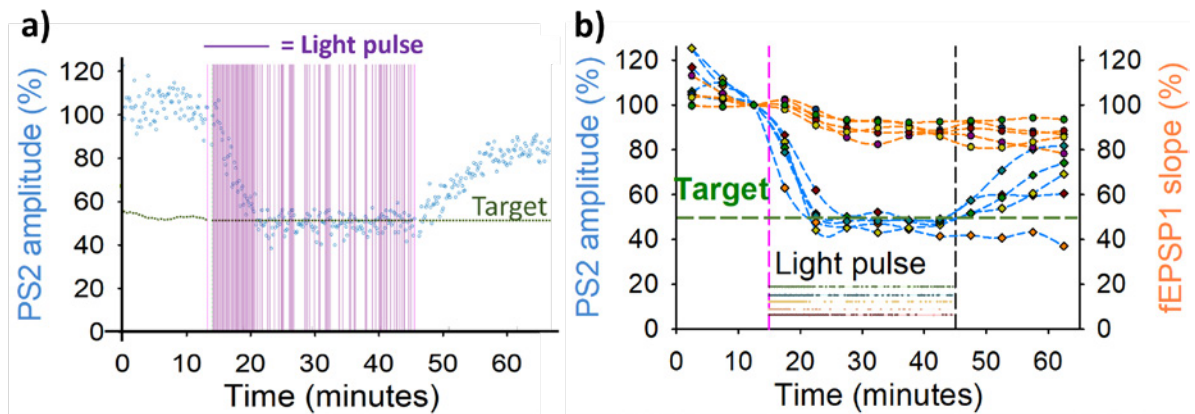

Figure 7: a) an example from a single slice recording in the dentate gyrus (DG) of hippocampal slices from epileptic tissue where the cCPA compound in combination with light was used to reduce the population spike amplitude of DG evoked potentials to ~50% of baseline levels. b) This finding was reproduced in a number (n=5) of consecutive slices from epileptic mouse brains.

Study in progress: *In vivo* control of excitability and suppression of spontaneous seizures in a mouse model of temporal lobe epilepsy

Since our *in vitro* experiments with both CPA and cCPA provided convincing evidence of being able to both inhibit evoked potentials and epileptiform activity, and control excitability in both healthy and epileptic tissue, we have initiated a series of experiments *in vivo*. This manuscript will contain the following data:

- Inhibition of dentate gyrus evoked potentials and spontaneous local field potentials with CPA. *Status: finalized.*
- Inhibition of dentate gyrus evoked potentials and spontaneous local field potentials with cCPA. *Status: increase number of animals*
- Suppression of spontaneous seizures in the kainic acid model of temporal lobe epilepsy with cCPA. *Status: finalized.*

The *in vivo* evoked potential experiments (1 and 2 above) were set up to deliver a proof of concept for the uncaging of cCPA *in vivo*. For these experiments, mice were anesthetized with isoflurane and fixed in a stereotactic frame. Stainless steel wire electrodes were implanted in the hilus of the DG for registration and a bipolar stimulation electrode was implanted in the perforant path. A Hamilton neurosyringe was then lowered to the level of the lateral ventricle, contralateral to the site from which evoked potentials where acquired, which allowed the infusion of either CPA (low dose = 0.25 µg or high dose = 1.25 µg, both dissolved in 5 µL of saline with 2.5% DMSO) or a vehicle solution. Following administration of CPA, there was a dose dependent suppression of both fEPSP amplitude and the population spike of the DG evoked potentials (**Figure 8**). These observations gave an indication of what we should expect to see with the cCPA if it is working as intended. We have thus completed initial experiments with the cCPA compound using same experimental setup described above, with the exception of adding a 400 µm optical fiber to the electrode used for evoked potential recordings, which allowed us to deliver light locally in the hippocampus for uncaging of the cCPA compound.

First, several exploratory experiments had been performed to find a suitable light protocol and optimal concentrations of cCPA needed to deliver our proof of concept for the uncaging of cCPA *in vivo*. The use of 100 ms light pulses of 8 mW at 0.1 Hz was found to be an effective and "safe" illumination protocol (without effects in the absence of cCPA). When testing several doses using this protocol, the proof of concept was initially achieved using 100 µg of cCPA, the maximal dose achievable in 5 µl of DMSO. While this resulted in clear and long-lasting effects, the high dose of the vehicle DMSO produced effects on evoked potentials and was deemed unsuitable for use in the following planned experiments in awake animals. Fortunately, we found that using the same concentration of cCPA dissolved in 100% DMSO (20 µg/µl) in lower volumes (25 µg cCPA in 1.25 µl DMSO and 50 µg cCPA in 2.5 µl DMSO) also allowed us to obtain reproducible effects of uncaging. With the 50 µg dose, effects also were long-lasting. In this case, we saw that illumination prior to cCPA administration had no effects on the evoked potentials (**Figure 9**). Administering the cCPA compound in the absence of light had no or minimal effects. However, application of light, both 10 minutes and 2 hours after injection, following cCPA administration induced a pronounced suppression of population spike amplitude, providing the proof of concept for local uncaging of cCPA, *in vivo.* This experiment will have to be repeated in additional animals (currently, n=3).
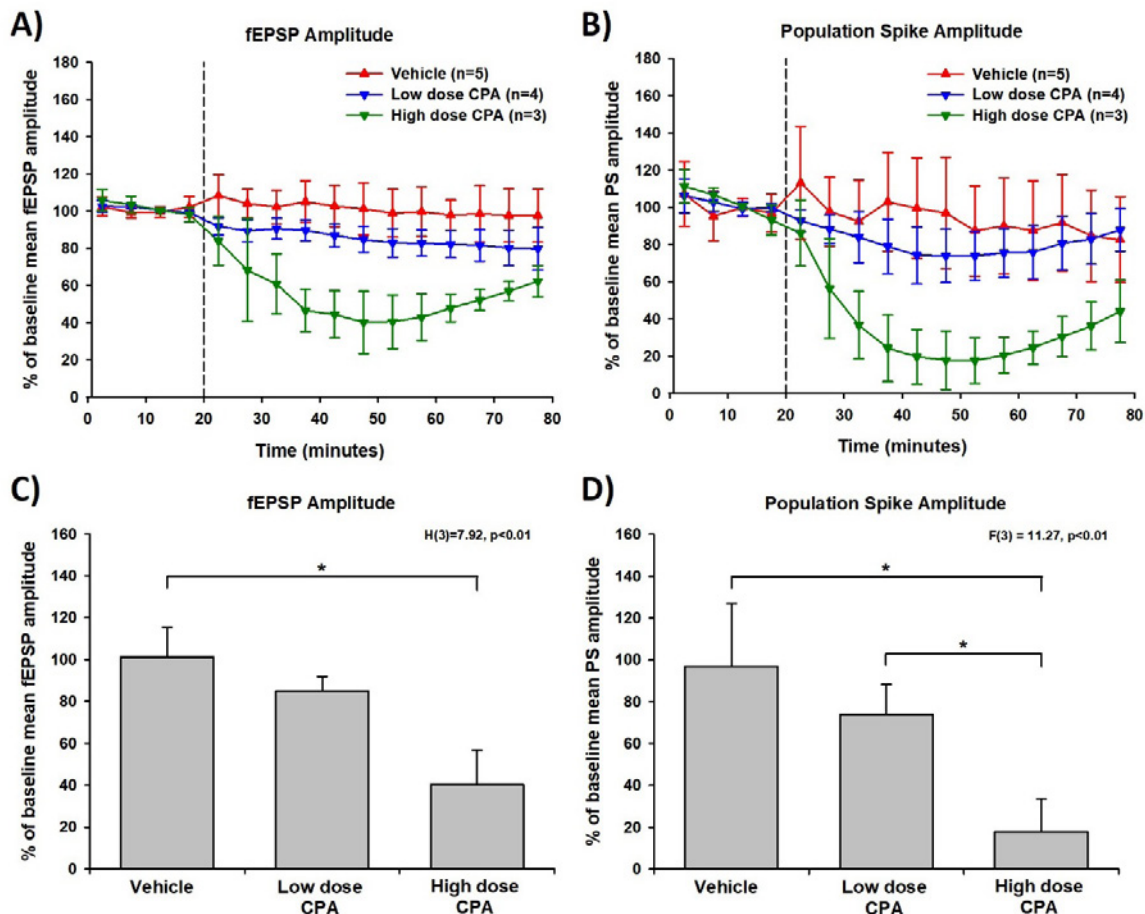
Figure 8: CPA administered intracerebroventricularly induces a dose-dependent inhibition of dentate gyrus EPs, reflected by a gradual reduction in both field excitatory postsynaptic potential (fEPSP) amplitude and population spike amplitude (A and B), which was significant 30 minutes after administration of CPA (C and D).
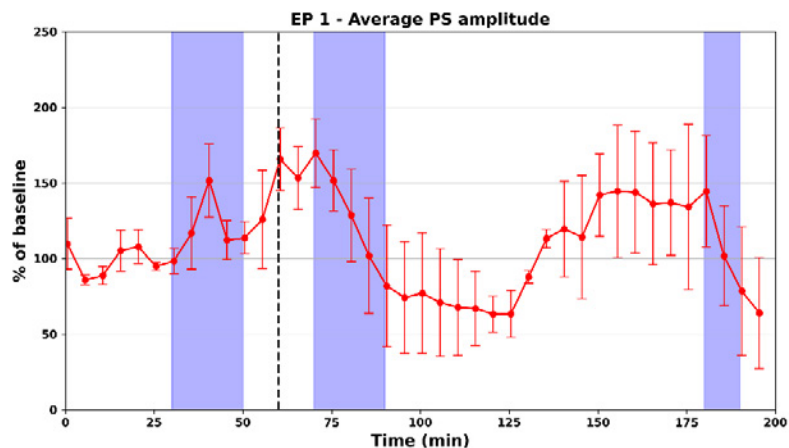

Figure 9: Effects of uncaging cCPA (50 µg) locally in the hippocampus following intracerebroventricular administration on evoked potentials recorded in the dentate gyrus. Light prior to cCPA administration had no effect on population spike amplitude. Following administration of cCPA, indicated with a dashed vertical line, light induced a strong suppression of both fEPSP slope and population spike amplitude. Data is presented as means ± SEM (n=3).

Based on these results, we have initiated experiments in the intrahippocampal kainic acid model of mice to try to suppress spontaneous seizures. Mice were initially injected intrahippocampally with kainic acid, resulting in a status epilepticus and subsequent development of spontaneous seizures over the following weeks. The 4Brain has years of experience with this model. Around 4 weeks after status epilepticus, mice were instrumented with the following:
- An intracranial electrode in the hippocampus for registration of seizure activity

- An intracranial optical fiber in the hippocampus for local light delivery and cCPA uncaging
- An intracranial guide cannula for injection of cCPA in the lateral ventricle

Subsequently, a cross over experiment was performed using an initial batch of 20 mice, of which only 7 mice with clear epileptic seizures were used for subsequent experiments. Three experimental conditions were included:
- Vehicle injection in combination with light delivery (injection control)
- cCPa injection without light (control for cCPA compound effects)
- cCPA injection with light (active treatment condition)

Experiments consisted of a baseline period of 2 hours, followed by injection of cCPA and continuous pulsing of light. Initial analysis shows that cCPA administration in combination leads to a significant reduction in seizure frequency relative to the two control conditions, which is a proof of concept for *in vivo* seizure suppression with photopharmacology.
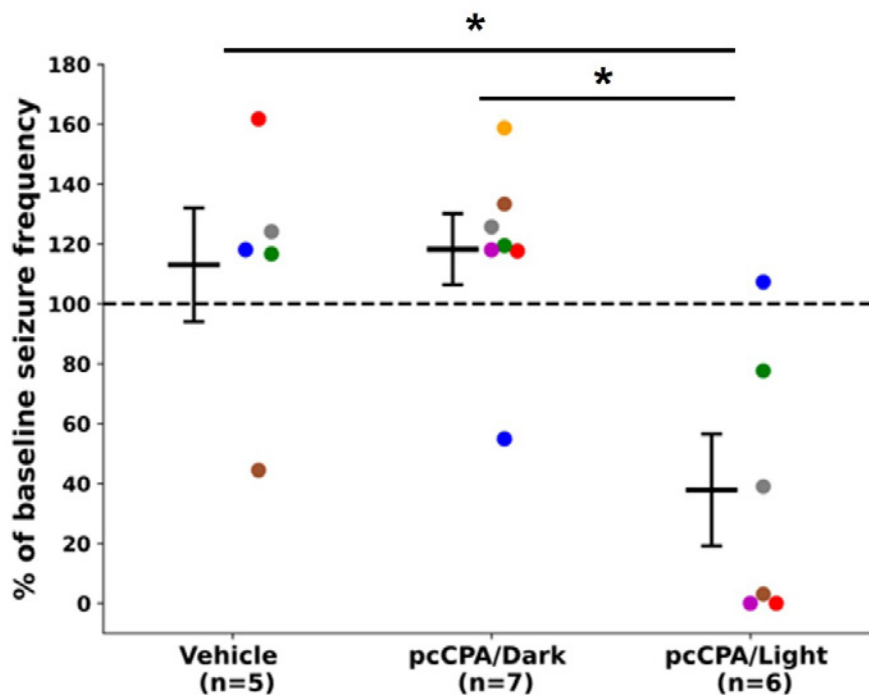
Figure 10: Relative changes in seizure frequency following vehicle/cCPA administration in combination with light. Asterisks denote significant differences between treatment conditions.

Final report of the research project of the young researcher

Aya Takeoka, PhD (IMEC)
Katholieke Universiteit Leuven (KU Leuven)

Aya Takeoka PhD
Principal Investigator at NERF, a joint research initiative by imec, VIB and KU Leuven
Assistant Professor, Department of Neuroscience @ KU Leuven
T +32 16 28 31 14
aya.takeoka@nerf.be
www.nerf.be
twitter.com/TakeokaLab

Learning to walk without the brain: Determining cellular signatures underlying age-dependent spinal cord plasticity

1. Aims and summary

Adult rodents with complete spinal cord transection (cSTX) at the thoracic level do not spontaneously regain the capacity to walk. Nevertheless, mice receiving the same injury at an early postnatal period (postnatal day 5, P5) exhibit proficient hindlimb locomotion on a motorized treadmill as adults. This is achieved despite the spinal cord circuits controlling hindlimb movements being functionally isolated from the brain. With support from GSKE/FMRE, **we uncovered the age of injury-dependent divergent synaptic connectivity from interneurons to motor neurons (**Bertels et al., *Nature Neuroscience*). Adult injury prompts neurotransmitter switching of excitatory interneurons to inhibitory phenotype, promoting inhibition at synapses interfacing motor neurons.

In contrast, neonatal injury causes synaptic sprouting of identical populations to facilitate excitation. Furthermore, genetic manipulation to mimic inhibitory phenotype observed after adult injury by these excitatory interneurons abrogates autonomous locomotor functionality in neonatally injured mice. In comparison, attenuating inhibitory phenotype improves locomotor recovery after adult injury. Together, our study demonstrates that flexible neurotransmitter phenotype of defined excitatory interneurons steers locomotor capacity after injury.

Finding 1. vGlut2^{ON} interneurons undergo neurotransmitter phenotype switch after adult injury.
Synaptic input from spinal interneurons to MNs is one of the factors regulating the final CNS output that controls muscle contractions. As inhibitory synaptic input to MNs is known to increase after injury, we asked whether the excitatory/inhibitory synaptic input ratio from spinal interneurons to MNs that innervate hindlimb muscles depends on injury age. To visualize excitatory and inhibitory synaptic terminals, we crossed major excitatory or inhibitory NT Cre-driver lines (*vGlut2^{cre}* or *vGAT^{cre}*) with *Tau$^{LSL-nlsLacZ-SynGFP}$* reporter mice to conditionally express Synaptophysin tagged with GFP (SynGFP^{ON}) in either excitatory or inhibitory spinal interneurons. This approach indelibly labeled presynaptic input derived from either genetically glutamatergic vGlut2^{ON} or inhibitory vGAT^{ON} interneuron populations to choline acetyltransferase^{ON} (ChAT^{ON}) MNs (Fig. 1a). This method shows high fidelity between genetically labeled excitatory or inhibitory terminals to assess protein expression of vGlut2 or vGAT with immuno-labeling (designated as vGlut2+ or vGAT+, as opposed to genetically labeled vGlut2^{ON} or vGAT^{ON}) in intact spinal cords (> 80%; Fig 1b-d).
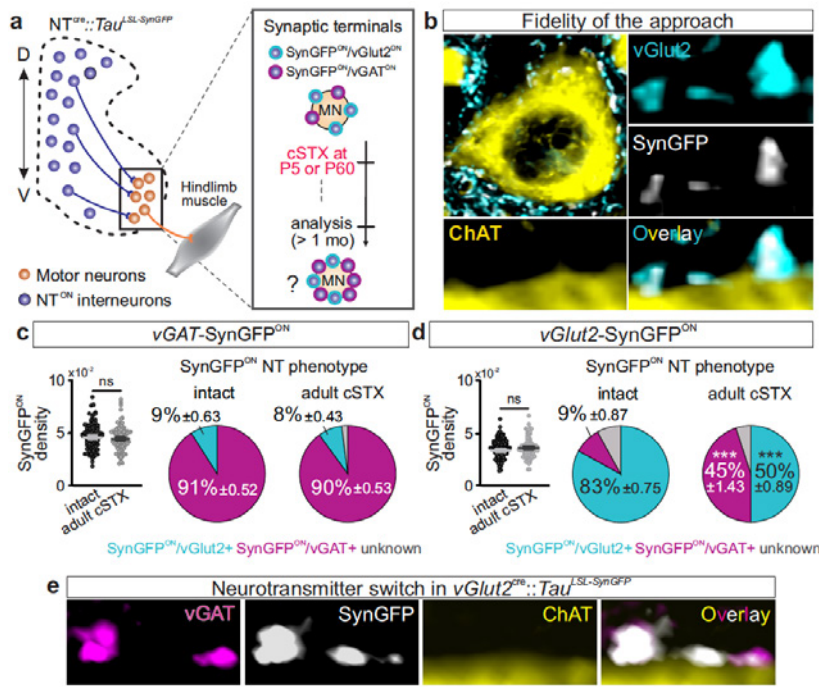
Fig 1. vGlut2^{ON} interneurons undergo neurotransmitter phenotype switch after adult injury.
a. Experimental scheme to visualize and quantify synaptic terminals derived from specific interneurons.
b. Representative image of synaptic apposition of SynGFP^{ON} terminals to a ChAT^{ON} motor neuron and colocalization of vGlut2 antibody in intact *vGlut2^{cre}::Tau$^{LSL-SynGFP}$* spinal cord.
c, d. Synaptic terminals derived from *vGAT^{ON}* **(c)** or *vGlut2^{ON}* **(d)** neurons depicted in the density of SynGFP^{ON} synaptic boutons (/µm^2) apposing MNs (left) and % antibody labeling of NT expression (vGlut2+ or vGAT+) with SynGFP^{ON} genetic markings to visualize NT phenotype (right) of intact and adult cSTX spinal cords. Each dot represents one MN. A low level of NT phenotype switch is detected in intact preparation for both intercrosses.
e. Genetically marked SynGFP^{ON} terminals co-immunolabeled for vGAT protein (vGAT+) in *vGlut2^{cre}::Tau$^{LSL-SynGFP}$* spinal cord after adult injury.

Surprisingly, we detected no increase in the number of synaptic terminals derived from genetically marked inhibitory terminals in *vGAT^{cre}::Tau$^{LSL-SynGFP}$* spinal cords after adult injury (Fig. 1c). Instead, we detected a five-fold increase of genetically marked excitatory terminals with vGAT+ expression (% SynGFP^{ON}/vGAT+) in *vGlut2^{cre}::Tau$^{LSL-SynGFP}$* spinal cords (Fig. 1d, 1e). The number of genetically marked SynGFP^{ON} terminals in the *vGlut2^{cre}* background remained unchanged after adult injury (SynGFP^{ON} density). In parallel, we found a decrease in % of SynGFP^{ON}/vGlut2+ and, conversely, a strong increase in SynGFP^{ON}/vGAT+ terminals, where almost half of the synaptic terminals derived from vGlut2^{ON} neurons became vGAT+ (Fig. 1d). Supporting this observation, we also found that vGlut2+ or vGAT+ expression at SynGFP^{ON} terminals is mutually exclusive (data not shown).

A phenomenon of activity-dependent NT phenotype switch in the brain is reported previously. To determine whether this observation at synaptic terminals is the case and, if so, whether the NT phenotype switch occurs uniformly among glutamatergic interneurons, we used *in-situ* hybridization of *vGlut2* and *vGAT* mRNA. In an intact spinal cord, we detected neurons with a singular expression of *vGlut2* or *vGAT* transcripts in equal abundance, with only a minor population of neurons co-expressing *vGlut2* and *vGAT* transcripts distributed sparsely along the dorsoventral axis (Fig. 2a-e). Together with the protein level analysis, we detected a low level of the opposite NT phenotype in genetically marked terminals (Fig. 2c, 2d). This result demonstrates that NT phenotype switch exists in an intact spinal cord. Adult cSTX significantly increased the density of neurons with *vGlut2/vGAT* co-expression in the dorsal and intermediate lamina (Fig. 2a-e). This shift paralleled a decrease in neurons with a singular expression of *vGlut2*, but no change in *vGAT* (Fig. 2e), a finding that suggests a fraction of dorsal and intermediate excitatory interneurons acquires inhibitory NT phenotype at the transcript level after adult injury. Together, our results identified cell type-specific NT phenotype switch as a pathophysiological response to a severe spinal cord injury impacting the mature nervous system.
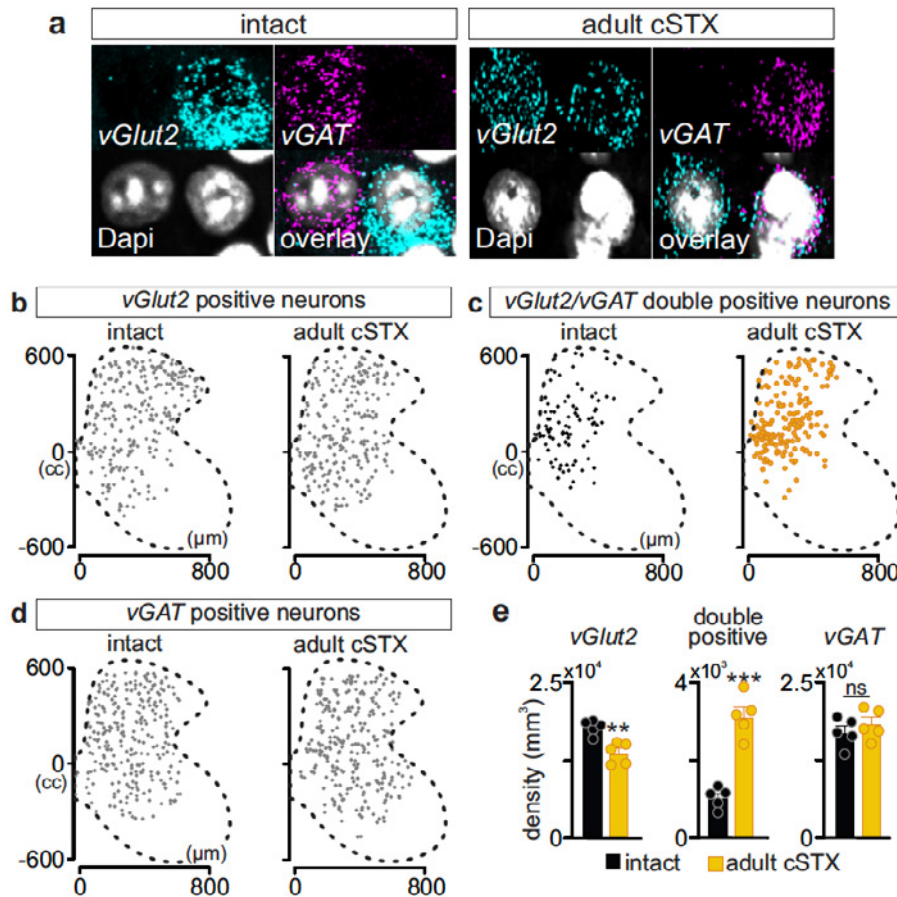
Fig 2. Dorsal and intermediate vGlut2^ON interneurons acquire vGAT phenotype after adult injury.
a. Representative *in-situ* hybridization example of the lumbar spinal cord (L4-6) sections with a singular expression of *vGlut2, vGAT*, or double-positive (*vGlut2/vGAT*), marked with DAPI.
b-d. Location of neurons with singular *vGlut2, vGAT,* or double *vGlut2/vGAT* expression for intact and adult cSTX experimental groups.
e. Density of singular *vGlut2*, double-positive and singular *vGAT* neurons of intact and adult cSTX mice. Each dot represents the mean of individual animals.

Finding 2. vGlut2^ON interneurons undergo synaptic sprouting after neonatal injury.

Next, we determined whether a similar NT phenotype switch occurred following neonatal injury. Much in contrast, we found no evidence of NT phenotype switch after neonatal injury. Instead, we observed a significant increase in genetically marked glutamatergic SynGFP^ON terminals to MNs in *vGlut2^cre::Tau^LSL-SynGFP* mice (Fig. 3a, 3b). Together, the two injury models revealed that the age of injury defines two opposing synaptic connectivity profiles of excitatory interneurons to motor neurons. We found genetically marked glutamatergic synaptic sprouting after neonatal injury, in contrast to NT switch after adult injury, which led to high vGAT+ synaptic input to MNs (Fig. 3c).
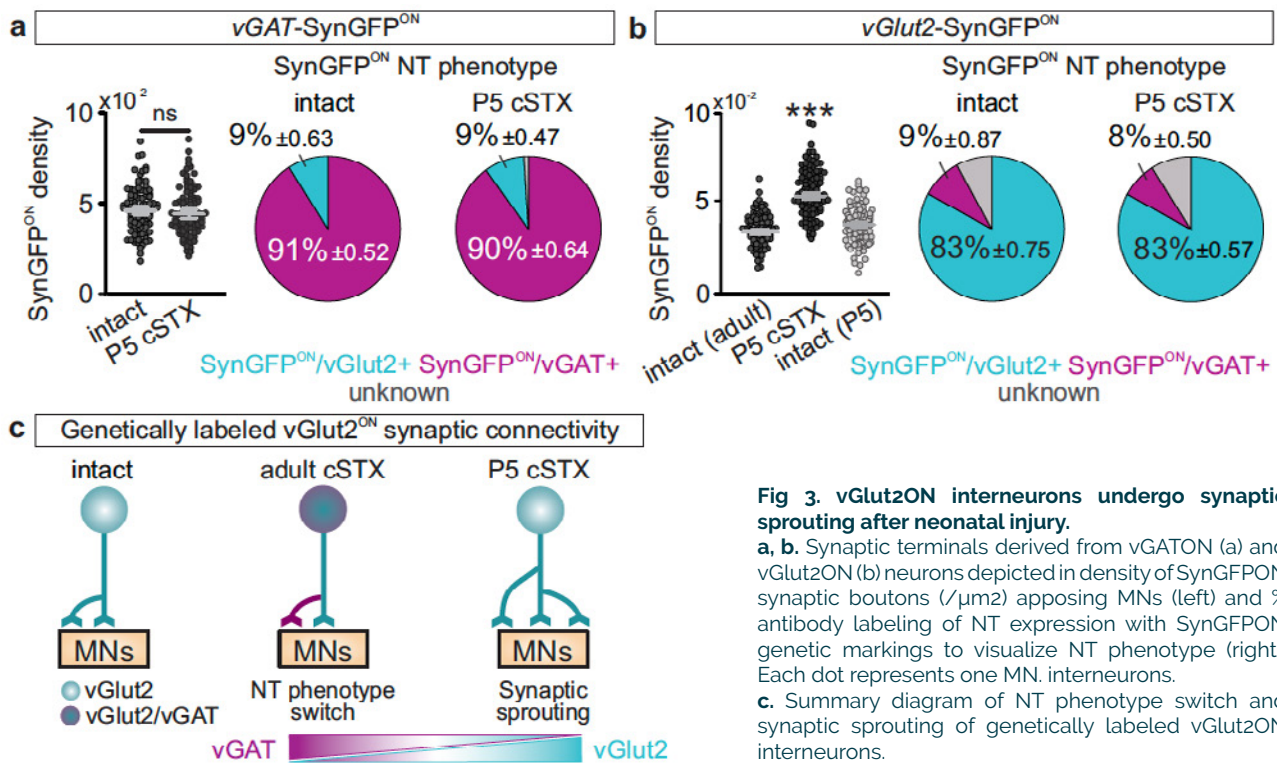
Fig 3. vGlut2ON interneurons undergo synaptic sprouting after neonatal injury.
a, b. Synaptic terminals derived from vGATON (a) and vGlut2ON (b) neurons depicted in density of SynGFPON synaptic boutons (/µm2) apposing MNs (left) and % antibody labeling of NT expression with SynGFPON genetic markings to visualize NT phenotype (right). Each dot represents one MN. interneurons.
c. Summary diagram of NT phenotype switch and synaptic sprouting of genetically labeled vGlut2ON interneurons.

Finding 3. Age of injury-dependent synaptic input reorganization from glutamatergic interneurons to MNs is subpopulation specific.

Our analysis of *vGlut2* and *vGAT* transcript expression after adult injury reveals that specific vGlut2^{ON} neurons residing in the dorsal and intermediate lamina are driving the process of NT phenotype switch (Fig. 2c). To gain genetic access to different subpopulations of excitatory interneurons residing along distinct dorso-ventral positions in the spinal cord (Fig. 4a), we used stratification by developmental origin. We used three transgenic mouse lines, each expressing Cre-recombinase under the control of a different progenitor domain (PD) specific transcription factor (*PD*^{cre}; Fig. 4b) and intercrossed with the *Tau*$^{LSL-SynGFP}$ reporter line to selectively visualize synaptic output derived from the selected PD population.

We found that both PD identity and age of injury determined the NT profile of their synaptic output. After the adult injury, *Tlx3*^{ON} (dI3 and dI5) and *Shox2*^{ON} (V2a), but not *Sim1*^{ON} (V3) interneurons, exhibited increased SynGFP^{ON}/vGAT+ and decreased SynGFP^{ON}/vGlut2+ terminals to MNs (Fig. 4c). After the neonatal injury, all three PD populations maintained their glutamatergic phenotype, consistent with the analysis on pan-vGlut2^{ON} interneurons (Fig. 3b). Interestingly, we found that the neonatal injury-dependent synaptic sprouting was also subpopulation-specific (Fig. 4c). We detected more SynGFP^{ON} boutons from *Tlx3*^{ON} and *Shox2*^{ON}, but not *Sim1*^{ON} interneurons to MNs, in P5 cSTX compared to the intact spinal cord. Together, we unraveled that the age of injury-specific NT identity switches and connectivity rearrangements to MNs occur with remarkable cell type specificity among excitatory interneurons.
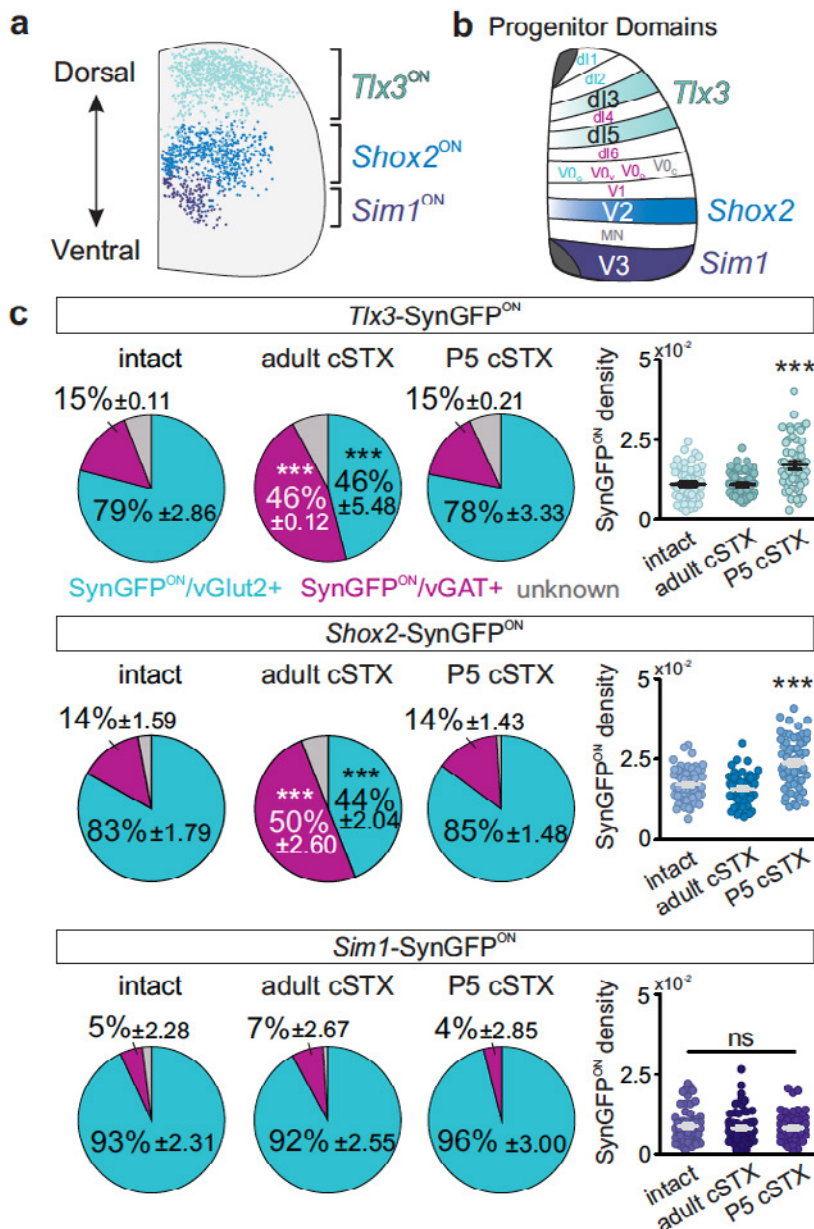
Fig 4. Age of injury-dependent synaptic profile of excitatory interneurons is subpopulation specific.

a, b. Scheme of analyzed excitatory subpopulations and their positions in the mature lumbar spinal cord **(a)** and transcription factor code of spinal cord progenitor domains (PD). PDs that give rise to vGlut2[ON] interneurons are magenta, vGAT[ON] interneurons in cyan, cholinergic interneurons, and MN in gray **(b,** PD; dI1-dI6, V0-V3, and MN, examined excitatory subpopulations: light blue *Tlx3*[ON], blue *Shox2*[ON], and purple *Sim1*[ON]).

c. Quantification of synaptic terminals derived from *Tlx3*[ON], *Shox2*[ON]. and *Sim1*[ON] neurons depicted in NT phenotype identity (left; NT+) and density of SynGFP[ON] synaptic boutons (/µm²) apposing MNs (right) in intact, adult cSTX and P5 cSTX spinal cords. Each dot represents one MN.

Finding 4. Overexpression of vGAT disrupts walking without the brain after neonatal injury.

Next, we asked whether maintaining the vGlut2[ON] phenotype is essential for proficient stepping without the brain. We performed an intraspinal injection of LoxP-flanked AAVs in the lumbar spinal cord to express vGAT (AAV-DIO-vGAT-Tag) by excitatory neurons. Broad injection of the virus across lumbar segments led to expression of the Tag at the cell body (data not shown). We then examined the locomotor ability of P5 cSTX mice with AAV-DIO-vGAT-Tag (P5 cSTX+vGAT) or control injection of AAV-DIO-Tag (P5 cSTX+control) at ~P60 (Fig. 5a).

Virus-mediated expression of vGAT after neonatal injury deteriorated locomotor performance. While P5 cSTX+control mice displayed alternation between left and right limbs, P5 cSTX+vGAT mice largely failed to develop a brain-independent locomotor capacity (Fig. 5b). However, we observed unilateral, non-weight bearing reflexive steps on rare occasions (Fig. 5b, right panel). Therefore, we reconstructed SynGFP[ON] terminals to MNs and quantified their NT phenotype as a proxy to validate viral transduction efficiency. We applied PC analysis on 94 parameters and then matched the % vGAT phenotype of synaptic terminals to each examined limb. Reconstructed PC

space segregated experimental groups primarily based on variability related to dragging-related parameters (Fig. 5c).

Furthermore, limb kinematics during treadmill locomotion broadly matched the extent of viral efficiency among experimental mice, i.e., hindlimbs with low vGAT % synaptic inputs to MNs display ambulatory phenotype and not dragging (Fig. 5d). Therefore, we conclude that acquiring vGAT accompanied by reduction of vGlut2 phenotype by dorsal and intermediate glutamatergic interneurons after neonatal injury deteriorates locomotor ability. Together, our results suggest causality between a NT shift by glutamatergic interneurons in the dorsal and intermediate lamina and locomotor capacity after injury, regardless of whether it is due to spontaneous shift after adult injury or virus-mediated shift after neonatal injury.
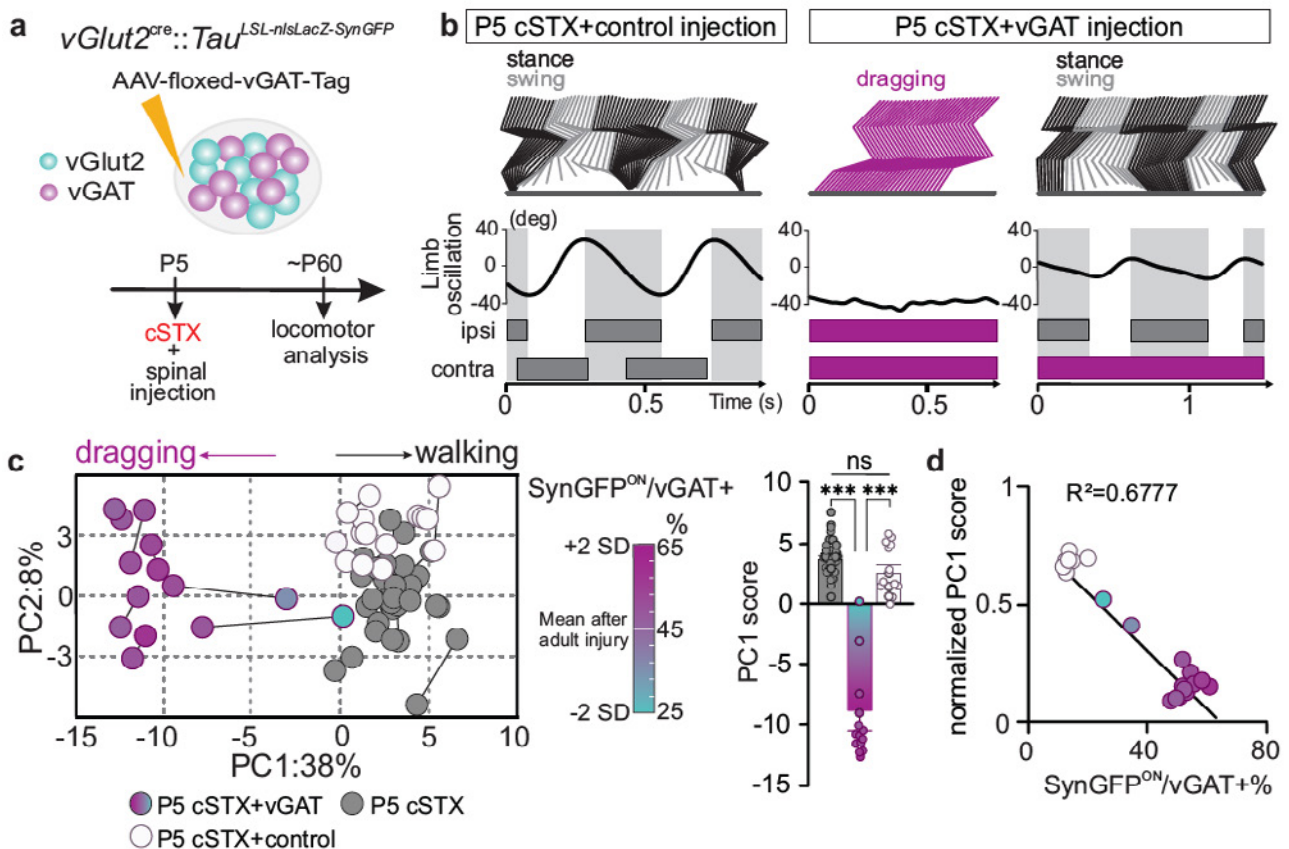

Fig 5. Overexpression of vGAT disrupts the ability to walk without the brain after neonatal injury.
a. Experimental strategy to transduce *vGAT* expression in *vGlut2*[cre] spinal interneurons and timeline. **b.** Stick decomposition, limb oscillation, and corresponding stance/swing phases of P5 cSTX+control injection and P5 cSTX+vGAT mice. Dark gray horizontal bars indicate stance, and empty spaces correspond to swing. Magenta bars indicate complete dragging of the hindlimbs. **c.** PC analysis was applied on mean values of 94 gait parameters. Each dot represents limb kinematics of either left or right hindlimb of one mouse. Color gradient ranges from 65% to 25% representing the highest (magenta) and the lowest (cyan) % SynGFP[ON]/vGAT+. PC1 scores of P5 cSTX+vGAT showed a significant difference compared to P5 cSTX and P5 cSTX+control injection. **d.** Linear regression analysis of locomotor capacity and NT composition of SynGFP[ON] synaptic terminals in P5 cSTX mice with control or AAV-vGAT injections. Individual PC1 values were normalized using z-score and scaled to [0,1].

Finding 5. Suppression of vGAT improves locomotor kinematics after adult injury.

Having established that defined subpopulations of vGlut2 interneurons undergo a NT phenotype switch after adult injury and that the vGlut2 neurotransmitter phenotype is critical for proficient locomotion after neonatal injury, we asked whether attenuating NT phenotype switch from vGlut2+ to vGAT+ facilitates locomotor improvement after adult injury. We devised an approach to conditionally downregulate vGAT expression in vGlut2 interneurons using an intraspinal injection of LoxP-flanked AAVs encoding short-hairpin RNA against vGAT gene expression

(*sh*RNA-vGAT-Tag; Fig. 6a). We then performed an intraspinal injection of AAV-floxed-*sh*RNA-vGAT in *vGlut2^(cre)::Tau^(LSL -SynGFP)* in the lumbar spinal cord followed by a complete transection and assessed stepping capability six weeks after injury (Fig. 6b). All mice with *sh*RNA-vGAT injection exhibited a few spontaneous consecutive steps, albeit limited and uncoordinated, compared to almost no steps by untreated mice (Fig 6c, 6d). Although only partially and variably, these data suggest that the treatment influences recovery. Lack of complete recovery is not surprising as a severe injury leads to other circuit changes independent of NT phenotype switch or maintenance. Therefore, we then combined this intervention with weight-supported locomotor training known to ameliorate such maladaptive circuit-wide plasticity.

We subjected subsets of adult cSTX mice with or without *sh*RNA-vGAT intervention to daily treadmill training of 20 minutes for four weeks (Fig. 6e). To train mice after adult injury, we used wide-spectrum serotonergic receptor agonists that acutely and temporally enable alternating weight-bearing stepping in rodents with complete spinal cord transection. These agonists elevate the excitability of the spinal cord and allow training without any apparent long-term effects.

After four weeks of training, we quantified spontaneous locomotor capacity based on 102 gait parameters without serotonergic agonists. Like *sh*RNA only group, the locomotor ability of the individual mouse was highly variable. Nonetheless, PC1 captured *sh*RNA-vGAT effects of both groups with and without training (33% of explained variance), where training further enhanced *sh*RNA-vGAT effects (Fig. 6f). Extraction and grouping of parameters highly correlated with PC1 demonstrate that *sh*RNA-vGAT combined with daily training significantly reduced the percentage of dragging and improved joint oscillation, measures associated with locomotor recovery (Fig. 6g). While training alone does not improve locomotor ability after an adult injury, a finding that is consistent with previous studies (Fig. 6f, 6g), we found that training alone partially prevented NT phenotype switch, i.e., reduced vGAT phenotype by dorsal and intermediate excitatory interneurons compared to no intervention (data not shown). Furthermore, training facilitated vGlut2^(ON) synaptic sprouting, a circuit reorganization signature we detected after neonatal injury (data not shown), a potential contributing factor to the added recovery observed in the *sh*RNA+training group.

Together, our results demonstrate that reducing neurotransmitter phenotype switch alone promotes locomotor pattern expression, and a combination of long-term locomotor training further facilitates distinct aspects of locomotor recovery after adult injury (Fig. 6h).
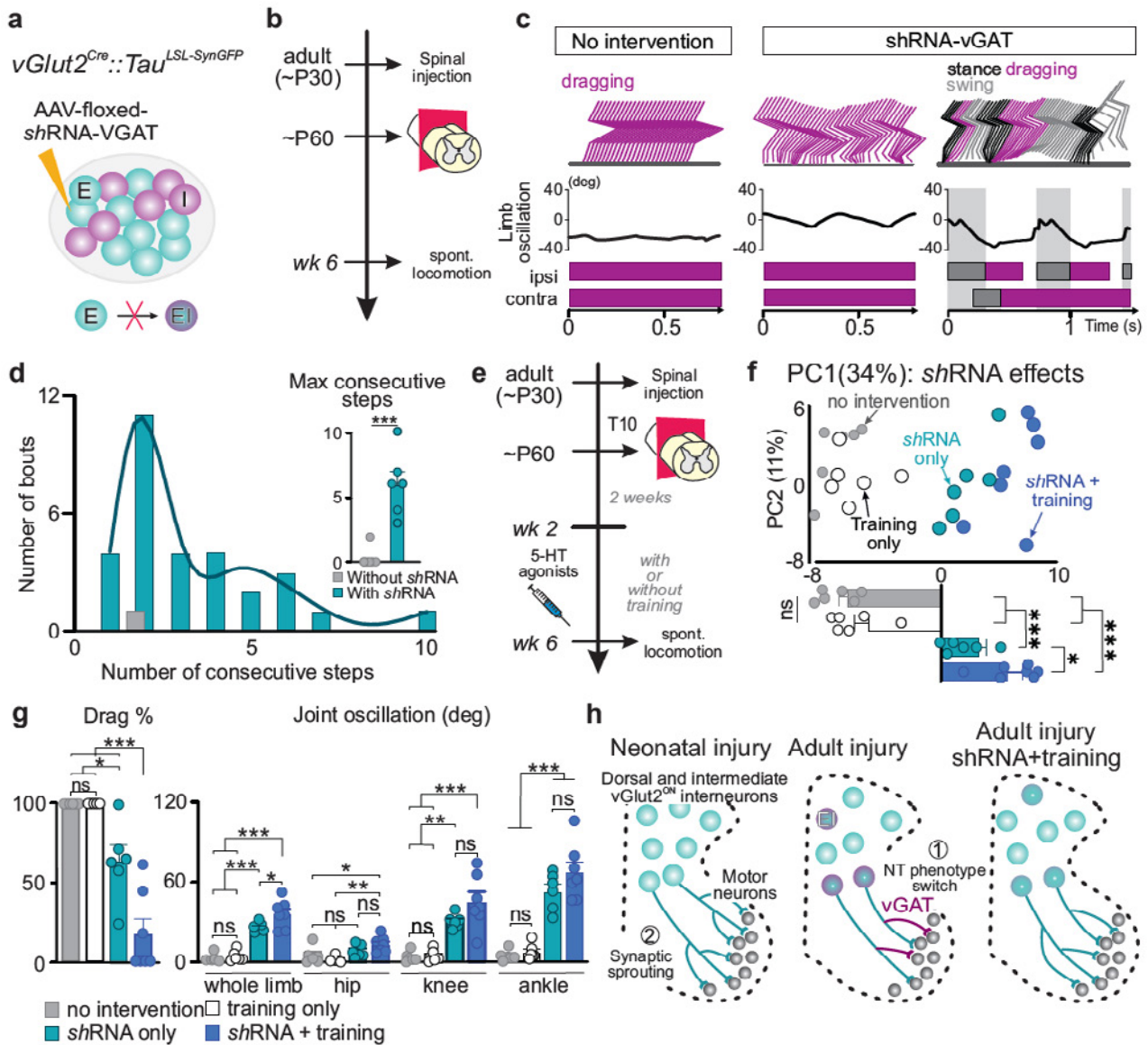
Fig 6. Suppression of vGAT expression by excitatory interneurons combined with locomotor training facilitates locomotor recovery after adult injury.

a, b. Experimental strategy and timeline to attenuate *vGAT* expression in genetically labeled *vGlut2*ON spinal interneurons after adult injury. **c.** Representative stick decomposition of adult cSTX mice with control (left) and *sh*RNA-vGAT (middle and right) injections at week 6. **d.** Frequency plot of stepping bouts and quantification of the maximum number of consecutive steps during a 30-sec recording session. **e.** Timeline to induce stepping after adult injury with or without daily locomotor training and the timeline. **f.** PC analysis of spontaneous stepping at week 6. Each dot represents one mouse. Histogram plots show differences in PC1 scores. **g.** Examples of kinematic parameters with additive effects of daily training combined with *sh*RNA-vGAT. **h.** Age of injury-dependent circuit signatures capture decreasing vGlut2 input due to NT re-specification of dorsal and intermediate excitatory interneurons after adult injury (1) in contrast to increasing vGlut2 premotor synaptic input derived from the same population to MNs after neonatal injury (2). *sh*RNA-vGAT and training interventions respectively minimize NT phenotype switch and facilitate synaptic sprouting, therefore likely contributing to added effects of recovery when combined.

2.   Future work

We demonstrate that neurotransmitter phenotype of a subpopulation of excitatory interneurons underlies one of the mechanisms that direct locomotor capacity after spinal cord injury. Given these observations, we hypothesized that transcriptomic profiles that define locomotor circuit plasticity are dramatically altered in an age of injury-dependent manner. We are currently working to determine the transcriptomic profiles of adult spinal cord injured as neonate versus adult. Knowledge gained from such experiments will allow us to determine positive/negative regulators beyond neurotransmitter phenotype that are potentially druggable targets. We will further determine the locomotor capacity of mice injured as adults with *in-vivo* manipulation that facilitates novel neural circuit connectivity and locomotor recovery.

3.   Manuscript acknowledging GSKE/FMRE support

Bertels H, Vicente-Ortiz G, El Kanbi, K, Takeoka A (2022). Neurotransmitter phenotype switching by spinal excitatory interneurons regulates locomotor recovery after spinal cord injury. *Nature Neuroscience* 25 (5) 617–629. Impact Factor: 24.8

Progress report of the research project of the young researcher

Dr. Valerie Uytterhoeven
Katholieke Universiteit Leuven (KU Leuven)

Dr. Valerie Uytterhoeven
Staff Scientist
Center for Brain & Disease Research, VIB-KU Leuven
Laboratory of neuronal communication
Herestraat 49 bus 602
3000 Leuven
Belgium
Tel: +32 16 37 61 03

Molecular mechanisms and inducers of chaperone mediated Tau autophagy in Alzheimer's disease

1. Abstract

Pathogenic Tau detaches from microtubuli and distributes to different compartments of the neuron, including presynapses. We show that increasing endosomal microautophagy with enhanced Hsc70-4 expression reduces Tau at presynapses in fruit flies expressing human pathogenic Tau^{P301L} but not in flies expressing human pathogenic Tau^{V337M}. Consequently, Tau mediated presynaptic dysfunction is rescued in Tau^{P301L} but not in Tau^{V337M} flies with increased endosomal microautophagy. In addition, double pathogenic Tau$^{P301L, V337M}$ flies, accumulate more Tau at presynapses compared to single pathogenic Tau flies, suggesting that multiple pathways contribute to the accumulation of Tau at presynapses. With a fluorescent timer attached to Tau and a Fluorescence Recovery After Photobleaching assay of Tau-GFP, we measured respectively more aged Tau^{V337M} compared to Tau^{P301L} at presynapses and increased mobility of Tau^{P301L} compared to Tau^{V337M} in axons. We propose that reduced Tau turnover at presynapses contributes to the accumulation of Tau^{V337M} and that increased detachment of Tau from microtubuli contributes to the accumulation of Tau^{P301L} at presynapses.

2. Introduction

The microtubule-associated protein, Tau, is linked with more than twenty neurodegenerative diseases [1]. Hyperphosphorylation or mutations in Tau is common to all of these diseases, collectively termed Tauopathies, and lead to detachment of Tau from microtubuli [2]. Tau is not simply an artefact of other pathological pathways during disease as in familial Alzheimer's disease (AD) mouse models producing excessive Aβ-amyloid, a decrease of Tau ameliorates neurotoxicity and cognitive deficits [3]. In addition, mutations in the Tau-encoding MAPT locus are causative of Frontotemporal dementia with parkinsonism linked to chromosome 17 (FTDP-17) [4]. Hence, Tau is a key mediator of neurotoxicity itself.

When Tau detaches from microtubuli, Tau mislocalizes to different compartments of the neuron including the presynaptic terminal. Tau physically associates with presynaptic vesicles via binding of the synaptic vesicle protein, Synaptogyrin 3 [5,6]. This interaction sequesters synaptic vesicles resulting in decreased synaptic vesicle mobility, neurotransmission and memory and cognition [5–7].

During the regulation of presynaptic activity and memory consolidation, protein turnover systems such as the endolysosomal system and autophagy play critical roles locally at the presynapse [8,9,18,10–17]. The importance of a correctly functioning protein turnover system becomes also apparent in disease. AD GWAS studies cropped up repeatedly several endolysosomal genes [19,20]. Pathological examinations of AD brains showed that abnormalities of the neuronal endolysosomal and autophagy systems are an early and prominent feature of AD [21–23]In addition, Tau is a target of the autophagic pathway. More specifically, insoluble Tau is degraded via macroautophagy [24] while soluble Tau is cleared by eMIA (eMIA) and chaperone mediated autophagy (CMA) [25,26]. eMIA or CMA take up proteins with a KFERQ-like motif directly in the late endosome via the formation of intraluminal vesicles (ILV) or lysosome through the LAMP2A

pore, respectively [9,12,27–31]. Tau contains two KFERQ-like motifs, which are situated between the microtubule binding repeat domain 3 and 4 and are thus present in all six Tau isoforms.

Heat shock cognate 71 kDa protein (Hsc70-4), member of the heat shock protein 70 family (Hsp70) and also known as HSPA8, plays an important role in cargo selection for eMIA and CMA by the recognition of KFERQ-like motifs in proteins such as Tau [32–35]. Unlike other HSPs, Hsc70-4 is constitutively expressed and is abundant in the cytoplasm [36]. In addition to its cargo selection function, Hsc70-4 has as well membrane deforming capacity which is necessary to form ILV and to advance eMIA [9].

Previously, we showed that the overexpression of Hsc70-4 increases eMIA at fruit fly presynapses resulting in increased turnover of resident presynaptic proteins harboring a KFERQ-like motif [9]. In this study, we tested if mislocalized Tau at fruit fly presynapses can be reduced by stimulating eMIA. We show that increasing the expression of Hsc70-4 in flies expressing human pathogenic Tau^{P301L} rescues increased Tau levels at presynapses and Tau associated defects such as reduced synaptic vesicle mobility, neurotransmission and neurodegeneration of the fly brain. However, the overexpression of Hsc70-4 in flies expressing human pathogenic Tau with a mutation in the first KFERQ-like motif, Tau^{V337M}, does not rescue presynaptic Tau levels and consequently also presynaptic dysfunction and neurodegeneration are not rescued. These results indicate that the recognition of Tau^{V337M} for degradation via eMIA is defective and may contribute to the accumulation of Tau^{V337M} at the presynapse. To further unravel this finding, we measured the relative age of Tau at presynapses using a fluorescent timer attached to Tau. We measured in Tau^{V337M} mutant presynapses an increase in Tau age, indicating that the turnover of pathogenic Tau^{V337M} is reduced at presynapses compared to Tau^{P301L}. In addition, in double mutant Tau$^{P301L, V337M}$ flies, presynaptic Tau levels are further increased compared to single Tau mutants, indicating that multiple pathways contribute to the accumulation of Tau at presynapses. Since the pathogenic P301L mutation is located in the second repeat domain of the microtubule binding domain, we tested the attachment of pathogenic Tau to microtubuli in axons using Tau-GFP FRAP. We show that pathogenic Tau^{P301L} is more mobile in axons compared to Tau^{V337M} , indicating that Tau^{P301L} detaches more rapidly from microtubuli compared to Tau^{V337M}. Together, our results give evidence that i) multiple mechanisms, including Tau detachment from microtubuli and defective Tau turnover, contribute to the accumulation of Tau at presynapses, ii) increasing eMIA by the expression of Hsc70-4 is beneficial to reduce presynaptic Tau pathology and neurodegeneration in neurons expressing pathogenic Tau^{P301L} but not in neurons expressing pathogenic Tau^{V337M}.

3.   Results and Discussion

3.1.   Increased eMIA reduces pathogenic Tau^{P301L} levels at fly presynapses

Previously, we showed that the expression of human pathogenic Tau in fruit flies results in the accumulation of Tau at presynapses [5–7]. In this study, we confirmed the accumulation of Tau at presynapses in flies expressing human Tau containing the same mutations as tested before (P301L and V337M mutations) but also two additional mutations (AA mutations disrupting both KFERQ-like motifs and double mutation P301L, V337M). Presynaptic Tau labeling intensity at neuromuscular junctions is significantly increased in all Tau mutant flies compared to control flies (Fig. S3, A and B). As Tau is a target for eMIA, [25] and we previously showed that increasing the expression of Hsc70-4 accelerates eMIA, we hypothesized that increasing eMIA with the expression of Hsc70-4 may rescue the accumulation of pathogenic Tau at presynapses [9]. Since loss of neuronal proteostasis is a common feature in neurodegenerative diseases, including different types of tauopathies, we first tested the eMIA capacity of Tau mutant presynapses [37–39]. We quantified levels of EndophilinA (EndoA), a presynaptic protein and known target for eMIA, in Tau mutant presynapses (Fig. S3, C, D, E and F) [9]. Presynapses with basal eMIA and high Tau levels show similar EndoA immunolabeling intensity as presynapses with wild type Tau levels (Fig. S3, C and D). In addition, the stimulation of eMIA by the overexpression of Hsc70-4 significantly reduced immunolabeling intensity of EndoA in Tau mutant presynapses compared to presynapses with basal eMIA levels (Fig. S3, E and F). Hence, the eMIA pathway in Tau mutant presynapses is still sufficient to sustain control levels of the eMIA client protein, EndoA, at basal conditions and still has the capacity to be further upregulated to increase EndoA turnover.

Since the eMIA capacity in Tau mutant synapses is still adequate to be upregulated, we tested if the increase of eMIA with the expression of Hsc70-4 reduces presynaptic Tau levels in flies expressing pathogenic Tau^{P301L}. Presynaptic Tau labeling intensity at neuromuscular junctions is significantly reduced with the expression of Hsc70-4 in flies expressing human pathogenic Tau^{P301L} (Fig. 1, A and B). Further indicating specificity, the expression of ATPase defective (D10N) Hsc70-4 [40], which still harbors membrane deforming capacity to advance eMIA, reduces Tau labeling intensity at presynapses to similar levels as the expression of wild type Hsc70-4 (Fig. 1, A and B). In addition, the expression of eMIA dead (3KA) Hsc70-4 [9] does not reduce presynaptic Tau^{P301L} labeling intensity (Fig. 1, A and B). Together, these data show that increasing eMIA by the expression of Hsc70-4 is an effective strategy to reduce Tau^{P301L} levels at presynapses.

3.2.   Tau^{P301L} mediated presynaptic dysfunction is rescued with increased eMIA

Increased Tau levels at presynapses sequesters synaptic vesicles, resulting in reduced mobility of synaptic vesicles and reduced neurotransmission [5,7]. To test if eMIA mediated reduction of presynaptic Tau rescues reduced vesicle mobility at Tau^{P301L} mutant presynapses, we performed a FRAP assay. In this FRAP assay, fluorescently labeled synaptic vesicles with the expression of Synaptotagmin-GFP (Syt-GFP) are photobleached in a defined area of the presynapse and the recovery of fluorescence is recorded over time. The rate of fluorescence recovery in the photobleached area is a measure for the mobility of synaptic vesicles [5,7,41]. At Tau^{P301L} mutant presynapses, the FRAP of Syt-GFP is significantly slower (Fig. S1 A and Fig. 1 C, D, E and F; grey) compared to control presynapses that do not express human Tau (Fig. S1 A and Fig. 1, D, E and F; black). This defect is rescued with increased eMIA by the expression of wild type Hsc70-4 in Tau^{P301L} mutant neurons (Fig. 1, C and D; orange). Accordingly to the rescue of Tau levels at presynapses, the expression of ATPase defective Hsc70-4 (D10N) rescues the reduced Syt-GFP FRAP rate (Fig. 1, C and E; blue) and the expression of eMIA defective (3KA) Hsc70-4 does not restore the Syt-GFP FRAP rate at boutons of Tau^{P301L} mutant neurons (Fig. S1 A and Fig. 1 F; red). Hence, reducing presynaptic Tau levels by the increase of eMIA in Tau^{P301L} mutant neurons

restores the mobility of synaptic vesicles comparable to the mobility of synaptic vesicles at wild type presynapses.

At low frequency stimulation (1Hz) excitatory junction potential (EJP) recordings at fly neuromuscular junctions are not different between control and Tau[P301L] mutants [5,7]. The expression of wild type, ATPase defective nor eMIA dead Hsc70-4 in Tau[P301L] mutants has an effect on basal EJP amplitude (Fig. S1 C). However, neurotransmission is not sustained over time during high frequency (10Hz) stimulation because reduced synaptic vesicle mobility in Tau mutant flies hampers the replenishment of synaptic vesicles in the vesicle cycle [5,7]. We tested if increasing eMIA is sufficient to restore reduced neurotransmission during high frequency stimulation at Tau[P301L] mutant presynapses. In accordance with our Tau[P301L] levels and vesicle mobility data at presynapses (Fig. 1, A-F), the increase of eMIA by the expression of wild type (orange) or ATPase defective (blue) Hsc70-4 rescues reduced neurotransmission during high frequency (10Hz) stimulation in Tau[P301L] mutant presynapses comparable to control presynapses (black) (Fig. 1, G and H and Fig. S1 B). In addition, the expression of eMIA dead (3KA) Hsc70-4 does not rescue reduced neurotransmission during high frequency stimulation (Fig. 1 G and H and Fig. S1 B; red). Together, the data support that the reduction of presynaptic Tau[P301L] levels by increasing eMIA is sufficient to rescue Tau mediated presynaptic dysfunction.

3.3. Rescue of Tau[P301L] mediated presynaptic dysfunction with increased eMIA prevents neurodegeneration of the aged fly brain.

Synaptic dysfunction and loss are key steps in the process of neurodegeneration [42,43]. In animal models expressing pathogenic Tau, including fly tauopathy models, Tau mediated changes in synaptic function contribute to brain neurodegeneration [44–48]. Neurodegeneration in the adult fly brain manifests as vacuoles and these are visualized in haematoxylin and eosin (H&E) stained paraffin sections. Young control flies and young flies expressing Tau[P301L] panneuronally do not show signs of neurodegeneration (Fig. 2, A and B). However, neurodegeneration, quantified as vacuole area and corrected for brain area, is significantly increased in 40-day old Tau[P301L] mutant flies compared to 40-day old control flies (Fig. 2, C and D). The increase of eMIA with the expression of wild type or ATPase dead (D10N) Hsc70-4 in aged Tau[P301L] mutant flies significantly reduced neurodegeneration comparable to control levels (Fig. 2, C and D). Together, the rescue of Tau mediated synaptic dysfunction with increased eMIA prevents neurodegeneration of the aged Tau[P301L] mutant fly brain.

3.4. Tampered KFERQ-like motifs in Tau block the rescue of Tau mediated presynaptic defects and neurodegeneration with increased eMIA

eMIA is selective for the degradation of proteins harboring at least one KFERQ-like motif. Further showing specificity, we tested if the reduction of Tau via the expression of Hsc70-4 is KFERQ-like motif selective at presynapses. We generated transgenic flies that express human Tau with mutated KFERQ-like motifs. In both KFERQ-like motifs, we substituted the uncharged amino acid, glutamine, and the hydrophobic amino acid, valine, with hydrophobic alanines (Tau[AA]). This substitution was shown before to disrupt the KFERQ-like motif in other proteins [9,49,50]. The introduction of these mutations in Tau does not block the expression of Tau protein but results in the accumulation of Tau[AA] at presynapses to a similar level as pathogenic Tau[P301L] (Fig. S3, A and B). In addition, the expression of wild type nor ATPase dead (D10N) Hsc70-4 in Tau[AA] mutant flies results in a reduction of Tau levels at presynapses (Fig. 3, A and B). Together, the loss of KFERQ-like motifs is sufficient for the accumulation of Tau at presynapses and the absence of presynaptic Tau reduction with increasing eMIA indicates that Tau[AA] is not recognized for degradation via eMIA.

Also pathogenic mutations in the first KFERQ-like motif of Tau are known, including the V337M mutation for which we showed in previous work that its expression results in the accumulation of Tau^{V337M} at presynapses [5,7]. The level of Tau^{V337M} accumulation at presynapses is comparable to the accumulation of Tau^{P301L} and Tau^{AA} (Fig. S3, A and B). Similar to mutant Tau^{AA} presynapses, increasing eMIA with the expression of wild type nor ATPase dead (D10N) Hsc70-4 has an effect on presynaptic Tau^{V337M} levels. As expected, the expression of eMIA dead (3KA) Hsc70-4 has no effect either (Fig. 3, C and D) on presynaptic Tau^{V337M} levels. Hence, our results indicate that the V337M mutation disrupts the KFERQ-like motif hereby interfering with the Hsc70-4 mediated recognition of Tau for degradation via eMIA.

Similar to Tau^{P301L}, Tau^{V337M} interacts with synaptic vesicles and reduces their mobility at presynapses [5,7]. However, the expression of wild type Hsc70-4 (WT, orange) nor ATPase dead (D10N, blue) rescues reduced FRAP of Syt-GFP at Tau^{V337M} mutant presynapses (Fig. 4, A-C and Fig. S2 A). In addition, the expression of eMIA dead Hsc70-4 (3KA, red) has no effect either on the reduced vesicle mobility at Tau^{V337M} mutant presynapses (Fig. 4 D and Fig. S2 A). Hence, in presynapses accumulating Tau^{V337M}, increasing eMIA is not sufficient to reduce presynaptic Tau^{V337M} and thus the interaction of Tau^{V337M} with synaptic vesicles continues hereby restricting vesicle mobility.

Tau^{V337M} mutant flies have normal basal neurotransmission as measured with EJP recordings at neuromuscular junctions [5,7]. In addition, the expression of wild type nor ATPase defective Hsc70-4 has an effect on the basal EJP amplitude in Tau^{V337M} mutants (Fig. S2 C). However, similar to Tau^{P301L} mutant neurons, neurotransmission is not maintained during a high frequency (10Hz) stimulation train of 10 minutes in Tau^{V337M} mutant neurons (Fig. 4, E and F and Fig. S2 B, grey) [5,7]. In accordance with our Tau^{V337M} immunolabeling intensity and vesicle mobility data (Fig. 3 and 4), the increase of eMIA by the expression of wild type (orange) nor ATPase defective (blue) Hsc70-4 rescues reduced neurotransmission during high frequency (10Hz) stimulation in Tau^{V337M} mutant presynapses (Fig. 4, E and F and Fig. S2 B). Because vesicle mobility is still restricted in Tau^{V337M} mutant neurons with increased eMIA, neurotransmission during high frequency stimulation is neither rescued.

Similar to 40-day aged Tau^{P301L} mutant fly brains, the quantification of vacuole area in H&E stained paraffin brain sections of 40-day old Tau^{V337M} mutant flies shows significantly increased neurodegeneration compared to 40-day old control flies (Fig. 3, E and F). However, the increased neurodegeneration in aged Tau^{V337M} mutant flies is not significantly reduced with the expression of wild type (WT), ATPase dead (D10N) Hsc70-4 or eMIA dead (3KA) Hsc70-4 (Fig. 3, E and F). Hence, when synaptic dysfunction is not rescued by the increase of eMIA also neurodegeneration is not rescued.

3.5. Reduced Tau turnover at presynapses and increased Tau mobility in axons mediate the accumulation of pathogenic Tau at presynapses.

Because increasing eMIA is not effective in reducing presynaptic Tau pathology in all Tau mutants, multiple pathways may be involved in the accumulation of Tau at presynapses. To test if multiple pathways contribute to the accumulation of Tau at presynapses, we generated transgenic flies expressing human double mutant Tau containing the P301L and V337M mutation (Tau$^{P301L, V337M}$). At double mutant Tau$^{P301L, V337M}$ presynapses, Tau levels increase significantly compared to single Tau mutants (Figure S3, A and B) and this increased accumulation of Tau at presynapses is accompanied with increased neurodegeneration in aged Tau^{P301L,V337M} double mutant fly brain compared to aged Tau single mutant fly brains (Fig. 5, B and C). Hence, the additive effect of double mutant Tau$^{P301L, V337M}$ on presynaptic Tau levels and neurodegeneration further confirms that multiple pathways contribute to presynaptic Tau pathology.

The pathogenic P301L mutation is located in the third microtubule binding domain, suggesting a defect in microtubuli binding and the pathogenic V337M mutation is located in the first KFERQ-like motif, suggesting a defect in Tau turnover (Fig. 5 A). Previously, we used a fluorescent timer to estimate the relative turnover of resident presynaptic proteins, such as nSynaptobrevin and Comatose [9,28]. To test if a defect in Tau turnover is involved in the accumulation of Tau at presynapses, we generated transgenic flies that express human mutant Tau linked to a fluorescent timer. A fluorescent timer is a modified GFP that shifts from blue to red over time and the red/blue intensity ratio is a measure of the level of old (red) versus young (blue) Tau protein. An increased red/blue ratio shows an older Tau protein pool indicating reduced protein turnover and vice versa. We measured an increased red/blue ratio in Tau^{V337M} and Tau^{AA} mutant presynapses compared to Tau^{P301L} mutant presynapses. However, the red/blue ratio in Tau$^{P301L, V337M}$ double mutant presynapses is not further increased but similar to Tau^{V337M} and Tau^{AA} single mutant presynapses (Fig. 5, D and E). Thus, the turnover of Tau protein containing mutations in the KFERQ-like motif (V337M and AA) is reduced, while the presence of the P301L mutation has no effect on Tau turnover.

To test the effect of the different Tau mutations on Tau microtubule attachment, we performed FRAP of wild type and mutant Tau-GFP in axons. FRAP of Tau-GFP is significantly increased in axons of neurons expressing mutant Tau compared to neurons expressing wild type Tau (black) (Fig. 5, F and G and Fig. S3 G), showing that mutant Tau is more mobile in axons compared to wild type Tau. In addition, Tau-GFP FRAP in Tau^{P301L} (brown) axons is significantly increased compared to Tau^{V337M} (pink) and Tau^{AA} (green) axons. However, TauGFP FRAP in Tau^{P301L,V337M} (blue) double mutants is not further increased but similar to Tau^{P301L} mutants (brown) (Fig. 5 F and G and Fig. S3 G). Hence, Tau protein containing the P301L mutation detaches faster from microtubuli compared to Tau containing mutations in the KFERQ-like motif (V337M and AA).

4.   Conclusion

Previously, we showed that pathogenic Tau accumulates at presynapses but the molecular pathways involved are not well understood. While much of the literature describes that pathogenic mutations in Tau interfere with microtubuli binding, a strong consensus on the impact of different pathogenic Tau mutations on Tau-microtubuli interactions is not yet shown [51–55]. In this study we show that the expression of human pathogenic Tau mutations P301L and V337M in flies both reduce the attachment of Tau to microtubuli but the P301L mutation in a much greater extent. Besides the attachment of Tau to microtubuli, we show that the turnover of Tau at presynapses plays an important role as well to regulate presynaptic Tau levels. The pathogenic Tau mutation, V337M, disrupts the eMIA recognition motif hereby reducing the turnover of Tau compared to the P301L mutation. We conclude that both detachment from microtubuli and reduced Tau turnover may contribute to the accumulation of Tau at the presynapse but the contribution ratio of both pathways is dependent on the mutation in Tau. The contribution of the pathogenic V337M mutation to presynaptic Tau accumulation is mainly a defect in Tau turnover while for the pathogenic P301L mutation detachment from microtubuli is more prominent (Fig. 5 H). Thus the nature of the mutation defines the main molecular route of Tau accumulation at the presynapse.

In addition, we show that increasing eMIA with the expression of Hsc70-4 is beneficial to rescue Tau^{P301L}-mediated presynaptic defects but not Tau^{V337M} mediated presynaptic defects. This insight shows that increasing eMIA would not be beneficial for patients with Tau^{V337M} mutation however this strategy may be beneficial for the many other tauopathies related to Tau mutations not affecting Tau eMIA recognition. Also for ALS, for which more and more data support a pathogenic

role of Tau in the disease ,an increase of eMIA may be beneficial. Coyne et al. showed in multiple models of ALS a reduction of Hsc70-4 and synaptic vesicle cycling defects [56]. Post-mortem studies of motor cortex and spinal cord of ALS patients showed a significant increase in total Tau and hyperphosphorylated Tau [57,58] and mislocalization of Tau to presynapses and synapse loss [59]. In addition, Tau is not the only protein containing KFERQ-like motifs that is involved in neurodegenerative diseases. Also Amyloid precursor protein (APP), best known as the precursor molecule whose proteolysis generates amyloid beta, the primary component of amyloid plaques found in the brain of Alzheimer's disease patients, contains KFERQ-like motifs. Xu et al. increased chaperone mediated autophagy with the viral mediated overexpression of Hsc70-4 in the brain of AD mice and measured reduced Ab plaque levels and reversed the molecular and behavioral AD phenotypes [60], however the effect on Tau was not measured. Hence increasing chaperone mediated autophagy/eMIA may be beneficial to reduce both pathological hallmarks of AD, Ab plaques and Tau tangles.

Tau level in presynapses at NMJs
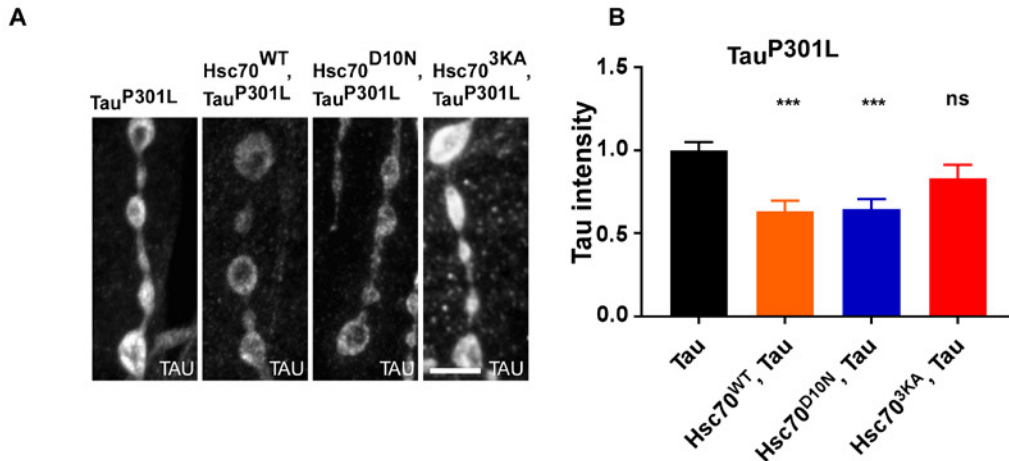
A

Tau^P301L | Hsc70^WT, Tau^P301L | Hsc70^D10N, Tau^P301L | Hsc70^3KA, Tau^P301L

B

Tau^P301L

Synaptic vesicle mobility with FRAP assay

C

Pre | 0s | 10s | 30s | 50s

Tau^P301L

Hsc70^WT, Tau^P301L

Hsc70^D10N, Tau^P301L

D

Hsc70^WT, Tau^P301L *
control *
Tau^P301L

E

Hsc70^D10N, Tau^P301L *
control *
Tau^P301L

F

Hsc70^3KA, Tau^P301L ns
control
Tau^P301L *

Neurotransmission with 10Hz Stimulation

G

control
Tau^P301L
Hsc70^WT, Tau^P301L
Hsc70^D10N, Tau^P301L
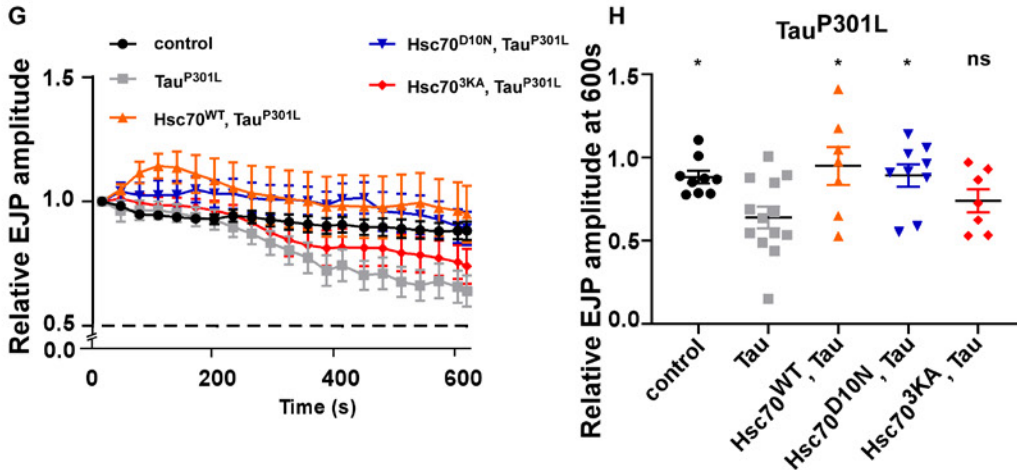Hsc70^3KA, Tau^P301L

H
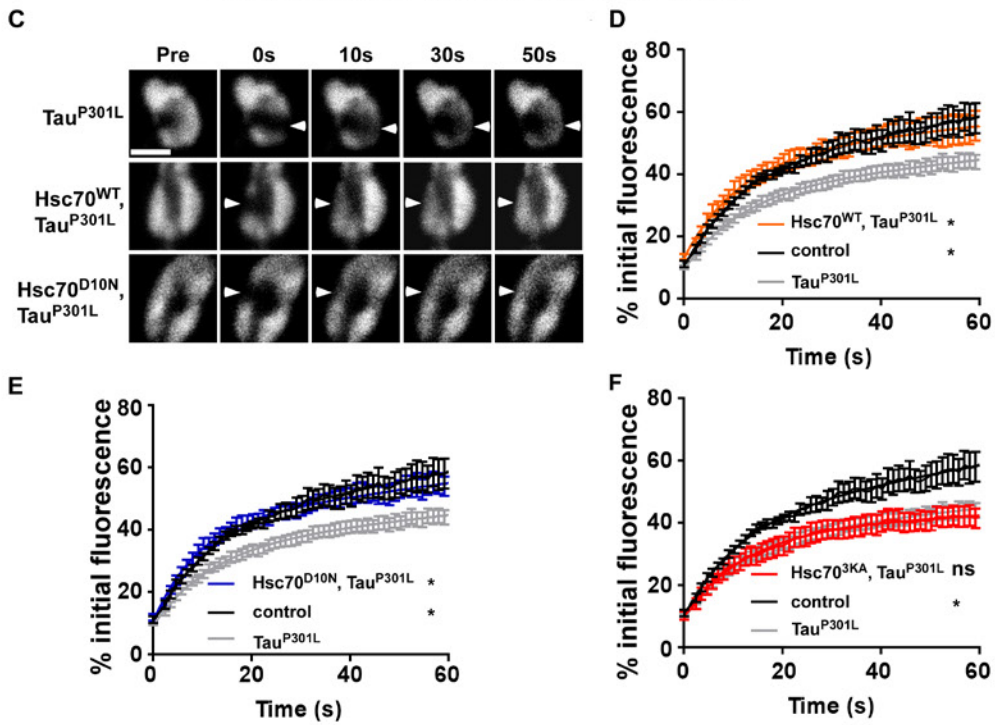
Tau^P301L

Figure 1. Increased eMIA rescues presynaptic defects in flies expressing human pathogenic Tau^{P301L}.

A) Representative images and **B)** quantification of Tau intensities in boutons of motorneurons expressing mutant Tau^{P301} without (nSyb-GAL4> Tau^{P301L} or nSyb-GAL4> Hsc70^{3KA}, Tau^{P301L}) or with increased eMIA (nSyb-GAL4> Hsc70^{WT}, Tau^{P301L} or nSyb-GAL4> Hsc70^{D10N}, Tau^{P301L}). Scale bar is 5µm. Bar graphs depict mean ± SEM. Number of larvae is 4-8 per genotype. **C)** Representative images of Syt-GFP FRAP in boutons at time points right before (pre) and after photobleaching of a small area (arrowhead) (0, 10, 30 and 50 seconds). Scale bar, 5 µm. An ordinary one-way ANOVA with Dunnett's correction for multiple comparison was performed; ns, not significant,***$p < 0.001$. **D-F)** Plots of Syt-GFP fluorescence recovery over time fit to a double-exponential curve and depict relative vesicle mobility in control (nSyb-GAL4>Syt-GFP, black), Tau^{P301L} mutants without increased eMIA (nSyb-GAL4>Syt-GFP; Tau^{P301L}, grey or nSyb-GAL4>Syt-GFP; Hsc70^{3KA}, Tau^{P301L}, red) or Tau^{P301L} mutants with increased eMIA (nSyb-GAL4>Syt-GFP; Hsc70^{WT}, Tau^{P301L}; orange or nSyb-GAL4>Syt-GFP; Hsc70^{D10N}, Tau^{P301L}; blue. Plots depict mean ± SEM (n is 8-23 boutons from ≥6 animals; A two-way ANOVA with Dunnett's correction for multiple comparisons was performed. **G–H)** Electrophysiological recordings of neurotransmitter release at NMJs. **G)** Plot of evoked junction potential (EJP) amplitudes in response to a 10Hz stimulation with 2 mM Ca^{2+} for 10 min in controls (nSyb-GAL4>; black) and Tau^{P301L} mutants without increased endosomal autophagy (nSyb-GAL4>Tau^{P301L}; grey or nSyb-GAL4>Hsc70^{3KA}, Tau^{P301L}; red) or Tau mutants with increased eMIA (nSyb-GAL4>Hsc70^{WT}, Tau^{P301L}; orange or nSyb-GAL4>Hsc70^{D10N}, Tau^{P301L}; blue). Plots depict mean ± SEM (n is 8-23 boutons from ≥6 animals. Amplitudes are binned at 30s intervals and normalized to the average amplitude of the first 15s. **H)** Relative EJP amplitude at 600 s plotted as individual data points. Graphs depicts mean ± SEM. Number of dots is number of NMJ recordings from ≥6 animals. An ordinary one-way ANOVA with Dunnett's correction for multiple comparison was performed; ns, not significant, *$p < 0.05$.
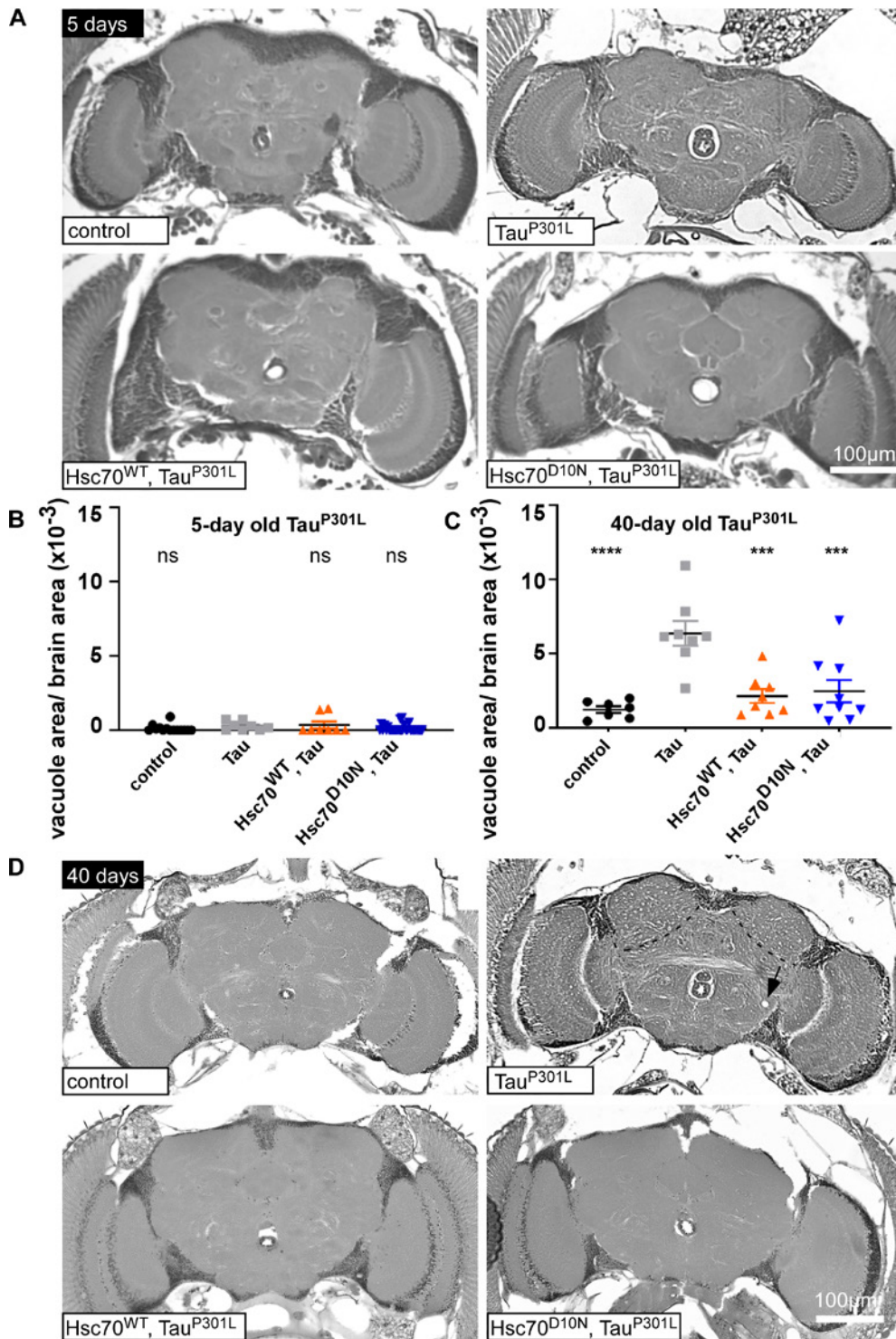
Figure 2. Tau^{P301L} induced neurodegeneration is rescued with increased eMIA
A and D) Representative brain sections stained with H&E and **B and C)** quantification of neurodegeneration by assessing vacuole area normalized over brain area of 5-day-old **(B)** and 40-day old **(C)** control (nSyb-GAL4>, black); and Tau^{P301L} mutants without (nSyb-GAL4> Tau^{P301L}, grey) and with increased eMIA (nSyb-GAL4> Hsc70^{WT}, Tau^{P301L} ; orange or nSyb-GAL4> Hsc70^{D10N}, Tau^{P301L}; blue). Arrow and encircled area indicate vacuolar degeneration. Graph represent the mean ± SEM and number of data points indicate the number of animals. An ordinary one-way ANOVA with Dunnett's correction for multiple comparison was performed. ns, not significant, *** $p<0.001$, **** $p<0.0001$.
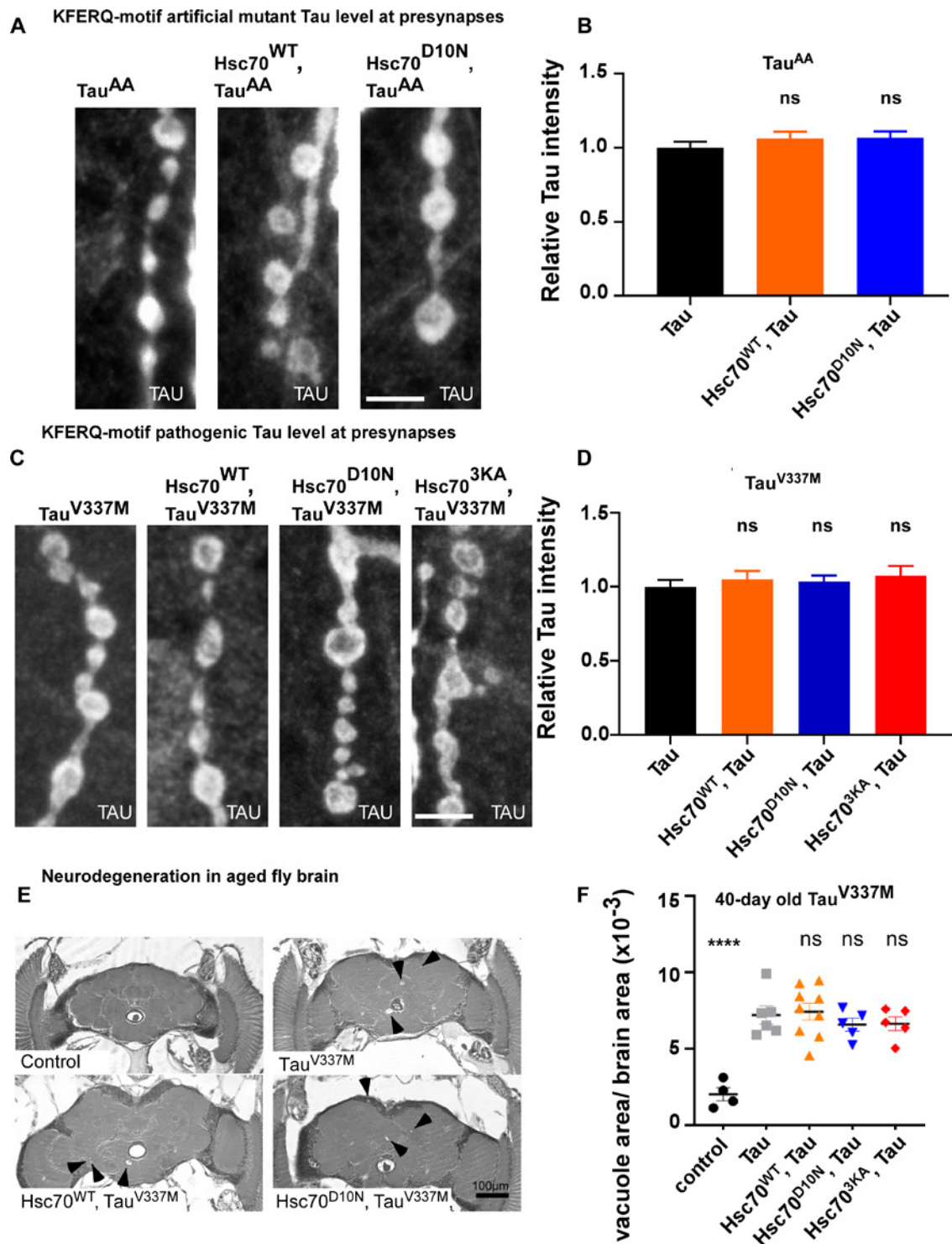
Figure 3. Presynaptic Tau levels and neurodegeneration are not rescued with increased eMIA in neurons expressing KFERQ-like motif mutant Tau.

A) Representative images and **B)** quantification of relative Tau intensities in boutons of motorneurons expressing KFERQ-like motif mutant Tau^{AA} without (nSyb-GAL4> Tau^{AA}; black) or with increased eMIA, (nSyb-GAL4> Hsc70^{WT}, Tau^{AA}; orange or nSyb-GAL4> Hsc70^{D10N}, Tau^{AA}; blue) **C)** Representative images and **D)** quantification of relative Tau intensities in boutons of motorneurons expressing KFERQ-like motif pathogenic Tau^{V337M} without (nSyb-GAL4> Tau^{V337M}; black or nSyb-GAL4> Hsc70^{3KA}, Tau^{V337M}; red) or with increased eMIA (nSyb-GAL4> Hsc70^{WT}, Tau^{V337M} ; orange or nSyb-GAL4> Hsc70^{D10N}, Tau^{V337M}; blue). Scale bars are 5μm. Bar graphs depict mean ± SEM. Number of larvae is 4-8 per genotype for **(A-B)** and 8 per genotype for **(C-D). E)** Representative images and **F)** quantification of neurodegeneration in H&E stained brain sections of 40-day old control flies (nSyb-GAL4>; black) and flies expressing human Tau^{V337M} without (nSyb-GAL4> Tau^{V337M}; grey or nSyb-GAL4> Hsc70^{3KA}, Tau^{V337M}; red) or with increased eMIA (nSyb-GAL4> Hsc70^{WT}, Tau^{V337M}; orange or nSyb-GAL4> Hsc70^{D10N}, Tau^{V337M}; blue). Arrowheads indicate vacuolar degeneration. Neurodegeneration is quantified by vacuole area normalized over brain area. Graph represents the mean ± SEM and number of data points indicate the number of animals. An ordinary one-way ANOVA with Dunnett's correction for multiple comparisons was performed for all quantifications. Ns; is not significant, **** $p<0.0001$.
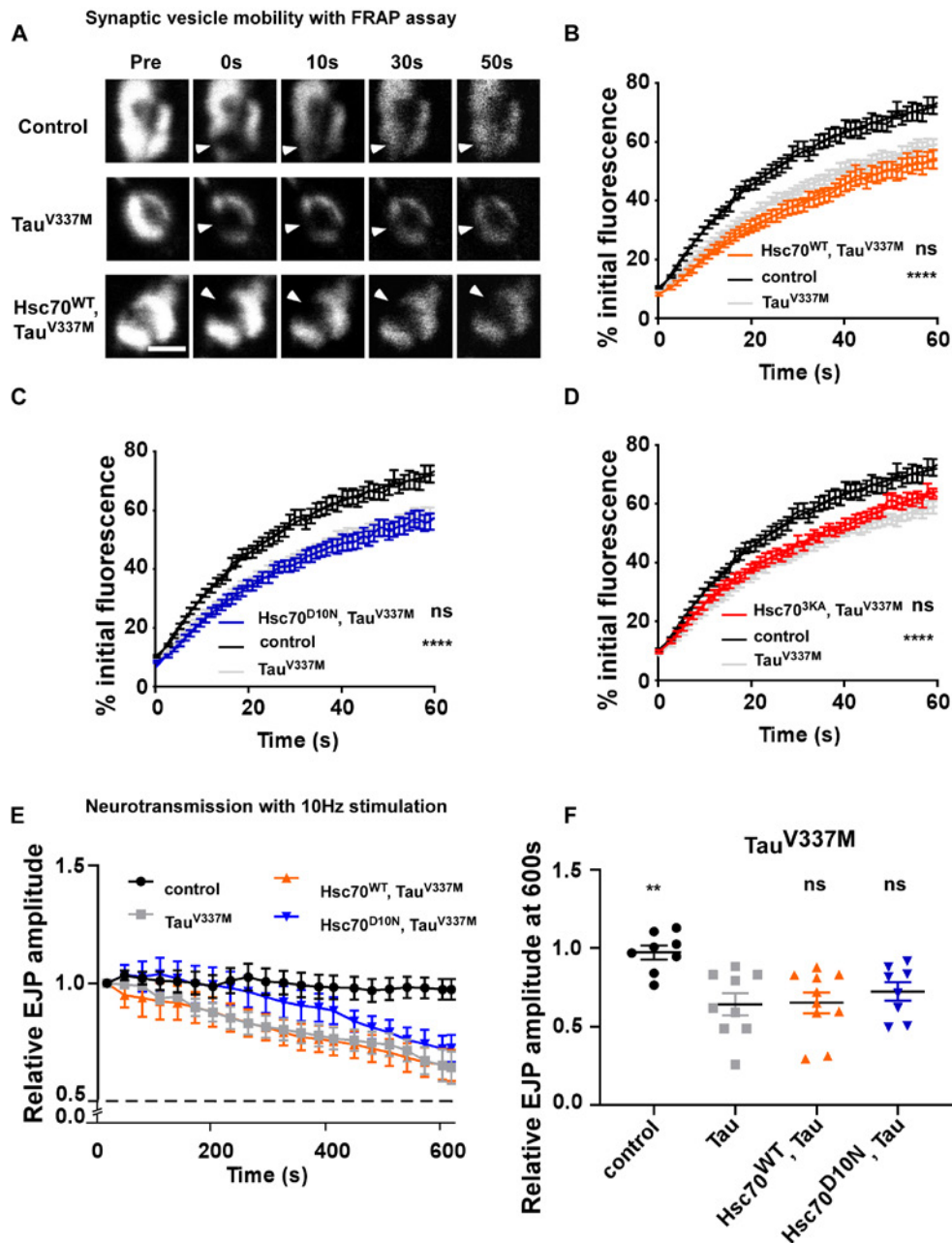
Figure 4. Tau^V337M mediated presynaptic dysfunction is not rescued with increased eMIA
A) Representative images of Syt-GFP FRAP in boutons at time points right before (pre) and after photobleaching of a small area (arrowhead) (0, 10, 30 and 50 seconds). Scale bar, 5 μm. **B-D)** Plots of Syt-GFP fluorescence recovery over time fit to a double-exponential curve depicting relative vesicle mobility in control (nSyb-GAL4>Syt-GFP; black), Tau^V337M mutant without increased eMIA (nSyb-GAL4>Syt-GFP; Tau^V337M; grey or nSyb-GAL4>Syt-GFP; Hsc70^3KA, Tau^V337M; red) and Tau^V337M mutant with increased eMIA (nSyb-GAL4>Syt-GFP; Hsc70^WT, Tau^V337M; orange or nSyb-GAL4>Syt-GFP; Hsc70^D10N, Tau^V337M; blue). Plots depict mean ± SEM (n is 8-23 boutons from ≥6 animals; A two-way ANOVA with Dunnett's correction for multiple comparisons was performed. ns is not significant, **** $p<0.0001$. **E–F)** Electrophysiological recordings of neurotransmitter release at NMJs. **E)** Plot of EJP amplitudes in response to a 10Hz stimulation with 2 mM Ca²⁺ for 10 min in control (nSyb-GAL4>; black); Tau^V337M mutants without increased eMIA (nSyb-GAL4> Tau^V337M; grey) and Tau mutants with increased eMIA (nSyb-GAL4> Hsc70^WT, Tau^V337M; orange or nSyb-GAL4> Hsc70^D10N, Tau^V337M; blue) mutants. Amplitudes are binned at 30s intervals and normalized to the average amplitude of the first 15s. **F)** Relative EJP amplitude at 600 s plotted as individual data points. Graphs depicts mean ± SEM. Number of data points is number of NMJ recordings from ≥6 animals. An ordinary one-way ANOVA with Dunnett's correction for multiple comparison was performed; ns, not significant, **$p < 0.01$.

A 0N4R Tau

P301L
V337M/AA

R1 R2 R3 R4

1 383

B Neurodegeneration in aged fly brain

Tau^P301L

Tau^V337M

Tau^AA

Tau^P301L,V337M

100μm

C

40-day old flies

**** ns ns **

vacuole area/ brain area (×10^{-3})

control Tau^P301L Tau^V337M Tau^AA Tau^P301L, V337M

D Tau turnover with Tau fluorescent timer

Tau^P301L Tau^V337M Tau^AA

E

*** **** **

Tau red/blue fluorescence

Tau^P301L Tau^V337M Tau^AA Tau^P301L, V337M

F Tau mobility with FRAP assay in axons

Pre 0s 10s 30s 50s

Tau^P301L

Tau^V337M

Tau^AA

G

% initial fluorescence

Tau^P301L, V337M
Tau^P301L
Tau^V337M
Tau^AA
Tau^WT

**** ****

Time (s)

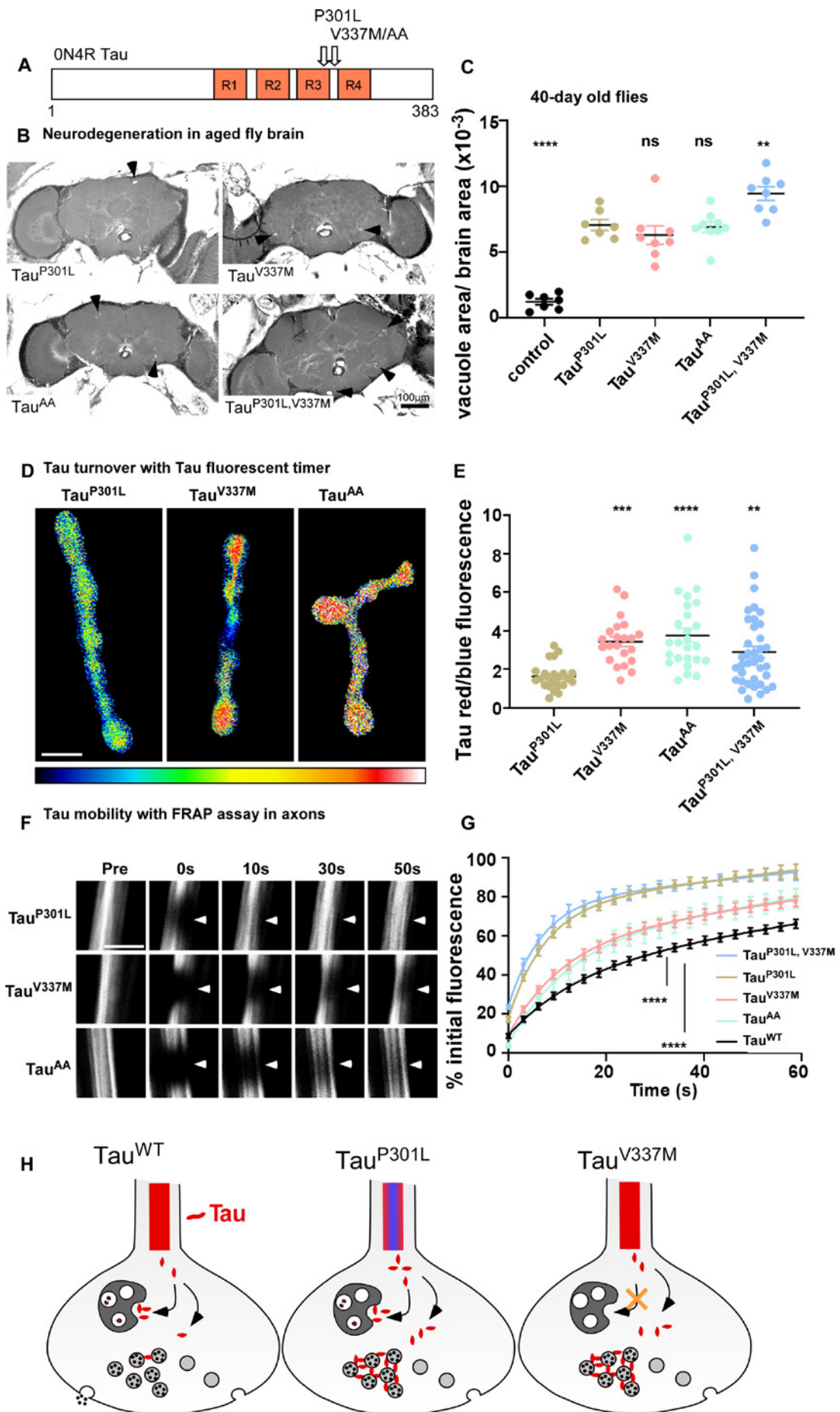**H** Tau^WT Tau^P301L Tau^V337M

Tau

Figure 5. Pathogenic Tau mutations differently affect presynaptic Tau turnover and axonal Tau mobility.
A) 0N4R human Tau contains four repeat domains, which interact with microtubuli. The pathogenic P301L mutation is located in the third repeat domain. The pathogenic V337M mutation and the artificial AA mutations are located between the third and fourth repeat domain and respectively disrupt the first or both KFERQ-like motifs. **B)** Paraffin embedded brain sections of 40-day old control flies (nSyb-GAL4>) or flies expressing human Tau^{P301L} (nSyb-GAL4> Tau^{P301L}) or Tau^{V337M} (nSyb-GAL4> Tau^{V337M}) or Tau^{AA} (nSyb-GAL4> Tau^{AA}) or Tau$^{P301L, V337M}$ (nSyb-GAL4> Tau$^{P301L, V337M}$) stained with H&E. Arrowheads indicate vacuolar degeneration. **C)** Neurodegeneration was assessed by quantification of vacuole area normalized over brain area. Graph represent the mean ± SEM and number of data points indicate the number of animals (≥7)). An ordinary one-way ANOVA with Dunnett's correction for multiple comparison was performed. **D)** Images of the ratio of red over blue fluorescence intensities at synaptic boutons using the indicated lookup table. Scale bar: 5µm. **E)** Quantification of Tau fluorescent timer red/ blue ratio in flies expressing human Tau attached to a fluorescent timer (nSyb-GAL4>Tau^{P301L}-FT-GFP or Tau^{V337M} nSyb-GAL4>Tau^{V337M}-FT-GFP or nSyb-GAL4> Tau^{AA}- FT-GFP or nSyb-GAL4> Tau$^{P301L, V337M}$ -FT-GFP). Graph represent the mean ± SEM and number of data points indicate the number of animals (≥7)). An ordinary one-way ANOVA with Dunnett's correction for multiple comparison was performed. **F)** Representative images of Tau-GFP FRAP at time points right before (pre) and after photobleaching of an area (arrowhead) (0, 10, 30 and 50 seconds) in axons. Scale bar: 5µm.**G)** Tau-GFP FRAP over time fit a double-exponential curve depicting relative Tau mobility in flies expressing human Tau (nSyb-GAL4>Tau^{WT}-FT-GFP or nSyb-GAL4>Tau^{P301L}-FT-GFP or Tau^{V337M} nSyb-GAL4>Tau^{V337M}-FT-GFP or nSyb-GAL4> Tau^{AA}- FT-GFP or nSyb-GAL4> Tau$^{P301L, V337M}$ -FT-GFP). Plot depicts mean ± SEM. n is 11-27 axons from ≥8 animals. A two-way ANOVA with Dunnett's correction for multiple comparisons was performed. ns is not significant, **p<0.01; ***p<0.001; **** p<0.0001 **H)** Model with neurons expressing wild type human Tau (Tau^{WT}) or pathogenic human Tau (Tau^{P301L} or Tau^{V337M}). Neuron that expresses Tau^{WT} shows minimal Tau detaching from microtubuli in axons and Tau that is distributed to the presynapse is recognized for degradation via eMIA keeping Tau levels at presynapses low. Neuron expressing pathogenic Tau^{P301L} shows excessive Tau detaching from the microtubuli in axons. High Tau^{P301L} levels distribute to the presynapse and are recognized for degradation via eMIA, however, the flow of Tau^{P301L} to the presynapse is too high to maintain wild type levels of Tau at presynapses. Neuron expressing pathogenic Tau^{V337M} shows less detachment of Tau^{V337M} from microtubuli compared to Tau^{P301L}. However, Tau^{V337M} is not recognized for degradation via eMIA and Tau^{V337M} accumulates at presynapses.

Synaptic vesicle mobility with FRAP assay

Neurotransmission with 10Hz stimulation

Supplemental Figure 1. Synaptic vesicle mobility and neurotransmission in Tau^{P301L} mutants with basal and increased eMIA.
A) Representative images of Syt-GFP FRAP in boutons at time points right before (pre) and after photobleaching of a small area (arrowhead) (0, 10, 30 and 50 seconds) in control (nSyb-GAL4>Syt-GFP) and Tau^{P301L} mutant boutons without increased eMIA (nSyb-GAL4>Syt-GFP; Tau^{P301L} or nSyb-GAL4>Syt-GFP; Hsc70^{3KA}, Tau^{P301L}). Scale bar, 5 µm. **B)** Representative raw data traces of evoked EJP amplitudes in response to 10Hz stimulation with 2mM Ca^{2+} for 10min in control (nSyb-GAL4>; black), Tau^{P301L} mutants without increased eMIA (nSyb-GAL4> Tau^{P301L} ; grey or nSyb-GAL4>Hsc70^{3KA}, Tau^{P301L}; red) and Tau^{P301L} mutants with increased eMIA (nSyb-GAL4> Hsc70^{WT}, Tau^{P301L}; orange or nSyb-GAL4> Hsc70^{D10N}, Tau^{P301L};blue). **C)** Relative first evoked EJP amplitude in response to 10Hz stimulation with 2mM Ca^{2+}. Graph depicts mean ± SEM. Number of data points is number of NMJ recordings from ≥6 animals. An ordinary one-way ANOVA with Dunnett's correction for multiple comparison was performed. ns, not significant
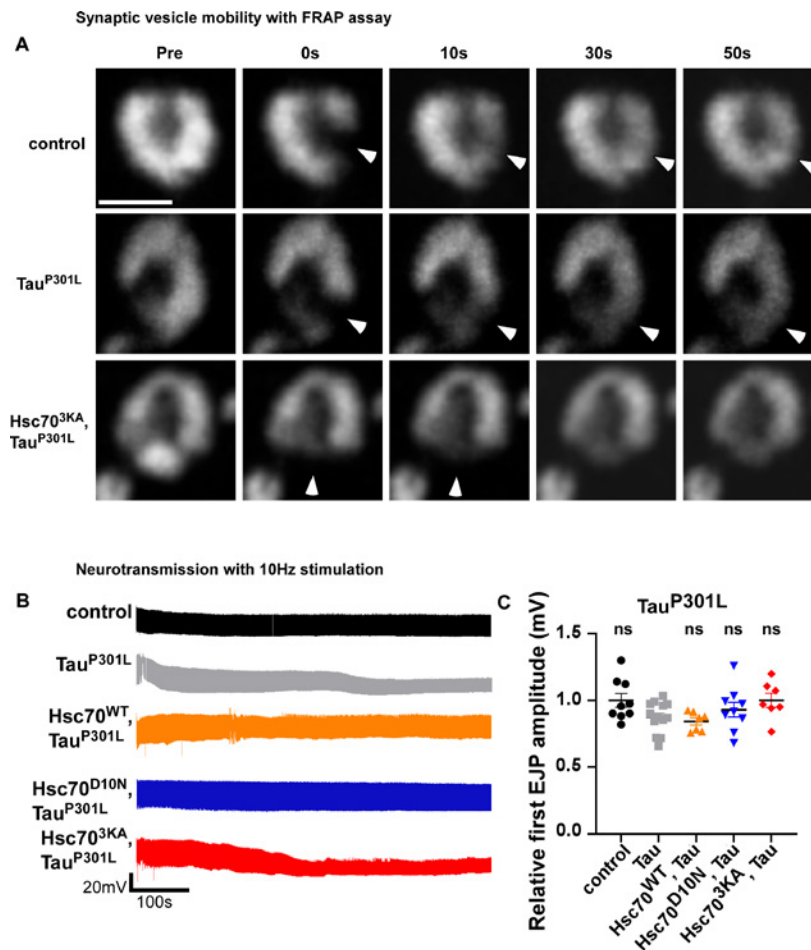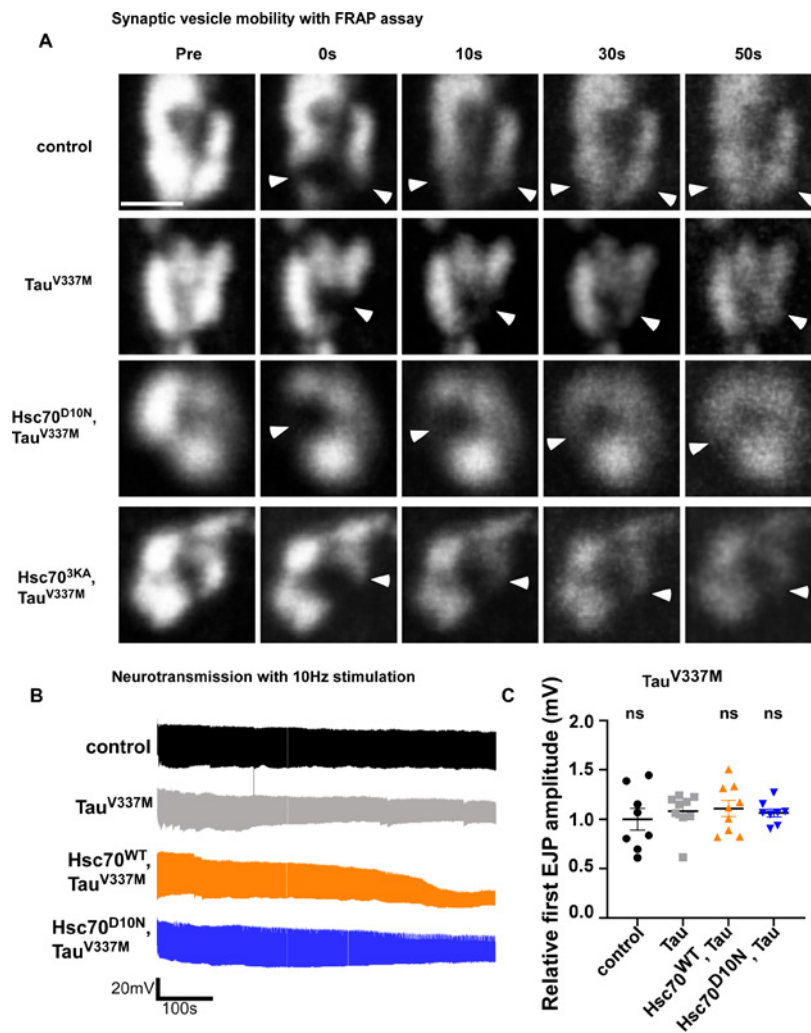
Supplemental Figure 2. Synaptic vesicle mobility and neurotransmission in Tau[V337M] mutants with basal and increased eMIA.
A) Representative images of Syt-GFP FRAP in boutons at time points right before (pre) and after photobleaching of a small area (arrowhead) (0, 10, 30 and 50 seconds) in control (nSyb-GAL4>Syt-GFP), Tau[V337M] mutants without increased eMIA (nSyb-GAL4>Syt-GFP; Tau[V337M] or nSyb-GAL4>Syt-GFP; Hsc70[3KA], Tau[V337M]) and Tau[V337M] mutants with increased eMIA (nSyb-GAL4>Syt-GFP; Hsc70[D10N], Tau[V337M]). Scale bar, 5 μm. **B)** Representative raw data traces of evoked EJP amplitudes in response to 10Hz stimulation with 2 mM Ca^{2+} for 10 min in control (nSyb-GAL4>; black), Tau[V337M] mutants without increased eMIA (nSyb-GAL4> Tau[V337M]; grey) and Tau[V337M] mutants with increased eMIA (nSyb-GAL4> Hsc70[WT], Tau[V337M]; orange or nSyb-GAL4> Hsc70[D10N], Tau[V337M]; blue). **C)** Relative first evoked EJP amplitude in response to 10Hz stimulation with 2mM Ca^{2+} Graph depicts mean ± SEM. Number of data points is number of NMJ recordings from ≥6 animals. An ordinary one-way ANOVA with Dunnett's correction for multiple comparison was performed. ns, not significant.
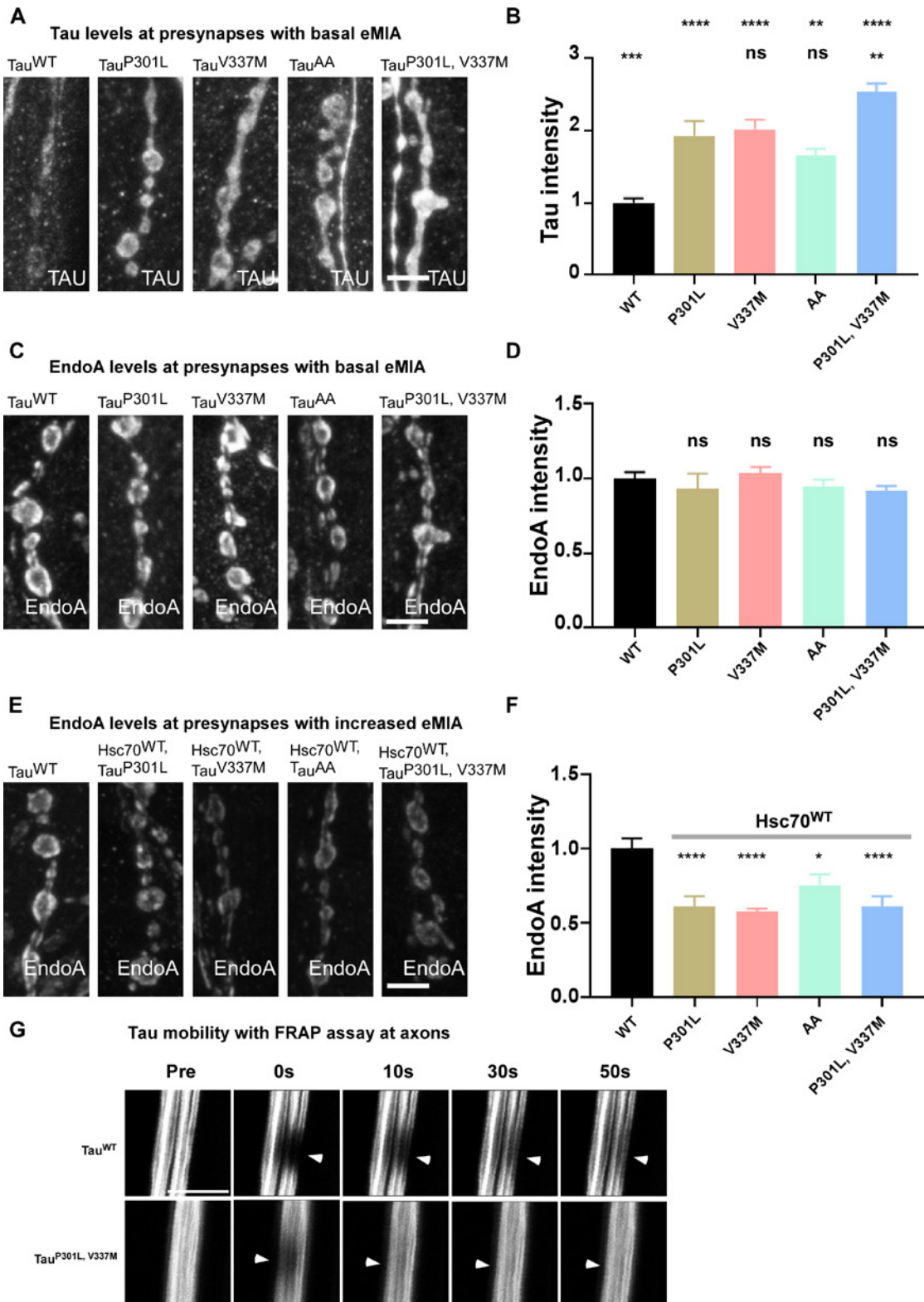
Supplemental Figure 3. Tau and EndoA levels and Tau mobility in TauP301L, V337M double mutants.
A) Representative images and **B)** quantification of Tau intensities in boutons of motorneurons expressing wild type (nSyb-GAL4> TauWT) or human mutant Tau (nSyb-GAL4> TauP301L or V337M or AA or P301L,V337M). Number of larvae is 4-8 per genotype. **C)** Representative images and **D)** quantification of EndoA intensities in boutons of motorneurons expressing wild type (nSyb-GAL4> TauWT) or human mutant Tau (nSyb-GAL4> TauP301L or V337M or AA or P301L,V337M). Number of larvae is 4-8 per genotype. **E)** Representative images and **F)** quantification of EndoA intensities in boutons of motorneurons expressing wild type (nSyb-GAL4> TauWT) or human mutant Tau with increased eMIA (nSyb-GAL4>Hsc70WT, TauP301L or V337M or AA or P301L,V337M). Number of larvae is 4-8 per genotype. **G)** Representative images of Tau-GFP FRAP at time points right before (pre) and after photobleaching of an area (arrowhead) (0, 10, 30 and 50 seconds) in axons of flies expressing human wild type Tau (nSyb-GAL4>TauWT-FT-GFP) or flies expressing human double mutant Tau (nSyb-GAL4>TauP301L,V337M-FT-GFP). An ordinary one-way ANOVA with Dunnett's correction for multiple comparison was performed for all analysis. ns, not significant; * $p<0.05$; ** $p<0.01$; *** $p<0.001$; **** $p<0.0001$. Scale bars: 5µm. Bar graphs depict mean ± SEM.

5. Follow up study: Targeting of pathogenic presynaptic Tau in human neurons in a chimeric Alzheimer's Disease mouse model

The follow up of our molecular work in fruit flies, showing rescue of synaptic dysfunction and neurodegeneration with the increase of Hsc70-4 levels, is to measure if the increase of Hsc70-4/HSPA8 also rescues synapse and neurodegeneration in human neurons transplanted in Aβ producing mice (APPNL-G-F Rag2-/-). Common in models used for AD research is a lack of neurodegeneration and Tau pathology [61]. A novel human-mouse chimera AD model (created in our institute) overcomes these important limitations [62,63]. In this model, human neuronal progenitors (NPCs) are grafted into an AD (APPNL-G-F Rag2-/-) mouse and differentiate and integrate into the mouse brain (Follow up Figure 1 E). When the host mice produce Aβ plaques, human transplanted (but not mouse transplanted) neurons develop Tau pathology and undergo neurodegeneration [62,63]. Hence, this chimeric mouse model is unique and an ideal model to study Aβ-induced Tau pathology and human disease-relevant processes of neurodegeneration and will identify if the increase of endosomal microautophagy is a relevant therapeutic candidate. An important aspect of the work is to follow synaptic decline (in addition to neurodegeneration), we therefore used CRISPR-Cas9 to knock in an HA-tag into the endogenous gene that encodes for the synaptic protein Synaptophysin (SYP) in human induced pluripotent stem cells (iPSCs) (Follow up Figure 1 A). We generated cortical neuronal progenitor cells (NPCs) of the genetic engineered iPSCs and differentiated them. After 55 days *in vitro*, we confirmed the expression of SYP-HA with immunostainings (Follow up Figure 1 B). We can also increase the expression of HSc70-4/HSPA8 by lentiviral expression in human neurons as confirmed with immunostainings and western blot (Follow up Figure 1 C and D). Since the genetically engineered NPCs differentiate and express SYP-HA, we xenotransplanted them in control mice (Rag2-/-) and Aβ producing mice (APPNL-G-F Rag2-/-) to check their graftability (Follow up Figure 2). The SYP-HA NPCs differentiate and integrate in the mouse brain (Follow up Figure 2A) and the expression of SYP-HA is confirmed with the anti-HA immunostaining on brain slices of the xenotransplanted mice (Follow up Figure 2B). Since, the SYP-HA cells integrate in the brain, we can use these cells (HA-SYP cells) to increase HSPA8 expression by lentiviral mediated expression. In the next step, we will assess human neuron synapse density using the HA-tag and neurodegeneration using qPCR. Finally, we will characterize pathological features such that we can compare signs of degeneration to the level of Tau and Aβ pathology in control human neurons versus human neurons with increased endosomal microautophagy by the overexpression of HSPA8.
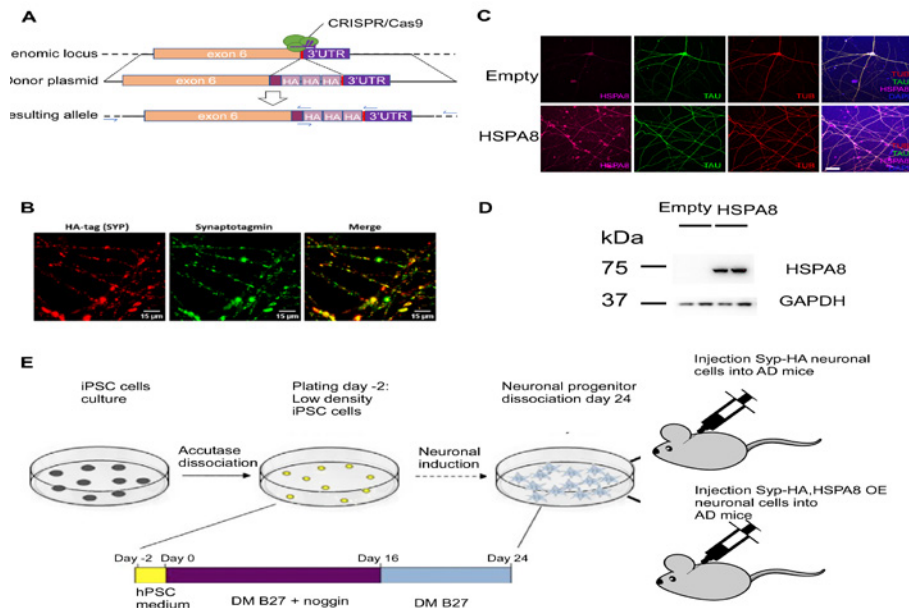
Follow up Figure 1. Generation of SYP-HA and Hsc70-4/HSPA8-myc overexpression neuronal cells to inject in AD mice APPNL-G-F Rag2-/-.
A) CRISPR/Cas9 mediated insertion of a triple HA tag at the C-terminus of Synaptophysin (*SYP*). B) Anti-HA and anti-Synaptotagmin labeling in SYP-HA cortical neurons (DIV 55) shows colocalization of SYP-HA with the synaptic protein Synaptotagmin. C) Lentiviral mediated expression of Hsc70-4/HSPA8-myc in cortical neurons confirmed with immunostainings against Hsc70-4/HSPA8, Tau and Tubulin (Tub) and nucleus (DAPI), scale bar 50µm C) and with western blot experiments. No expression of Hsc70-4/HSPA8-myc was observed in human neurons transduced with empty lentiviral vector (empty) D). E) Scheme for the generation of neuronal progenitor cells (SYP-HA and HSPA8 overpexpression (OE)) and the injection thereof in pups (P0) of AD mice.
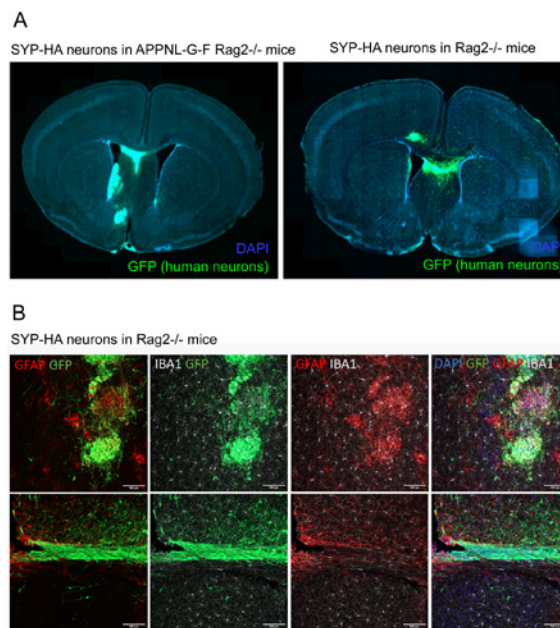
Follow up Figure 2. Generation of SYP-HA and Hsc70-4/HSPA8-myc overexpression neuronal cells to inject in AD mice APPNL-G-F Rag2-/-.
A) Coronal brain slices of APPNL-G-F Rag2-/- and Rag2-/-mice one month past transplantation with human SYP-HA neurons (green). B) Anti-HA and anti-GFP (human neurons) immunolabeling shows integration and synapse formation of SYP-HA cortical neurons in the brain.

6.   Publications GSKE funded

In preparation:
– Uytterhoeven, V. et al. (2023) Independent pathways contribute to the accumulation of pathogenic Tau at presynapses.

7.   References

1.   Wang, Y. and Mandelkow, E. (2016) Tau in physiology and pathology. *Nat. Rev. Neurosci.* 17, 5–21
2.   Ballatore, C. et al. (2007) Tau-mediated neurodegeneration in Alzheimer's disease and related disorders. *Nat. Rev. Neurosci.* 8, 663–672
3.   Roberson, E.D. et al. (2007) Reducing endogenous Tau ameliorates amyloid beta-induced deficits in an Alzheimer's disease mouse model. *Science (80-.).* 316, 750–753
4.   Hutton, M. et al. (1998) Association of missense and 5'-splice-site mutations in tau with the inherited dementia FTDP-17. *Nature* 393, 702–704
5.   McInnes, J. et al. (2018) Synaptogyrin-3 Mediates Presynaptic Dysfunction Induced by Tau. *Neuron* 97, 823-835.e8
6.   Largo-Barrientos, P. et al. (2021) Lowering Synaptogyrin-3 expression rescues Tau-induced memory defects and synaptic loss in the presence of microglial activation. *Neuron* 109, 767-777.e5
7.   Zhou, L. et al. (2017) Tau association with synaptic vesicles causes presynaptic dysfunction. *Nat. Commun.* 8, 1–29
8.   Wucherpfennig, T. et al. (2003) Role of Drosophila Rab5 during endosomal trafficking at the synapse and evoked neurotransmitter release. *J. Cell Biol.* 161, 609–24
9.   Uytterhoeven, V. et al. (2015) Hsc70-4 Deforms Membranes to Promote Synaptic Protein Turnover by Endosomal Microautophagy. *Neuron* 88, 735–748
10. Taoufiq, Z. et al. (2020) Hidden proteome of synaptic vesicles in the mammalian brain. *Proc. Natl. Acad. Sci. U. S. A.* 117, 33586–33596
11. Soukup, S.F. et al. (2016) A LRRK2-Dependent EndophilinA Phosphoswitch Is Critical for Macroautophagy at Presynaptic Terminals. *Neuron* 92, 829–844
12. Uytterhoeven, V. et al. (2011) Loss of Skywalker Reveals Synaptic Endosomes as Sorting Stations for Synaptic Vesicle Proteins. *Cell* 145, 117–132
13. Shen, W. and Ganetzky, B. (2009) Autophagy promotes synapse development in Drosophila. *J. Cell Biol.* 187, 71–79
14. Tang, G. et al. (2014) Loss of mTOR-Dependent Macroautophagy Causes Autistic-like Synaptic Pruning Deficits. *Neuron* 83, 1131–1143
15. Stavoe, A.K.H. et al. (2016) KIF1A/UNC-104 Transports ATG-9 to Regulate Neurodevelopment and Autophagy at Synapses. *Dev. Cell* 38, 171–185
16. Hernandez, D. et al. (2012) Regulation of Presynaptic Neurotransmission by Macroautophagy. *Neuron* 74, 277–284
17. Kuijpers, M. et al. (2021) Neuronal Autophagy Regulates Presynaptic Neurotransmission by Controlling the Axonal Endoplasmic Reticulum. *Neuron* 109, 299-313.e9
18. Glatigny, M. et al. (2019) Autophagy Is Required for Memory Formation and Reverses Age-Related Memory Decline. *Curr. Biol.* 29, 435-448.e8
19. Bellenguez, C. et al. (2021) New insights on the genetic etiology of Alzheimer's and related dementia. *medRXiv* 17, 10
20. Wightman, D.P. et al. (2021) A genome-wide association study with 1,126,563 individuals identifies new risk loci for Alzheimer's disease. *Nat. Genet.* 53, 1276–1282
21. Lai, S.S.M. et al. (2021) Endosomallysosomal dysfunctions in Alzheimer's disease: Pathogenesis and therapeutic interventions. *Metab. Brain Dis.* 36, 1087–1100
22. Piras, A. et al. (2016) Autophagic and lysosomal defects in human tauopathies: analysis of post-mortem brain from patients with familial Alzheimer disease, corticobasal degeneration and progressive supranuclear palsy. DOI: 10.1186/s40478-016-0292-9
23. Nixon, R.A. (2013) The role of autophagy in neurodegenerative disease. *Nat. Med. 2013 198* 19, 983–997
24. Krüger, U. et al. (2012) Autophagic degradation of tau in primary neurons and its enhancement by trehalose. *Neurobiol. Aging* 33, 2291–2305
25. Caballero, B. et al. (2018) Interplay of pathogenic forms of human tau with different autophagic pathways. *Aging Cell* 17,
26. Wang, Y. et al. (2009) Tau fragmentation, aggregation and clearance: The dual role of lysosomal processing. *Hum. Mol. Genet.* 18, 4153–4170
27. Kaushik, S. and Cuervo, A.M. (2012) Chaperone-mediated autophagy: A unique way to enter the lysosome world. *Trends Cell Biol.* 22, 407–417

28. Fernandes, A.C. *et al.* (2014) Reduced synaptic vesicle protein degradation at lysosomes curbs TBC1D24/sky-induced neurodegeneration. *J. Cell Biol.* 207,

29. Pan, P.Y. *et al.* (2020) Synj1 haploinsufficiency causes dopamine neuron vulnerability and alpha-synuclein accumulation in mice. *Hum. Mol. Genet.* 29, 2300–2312

30. Sheehan, P. *et al.* (2016) Activity-Dependent Degradation of Synaptic Vesicle Proteins Requires Rab35 and the ESCRT Pathway. *J. Neurosci.* 36, 8668–8686

31. Jin, E.J. *et al.* (2018) Live Observation of Two Parallel Membrane Degradation Pathways at Axon Terminals. *Curr. Biol.* 28, 1027-1038.e4

32. Tekirdag, K. and Cuervo, A.M. (2018) Chaperone-mediated autophagy and endosomal microautophagy: Jointed by a chaperone. *J. Biol. Chem.* 293, 5414

33. Sahu, R. *et al.* (2011) Microautophagy of Cytosolic Proteins by Late Endosomes. *Dev. Cell* 20, 131–139

34. Massey, A.C. *et al.* (2006) Consequences of the selective blockage of chaperone-mediated autophagy. *Proc. Natl. Acad. Sci. U. S. A.* 103, 5805–5810

35. Chiang, H.L. and Dice, J.F. (1988) Peptide sequences that target proteins for enhanced degradation during serum withdrawal. *J. Biol. Chem.* 263, 6797–6805

36. Hageman, J. and Kampinga, H.H. (2009) Computational analysis of the human HSPH/HSPA/DNAJ family and cloning of a human HSPH/HSPA/DNAJ expression library. *Cell Stress Chaperones* 14, 1–21

37. Nixon, R.A. *et al.* (2005) *Extensive Involvement of Autophagy in Alzheimer Disease: An Immuno-Electron Microscopy Study*, 64

38. Morimoto, R.I. and Cuervo, A.M. (2014) Proteostasis and the Aging Proteome in Health and Disease. *Journals Gerontol. Ser. A* 69, S33–S38

39. Menzies, F.M. *et al.* (2015) Compromised autophagy and neurodegenerative diseases. *Nat. Rev. Neurosci. 2015 166* 16, 345–357

40. Huang, S.P. *et al.* (1993) Aspartyl residue 10 is essential for ATPase activity of rat hsc70. *J. Biol. Chem.* 268, 2063–2068

41. Shupliakov, O. *et al.* (2011) How synapsin I may cluster synaptic vesicles. *Semin. Cell Dev. Biol.* 22, 393–399

42. Selkoe, D.J. (2002) Alzheimer's disease is a synaptic failure. *Science* 298, 789–91

43. Jackson, J. *et al.* (2019) Targeting the synapse in Alzheimer's disease. *Front. Neurosci.* 13, 1–8

44. Wittmann, C.W. *et al.* (2001) Tauopathy in Drosophila: neurodegeneration without neurofibrillary tangles. *Science* 293, 711–4

45. Devos, S.L. *et al.* (2018) HHS Public Access. 9, 1–30

46. Yoshiyama, Y. *et al.* (2007) Synapse Loss and Microglial Activation Precede Tangles in a P301S Tauopathy Mouse Model. *Neuron* 53, 337–351

47. Hardy, J. *et al.* (2014) Pathways to Alzheimer's disease. *J. Intern. Med.* 275, 296–303

48. Passarella, D. and Goedert, M. (2018) Beta-sheet assembly of Tau and neurodegeneration in Drosophila melanogaster. *Neurobiol. Aging* 72, 98–105

49. Jacomin, A.-C. *et al.* (2020) Degradation of arouser by endosomal microautophagy is essential for adaptation to starvation in Drosophila. DOI: 10.26508/lsa.202000965

50. Kirchner, P. *et al.* (2019) Proteome-wide analysis of chaperone-mediated autophagy targeting motifs. DOI: 10.1371/journal.pbio.3000301

51. Barghorn, S. *et al.* (2000) Structure, microtubule interactions, and paired helical filament aggregation by tau mutants of frontotemporal dementias. *Biochemistry* 39, 11714–11721

52. Deture, M. *et al.* (2000) Missense tau mutations identified in FTDP-17 have a small effect on tau-microtubule interactions. *Brain Res.* 853, 5–14

53. Xia, Y. *et al.* (2019) Impaired tau-microtubule interactions are prevalent among pathogenic tau variants arising from missense mutations. *J. Biol. Chem.* 294, 18488–18503

54. Di Primio, C. *et al.* (2017) The distance between N and C termini of tau and of FTDP-17 mutants is modulated by microtubule interactions in living cells. *Front. Mol. Neurosci.* 10,

55. Konzack, S. *et al.* (2007) Swimming against the tide: Mobility of the microtubule-associated protein tau in neurons. *J. Neurosci.* 27, 9916–9927

56. Coyne, A.N. *et al.* (2017) Post-transcriptional Inhibition of Hsc70-4/HSPA8 Expression Leads to Synaptic Vesicle Cycling Defects in Multiple Models of ALS. *Cell Rep.* 21, 110–125

57. Ayaki, T. *et al.* (2018) Multiple proteinopathies in familial ALS cases with optineurin mutations. *J. Neuropathol. Exp. Neurol.* 77, 128–138

58. Stevens, C.H. *et al.* (2019) Increased tau phosphorylation in motor neurons from clinically pure sporadic amyotrophic lateral sclerosis patients. *J. Neuropathol. Exp. Neurol.* 78, 605–614

59. Petrozziello, T. *et al.* (2022) Targeting Tau Mitigates Mitochondrial Fragmentation and Oxidative Stress in Amyotrophic Lateral Sclerosis. *Mol. Neurobiol.* 59, 683–702

60. Xu, X. *et al.* Correction to: Metformin activates chaperone-mediated autophagy and improves disease pathologies in an Alzheimer disease mouse model (Protein & Cell, (2021), 12, 10, (769-787), 10.1007/s13238-021-00858-3). , *Protein and Cell*, 13. (2022) , 227–229

61. Drummond, E. and Wisniewski, T. (2017) Alzheimer's disease: experimental models and reality. *Acta Neuropathol.* 133, 155–175

62. Espuny-Camacho, I. *et al.* (2017) Hallmarks of Alzheimer's Disease in Stem-Cell-Derived Human Neurons Transplanted into Mouse Brain. *Neuron* 93, 1066-1081.e8

63. Balusu, S. *et al.* (2022) Long noncoding RNA MEG3 activates neuronal necroptosis in Alzheimer's disease. *bioRxiv* DOI: 10.1101/2022.02.18.480849

Progress report of the research project of the young researcher

Dr. Emanuel van den Broeke
Université Catholique de Louvain (UCLouvain)

Dr. Emanuel van den Broeke
Postdoctoral researcher, laboratory Algology (prof. André Mouraux),
Institute of Neuroscience (IONS),
division Systems and Cognition (COSY),
UCLouvain, Brussels
www.nocions.org/emanuel-vandenbroeke

The involvement of top-down facilitatory serotonergic pathways in nocebo-induced pain hypersensitivity.

Compared to previous report, the aim remains to find an effective protocol for inducing negative expectations on pain that can be used to conduct the planned pharmacological study. As the experimental results have been disappointed so far (in terms of effectiveness), and because there is only one more year left, it will not be possible to conduct the pharmacological study within the time of the grant. Unfortunately, I was not granted the Chercheur Qualife provided by the FNRS, despite being ranked twice A+. This means that my contract at UCL will end 31 of December 2023 (end of the grant). I will continue my post-doctoral fellowship at KUL.

1.   Ongoing studies

We have just finished a study investigating the effect of negative expectations of pain on the development of secondary hyperalgesia. The manuscript is in preparation. Despite the fact that we found an effect of the negative expectations on our test stimuli, indicating that the intervention was effective, no differences were found in the perceived pain and hyperalgesia between the control group and intervention group.

We have set up three new studies. The first one is a modified version of the one mentioned above. We hope that the intervention will be more effective. Two other studies will be carried out at KUL under my supervision. One will make an attempt to replicate the original study (van den Broeke et al. 2014) that was the basis of the FMRE grant. The other study will use fear induction to increase pain and hyperalgesia.

The aim of these studies is to find a protocol that robustly induces negative expectation or fear that increases pain and hyperalgesia.

2.   Output:

2.1.   Congress
I have organized as Chair a topical workshop: "Understanding the Role of Psychological Factors in Pain Amplification: Insights from Experimental and Clinical Research" at the 2023 International Convention of Psychological Science (ICPS), 9th to 11th March 2023 in Brussels, Belgium. The funding of the FMRE will be acknowledged.

2.2.   Publications
– Torta DM, Meyers E, Polleunis K, De Wolf S, Meulders A, van den Broeke EN. The Effect of Observing High or Low Pain on the Development of Central Sensitization. J Pain. 2023 Jan;24(1):167-177. doi: 10.1016/j.jpain.2022.09.009. The funding of the FMRE is acknowledged.

3. Publications

3.1. Published
– **van den Broeke EN**, Crombez G, Vlaeyen JWS. Reconceptualizing sensitization in pain: back to basics. Pain Rep. 2024 Jan 15;9(1):e1125. doi: 10.1097/PR9.0000000000001125.
– Gousset S, Torta DM, Mouraux A, Lambert J, **van den Broeke EN**. Pinprick-induced gamma-band oscillations are not a useful electrophysiological marker of pinprick hypersensitivity in humans. Clin Neurophysiol. 2023 Sep;153:102-110. doi: 10.1016/j.clinph.2023.06.018.
– Meyers E, Vlaeyen JWS, **van den Broeke EN**, von Leupoldt A, Palmer AJ, Torta DM. The effect of high versus low cognitive load on the development of nociceptive hypersensitivity: The roles of sympathetic arousal, sex and pain-related fear. Eur J Pain. 2023 Jul;27(6):682-698. doi: 10.1002/ejp.2098.

3.2. Under Review
– Gousset S, Cayrol T, Papleux M, Meulders A, Mouraux A, **van den Broeke EN.** Do you get what you expect? Studying the effect of expectations on high-frequency electrical stimulation-induced pain and pinprick hypersensitivity. J Pain.

3.3. In preperation
– **Van den Broeke EN**, Wijns K, Bouwer B, Torta D and Vlaeyen JWS. No evidence that fear of electrically-evoked pain affects mechanical pinprick perception.
– De Voeght L, Kinnart M, Jeltare K, D'agostini M, Torta D and **van den Broeke EN**. A partial replication of the effect of negative expectations on the development of heterotopic mechanical hyperalgesia: A behavioural and psychophysiological approach.
– Della Porta D, Boutachkourt A, Gousset S, **van den Broeke EN**. Experimentally testing the pain-enhancing effect of a nocebo manipulation on the induction of secondary hyperalgesia.
– Meyers E, Della Porta D, Torta DM, and **van den Broeke EN**. The role of psychological factors in the development and modulation of secondary hyperalgesia as a marker of central sensitization: A narrative review.

4. Development of an upgraded robot-controlled mechanical pinprick stimulator

Together with our technical department (Mr. Lambert) we are building a new robot-controlled mechanical pinprick stimulator. Such a robot increases the reliability of the forces applied onto the skin and works operator-independent. The robot that is currently built is an upgraded version of a prototype built some years ago as a first attempt. The idea is to make the design of the robot open hardware so that the whole scientific society can benefit from it.

5. Final conclusions

The aim of the originally proposed project was to investigate the effect of a 5-HT3 receptor antagonist (ondansetron) on nocebo induced hyperalgesia. Unfortunately, we could not replicate the nocebo effect as found in the original paper (van den Broeke et al. 2014), which was the basis of our application. We conducted a series of experiments using different approaches to induce nocebo responses. In most experiments we did not observe an effect of nocebo on HFS and pinprick hypersensitivity and in those experiments were we did manage to induce a nocebo effect, the effect on HFS-pain and/or pinprick hypersensitivity was absent, or very small. Taken together, our results suggest that it is difficult to induce a nocebo effect that modulates HFS-pain and pinprick hypersensitivity. This casts doubt about the feasibility of conducting a pharmacological study with these experimental designs as large numbers of participants are needed.

Of note: our collaborators in Germany have in the meantime conducted an experiment investigating the effect of Ondansetron on HFS and pinprick hypersensitivity (without nocebo). They found no effect of Ondansetron on the pain ratings during HFS or on pinprick hypersensitivity. So either a single oral application of 40 mg Ondansetron is not sufficient to modulate HFS-evoked pain and pinprick hypersensitivity or 5-HT3 does not play a significant role in HFS-evoked pain and pinprick hypersensitivity. However, it remains to be investigated the role of 5-HT3 in *nocebo responses* in the context of HFS and pinprick hypersensitivity.

Progress report of the research project of the young researcher

Eline Wauters, PhD (VIB)
Universiteit Antwerpen (UAntwerpen)

Eline Wauters, PhD (VIB)
Neurodegenerative Brain Diseases,
VIB Center for Molecular Neurology,
Laboratory of Neurogenetics,
Institute Born-Bunge,
University of Antwerp,
Antwerp, Belgium

Onset age variability in *GRN*-associated frontotemporal lobar degeneration: identification of a functional onset age modifier

1.   Research Summary

Frontotemporal lobar degeneration (FTLD) is the most common cause of neurodegenerative dementia at young age after Alzheimer's disease (AD). Mutations in the progranulin gene (*GRN*) are a major cause of FTLD, accounting for up to 11.2% of patients. The onset age of *GRN* mutation carriers ranges from 25 to 90 years. This broad onset age range points to the existence of modifiers that affect the onset age of *GRN*-related neurodegeneration. Identifying these factors is of importance as they might represent targets for disease-delaying therapies.

In an extended Belgian founder family, segregating the *GRN* IVS1+5 G>C null mutation, patients present with disease at onset ages ranging from 45 to 80 years. In this family, we have previously identified a quantitative trait locus (QTL) for onset age. The aim of the project is to identify the functional gene and variant underlying the onset age variability, to study the modifier effect in induced pluripotent stem cell (iPSC) derived neurons and microglia, and to extend the findings to international patient cohorts.

2.   Progress Report

Please note that the planned execution of this project has been delayed due to the COVID-19 pandemic, leading to a mandatory lockdown and to delays in delivery of consumables, and due to my pregnancy.

2.1.   Identification of functional QTL SNPs with a significant effect on onset age

From whole genome (n=23) and exome sequencing data (n=41) of *GRN* founder mutation carriers, I have selected variants located within the onset age QTL (n=635 variants, 620 of which are located in intronic and intergenic regions). To bridge the gap between a genomic locus and mechanisms, I am performing an unbiased high-throughput screen to prioritize functional variants. This technology, REEL-Seq (Regulatory Element Sequencing, (1)), progressed from the SNP-seq technology which I originally envisaged to use (2). I have performed a research stay in the lab of Dr. Li, who introduced both these innovative technologies (University of Pittsburgh (USA), August 2019). REEL-Seq is based on the design of two oligonucleotides for each studied variant – one with the wild-type and one with the alternative allele. This library of oligonucleotides will be incubated with nuclear extract. By performing consecutive cycles of incubation with nuclear extract, gel electrophoresis and PCR amplification, the sequences containing a functional SNP will be enriched in the sequence pool.

I have performed a first REEL-seq experiment in house, using an oligonucleotide library containing QTL variants (Twist Bioscience) and nuclear extract derived from HEK293T cells. The resulting libraries have been sequenced on the NextSeq platform to quantify the sequences. (Neuromics Support Facility). These data will be analyzed to know which sequences are enriched in the sequence pool and thus contain a functional SNP. Afterwards, I will genotype the identified functional variants in the complete founder family and perform reporter gene assays to determine the effect of the variants on expression.

Fifteen of the 635 variants are located in exons (coding and non-coding). While these are also included in the REEL-seq library, I have moved forward with these variants in a parallel trajectory given the known relevance of variants in this region for protein function or expression.

I have genotyped the 15 exonic variants in members of the *GRN* founder family (n=170 individuals, including 79 *GRN* founder mutation carriers). Genotyping was performed via multiplex PCRs for target enrichment of the regions encompassing the exonic variants (3). The amplicon libraries were sequenced (MiSeq, Illumina). Adapters were trimmed using Fastq-mcf. Reads were aligned to the reference genome hg19 with the Burrows-Wheeler Aligner (4). Variant calling and annotation were performed using GATK (5) and the GenomeComb package (6). For each variant I have estimated the effect on onset age in the *GRN* founder family using Loki (7). This analysis indicated that seven exonic variants have a significant effect on onset age (p<0.05). Six variants are located in 5' or 3' untranslated regions (UTR). One variant is located in a coding exon, leading to a missense mutation. We will evaluate the functional effect of the UTR variants using luciferase reporter assays. To assess the functionality of the missense mutation, we will overexpress the wild-type and mutant protein in a cell model and evaluate effects of the mutation on the known protein function.

For the luciferase reporter assays, the coding sequence of secreted *Nanoluc* luciferase was synthesized (Integrated DNA Technologies, IDT) and cloned into the BamHI and NotI restriction sites of a pGL4 expression vector (Promega) under the TK promoter, thereby substituting the *Gaussia* luciferase coding sequence. Fragments containing the UTR sequences were amplified from cDNA using specific primers and cloned into this plasmid via In-Fusion cloning (Takara Bio). 5' UTR sequences were cloned upstream of the *Nanoluc* luciferase, and 3' UTR sequences downstream of the luciferase. Genetic variants were generated by site-directed *in vitro* mutagenesis. All constructs were validated by Sanger sequencing. HEK293T cells were co-transfected with the *Nanoluc* luciferase construct and a *Firefly* luciferase plasmid (under the SV40 promoter, Promega). The signal for both luciferases was generated using the Dual-Luciferase Reporter Assay System (Promega), after which luminescence was measured. One variant, located in a 3'UTR, lowered expression to 55-70% in comparison to the wild-type sequence (p=0.00512, Mann-Whitney U test). Additional experiments will be performed to confirm this effect. In the founder family, homozygous carriers of the wild-type allele developed disease on average 8.5 years earlier in comparison to homozygous carriers of the variant allele (p=0.00018).

2.2. Compare gene expression in biomaterials of patients with early and late onset of disease

To study differential gene expression between early- and late-onset disease, we have compared expression levels between individuals with different genotypes at a QTL variant with a significant effect on onset age. For this variant, heterozygous (AB) and homozygous (BB) variation carriers developed disease on average 9.0 and 7.9 years later in comparison to homozygous wild-type allele carriers (p<0.00001 and p=0.0002, respectively) (**Figure 1**). Transcriptome profiling was performed on lymphoblastoid cell line (LCL)-derived RNA of eight *GRN* founder mutation carriers with different genotypes for the QTL variant. Six carriers had onset ages ranging from 56 to 68 years, and two carriers were unaffected at ages 72 and 75. The coding transcriptome was captured and sequenced (TruSeq Stranded mRNA Library Prep kit, NextSeq, Illumina). We identified 475 differentially expressed genes between four homozygous carriers of the wild-type allele (AA) and four homozygous carriers of the QTL variant (BB) (Padj < 0.1). Enrichment analysis (GOrilla, 8) indicated an important role for endoplasmic reticulum (ER) unfolded protein response and ER stress.
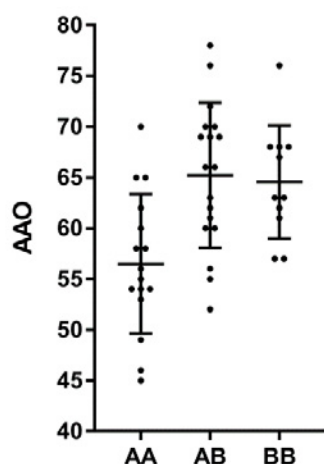
Figure 1: Onset age distributions in the *GRN* founder family for one of the QTL variants with a significant effect on onset age. Patients with known onset age and genotype were included. The mean onset age for each genotype and the standard deviations are visualized. AAO: age at onset. AA/AB/BB: genotypes.

We have expanded our transcriptomics studies and performed QuantSeq 3' mRNA sequencing (Lexogen) on LCLs (n=58) and brain material (n=9) of *GRN* founder mutation carriers and non-carriers (n=14 LCLs, n=6 brain). When comparing expression levels in LCLs between carriers homozygous for the wild-type allele (AA, n=21) and homozygous variant carriers (BB, n=14), only ten differentially expressed genes (Padj < 0.1) were identified. Validation on the protein level in LCLs is ongoing.

2.3. A GRN-FTD iPSC model to identify the functional onset age modifier

We have differentiated control iPSCs to cortical neurons following the feeder-free protocol implemented by the Stem Cell Institute Leuven (SCIL) (protocol adapted from (9)), and to macrophages following the protocol described by *Haenseler et al* (10). We have evaluated the RNA expression of *GRN* and of the genes located in the onset age QTL in undifferentiated iPSCs, in cortical neurons (22 days *in vitro*), and in macrophages using SYBR green-based quantitative PCR. This analysis indicated that *GRN* and the onset age QTL genes are indeed expressed in the differentiated cortical neurons and macrophages. We have also investigated the expression of marker genes; the pluripotency marker *Oct4* shows clear expression in the undifferentiated iPSCs, while this is not the case in the neurons and macrophages. Conversely, transcript levels of the cortical marker *Tbr1* were dramatically increased in the cortical neurons, while the expression of microglia/macrophage markers *MERTK*, *GPR34* and *P2RY12* was highly increased in the macrophages in comparison to the iPSCs.

I have created heterozygous *GRN* knockout lines using CRISPR-Cas9 genome editing starting from control iPSCs, with the aim of using this model to investigate the effect of candidate onset age modifiers on disease-related characteristics such as *GRN* expression, expression of lysosomal proteins, corticogenesis, and TDP-43 accumulation and localization.

2.4. Investigation of the role of the QTL in onset age modification in international patient cohorts

Unrelated FTD patients without GRN mutation

We have evaluated the onset age modifying effect of the QTL in unrelated Belgian frontotemporal dementia (FTD) patients without *GRN* mutations (n=293; mean onset age 62.9 ± 10.5 y) by genotyping QTL tagging variants (n=21). Homozygous carriers of the top associated SNP developed disease on average 3.7 years later in comparison to patients homozygous for the wild-type allele (p=0.010, Mann-Whitney U), indicating that the modifier locus also has an effect

in *GRN*-unrelated FTD. To verify a possible effect on disease risk, I genotyped the same set of variants in a cohort of Belgian control individuals (n=684, age at inclusion range 60 to 98 years). We calculated association with disease (genotypic logistic regression, covariate: gender), and obtained significance for four variants (p<0.05).

Alzheimer dementia patients
A genetic, clinical, and pathological overlap exists between neurodegenerative disorders such as FTD and AD. It is thus conceivable that QTL variants would affect the onset age of AD patients. To test this hypothesis, we have genotyped the QTL tagging variants in a cohort of unrelated Belgian AD patients (n=559; mean onset age 73.0 ± 9.3 y) and calculated association with onset age (univariate tests, covariates: APOE, gender). This indicated no significant effect (p>0.05).

GRN LOF mutation families
The candidate onset age modifiers were identified in an extended Belgian founder family, segregating the *GRN* IVS1+5 G>C null mutation. To allow evaluation of candidate onset age modifying variants in other families with a *GRN* LOF mutation, we have biomaterials available of 62 other Belgian *GRN* LOF mutation carriers, including 26 index patients. We will genotype the QTL tagging variants in this cohort and evaluate their effect on onset age.

We continuously update this cohort, and we identified a novel *GRN* mutation p.E393A in a non-fluent variant primary progressive aphasia patient with a positive family history of dementia (*Wauters, Gossye, et al, submitted*). This mutation has to the best of our knowledge not been reported before and is absent from mutation databases. It is located in the last codon of exon 10, in the splice donor sequence. The mutation leads to aberrant splicing, namely partial intronic read-through into intron 10 and usage of a cryptic intronic splice donor site. Long-read sequencing of a cycloheximide-treated RNA sample derived from mutation carrier's lymphoblasts (Flongle, Oxford Nanopore Technologies) shows a transcript that reads through 35 bases into intron 10 and continues in exon 11 (**Figure 2**). This out-of-frame 35 bases retention would result in a frameshift, a premature termination codon in exon 11 and nonsense-mediated mRNA decay of the mutant transcript (p.E393AfsTer31). PGRN protein levels are reduced in serum of the carriers to levels comparable to other known LOF mutations (**Figure 2**). Neuropathological examination of the index patient indicated Alzheimer's dementia pathology and FTLD-TDP type A pathology, characteristic for *GRN*-related FTLD. Our data demonstrate that careful examination of resequencing data is mandatory, as the mutation was annotated as a missense mutation in our sequencing dataset. In this way, pathogenic LOF mutations can be overlooked and hastily misinterpreted as missense mutations of unknown significance.
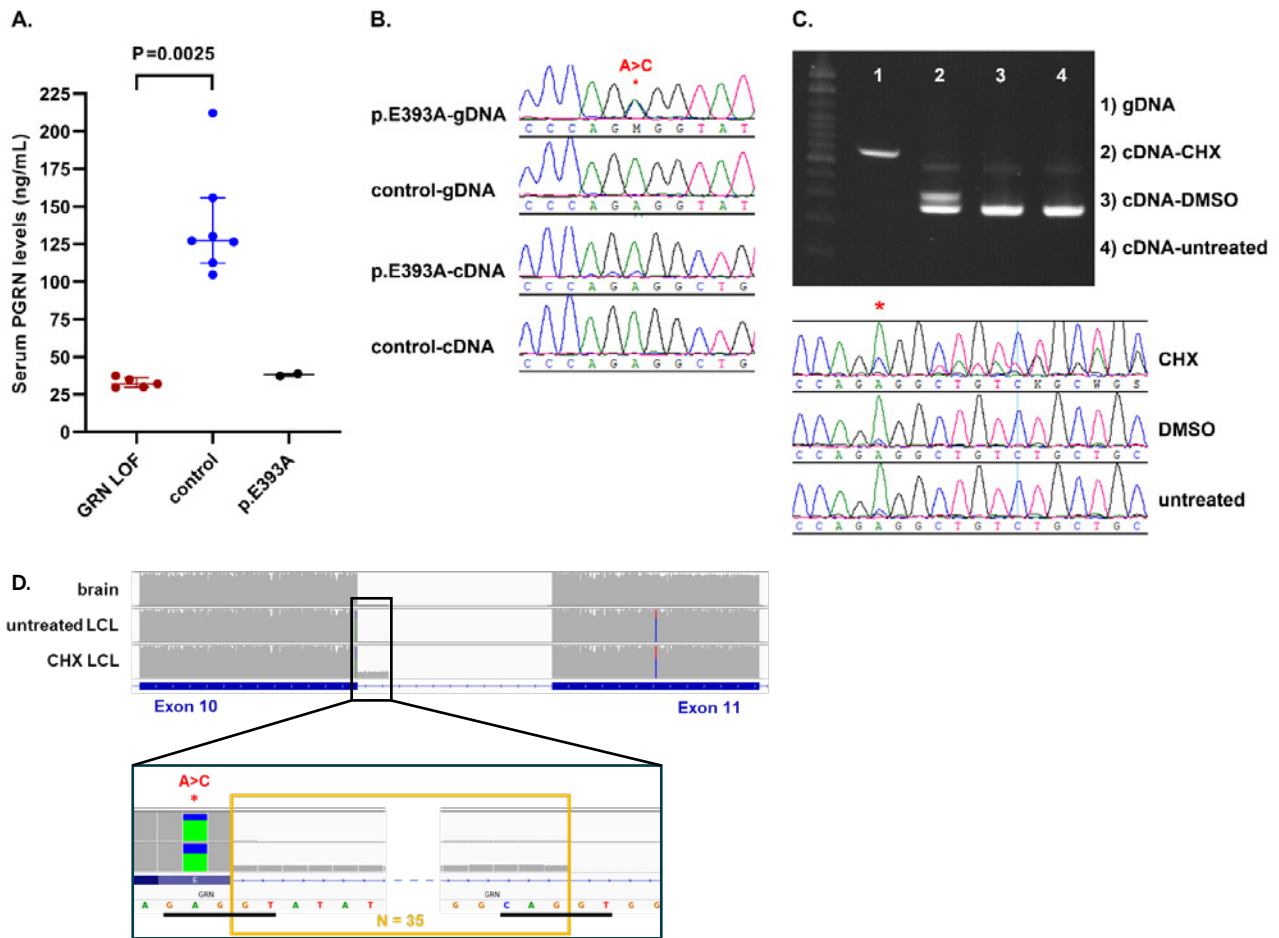
Figure 2: A) Serum PGRN levels measured in carriers of the *GRN* p.E393A mutation (n=2), *GRN* LOF mutations (n=5) and control individuals (n=7). PGRN levels are measured using ELISA (Adipogen). Horizontal lines: median levels, whiskers: interquartile range. Mann-Whitney U test was performed to compare PGRN levels between '*GRN* LOF' and 'control'. **B) LCL cDNA Sanger sequencing.** Electropherograms show the results of gDNA and cDNA Sanger sequencing in presence of the mutation. **C) NMD experiment.** Agarose gel picture shows the results of the exon 9 to 11 fragments amplification. The wild-type amplicon is 697 bases in size on gDNA level (1), and 388 bases on cDNA level (2-3-4). CHX treatment (2) results in an extra larger fragment, suggesting the presence of an alternative transcript which is degraded by NMD. Electropherograms show the results of the cDNA Sanger sequencing of CHX treated, DMSO treated and untreated LCLs of the mutation carrier. The red asterisk indicates the location of the mutation. **D) Long-read brain and LCL cDNA sequencing.** IGV visualization of Flongle sequencing data of brain-derived cDNA and CHX treated and untreated LCL-derived cDNA. Flongle CHX treated LCL cDNA sequencing shows read-through of 35 bases into intron 10. Zoom in on this region highlights the 35 bases intronic read-through in a yellow box. The presence of reads with the "C"-allele in the untreated sample demonstrates that not all mutated transcripts are degraded.

Abbreviations: cDNA: complementary DNA, ELISA: enzyme linked-immunosorbent assay, gDNA: genomic DNA, *GRN*: progranulin gene, LCL: lymphoblastoid cell line, LOF: loss-of-function, PGRN: progranulin protein

3.   References

1.   Zhao et al, Nat Commun, 2020
2.   Li et al, Nat Genet, 2018
3.   Goossens et al, Hum Mutat, 2009
4.   Li and Durbin, Bioinformatics, 2009
5.   McKenna et al, Genome Res, 2010
6.   Reumers et al, Nat Biotechnol, 2012
7.   Heath, Am J Hum Genet, 1997
8.   Eden et al, Bioinformatics, 2009
9.   Shi et al, Nat Neurosci, 2012
10. Haenseler et al, Stem Cell Rep, 2017

Geneeskundige **S**tichting **K**oningin **E**lisabeth
Fondation **M**édicale **R**eine **E**lisabeth
Königin-**E**lisabeth-**S**tiftung für **M**edizin
Queen **E**lisabeth **M**edical **F**oundation

Geneeskundige Stichting Koningin Elisabeth – G.S.K.E.

Fondation Médicale Reine Elisabeth – F.M.R.E.

Queen Elisabeth Medical Foundation – Q.E.M.F.

Mailing address:

The scientifique director:
Prof. dr. Jean-Marie Maloteaux
3, avenue J.J. Crocq laan
1020 Bruxelles - Brussel
Belgium
Tel.: +32 2 478 35 56
E-mail: jean-marie.maloteaux@uclouvain.be

Secretary:
Mr. Erik Dhondt
3, avenue J.J. Crocq laan
1020 Bruxelles - Brussel
Belgium
Tel.: +32 2 478 35 56
E-mail: fmre.gske@skynet.be
           erik.dhondt@skynet.be
           e.l.dhondt@skynet.be

www.fmre-gske.be
www.fmre-gske.eu
www.fmre-gske.com